Wide angle reflection studies at sea

Walker, Christopher David Terence

"Wide Angle Reflection Studies At Sea"

by

Christopher David Terence Walker

submitted for the degree of

Doctor of Philosophy

University of Durham

Department of Geological Sciences

Nineteen Hundred and Seventy Seven

CONTENTS

Illustrations			Page No.
Fig. 1.1		Example of Real Amplitude Processing - Normal Section	15
	1.2	Real Amplitude Playback of Fig. 1.1	16
	1.3	a, b Single Ship Seismic Systems	19
	1.3	c, d Single Ship Seismic Systems	20
	1.4	Ambient Acoustic Noise Spectrum	22
Fig. 2.1		Lateral View of Sonobuoy	30,31
	2.2	Block Diagram of Digress System	32
	2.3	Top View of Internal Housing	34
	2.4	Record Electronics	35
	2.5	Timing Electronics	36
	2.6	Hydrophone Deployment	37
	2.7	Hydrophone Electronics	40
	2.8	Hydrophone Frequency Response	41
	2.9	+15v Regulator	42
	2.10	-15v Regulator	43
	2.11	+5v Regulator	45
	2.12	Gain Ranging Board	46
	2.13	ADC Board	47
	2.14	Schematic Diagram of Crystal Oscillator Board	48
	2.15	Clock Circuit	49
	2.16	Internal Clock Schematic	51
	2.17	Sequence Control Unit Schematic	53
	2.18	Matrix Timing Board Schematic	54
	2.19	Sequence Control Operation	56
	2.20	Timer Circuit	59
	2.21	Matrix Board Operation - Case 1	60
	2.22	Matrix Board Operation - Case 2	61
	2.23	Tape Format	63, 64

Page No.

Acknowledgment

The author would like to thank the following, without whose help and assistance this work could not have been accomplished: Professor M.H.P. Bott, Professor J. Willis, Mr. D.W. Asberry, Mr. J.H. Peacock, Mr. R. Reeve, Dr. L.A. Arnold and the officers and crew of the R.R.S. 'Shackleton'.

Thanks also to Mrs. K. Waldron for her diligence in producing the text.

The research studentship for this project was granted by the former Ministry of Education for Northern Ireland.

"all ignorance toboggans into know

and trudges up to ignorance again."

- e.e. cummings.

A B S T R A C T

A self contained, free floating, recoverable sonobuoy system is described, for use in marine reflection and refraction surveys, together with a mathematical derivation of the wave amplitudes to be expected in such investigations. A detailed examination of the reflection and refraction results from several areas in the North Atlantic, obtained in the summers of 1973 and 1974 during the course of two Durham University Geophysical Surveys, is presented, in conjunction with simple processing procedures designed to extract information concerning the physical composition of the sea floor sediments, on the basis of the theory developed in the text.

CHAPTER ONE

INTRODUCTION

The usual procedure undertaken when a marine seismic investigation is made of a particular region is to examine the range of compressional and transverse wave velocities obtained by the various reflection and refraction methods, together with their corresponding interface depths (Ref. 1.1).

These kinematic properties can provide an enormous amount of information about each particular reflecting and/or refracting horizon present in the area surveyed, as is well known (Ref. 1.2), but for the most part the dynamic characteristics of the waves - the amplitude, spectra, change of wave shape upon reflection or refraction, are largely ignored.

When one considers the amplitude of a reflected-wave, even a simple analysis can provide information about the reflecting medium for instance, in a normal incidence reflection survey, the 'Bright' or 'Hot' Spot technique (Ref. 1.3).

In this system a real amplitude, as opposed to a gain controlled, plot of the arrival is made, and can clearly (Fig. 1.1, 1.2), reveal trapped gas deposits, for instance, very readily since the amplitude of the wave reflected from the gas saturated rock is many times that of the non-saturated surrounding rock.

It is hoped that examination of the reflected amplitude from a given interface with increasing angles of incidence may enable some information concerning the acoustic parameters of the interface to be determined. In particular, the behaviour of the amplitude as the angle of incidence approaches the critical angle is of interest, since it is at this angle that head waves are produced along the lower surface of the interface.

Having decided to examine the reflected wave amplitudes at varying angles of incidence, at sea, the problem of the design of a suitable experiment to permit this investigation arises. Dividing

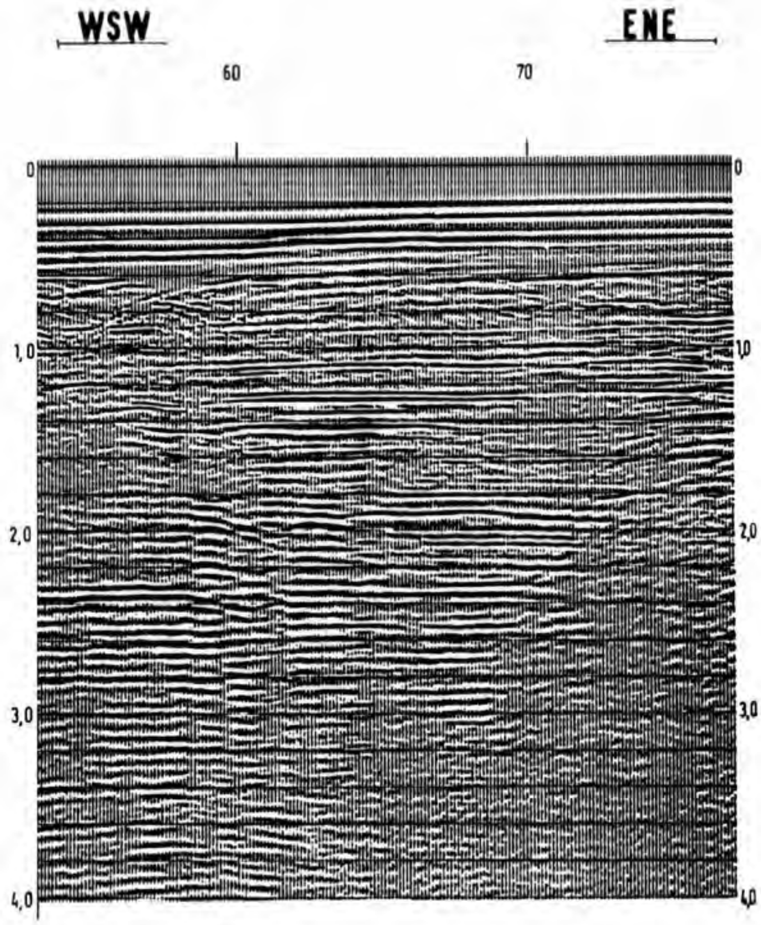

Fig. 1.1 Example of Real Amplitude Processing (Bright Spot Technique)
Normal Section

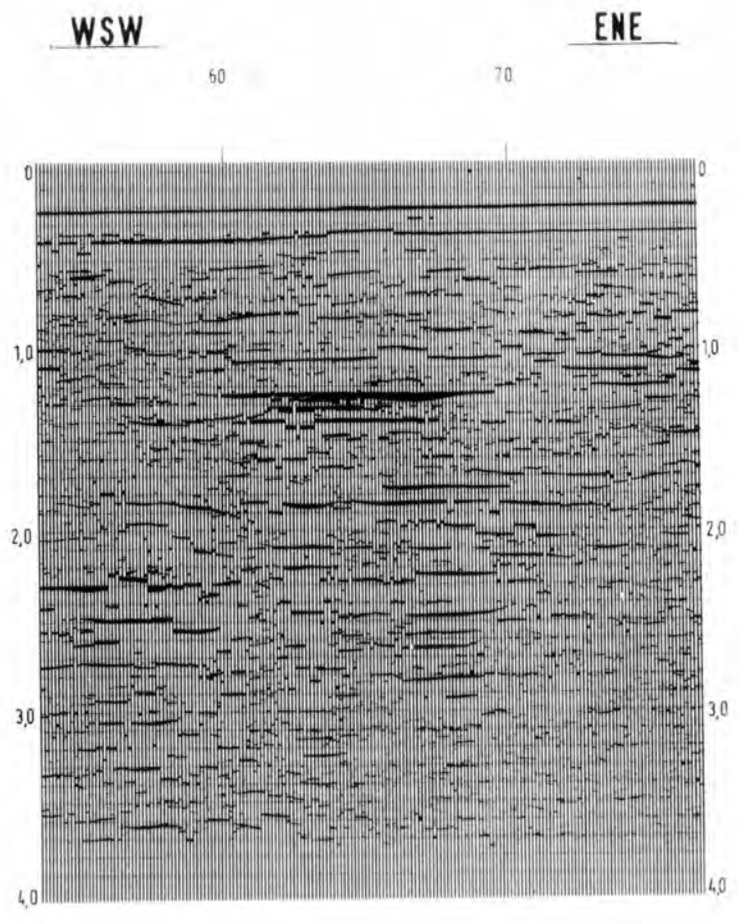

Fig. 1.2 Playback of Fig. 1.1 Section Using Real Amplitude Processing

the procedure into three parts, one obtains the following structure:

i) Data Acquisition System.

ii) Development of mathematical techniques, if necessary to provide theoretical expectations for the examination.

iii) Data Reduction and Processing to produce experimental results which may be compared to and contrasted with, those results obtained theoretically.

<u>Data Acquisition System</u>

Given the limitation imposed by having access to a single ship for marine geophysical surveying purposes, there are several possible single ship systems (Fig. 1.3 a-d).

a) Shooting at sea, Receiving on land (Fig. 1.3a).

This is technically the simplest way of recording marine seismic data, but for an amplitude study, the problem of differing structures beneath ship and station(s), presents a difficulty as regards interpretation. An entire array of stations would be required to calculate individual station delays and the logistics involved in setting up and maintaining such an array are considerable. A slightly different approach would be to use a single station, close to the coast and allow the ship to sail from close to shore seawards.

The problem with this system is that being close to the sea, such a station would be very prone to tidal and wave noise, and this, combined with the inevitable difficulty of having to use a high energy acoustic source to introduce energy across the sea/land interface, makes such a system unacceptable.

b) Towed Arrays/Single Hydrophone (Fig. 1.3b).

A hydrophone array streamer, towed behind the survey ship gives excellent quality data on near vertical incidence reflections but does not, in deeper water, cover a large enough angle of incidence range. Obviously, such a system suffers from towed body noise (Ref. 1.4), due to its relatively rapid motion through the water, and also from transmitted ship noise, both through the towing cable and in direct and multiple reflected waves emanating from the ship itself.

Similar drawbacks face a towed single hydrophone system, which could be towed at ever increasing separations to enable it to encompass the wide angle reflections. Practically, however, this is extremely inconvenient, reducing the manoeuvreability of the

Single Ship Seismic Systems

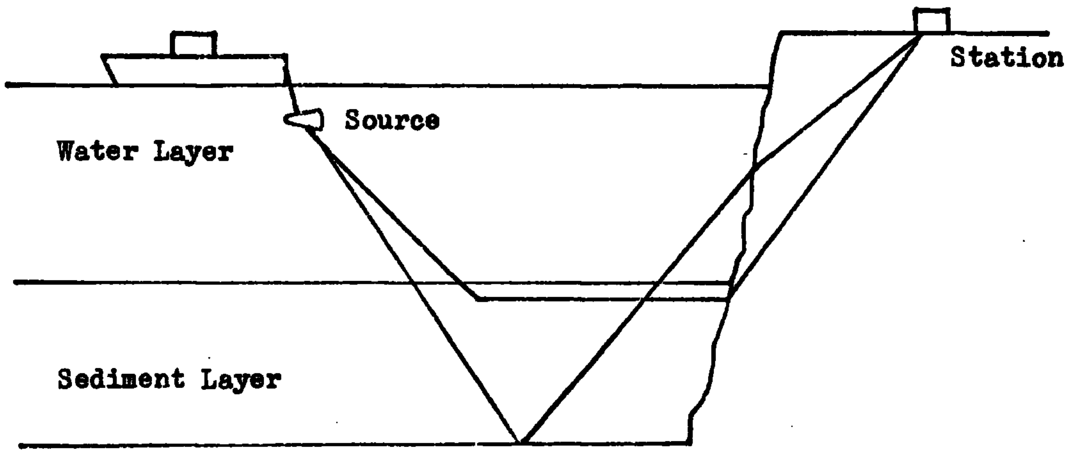

Fig. 1.3(a) Ship at Sea, Station on Land

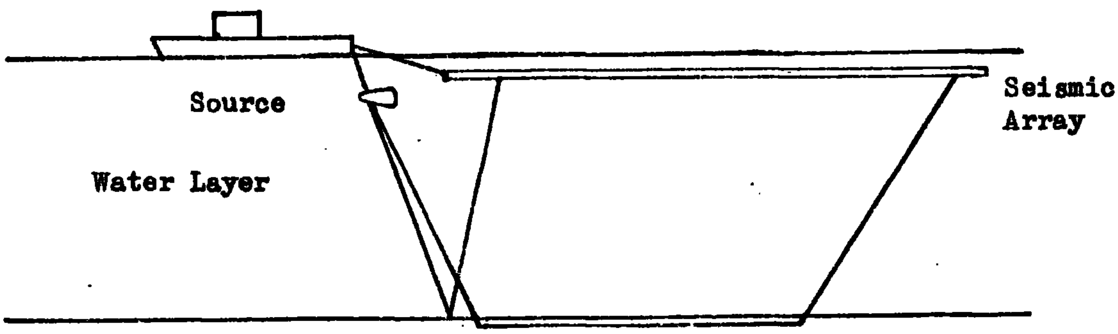

Fig. 1.3(b) Towed Array/Hydrophone

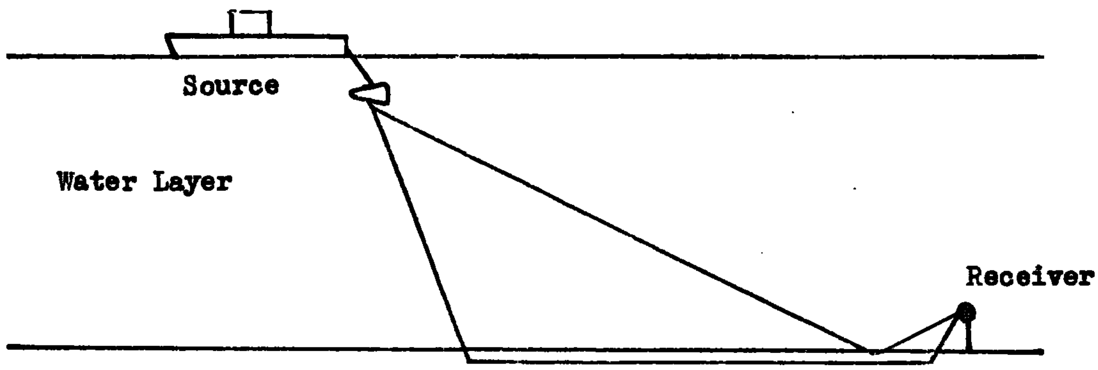

Fig. 1.3(c) **Bottom Mounted System**

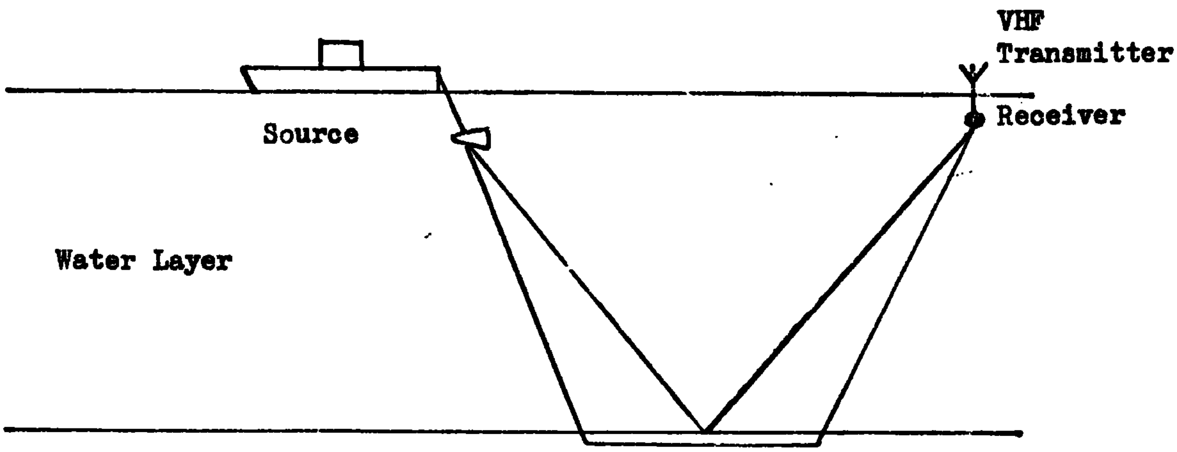

Fig. 1.3(d) **Free Floating Sonobuoy System**

towing ship and presenting somewhat of a hazard to shipping in the area, a limitation which affects all marine systems to a greater or lesser extent.

c) Bottom Systems (Fig. 1.3c).

The immediate advantage of this type of system is that it is remote from interference by man or surface weather conditions (Ref. 1.5). According to Wenz, (Ref. 1.6), the r.m.s. noise levels obtained in a typical bottom environment are of the order of 6dB less than shallow water noise levels (Fig. 1.4).

The bottom mounted system is simply lowered over the side of the ship and left weighted, on the bottom until the particular experiment has been completed, whereupon an acoustic release mechanism is activated allowing the instrument to rise to the surface under its own buoyancy, having left the weight on the sea bed behind (Ref. 1.7). This would seem to be the ideal solution to the situation to be investigated, at first sight, but on consideration there are several drawbacks, primarily the cost of the pressure housing, which is exorbitantly expensive. This, coupled with the fact that the areas to be examined are in fishing grounds, where the loss rate of scientific equipment in general is high, decided against this technique.

d) Moored/Free Floating Sonobuoys (Fig. 1.3d).

Following the successful use of disposable free floating sonobuoys by various researchers (Ref. 1.8), it was found (Ref. 1.9) that given adequate decoupling of the hydrophone from surface motion and reasonable sea states, the noise levels encountered are not significantly worse than those obtained using bottom systems (Ref. 1.10).

One particular advantage of this system is the relative ease of development and recovery of the buoy, the techniques of Dhan Buoy handling for oceanographic purposes being well established. The free

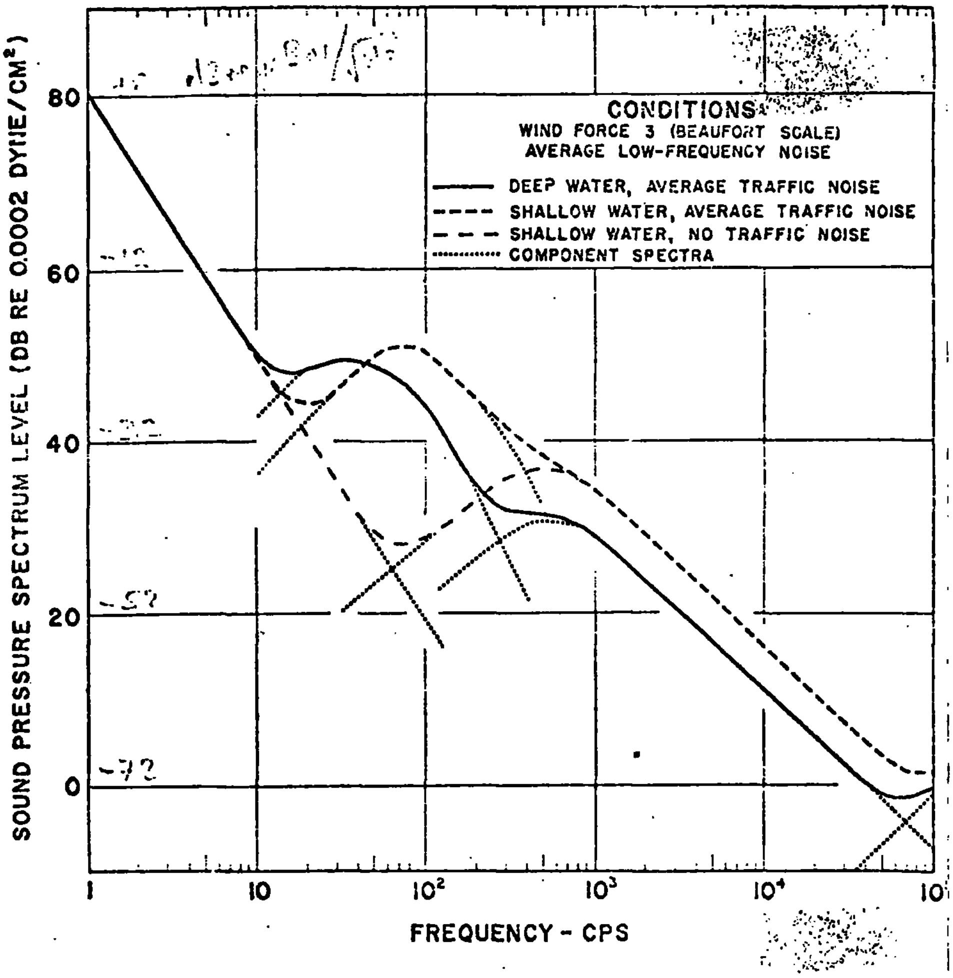

Fig. 1.4 Ambient Noise Spectrum

floating hydrophone should have a better signal to noise ratio but may present somewhat of a danger to shipping, whilst both options run the risk of being 'acquired' by fishing trawlers, either intentionally or by being accidentally caught in the nets. By attaching the buoy to a moored Dhan buoy, with its standard radar reflector, the problem of relocation would be eased but the flow noise is likely to be higher.

This final system was the one decided upon having taken cost, feasibility and fitting in with other departmental research programmes into consideration.

System Requirements

i) large dynamic range;

ii) large geographical range;

iii) low power consumption;

iv) physical reliability.

i) Dynamic Range.

The dynamic range of the system must be sufficient to cope with the large variation in signal strength encountered by such a system. At close ranges from the ship, the amount of reflected and directly received energy is large and both the hydrophone and amplifiers must be able to deal with this, whilst still being sufficiently sensitive to be able to detect the lower energy longer range refracted arrivals.

A wide band hydrophone is also required since at close range, there is a large high frequency content in the received signal, whilst at greater distances the dominant frequency shifts to the lower end of the frequency spectrum. Similar considerations apply to the amplifier.

In order to carry out digital processing on the received data, a dynamic range of at least 86dB is necessary for reflection work, or 60dB for refraction results (Ref. 1.11), which automatically necessitates the use of digital recording, since at the very best an F.M. recording system, incorporating flutter compensation can achieve 55-60dB of dynamic range.

ii) Geographical Range.

At close separations of ship and buoy the combination of large signal amplitude and good radio contact with the buoy is sufficient to allow the use of an F.M. link (Ref. 1.12). The analogue signal is frequency modulated onto a carrier which is telemetered back to the ship for recording on F.M. tape. This improves the range of the buoy since the internal tape unit envisaged (see Chapter II) need only begin operation once the F.M. signal falls below an acceptable level. The range limitation is then imposed by the length of running time available on the recorder itself and the seismic source utilised. When recording digitally, the maximum packing density acceptable is of the order of 1000 bits per inch, which for moderate digitisation rates implies that a tape speed of at least 1"/sec. must be used. For a standard 3600' tape, this gives an operating time of 12 hours continuously, representing a ship travel distance of approximately 72 nautical miles, at the standard towing speed of 6 knots.

This may not be sufficient, if large scale refraction work is to be undertaken, and so, to increase the system range, intermittent operation of the tape deck is necessary. For long range work, also, the standard "air-gun" system (Ref. 1.13) does not have sufficient power to provide significant amplitude levels and hence an explosive source is normally used, which can only be detonated at certain definite intervals. By arranging that the tape unit is on for, say 6 minutes, in every half hour, after five hours of continuous operation, the system range is increased to 280 nautical miles.

These figures represent the maximum attainable and are dependent on tape speed. If a speed of 1.5"/second is used the range falls to 180n.m. approximately, which is still sufficient for refraction studies.

iii) Power Consumption.

In order to allow the system to operate for long periods of time, power consumption must be kept to a minimum. M.O.S. (Metal Oxide Silicon) Logic provides digital circuitry in robust packages with low power consumption and high noise immunity. Hence, it was decided to use as much MOS logic as possible in the sonobuoy. Rechargeable nickel-cadmium cells provide the greatest power to weight ratio but are prohibitively expensive, so that the non-spill lead acid batteries commonly used in motorcycles and small boats were chosen.

iv) Physical Considerations.

The physical environment in which the system is to operate decides the design of the sonobuoy to a great extent.

The buoy must be such that it is not easily damaged, either by mishandling during launch or re-acquisition, or by heavy seas that it might encounter. At the same time, it must be sufficiently light to allow ease of handling, and the compromise solution is to use a glass reinforced plastic (G.R.P.) body which is ribbed vertically, to provide protection during handling and strength to withstand wave bombardment.

By using well tested peripheral equipment, flashing light for recovery, hydrophone, the reliability of the system is increased without excessive cost, so these items were bought in.

Mathematical Analysis

The problems of reflection and refraction of elastic waves in a layered medium have been extensively studies in the past, notably by Cagniard(Ref. 1.14), Rayleigh (Ref. 1.15), Lamb (Ref. 1.16), Sommerfeld (Ref. 1.17), Smirnov and Sobolev (Ref. 1.18), Spencer (Ref. 1.19), Pekeris (Ref. 1.20), Petrashen (Ref. 1.21) and Sherwood (Ref. 1.22).

Given the two layer situation which is the simplest to consider, and that most extensively studied, in trying to obtain the amplitude of the reflected wave for all angles of incidence, the first approach is to examine the behaviour of plane waves.

Since the original papers by Zoeppritz (Ref. 1.23) and Knott (Ref. 1.24), numerous authors have developed and published various forms of Zoeppritz' amplitude and Knott's energy equation (Ref. 1.25 - 1.37), with some confusion as to the computation and physical interpretation of these equations, due to differing notation and nomenclature (Ref. 1.38).

The plane wave is, however, not sufficient to cope with the problems of wide angle reflections (Ref. 1.39) but it is extremely useful in developing some insight into the problem and in providing some concepts which simplify the exposition of the behaviour of the more complicated spherical waveform used subsequently.

The spherical wave has been analysed by several authors, and the work detailed in Chapter III follows on from that undertaken by Brekoskikh (Ref. 1.40), Cerveny (Ref. 1.41) and others based on the theoretical development of spherical wave analysis, to suit the particular requirements of the marine survey described above, by introducing a different approximation in the method of steepest descents, leading to a new solution.

Data Processing

Once the data has been obtained using the sonobuoy described and disposable sonobuoys where time considerations do not permit a return to locate and recover the re-useable buoy, the question of data analysis arises and in particular the level of sophistication necessary in the first instance, to obtain experimental results which may be compared with theoretical predictions.

As the behaviour of the waves at wide angles is not well defined, the most obvious method is to approach the data in the simplest way consistent with obtaining valid results to compare theory and experiment.

Once the existence of some agreement between the two has been proven, the next stage is to increase the complexity of the data processing techniques. Clearly, signal enhancement procedures, deconvolution, filtering, improve the quality of the results, but it must be borne in mind the considerable amount of time and effort involved in producing such results on the equipment available. Thus, before this time consuming step is undertaken, an initial amplitude analysis will be performed using simple high cut filtering to remove unwanted noise, and linear interpolation for signal recovery.

CHAPTER TWO

INTRODUCTION

The DIGitally REcording Sonobuoy System (DIGRESS) comprises a digital tape recorder and an F.M. transmitter, for close range work, housed in a Glass Reinforced Plastic body, (Fig. 2.1). A block diagram of the complete system is given in Fig. 2.2. The electronics inside the buoy consists of two main parts; the record electronics and a timing unit. The record electronics converts the analogue hydrophone input signal into digital form which is then recorded on $\frac{1}{4}$" magnetic tape, together with time information. The timing unit provides both a binary coded decimal (BCD) time code for writing onto tape and a facility for remote (programmable) intermittent operation of the tape deck.

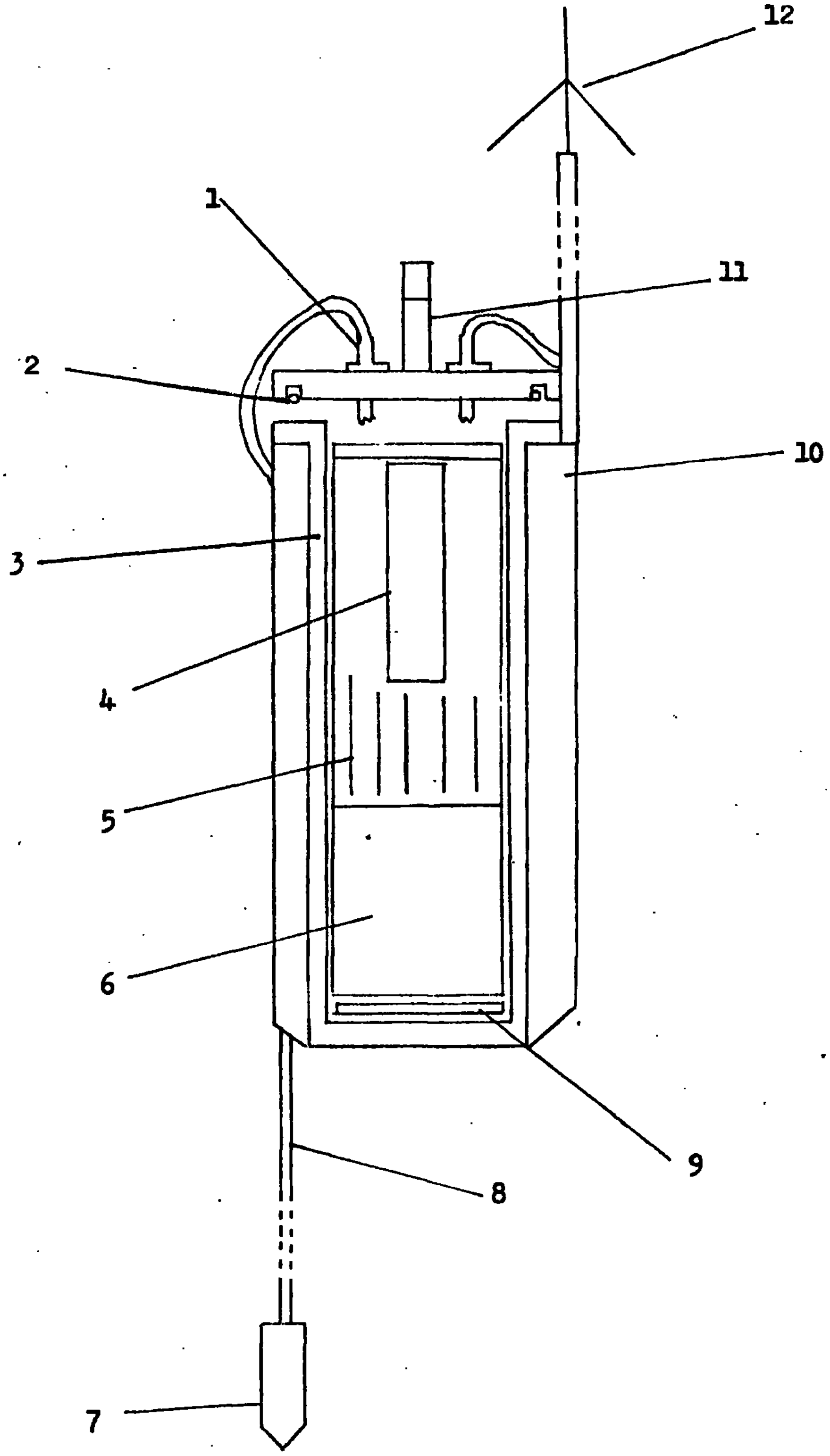

Fig. 2.1 **Lateral View of Sonobuoy**

Key

1	-	Boston Insulated'Watertite'Connector
2	-	'0'-ring seal
3	-	GRP Outer Case
4	-	Vertically Mounted Tape Transport Unit
5	-	Electronic Boards
6	-	Battery Housing
7	-	Hydrophone
8	-	Hydrophone Cable
9	-	Floatation Adjusting Weights
10	-	GRP Strengthening Rib
11	-	Flashing Light
12	-	Transmitter Aerial

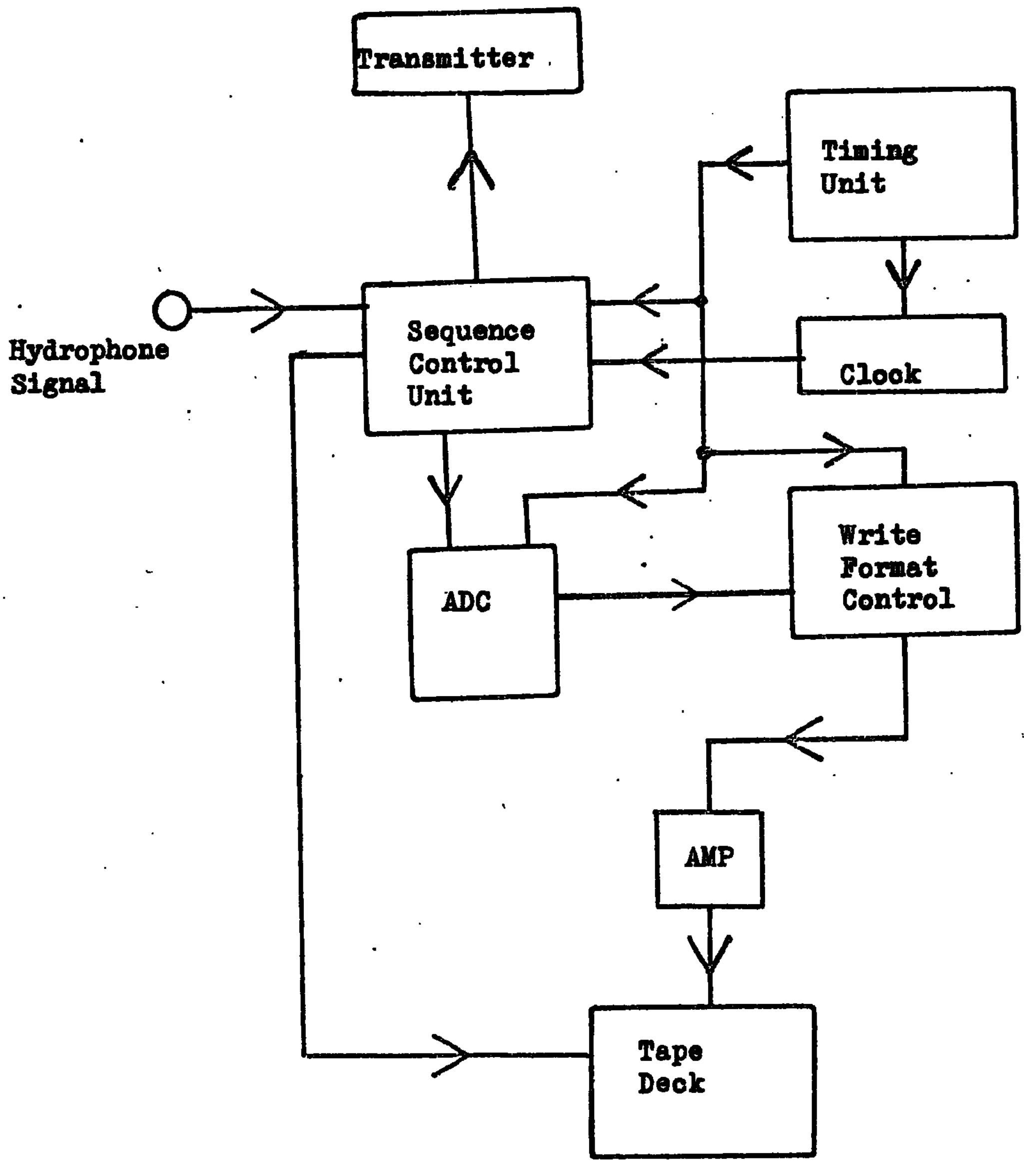

Fig. 2.2 **Block Diagram of Digress System**

GENERAL DESCRIPTION

DIGRESS ELECTRONICS

The DIGRESS electronics are contained in a cylindrical aluminium container which fits exactly inside the GRP body. Fig. 2.2 shows the complete system.

The uppermost surface of the GRP body is detachable, allowing removal of the internal housing, while O ring seals in a recessed groove inside the lid maintain a watertight seal. Electrical connections between the internal electronics and the external fittings are made through Boston Insulated connectors.

The hydrophone unit is deployed beneath the buoy, according to the arrangement shown in Fig. 2.6, with the hydrophone suspended neutrally at the end of a system of 'bites' which decouple the hydrophone from the surface motion of the instrument housing.

ELECTRICAL

RECORD

The output from the Mark Products P.27 Hydrophone (Ref. 2.1) is fed to an analogue to digital converter and gain control unit. The digital information is arranged into the chosen format on the WRITE board and written onto ¼" tape using an 8-track head.

The 5 MHz output from an SEI Type 512704 Quartz Crystal Oscillator is counted down by a frequency divider circuit to produce both control signals to operate the tape recorder cycling, and clock timing signals (Fig. 2.4).

Stabilised supplies for all the electronics are provided by the ±15V, +5V stabilised power supplies.

TIMING UNIT

As well as providing clock pulses this unit also supplies time signals for remote programmable operation of the tape recorder (Fig. 2.5).

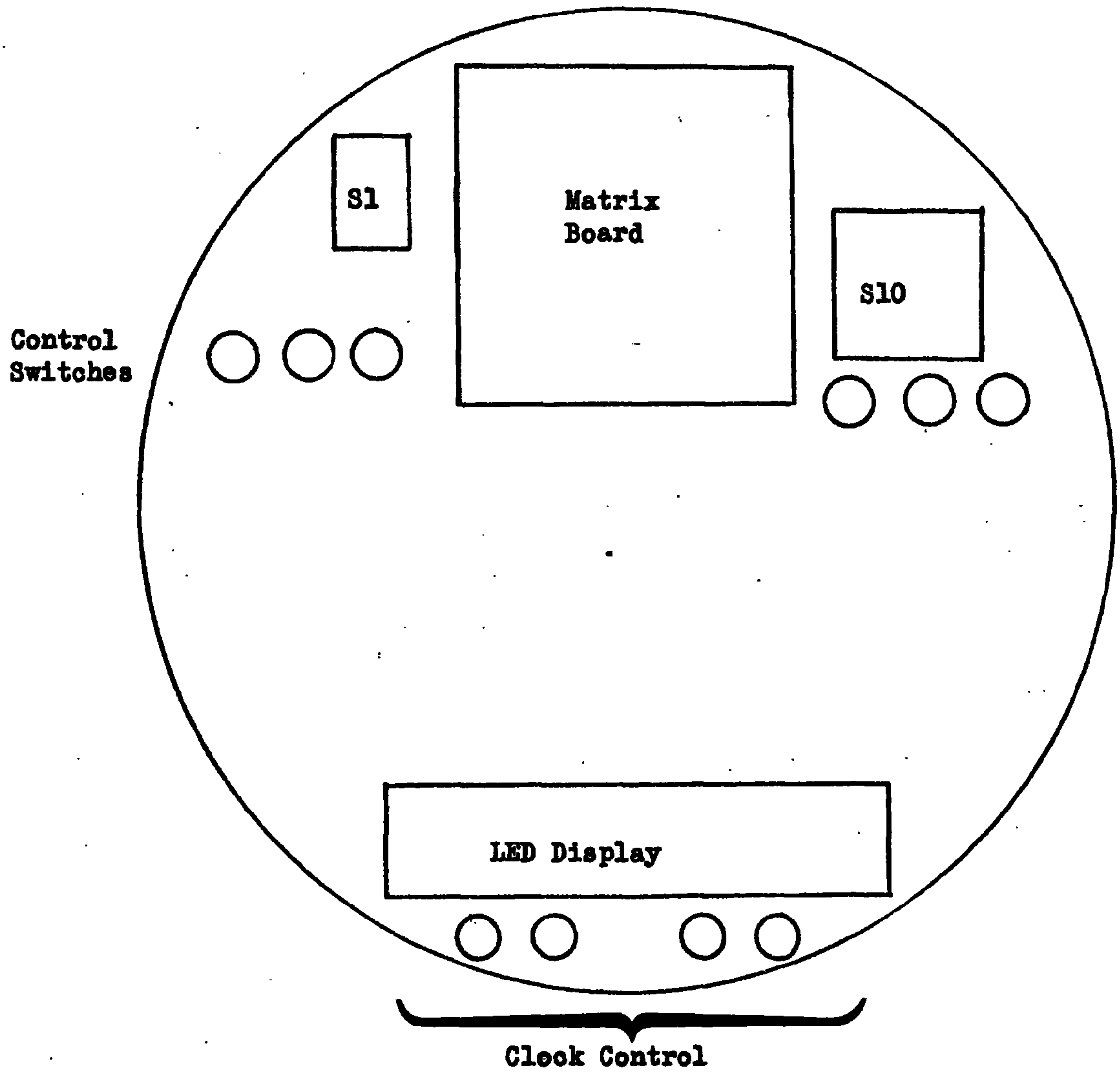

Fig. 2.3 Top View of Internal Housing

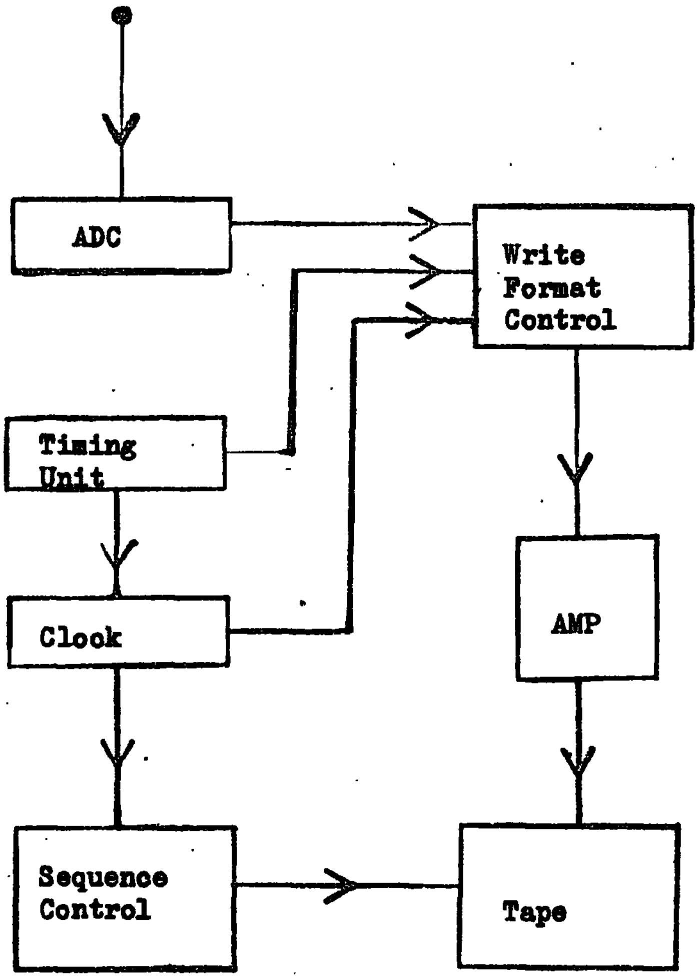

Fig. 2.4 Record Electronics

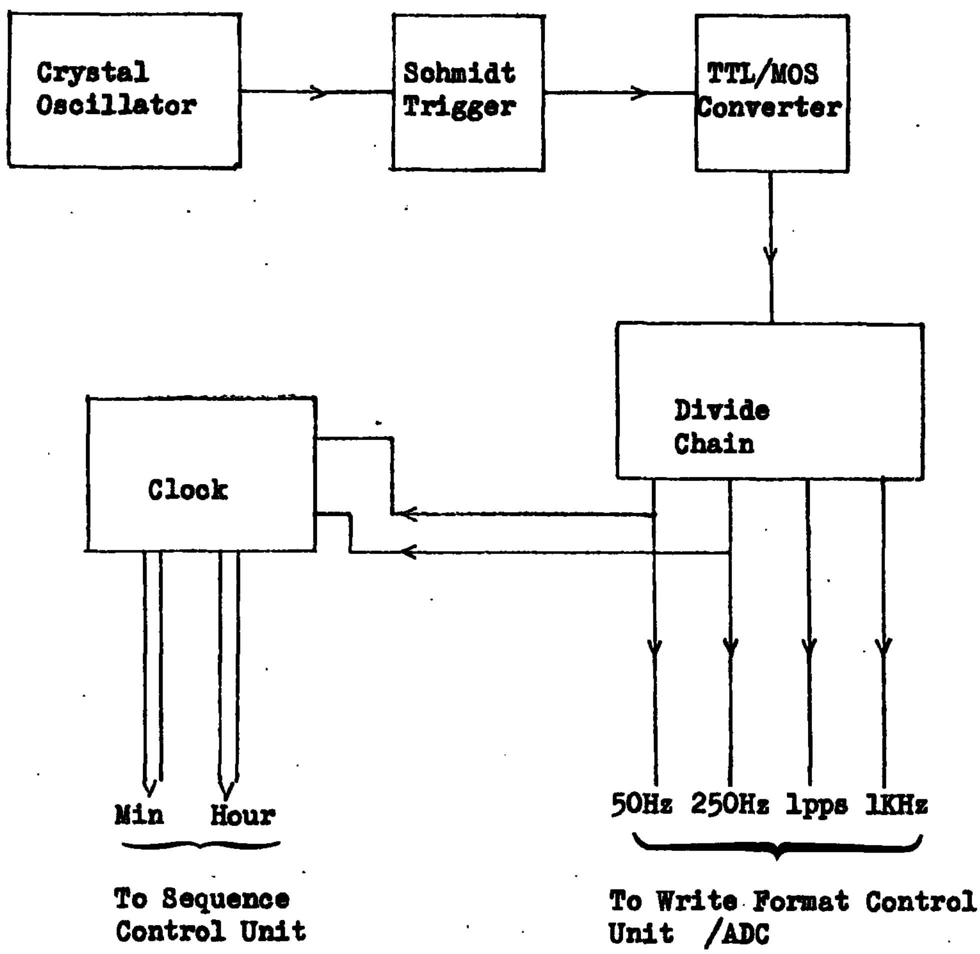

Fig. 2.5 **Timing Electronics**

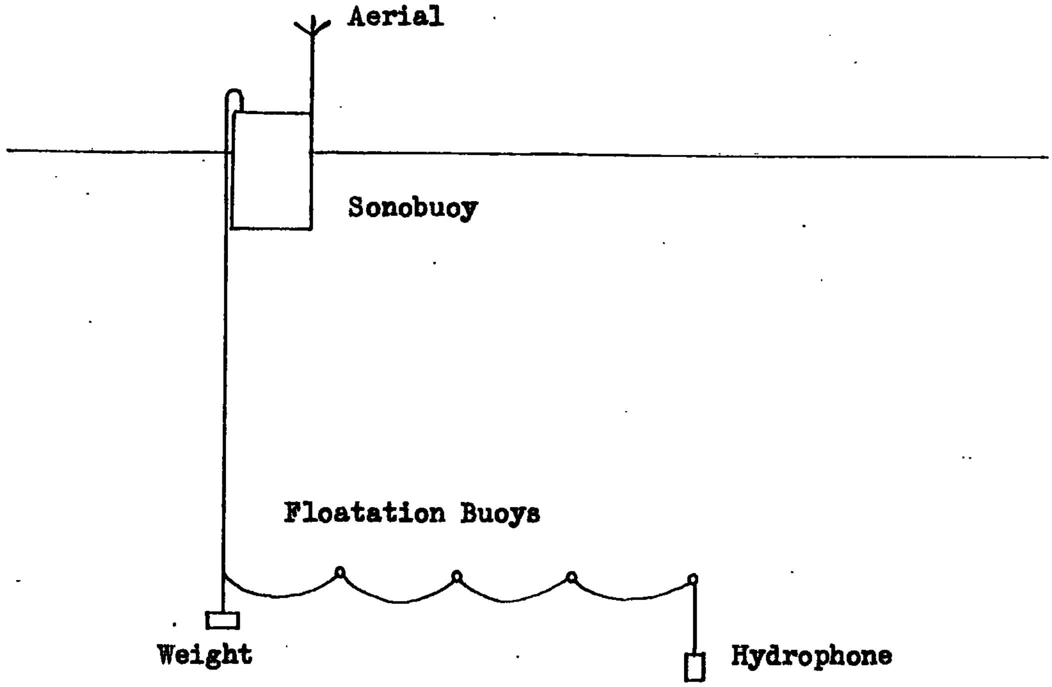

Fig. 2.6 Hydrophone Deployment

The system can function in any of the following modes:

i) transmitter only,

this is for short range work only;

ii) transmitter, then tape,

tape either intermittent (preselected) or continuously;

iii) tape only,

as above;

iv) tape only,

in a repetitive 1 hour cycle.

There is also an option of up to nine hours delay before allowing commencement of any of the above operating modes.

CIRCUIT DESCRIPTION

RECORD ELECTRONICS

HYDROPHONE

The seismic hydrophone is a Mark Products P-27 low frequency deep water hydrophone, consisting of a piezo electric ceramic element, a current amplifier and a rechargeable Nickel-Cadmium cell.

The output impedance of the hydrophone is $50\,\Omega$, and the sensitivity a standard temperature and pressure is $30\mu V/\mu bar$. A schematic diagram is given in Fig. 2.7. The hydrophone was chosen because it exhibited an extremely flat wide band response (Fig. 2.8) combined with high sensitivity, together with long operating time at low current levels.

STABILISED SUPPLIES

The +15V stabiliser (Fig. 2.9) is contained on the Matrix timing board and provides a +15V supply line from an 18.4 - 24V unstabilised battery source. The circuit incorporates an SGS L123 precision voltage regulator with an external BUY24 power transistor to increase the output current. The L123 comprises a temperature compensated reference amplifier, an error amplifier, a power series pass transistor and current limiting circuitry. The advantages of this particular device are that it has:

i) a low standby current;

ii) low temperature drift; typically $0.003\%/^{\circ}C$ $0^{\circ}C \leq T \leq 70^{\circ}C$;

iii) high ripple rejection,

the output power transistor increases the current output to 1 Amp.

The -15V stabilised supply (Fig. 2.10) is achieved using a second SGS L123 with an external BFX 39 output transistor. The -15V line is generated from a -18.4 to -24V unregulated battery supply.

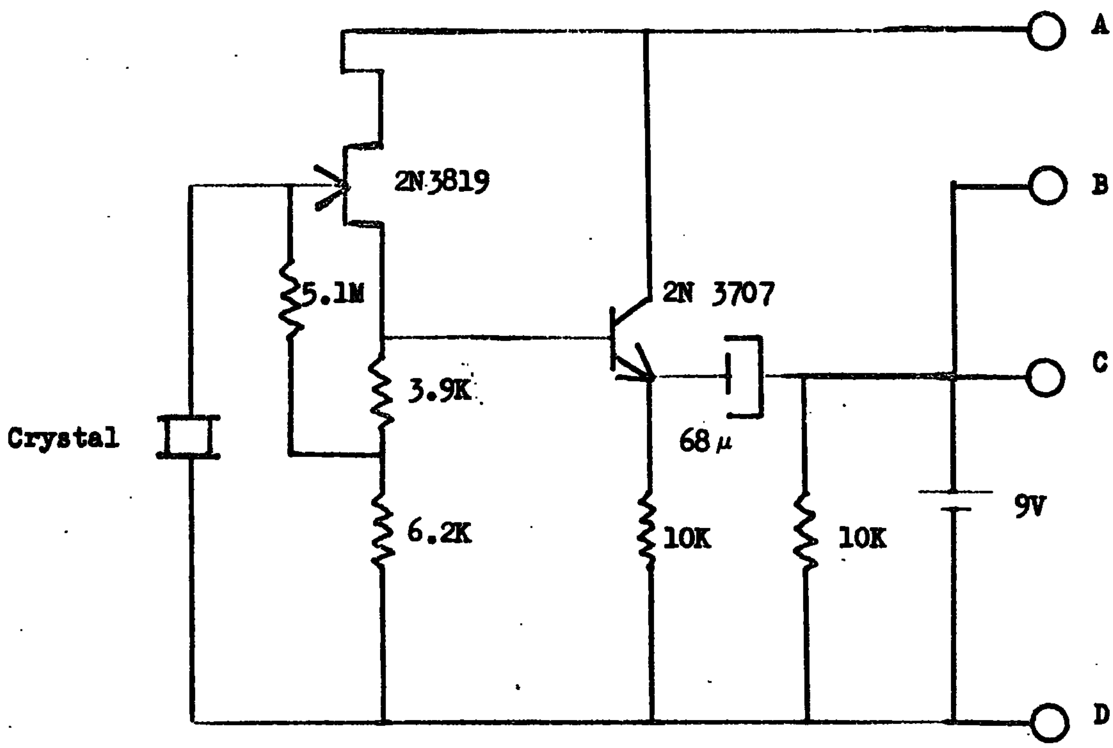

All Resistors ½W -5%

Fig. 2.7 Hydrophone Electronics

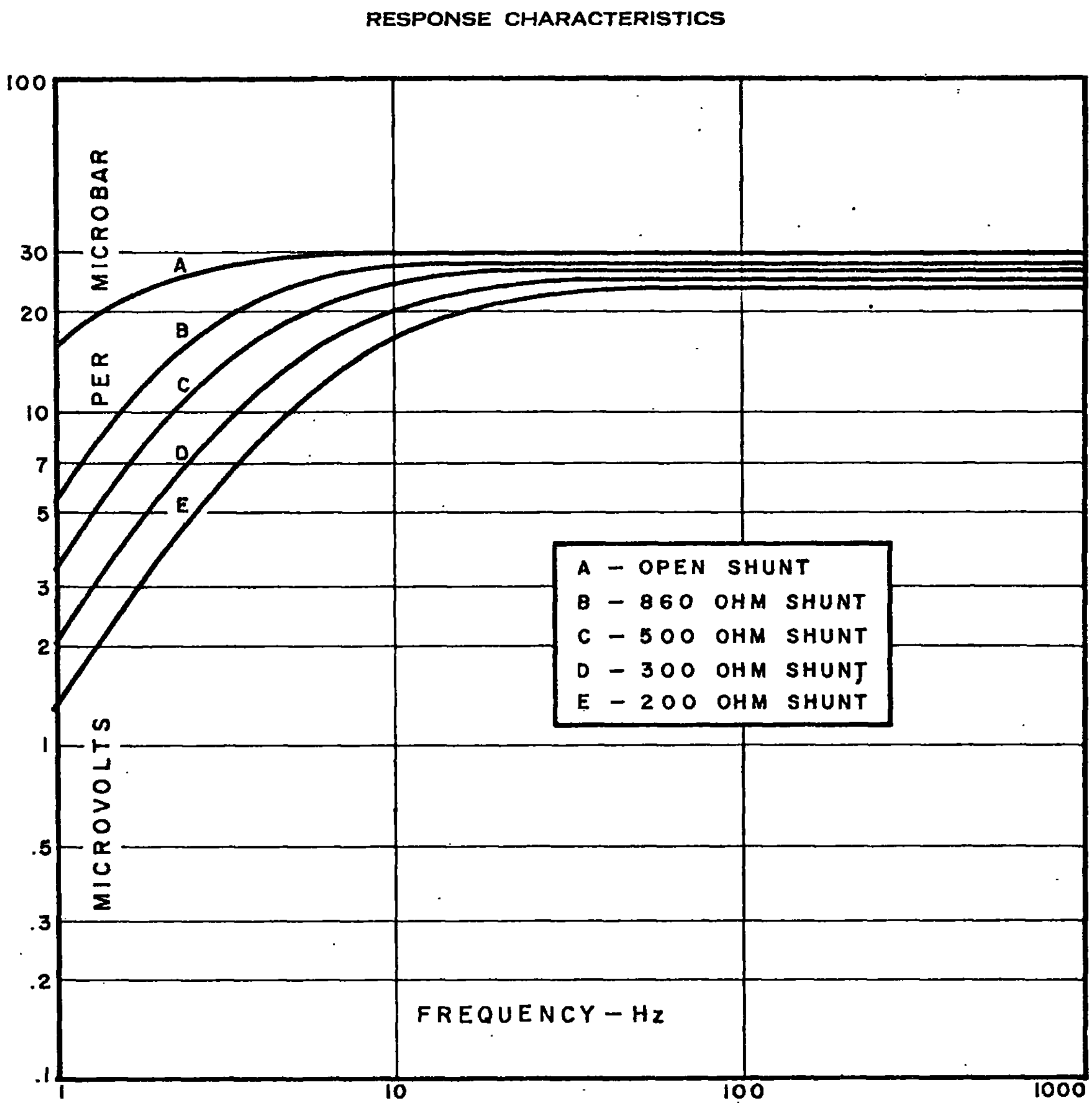

Fig. 2.8 **Hydrophone Frequency Response**

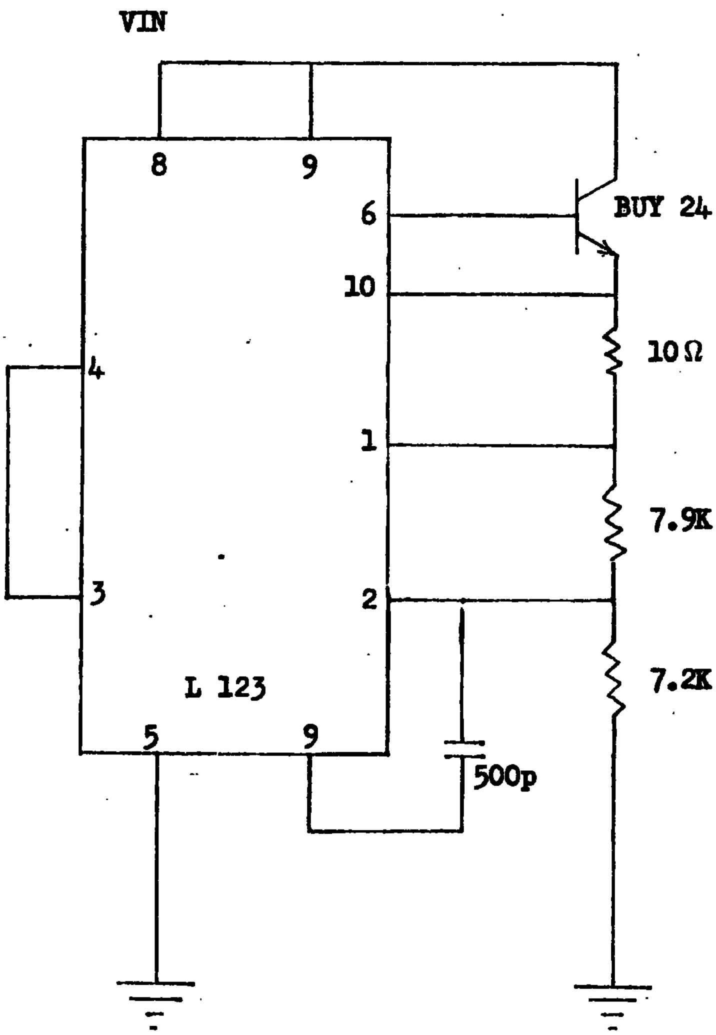

Fig. 2.9 +15V Regulator

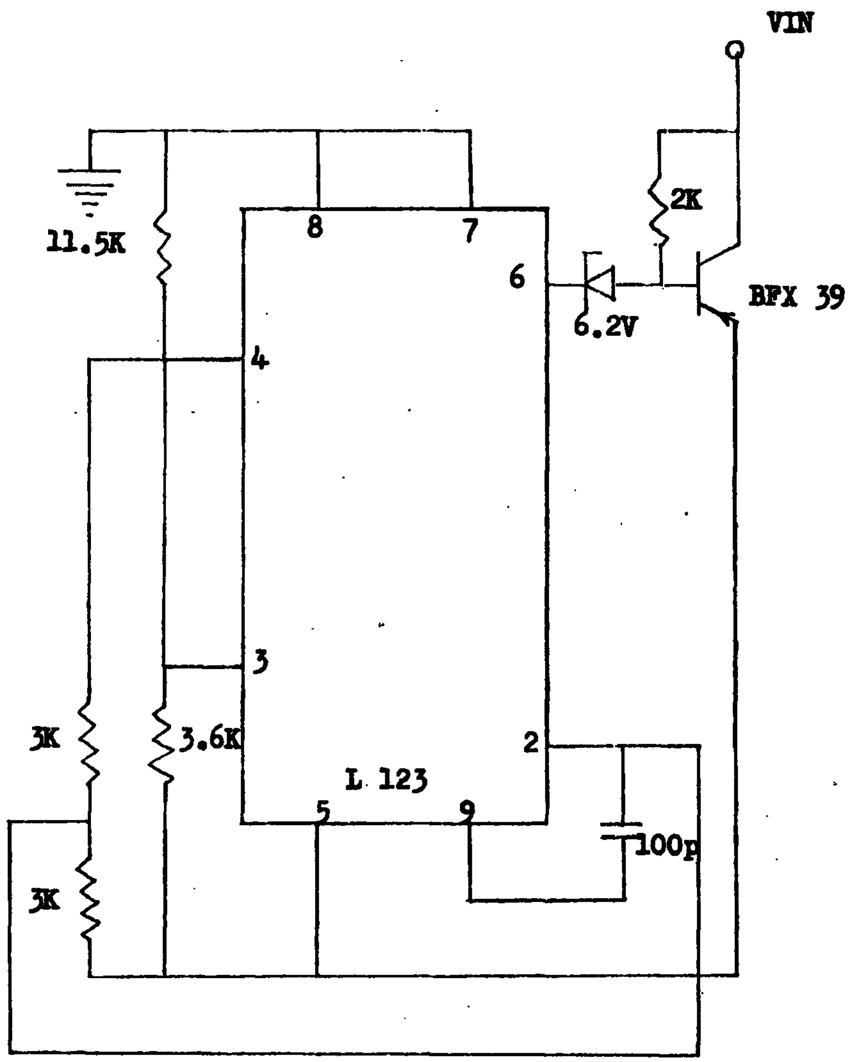

Fig. 2.10 **-15V Regulator**

ANALOGUE TO DIGITAL CONVERTER AND GAIN CONTROL (Ref. 2.2)

The analogue input signal fed through a binary gain switching board (Fig. 2.13) incorporating fast comparator circuits, to a BURR BROWN 12-bit Analogue/Digital Converter.

The gain of the system is set using the L.E.D's mounted on the top panel of the board (Fig. 2.12) as an indication of saturation and the rotary preset gain control potentiometer. The automatic binary gain switching (3 bits) increases the effective dynamic range of the converter to 90 dB.

To ensure that the response of the ADC system was linear considerable care was taken in the initial gain setting of the component amplifiers whose gains were adjusted by means of trimming resistors (see inset Fig. 2.12).

CRYSTAL OSCILLATOR

The fundamental clock frequency of 5MHz is generated by the SEI crystal oscillator, the output of which is amplified by VTI and fed to the TTL divide by five chain comprosing R1, R2 and IC1 to give 1 MHz input to the subsequent MOS logic (Fig. 2.14). The 1 MHz signal is used as an input to a Schmidt trigger (IC2) and pulled up to a +15V positive logic level using R3.

The crystal frequency is continually counted down to 1k Hz at the output of IC5, by IC3 and IC4. IC6 produces a 100 Hz output to IC7, which reduces this via IC8 and IC9 to provide 50 Hz and 1 Hz outputs. IC10 provides a 250 Hz signal from the kilohertz input. All the output frequencies are synchronous.

CLOCK

The basis of the clock unit is a National Semiconductor MM5311 D.I.L. clock (Fig. 2.15). The 50 Hz signal from IC7 is fed to an

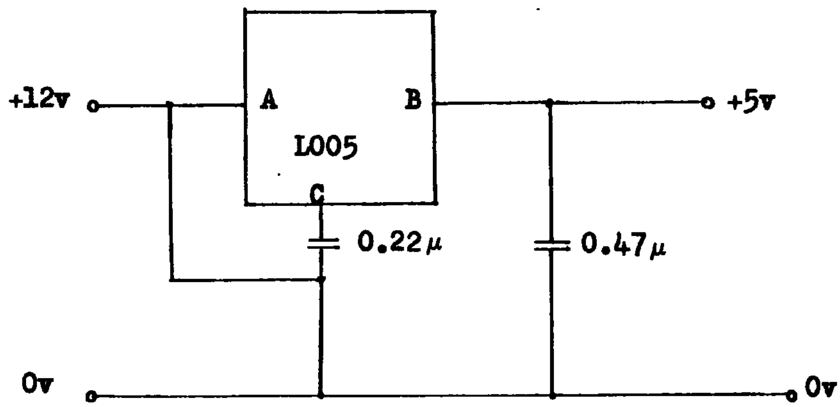

Fig. 2.11 +5v Regulated Supply

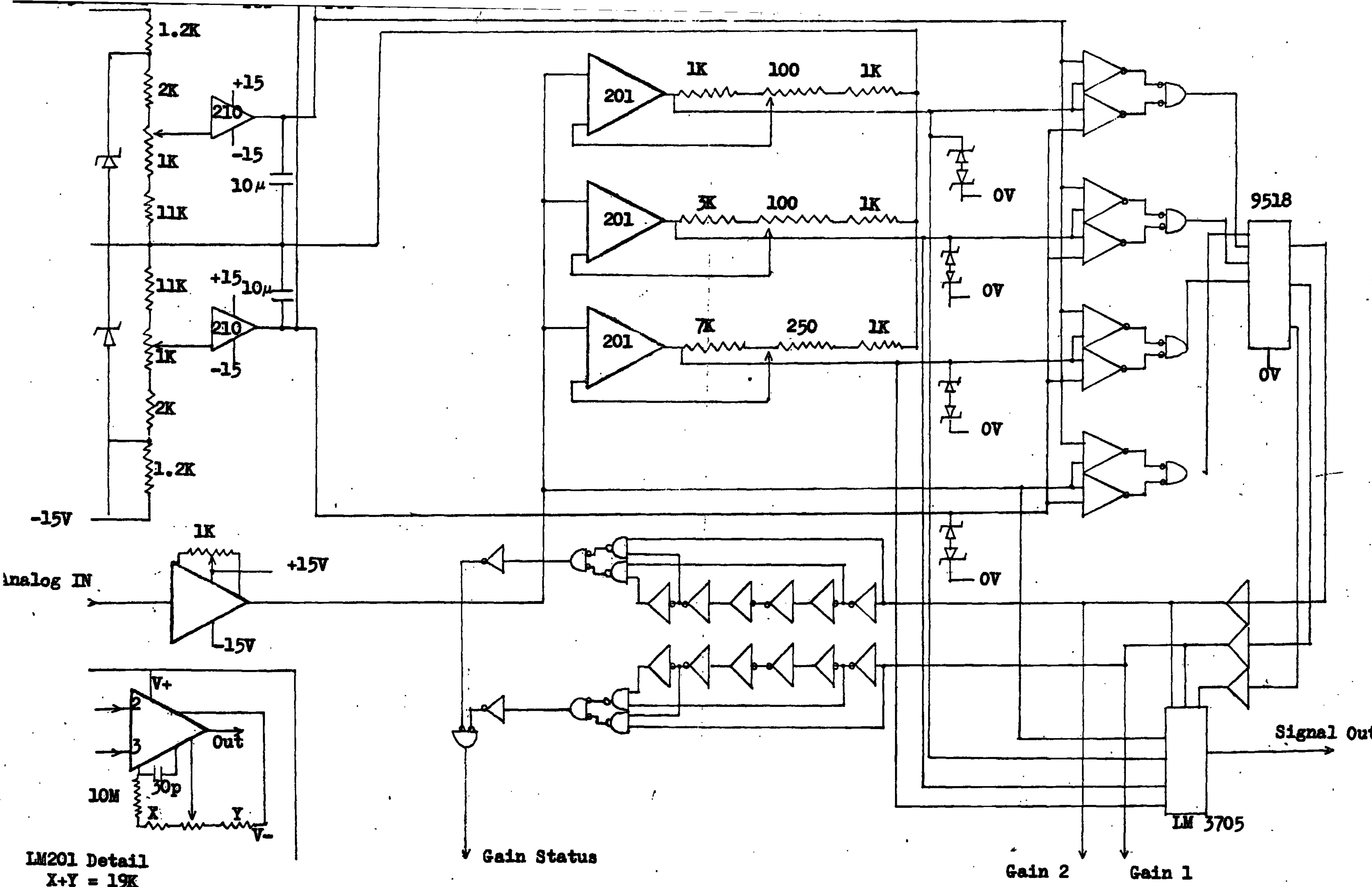

Fig. 2.12 **Gain Ranging Board**

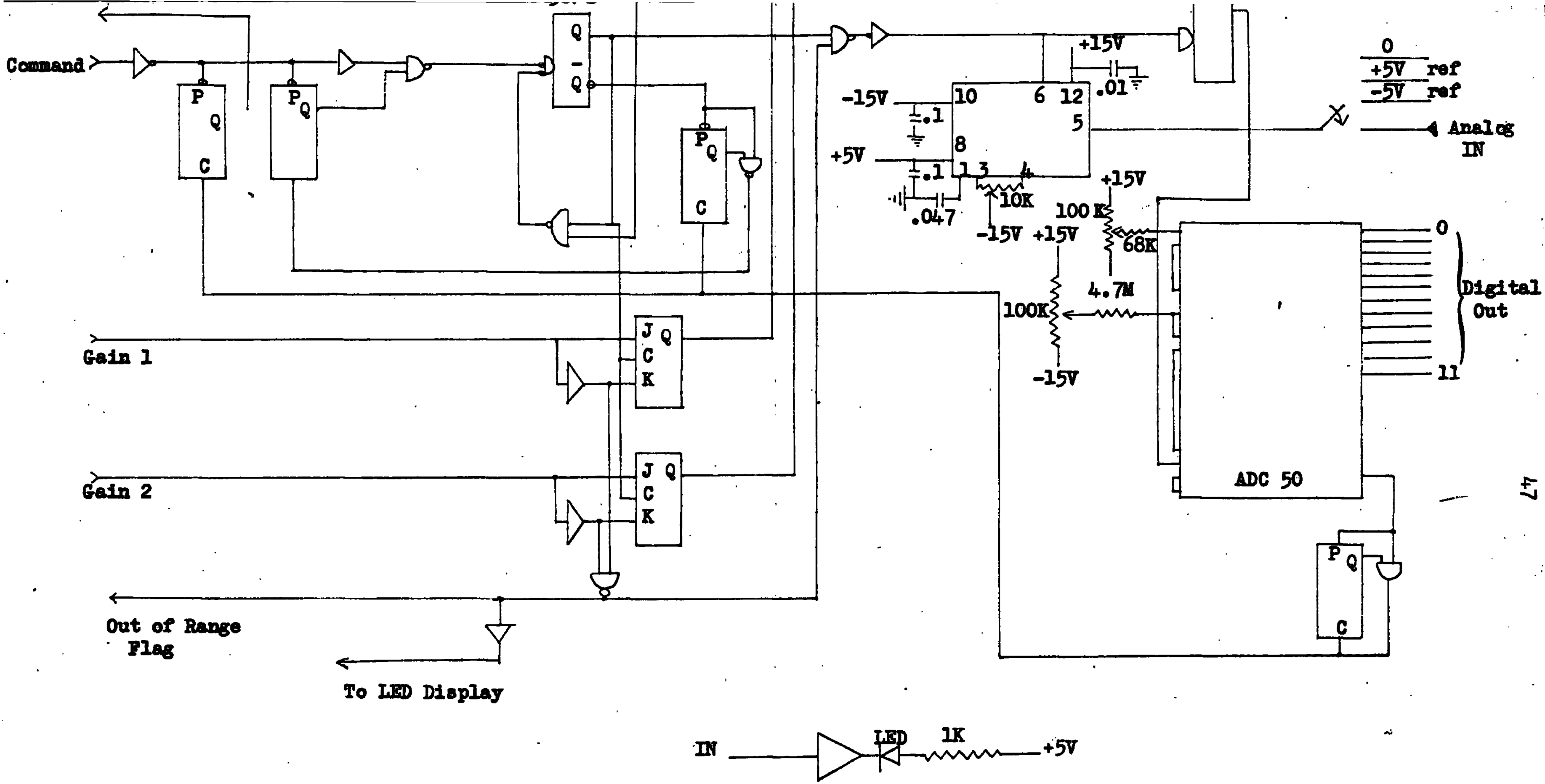

Fig. 2.13 ADC Board

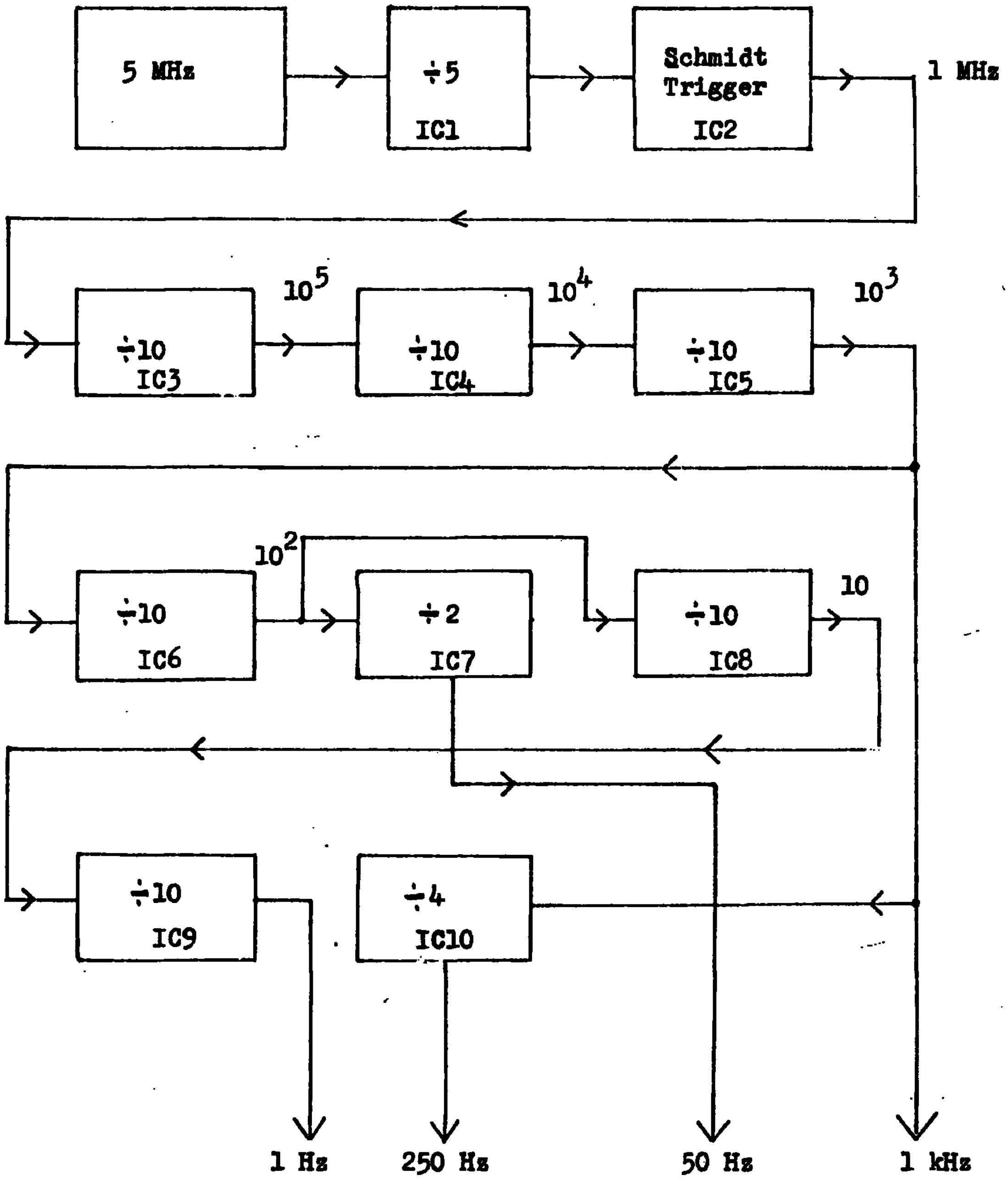

Fig. 2.14 Schematic Diagram of Crystal Oscillator Board

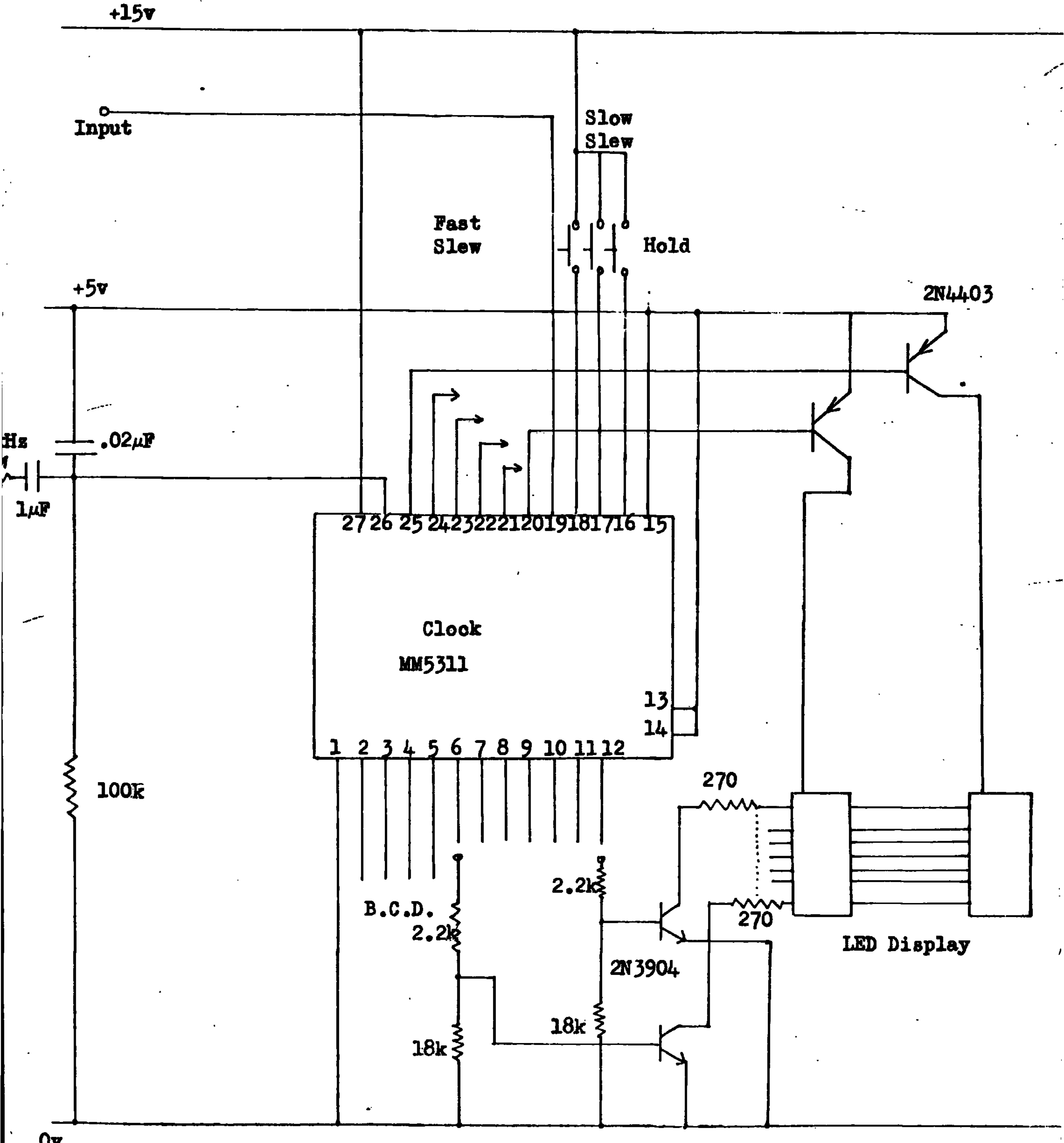

Fig. 2.15 **Clock Circuit**

internal Schmidt trigger shaping circuit which provides approximately 5 volts of hysteresis. The shaper output drives a function chain which performs the time keeping functions.

Both fast and slow setting inputs, as well as a hold input are provided. Internal 20K pull up resistors provide the normal time keeping function. Switching any of the inputs to VDD (ground) results in the desired time setting function.

The three gates in the counter chain (Fig. 2.16) are used for time setting. During normal operation gate A connects the shaper output to a prescale counter (÷50); gates B and C cascade the remaining counters. Gate A is used to inhibit the input to the counters for the duration of a slow, fast or hold time setting input activity. Gate B is used to connect the shaper output directly to a seconds (÷60) counter - the condition for slow slew. Similarly gate C connects the shaper output to a minutes counter (÷60) for fast slew.

Fast slew advances the hours information at one hour/second, slow slew the minute information at one minute/second.

The seconds, minutes and hours counters continuously reflect the time of day. Outputs from each counter (indicative of both units and tens of seconds, minutes and hours) are time division multiplexed to provide digit sequential access to the time data. The multiplexer is addressed by a multiplex divider decoder driven by a multiplex oscillator. This multiplex element is itself driven through a variable 1-k preset, and a 1μF capacitor at 250 Hz, (Fig. 2.15).

The preset is necessary to prevent the clock from going into oscillation, which occurs when the 250 Hz multiplex frequency is of the same amplitude as the 50 Hz clock driving signal. The preset is adjusted so that oscillation does not occur, and is 8% down on its normal amplitude for stable operation.

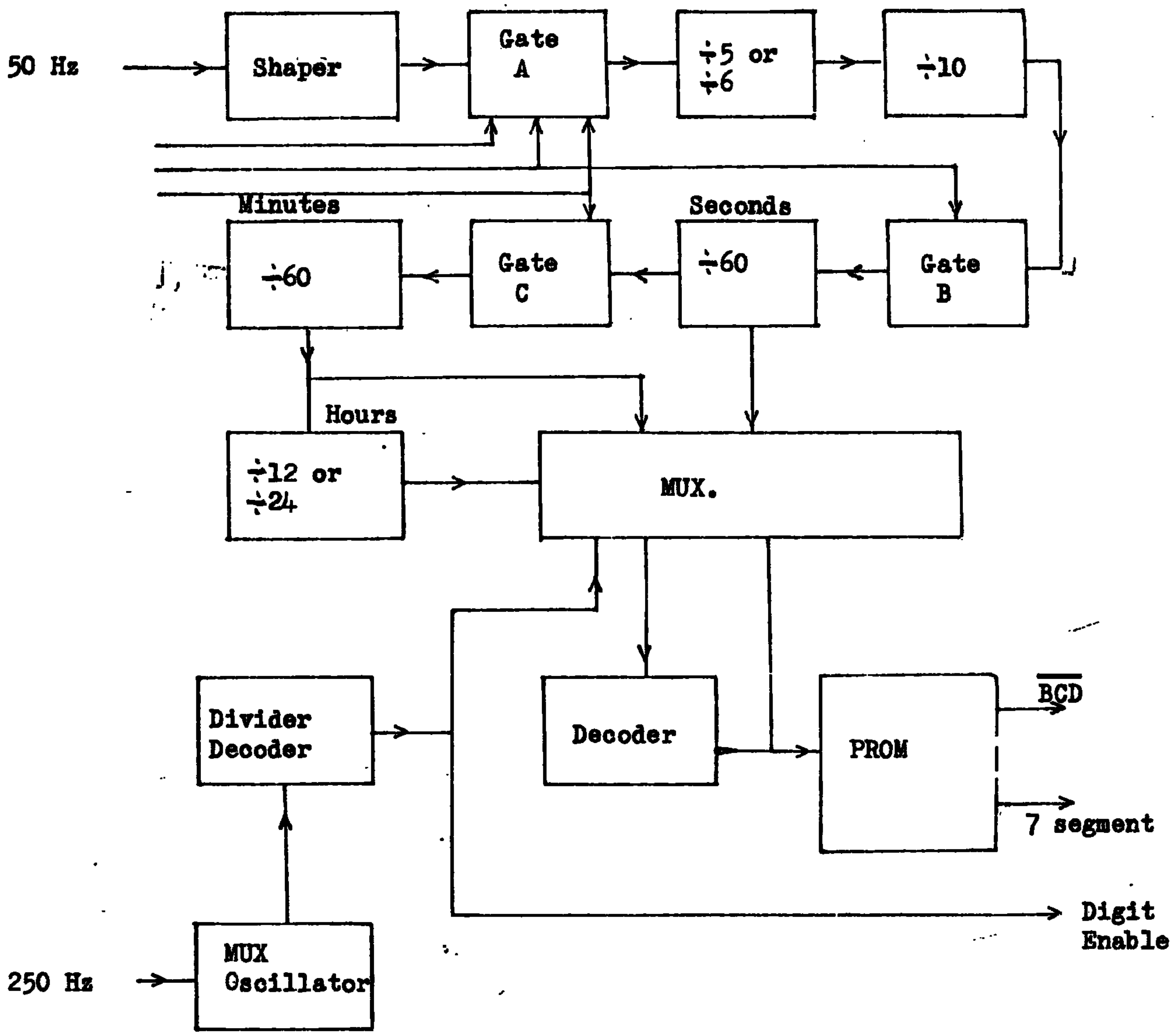

Fig. 2.16 Internal Clock Schematic

The multiplex addresses also become the display digit enable outputs, which are hence observed at 250/6 Hz, i.e. approximately 40 Hz which is just sufficient for flickerless viewing. The multiplex outputs are applied to a decoder which, in turn, is used to address a PROM. This PROM generates the final output codes - $\overline{\text{BCD}}$ and 7 segment. The sequential output is from unit seconds to tens of hours. The digit enable lines turn on the enabling transistors, (2N3904) and hence the L.E.D. display.

To ensure a good wave shape to the digit enable and inverse BCD outputs, for recording purposes, dropping resistors, R are wired in between output and ground. The positive logical voltage is dropped to 13.7 volts on the digit enable lines but this is still well within the MOS logic acceptance level (45% noise immunity).

The clock output goes to an L.E.D. display which is disconnected once the initial time setting operation is accomplished.

MATRIX TIMING CIRCUIT

This provides the pulses for timing the remote programmable operation of the tape transport system. The 1 Hz signal from IC9 is fed to IC12, a decade divider whose 0.1 output is divided by 36 using IC13 and 14, (Fig. 2.17), to give a pulse every 6 minutes. IC15 provides a decoded decade output of these 6 minute pulses.

The 6 minute outputs are fed through protection diodes to the first ten columns of the matrix board; column 1 corresponds to minutes zero to six, column 2 to M_{6-12} etc.

The carry out signal from IC15 (1 pulse/hour) is used to drive two sequential decade counters, HRST1 and HRST2 (IC16 and 17), which provide an hours count (Fig. 2.18). Each hour line output from IC16 and IC17 is connected to one input of an AND gate, the other input coming from a Row of the matrix board, i.e. hour line zero to one (H_{0-1}) is ANDed with matrix Row 1, H_{1-2} is ANDed with matrix Row 2 and so on down to H_{18-19} which is ANDed with matrix Row 19, (Fig. 2.18).

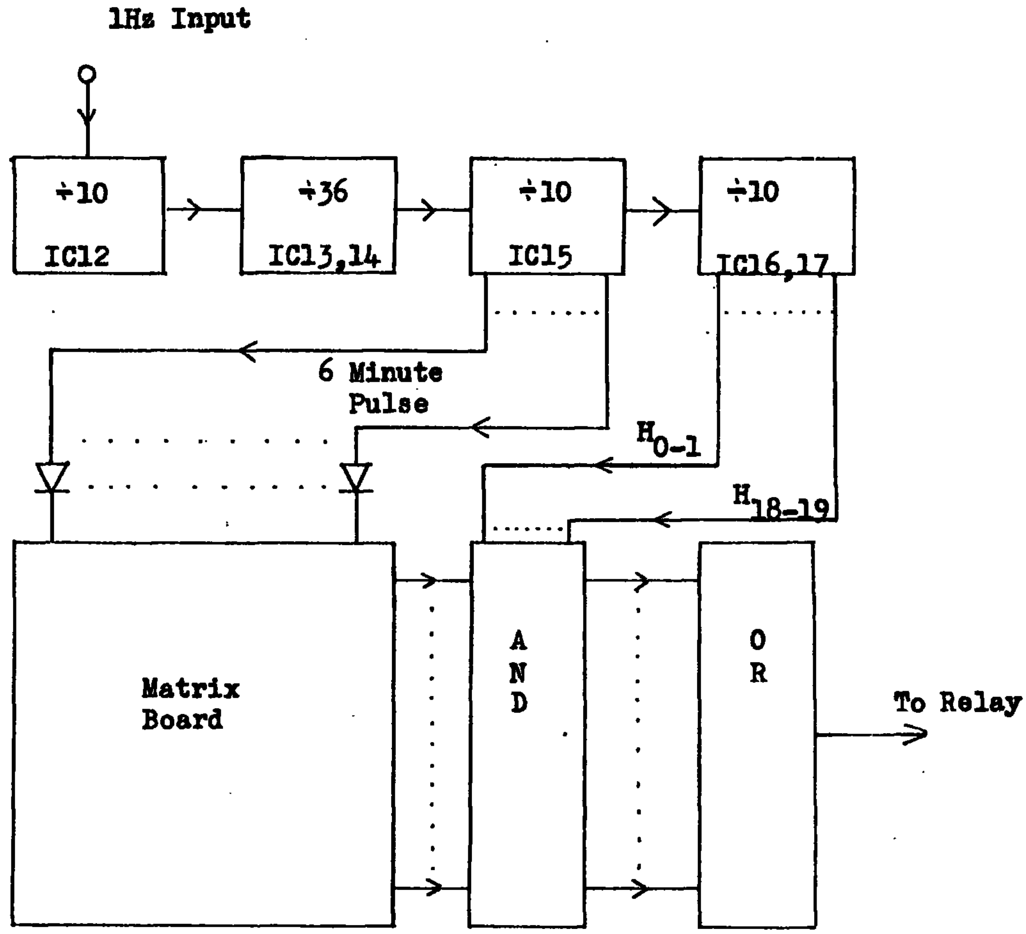

Fig. 2.17 Sequence Control Unit Schematic

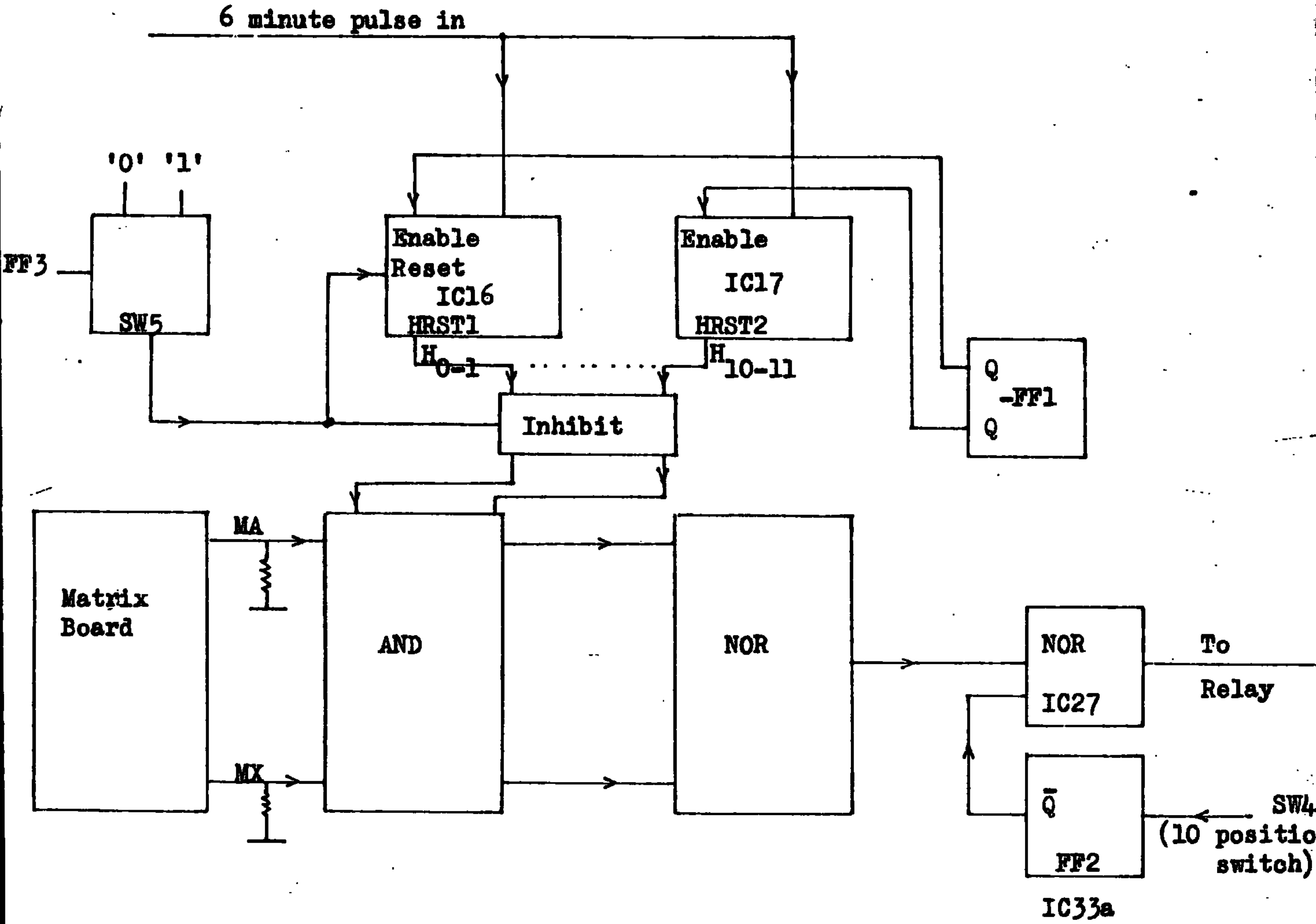

<u>Fig. 2.18</u> <u>Matrix Board Timing Schematic</u>

SEQUENCE CONTROL UNIT

The placing of a pin in column C, row R, of the matrix board makes an electrical connection between the input line connected to column C and the output row R, Fig. 2.19. If the 6-minute line corresponding to Column C is on, i.e. high, true and the hour line ANDed with row R is also high, then the AND output gate will be high. The outputs from all the AND gates are ORed together so that any 6-minute and hour line will provide an output, provided that a pin is placed in the appropriate row of column of the matrix board.

The output from the OR gate drives a feed relay connecting power to the tape deck. There are, however, several sophistications to this basic unit, allowing a certain amount of flexibility of operation.

1. DELAYED OPERATION

Once the timing unit has been started one input to the final output NOR gate (IC27) before the relay driving the tape deck, is held at logical zero by the $\bar{Q}$ output of IC33 (FF2). FF2 is a D-type flip-flop driven from the 10 position switch, SW4, which is in turn connected to the output of IC16, the HRST1 hours counter. If SW4 is set to 8, FF2 will set and hence $\bar{Q}$ go low, if and only if, the H_{8-9} line goes high. Hence the NOR gate is opened. In this manner a delay of up to 9 hours may be achieved before operation of the tape deck commences.

2. PROGRAMMED OPERATION

Once FF2 has set, programmed operation may begin provided SW5 is set to logical zero. SW5 controls the NAND gates (IC23) on the H_{0-1} and H_{10-11} lines. If SW5 is set to zero, these NAND gates are opened and operation according to the distribution of pins in the matrix board ensues.

3. CYCLICAL MODE

Once FF2 is set, with SW5 set to logical one, the H_{0-1} and H_{10-11} lines of IC16 and IC17 are disabled, since the NAND gates are closed. The NAND gate on matrix row X, is opened and hence operation according

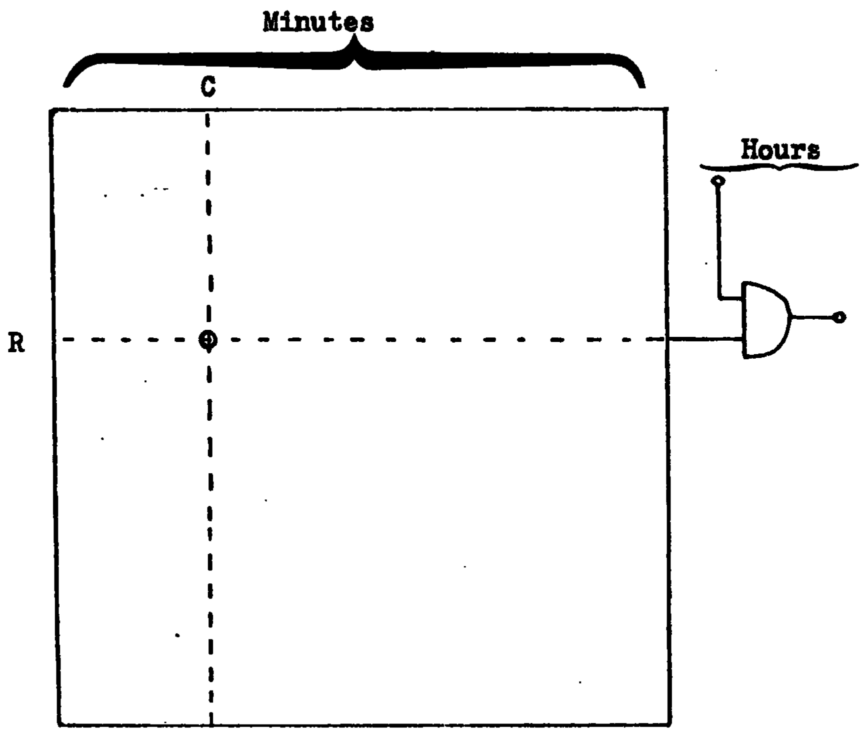

Fig. 2.19 Sequence Control Operation

to the pins in row X begins, and thus instead of moving down the matrix board, row by row, the operation will cycle through according to row X, every hour.

4. NO DELAY

If no delay is required before beginning the cyclic mode of operation then SW5 is set to position '2', in which it is connected to the output of FF3 (IC33) which is clocked by the H_{0-1} line of HRST1. In this state, SW5 goes high, and cyclic operation begins when FF3 sets, at the H_{0-1} transition.

5. DELAY, PROGRAMMED OPERATION AND CYCLICAL MODE

Delay is achieved as in 1. ($\leqslant 9$ hours); programmed operation as in 2. until H_{cyc} occurs ($H_{cyc} \leqslant 19$ hours), where H_{cyc} is the hour at which the tape goes from programmed to cyclical operation. The H_{cyc} line is wired in as a clock line for FF3 and the sequence is as follows:

The H_{cyc} line goes high, setting FF3, putting SW5 to '1'. This resets the HRST1 counter to its zero count and enables cyclical mode operation as in 3.

6. ITERATIVE

If no H_{cyc} line is wired into FF3, the HRST1 and HRST2 counters will count on automatically. The clock input of FF1 (IC33) is driven by the carry out signal from HRST1. When this goes high at the end of 10 hours of counting, it sets the flip-flop whose Q output disables the HRST1 counter in its H_{0-1} count. The Q output of FF1 also opens the H_{10-11} AND gate, previously held shut during the cycle of HRST1 by this Q output. The $\overline{Q}$ output of FF1 enables the previously disabled HRST2 counter and shuts the H_{0-1} AND gate so that operation according to matrix row M begins. When H_{19-20} goes high on HRST2, FF1 is reset disabling HRST2, enabling HRST1 which jumps into its H_{1-2} count, having been held at its H_{0-1} count during the HRST2 cycle.

Hence iterative operation begins, H_{0-1}, H_{1-2}, ... , H_{9-10}, H_{10-11}, H_{11-12}, ... , H_{18-19}, H_{1-2}, ... etc., until the end of tape marker is detected.

In order to allow the tape speed to settle down to 1.5"/sec., a slight delay occurs between the starting up of the deck and the operation of the WRITE board, described in the next section. This delay is achieved using an RS 555 timer circuit which holds off the power to the WRITE board for 1.8 seconds (Fig. 2.20).

To ensure correct operation of the tape deck the following must be noted:

i) at least one column of the matrix board must be occupied for every hour. If operation is not required during a particular hour, a pin must be placed in column 20, the dummy column, at that row. This is necessary as otherwise the input to the HOURS AND gate would float high and give a spurious command pulse.

ii) in the case shown in Fig. 2.21 there is electrical continuity between A and C through B if ordinary pins are used. This would lead to operation of the tape deck during H_{24-30} in Hour 1, which is not required. In this instance, a diode pin (type 2) is used, which allows only one way connection (horizontal) to occur.

The situation becomes that shown in Fig. 2.22, so that when column 6 goes high (H_{24-30}) in hour 1, the diode prevents the input to the H_{0-1} AND gate going high.

<u>WRITE BOARD</u>

This presents the data in a suitable format for writing onto tape. The information to be written onto tape comprises two distinct parts:

a) the data from the ADC and gain ranging boards, which is divided up into 2 segments, the 2 bits of binary gain,

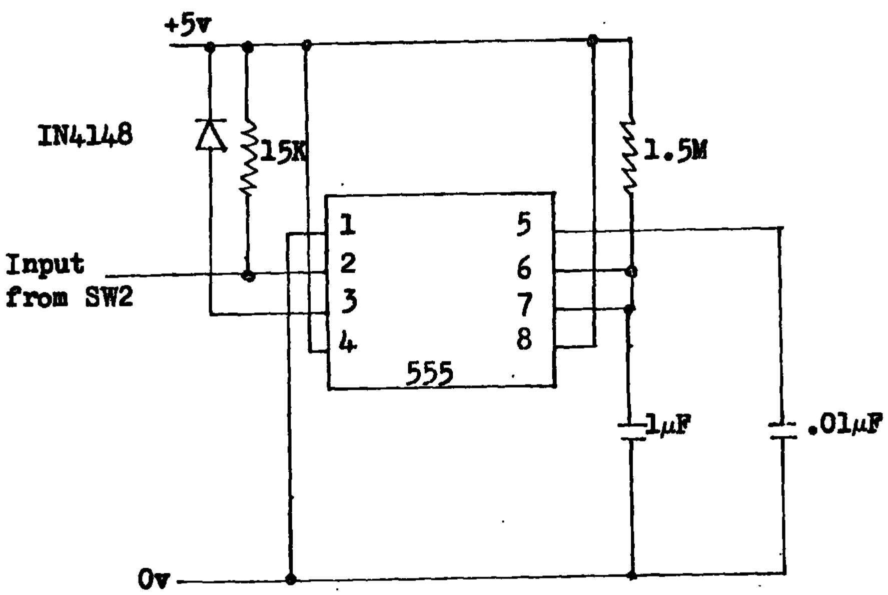

Fig. 2.20 Timer Circuit

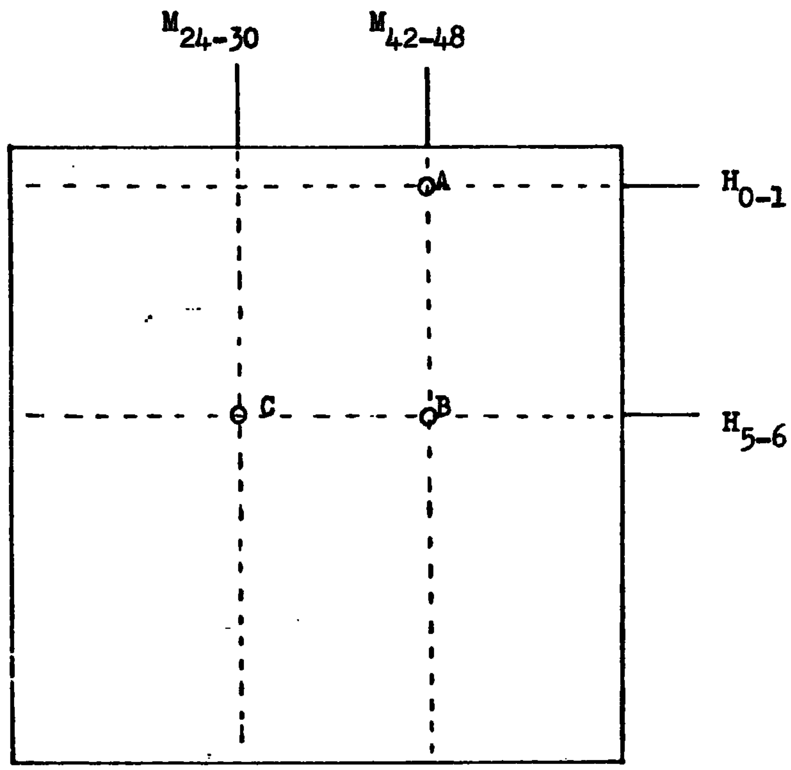

Fig. 2.21 Matrix Board Operation - Case 1

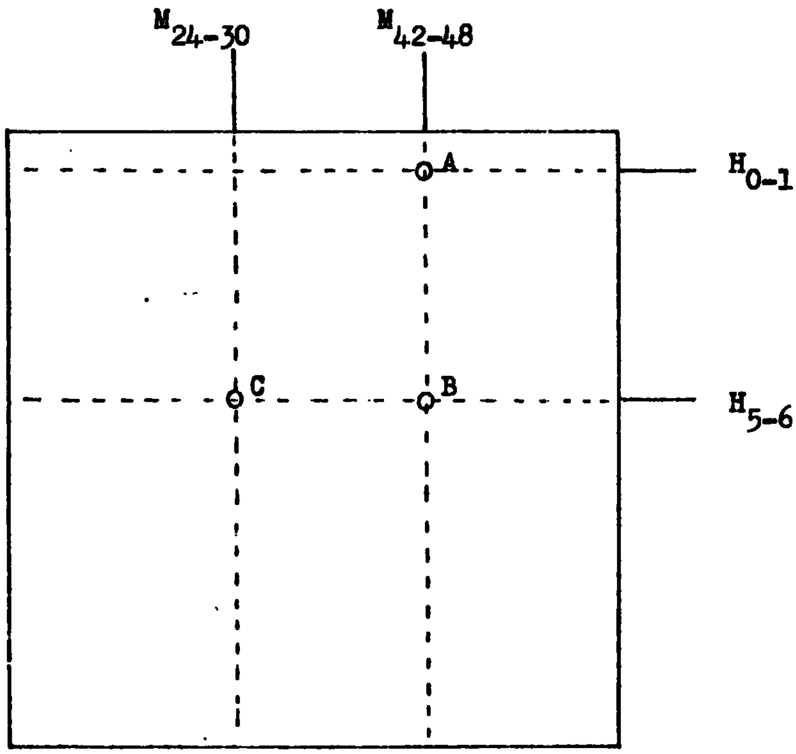

Fig. 2.22 Matrix Board Operation - Case 2

g(1), g(2) and the 5 most significant date bits (m.s.b.) and the seven least significant bits (l.s.b.).

b) time, which is obtained from the $\overline{BCD}$ output from the clock.

The format is arranged so that the tape may be uniquely decoded, and the following scheme meets this requirement (Fig. 2.23).

The information is written in 4 500μsec blocks with a mark/space ratio of 1:1, between blocks giving a 4ms cycle time.

BLOCK 1 is reserved for decoding purposes.

BLOCK 2 is used for time and decoding.

BLOCK 3 is a data block - g(1), g(2) and m.s.b. - 8th m.s.b.

BLOCK 4 is a data block, the seven l.s.b's. This unique coding is accomplished by arranging that all of BLOCK 1 is '0' followed by all of BLOCK 2 '1' at the beginning of each second.

The centre track (TRACK 4) is used for strobe purposes by writing a continuous 1 kHz signal onto it. There are hence 7 tracks available for information and the second identification code is termed a 0, 7 recognition pulse.

In every 4ms BYTE in between each second, one track of BLOCK 1 is held high and one track of BLOCK 2 is held low to prevent mis-recognition on playback.

If bits 1-5 are zero then g(1), g (2) will be high, ensuring that BLOCK 3 is never '0'. If BLOCK 4 is '0', the coding ensures that BLOCK 1 has at least one '0' track.

BLOCK 2 is only '7' or all '1' at each second pulse, the BCD output from the clock being such that only 4 of the seven available tracks are ever used at once. To provide time identification the S_1 digit enable line from the clock is indexed into BLOCK 1, on track 6. This digit enable line goes low only whenever the time digit value at the BCD output is accessed, i.e. BLOCK 1 track six is '0' only when the time data in BLOCK 2 following is S_1, S2, S4, S8.

TRACK																													
1	'0'	'1'	4	11	'0'	'1'	4	11	'0'	'1'	4	11	'0'	'1'	4	11	'0'	'1'	4	11	'0'	'1'	4	11	'0'	'1'	4	11	
2	'0'	'1'	3	10	'0'	H_{10}	3	10	'0'	H_1	3	10	'0'	M_{10}	3	10	'0'	M_1	3	10	'0'	S_{10}	3	10	'0'	S_1	3	10	continue until next second ident. pulse
3	'0'	'1'	G_1	7	H_I	'0'	G_1	7	H_I	H_2	G_1	7	H_I	M_{20}	G_1	7	M_I	M_2	G_1	7	M_I	S_{20}	G_1	7	M_I	S_2	G_1	7	
4	CLOCK STROBE →																												
5	'0'	'1'	G_2	6	H_I	'0'	G_2	6	H_I	H_8	G_2	6	H_I	0	G_2	6	H_I	M_8	G_2	6	H_I	'0'	G_2	6	H_I	S_8	G_2	6	
6	'0'	'1'	1	8	S_I	'0'	1	8	S_I	H_4	1	8	S_I	M_{40}	1	8	S_I	M_4	1	8	S_I	S_{10}	1	8	S_I	S_4	1	8	
7	'0'	'1'	2	9	'0'	'1'	2	9	'0'	'1'	2	9	'0'	'1'	2	9	'0'	'1'	2	9	'0'	'1'	2	9	'0'	'1'	2	9	
8	'0'	'1'	5	12	'0'	'1'	5	12	'0'	'1'	5	12	'0'	'1'	5	12	'0'	'1'	5	12	'0'	'1'	5	12	'0'	'1'	5	12	

4ms (one block of four columns)

28ms (whole sequence)

Key overleaf......

Fig. 2.23 **Tape Format**

KEY

'0' and '1'	-	refer to logical 0 and logical 1
1	-	refers to the most significant bit
11	-	refers to the least significant bit
G_1, G_2	-	are binary gain values
H_1	-	HOUR x 1 count
H_{10}	-	HOUR x 10 count
S_1	-	SECOND x 1 count
M_{10}	-	MINUTES x 10 count
H_I	-	Hours identification mark
S_I, M_I	-	Second, Minute identification mark

Similarly M_1 - the single minute digit enable line is indexed into track 3 of BLOCK 1 and H_1, the single hour digit enable line to track 5.

The appropriate 250Hz timing pulses are obtained from the frequency divide network and the combination of logic gates as shown in Fig. 2.24 a→g, are used to arrange the data into the required format for each track.

The information thus arranged is presented to each of the seven multi-channel data selectors (MC14512), which are driven at 1kHz by the A_1 and B_1 outputs from a BINARY 4 counter (IC10) Fig. 2.25.

The multiplexed outputs, together with the 1kHz strobe signal are fed to the tape heads via a simple head driver circuit, which simply provides enough current to drive the heads (Fig. 2.26).

TAPE RECORDER

The tape transport system used is a NAGRA IV L deck, fitted with a Nagra IV-SJ speed and tension stabiliser board (Figs. 2.27 and 2.28). The deck is adjusted to run at 1.5"/sec. The power to run the tape is provided by the -24V battery supply. The tape deck is fitted with two 8-track ¼" Phi Magnetronics digital heads, type DHM/030. Signal leads to the heads are brought out to a VERO edge connector which is fitted to the head drive board mounted, in turn, on the underside of the chassis of the deck.

TAPE HEAD DETAILS

PHI MAGNETRONICS	DHM/030
Dimensions	50" x 50" x 65"
Track Width	.020"
Track Pitch	.0318"
Gap Spacer	.0001"
Face Form	hyperbolic
Inductance a 1kHz	30mH ± 20%

Track 1

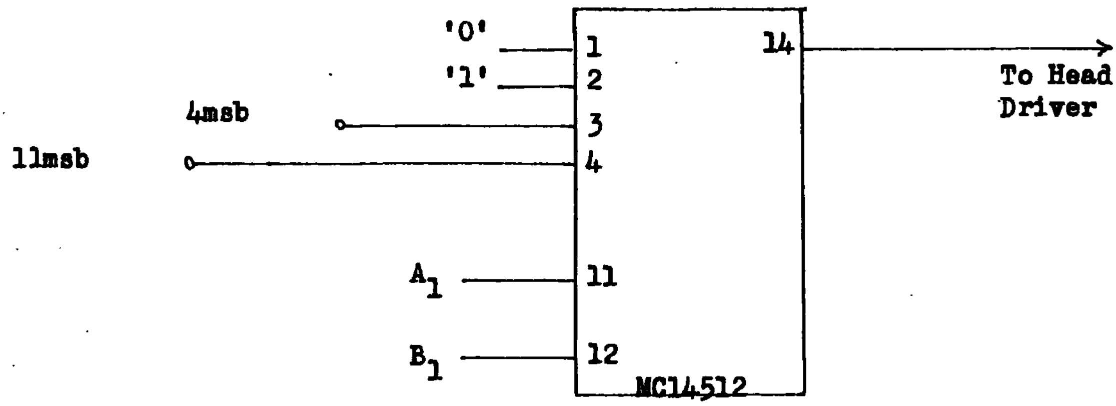

Fig. 2.24(a) Write Logic

Track 2

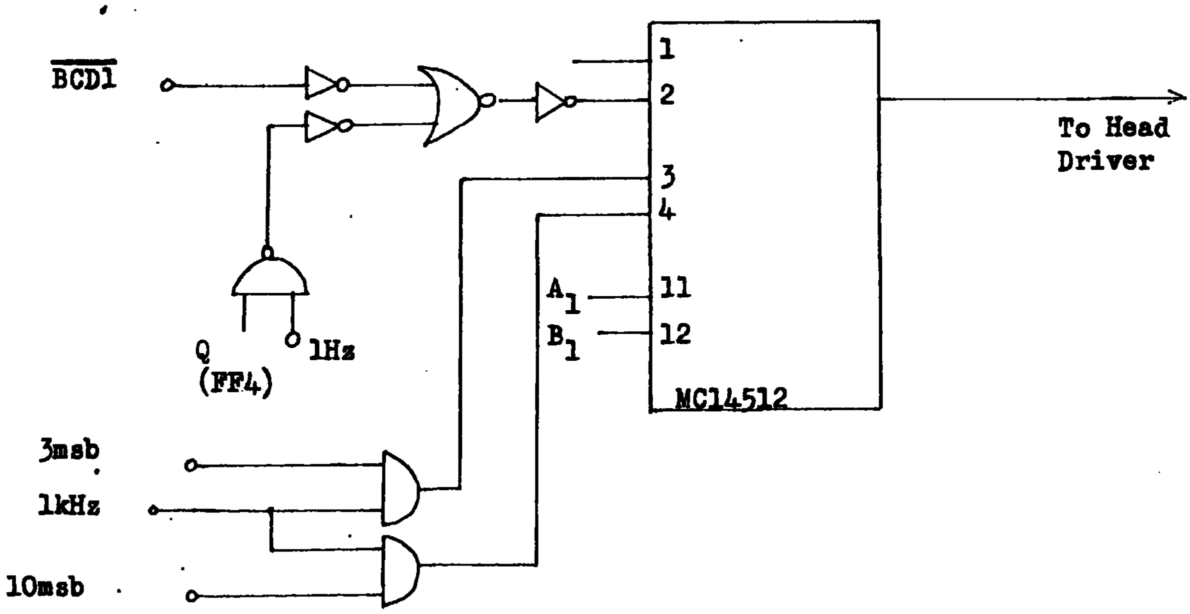

Note 1Hz NANDED with Q(FF4) gives a 4msec low pulse at each second pulse, with priority over time.

Fig. 2.24(b) Write Logic

Track 3

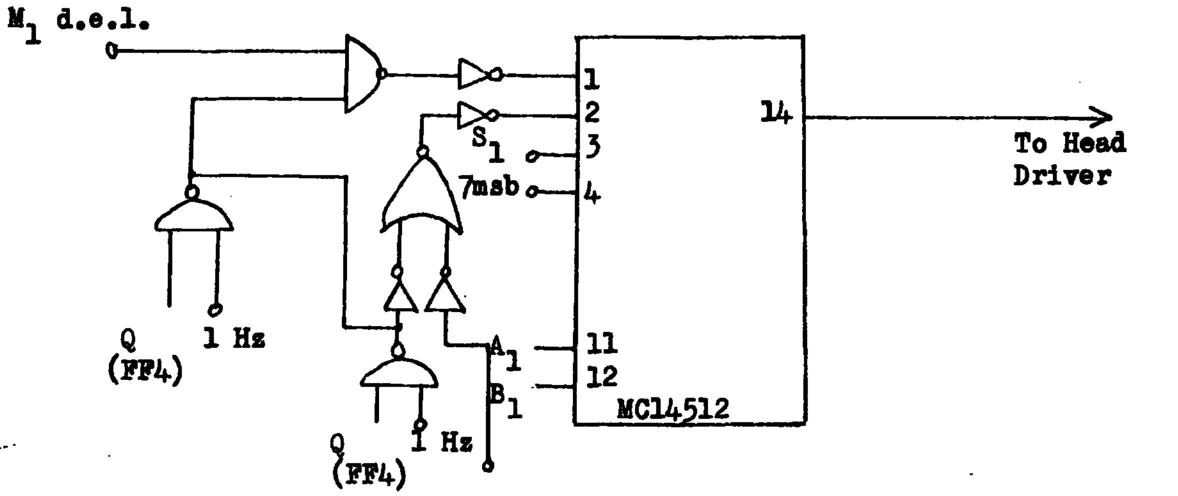

Fig. 2.24(c) Write Logic

Track 5

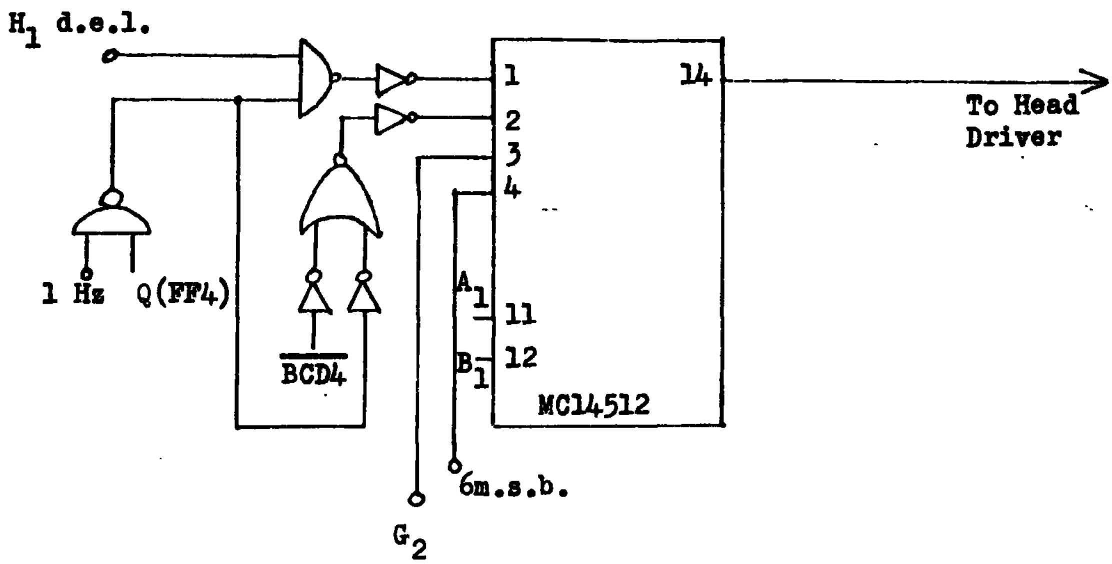

Fig. 2.24(d) Write Logic

Track 6

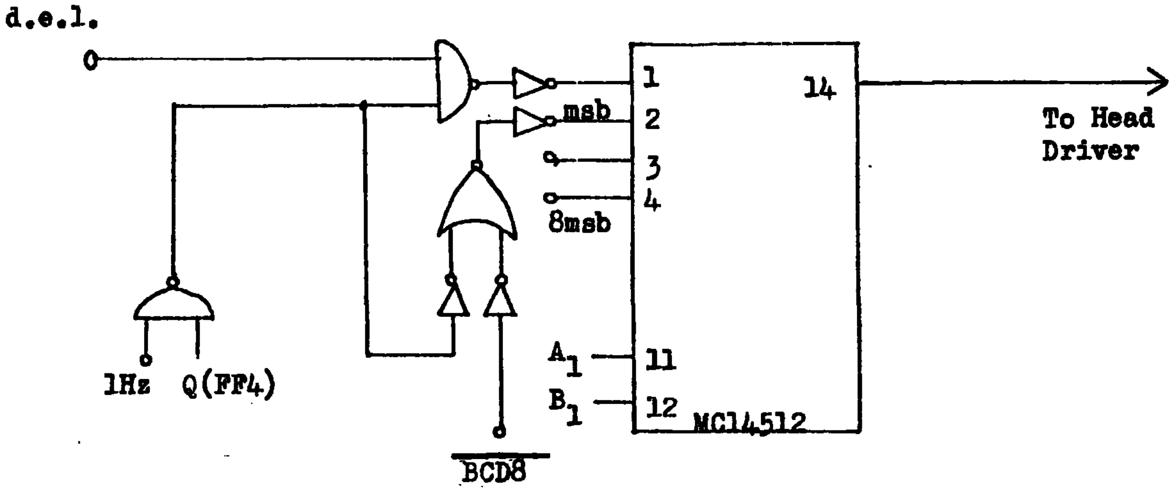

Fig. 2.24(e) Write Logic

Track 7

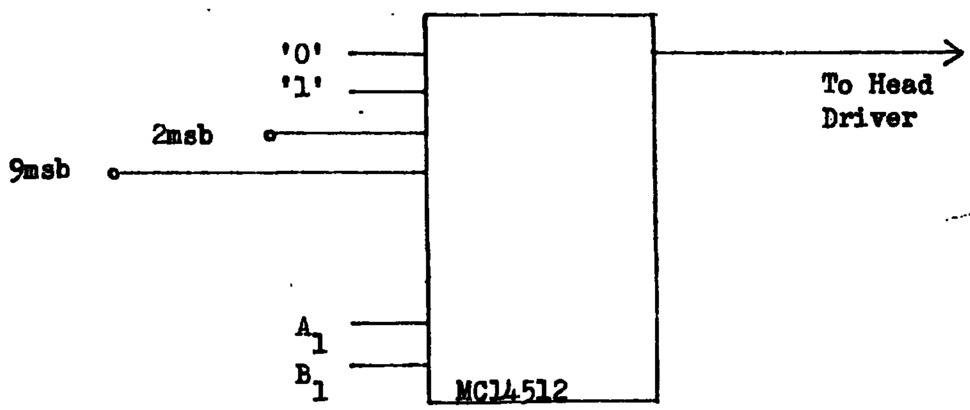

Fig. 2.24(f) Write Logic

Track 8

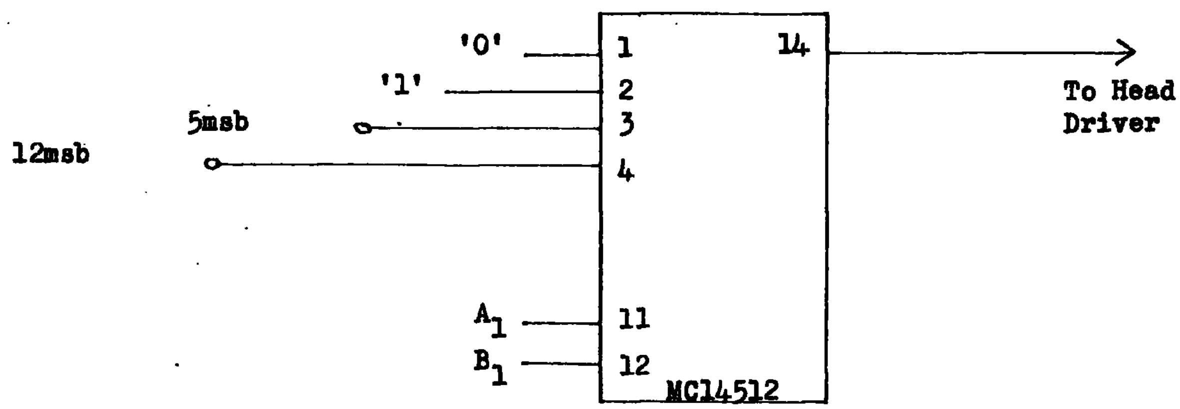

Fig. 2.24(g) Write Logic

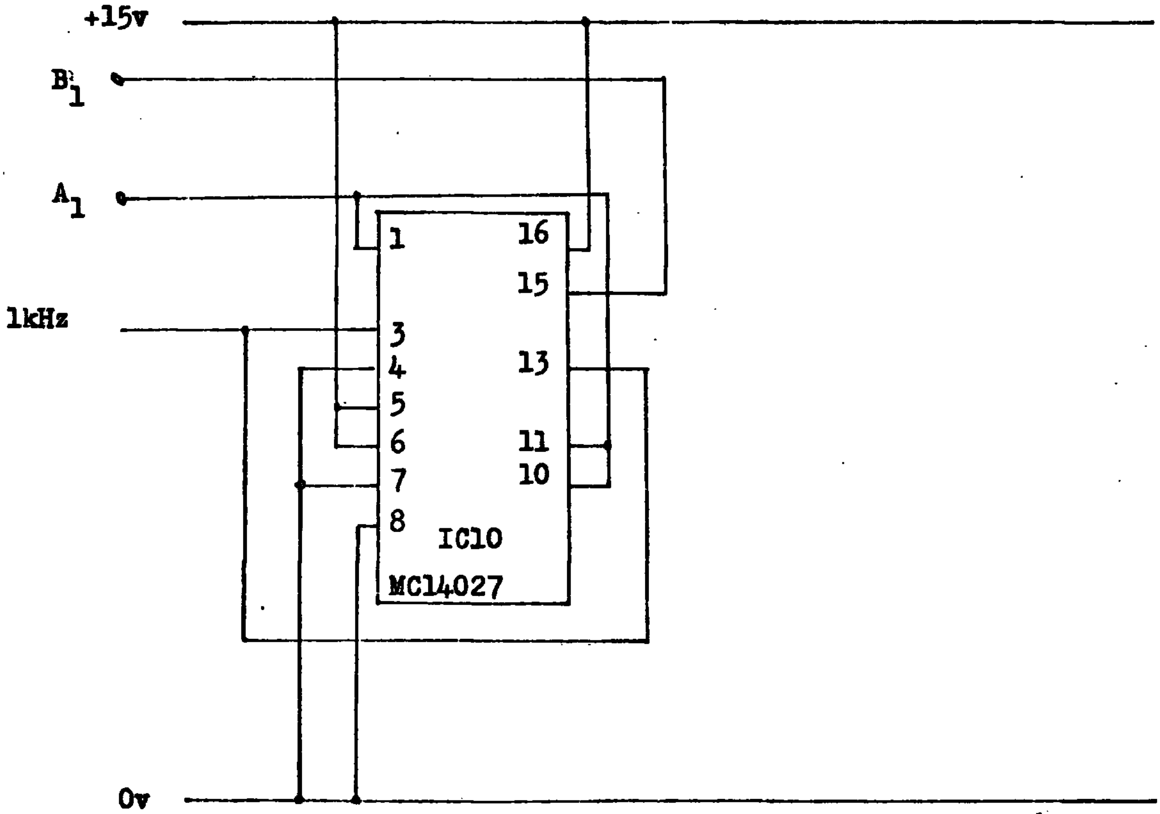

Count	A_1	B_1
0	0	0
1	1	0
2	0	1
3	1	1
0	0	0

<u>Fig. 2.25</u> <u>Binary 4 Counter</u>

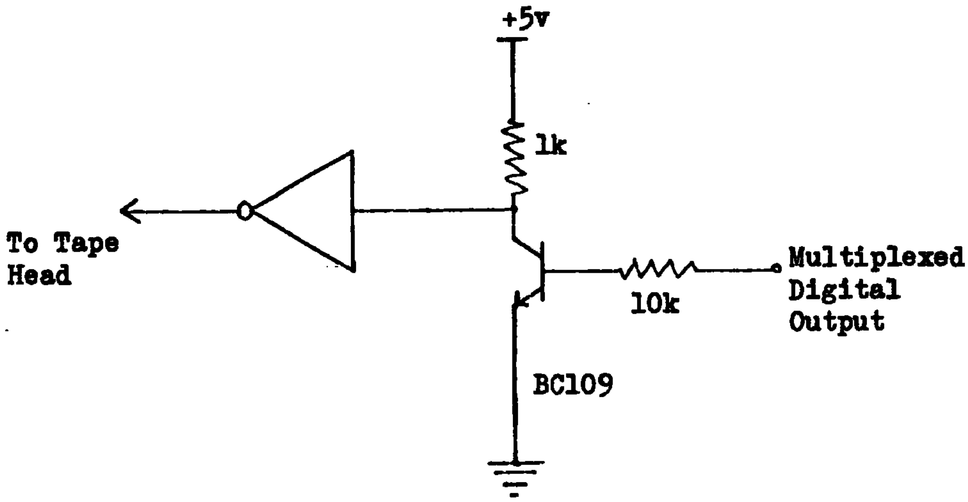

Fig. 2.26 **Head Driver Schematic**

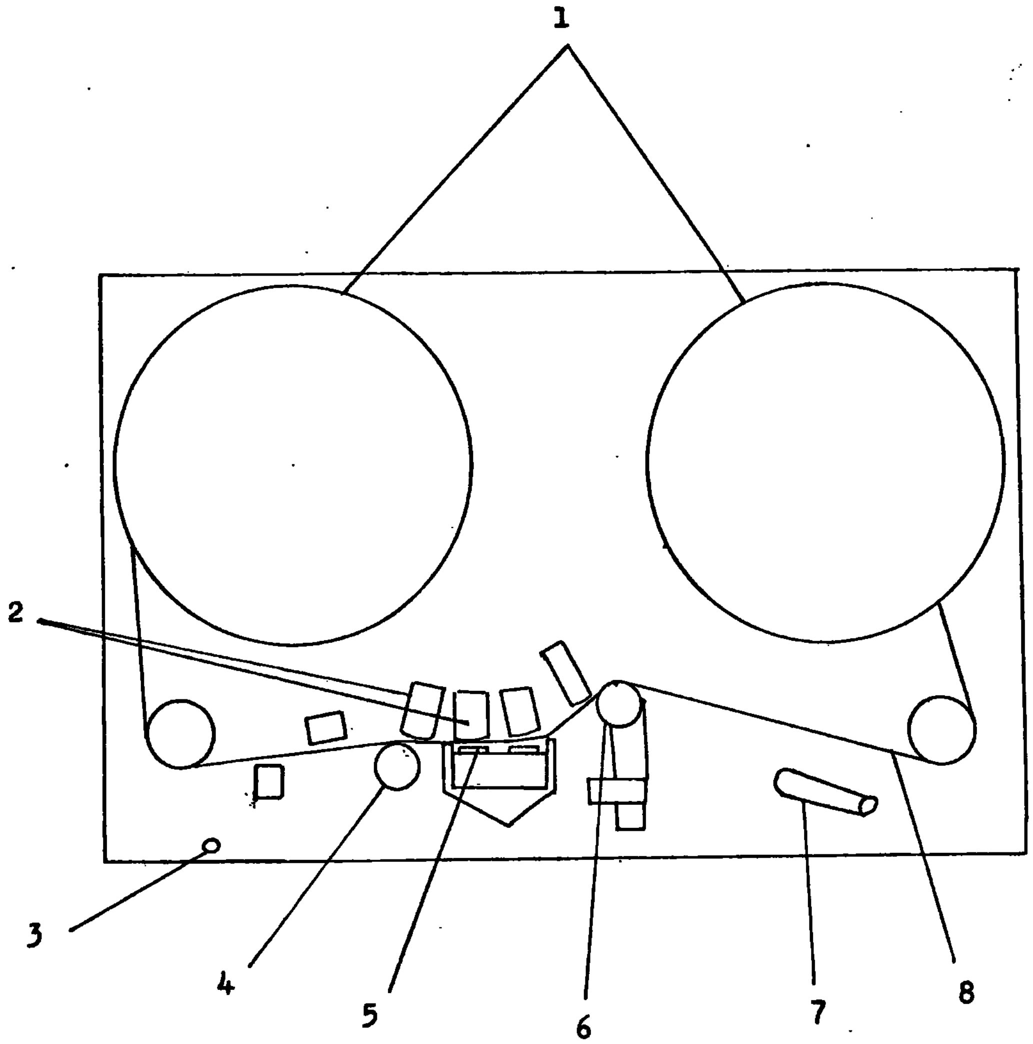

see over

Fig. 2.27 Tape Recorder - Top View

<u>Key</u>

1	Tape Spool
2	Erase, Record Heads
3	Fast Wind/Rewind Switch
4	Tape Speed Sensor
5	Pressure Pad
6	Pinch Roller
7	Function Switch
8	Tape

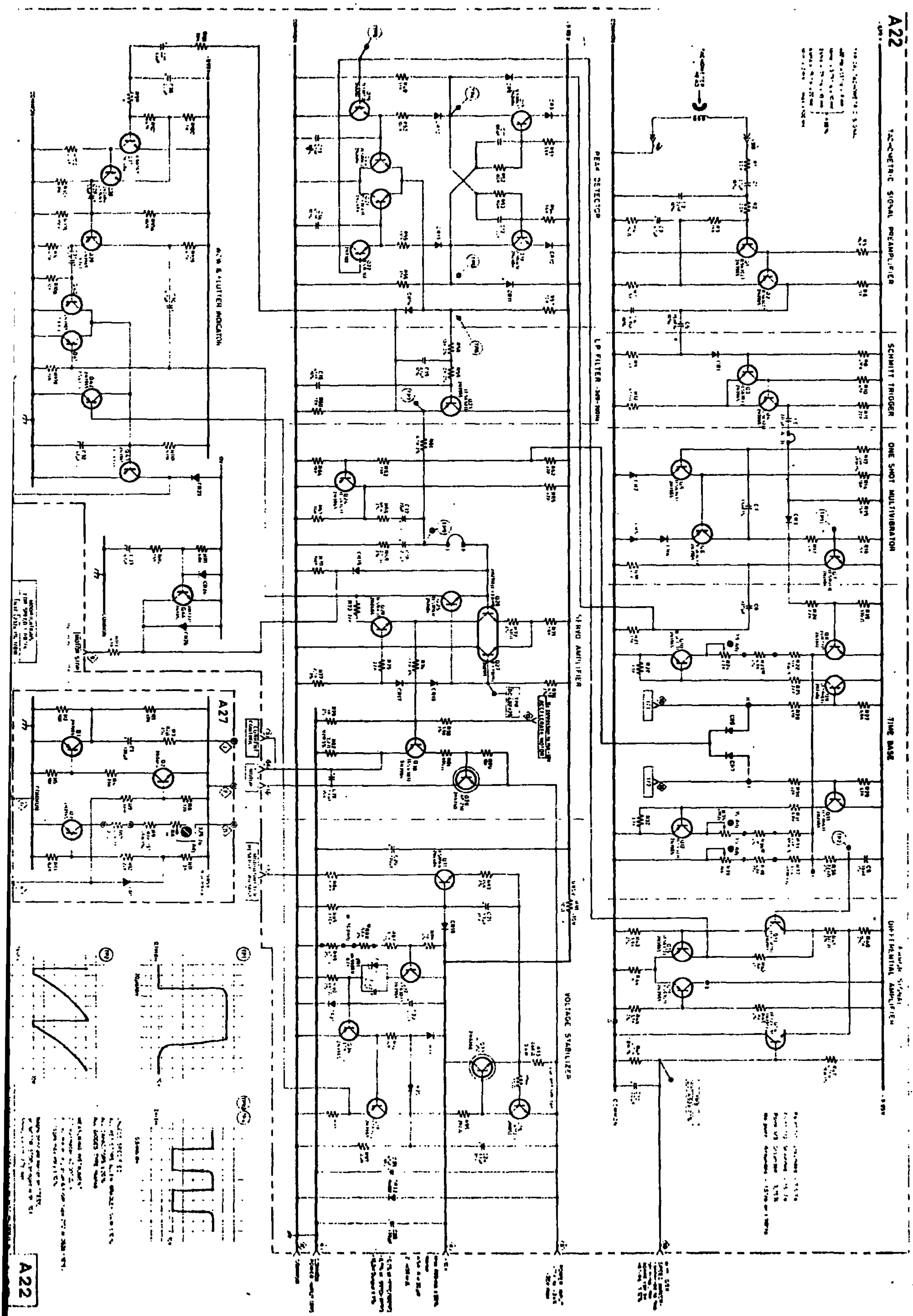

Fig. 2.28 Speed Control Board

Playback Level	85V ± 1.5dB
WRITE Current	10mA p-p.
Output	2.5mV ± 20% p-p.

TRANSMITTER

This is taken from an Ultra Electronics disposable sonobuoy (Fig. 2.29), and mounted, screened inside the instrument housing of the buoy, next to the electronics container. The transmitter consists of a modulated crystal controlled R-F oscillator-doubler, two frequency doubler amplifiers and a final RF power amplifier. Modulation is accomplished in the oscillator stage by means of a variable reactance diode in series with the crystal, and thus the oscillator frequency is varied by the audio input.

The transmitter is disconnected once the tape deck begins to operate, to prevent any R.F. interference which might cause the A/D converter to malfunction.

The power for the x-mitter is dropped from the unregulated 12v battery supply to 10.1 volts using a Zener diode arrangement. The aerial of the transmitter is mounted on a 19' two section hollow glass fibre pole, to increase the system's range.

FLASHING LIGHT

This is an OAR submersible flasher, type SF-500-1-100 which operates for over 100 hours at 1 flash every 2 seconds. It is mounted externally, clamped to one of the strengthening struts (Fig. 2.1).

BATTERY SUPPLIES

The +24V input to the +15V power regulator is provided by two Exide type 166 12 volt motorcycle batteries, fitted with non-spill caps. One of these batteries also provides the 12V supply to the 5V power regulator.

The -15V stabiliser is driven from two Lucas MCZ7/9A-8 motorcycle batteries again fitted with non-spill caps.

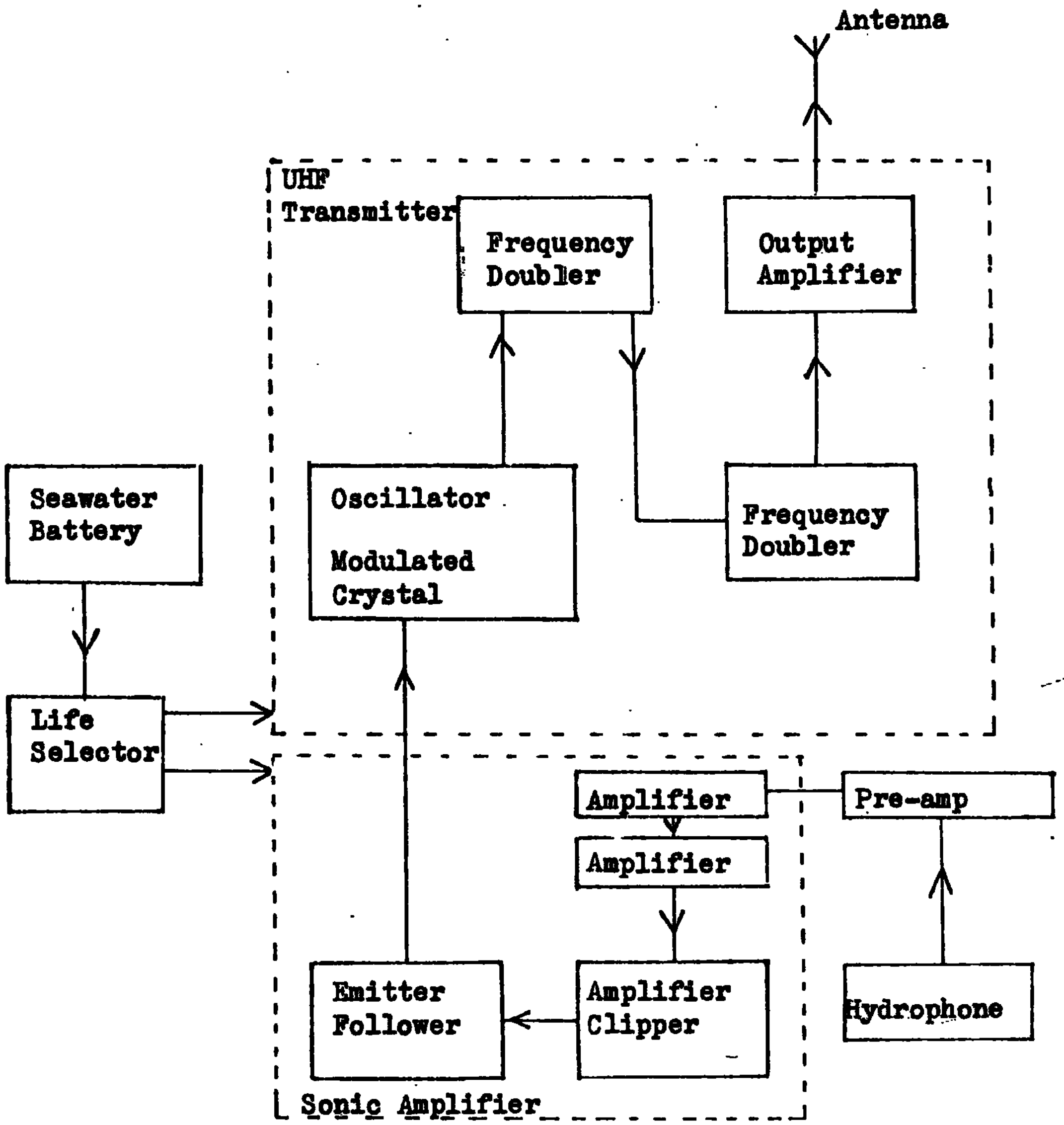

Fig. 2.29 Sonobuoy Type SB6E4 Block Diagram

Fig. 2.30 Sonobuoy About to be Launched

A Lucas PUZ5A 12 volt battery supplies the UEL transmitter. A schematic diagram of the power supply system is shown in Fig. 2.31.

The electronic boards are housed in an aluminium container which is mounted as shown in Fig. 2.1. The container may be removed for circuit analysis, while still connected.

50-way and 13-way sockets on either side of the container link the internal electronics to the tape deck, control switches matrix board, L.E.D. display and power supply.

The top view of the arrangement inside the buoy is shown in Fig. 2.3. The tape deck is held in position by spring-loaded runners, which fit inside a groove mounted on the inside walls of the container.

The batteries are mounted in the lower half of the instrument housing using formers designed to hold them securely in place.

OPERATION

The setting up procedure for operation of the buoy is described below.

1. The batteries are connected up and a d.v.m. used to check that the correct working voltages are being generated.

2. The 7-segment display for the clock is enabled using SW7, and the clock set up to its zero count using the fast or slow slew controls. The clock is held at this initial count until just prior to buoy drop. The display is then turned off to conserve power.

3. The tape deck is removed from the buoy in order that 3600' of Ampex tape may be fitted and the gain of the A/D converter and gain control board is adjusted using the rotary gain control switch so that saturation does not occur. This is indicated by the L.E.D. displays on the panel of the gain control board.

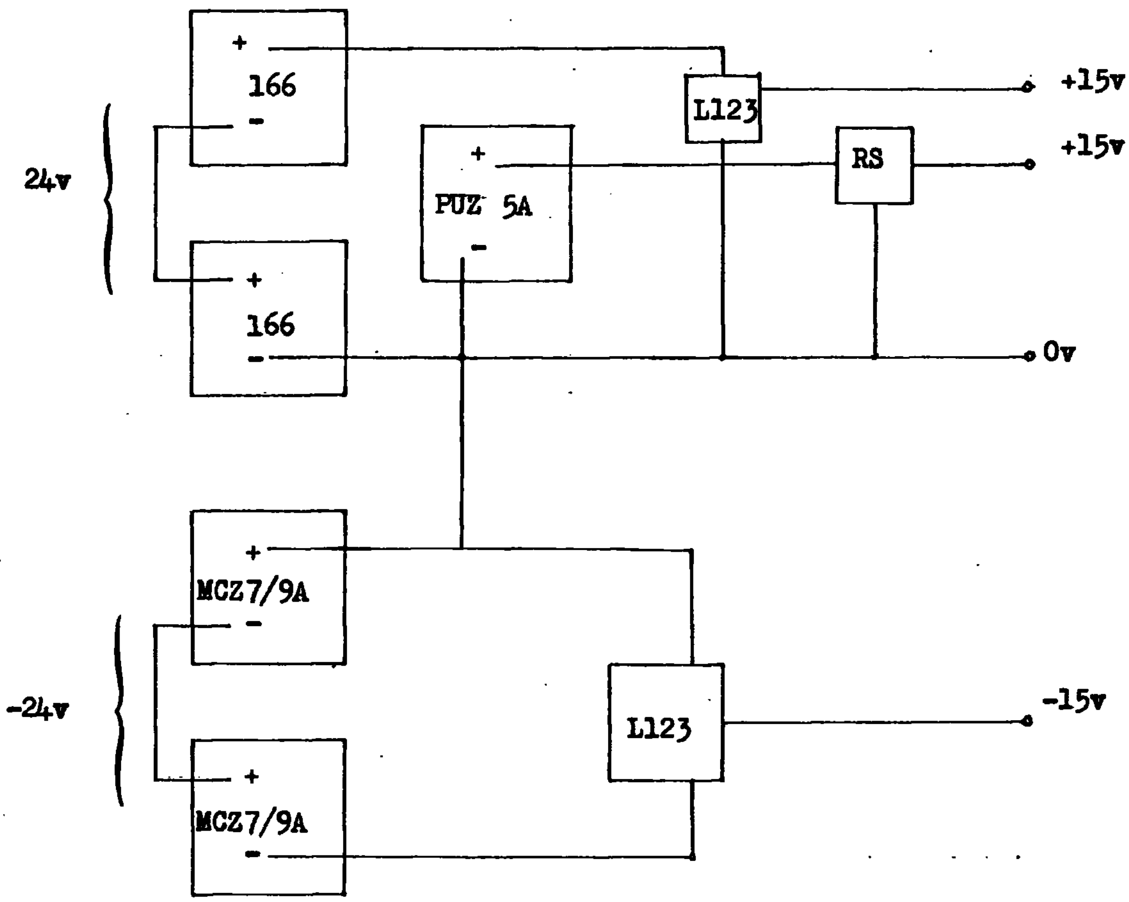

Fig. 2.31 Battery Schematic

4. Once the gain level has been set, this display is disabled in the interests of power conservation.

5. The tape deck is replaced and the timing counter chain including the 6-minute and hours counter stages are reset using the master reset button. BINARY 4 counter controlling the data selection is also reset by this switch.

6. The appropriate mode of operation is selected (SW5 in position 0, 1 or 2) and matrix pins placed in the required (or default) positions.

7. The hold of the clock is switched off and the lid of the buoy firmly secured.

8. The flashing light is activated and the buoy is ready for launching, once power to the hydrophone has been supplied by attaching the hydrophone cable.

The individual component circuits comprising the Digress electronics and the system in toto were temperature cycled in so far as was possible without a controlled environment chamber, to ascertain that the cold water conditions in which the buoy was to be used would not cause instability or excessive drift in the timing and clocking functions of the buoy.

In the range 0-15°C, approximately,no discernible temperature dependent drift could be found after an initial settling period of some three minutes, during which time, presumably, the l.s.i. circuits were achieving their operating temperatures.

Replay

Although some time was spent designing TTL circuitry to decode the digital signals recorded onto tape, a PDP8 mini computer was purchased by the Department of Geological Sciences before the playback system was built, and it was a straightforward matter to use this computer to replay the digital tapes.

With knowledge of the tape format (Fig. 2.23), the decoding and demultiplexing of the digital data is simple, once the '0, 7' recognition pulse has been detected. The tape from the sonobuoy is replayed on a Ferrograph Series 7 deck only unit, fitted with the same recording heads as the Nagra machine. This Ferrograph deck had been modified to enable it to be remotely operated.

The computer waits for receipt of a '0, 7' pulse, whereupon the digital data blocks immediately following are stored in the core memory. Each bit is assigned to a location corresponding to its binary weighting and the binary gain values, data block 3, tracks 3 and 4 are used to convert the 12 bits into real amplitudes. The signal is output through a digital-to-analogue converter to the Geospace V.A.D. system (Chapter V). The computer decodes the time data presented to it, simultaneously, the second, minute and single hours indicators, S_I, M_I, H_I, being used to identify the appropriate time data, and displays it on a 6 digit L.E.D. display, similar to that used inside the buoy.

The system was carefully checked in the laboratory and found to behave well when using digital test signals. For analogue test, sinusoidal oscillations, between 3Hz and 80Hz were input to the digital tape recorder and replayed subsequently to examine distortion and non-linearity (Fig. 2.32).

A sample of the data obtained using the U.E.L. disposable sonobuoys was input similarly and replayed to the jet pen system (Chapter V) for visual comparison (Fig. 2.33).

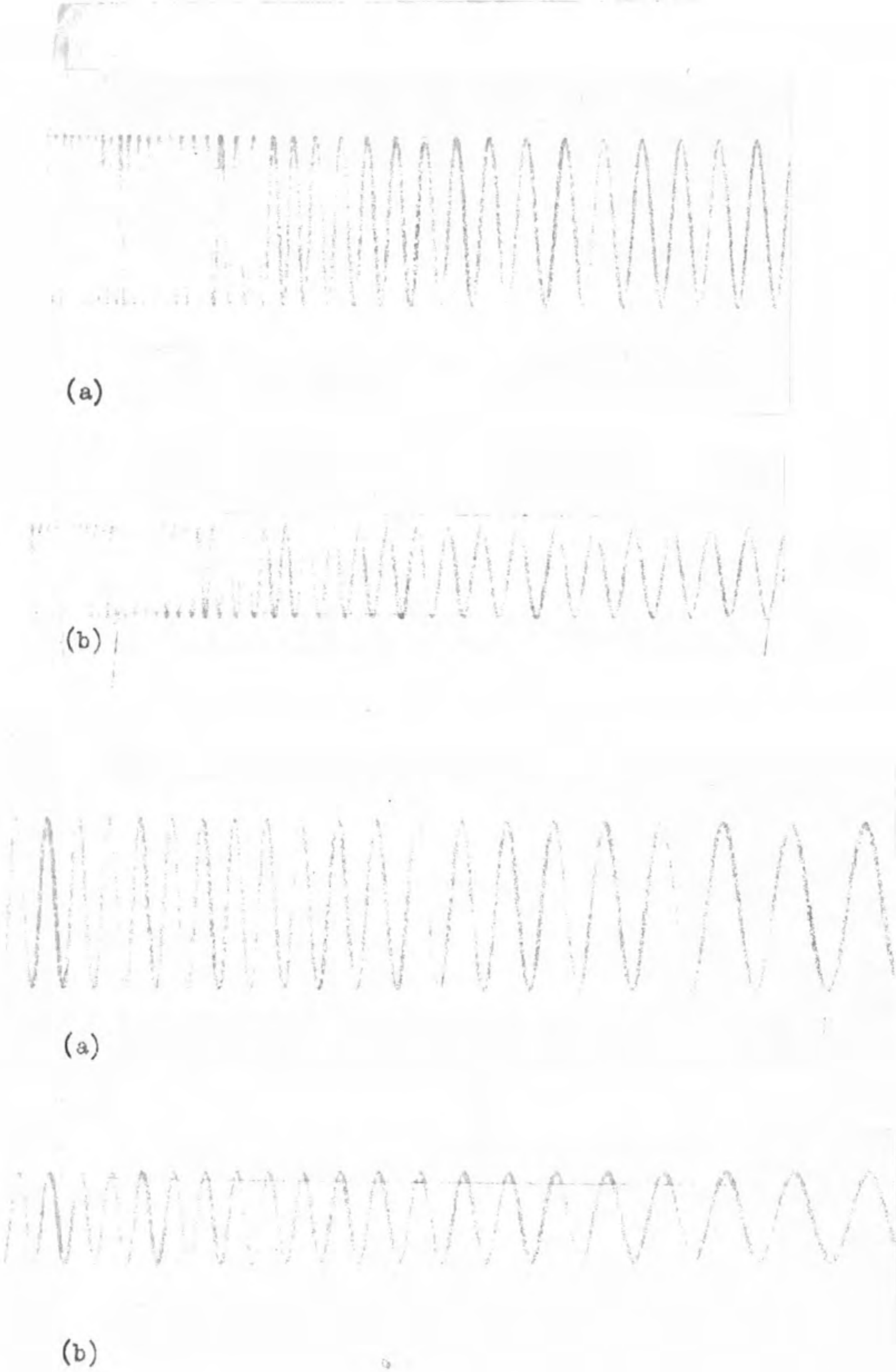

Fig. 2.32 Sinusoidal Input (a) and Replay (b)

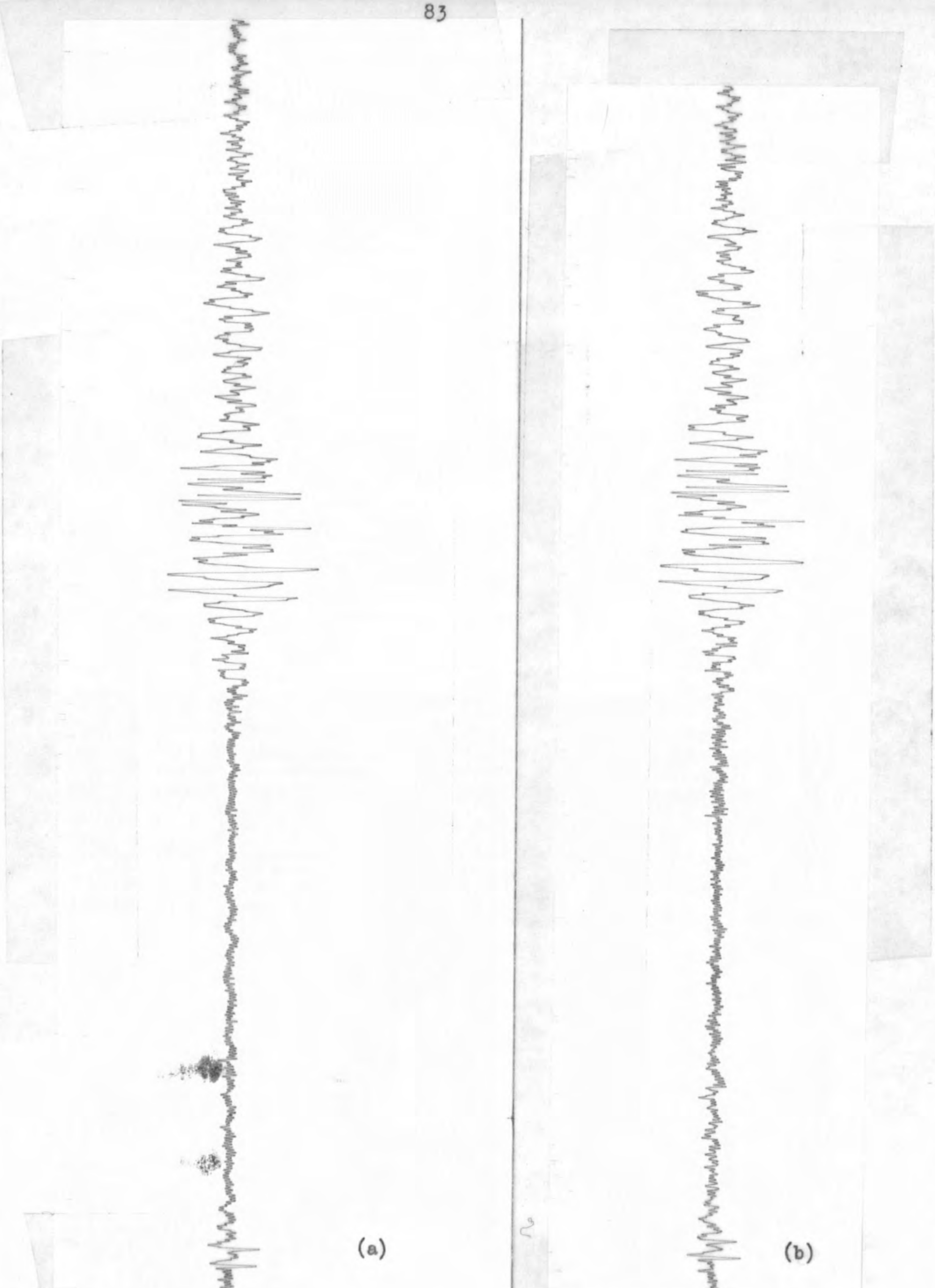

Fig. 2.33 Sample Input (a) and Replay (b)

It should be noted at this point that owing to certain difficulties, both at Durham and whilst at sea in the summer of 1974 the sonobuoy described in this chapter was not used at sea and the amplitude analysis and velocity-depth information presented subsequently, were obtained from the U.E.L. disposable sonobuoys, in conjunction with a a Bolt Airgun system. It had been hoped to perform some longer range refraction work in 1973 but the 'Aquaflex' explosive was found to be unusable because of corrosion, and similar investigations in 1974 were curtailed because of operational constraints.

Note:-

The books and articles listed in the bibliography for this chapter are not numbered specifically as general reference was made to them all in the design, construction and testing of the sonobuoy.

CHAPTER THREE

THEORY

Plane Wave Reflection

Since the plane wave concept is used as the basis for wave analysis, the following is given in introduction.

The plane wave is the simplest form of wave motion and, in general, acoustic scalar and vector potentials, Φ and $\underline{\Psi}$, may be assumed, such that (Ref. 3.1)

$$\underline{v} = \operatorname{grad} \phi + \operatorname{curl} \underline{\Psi} \qquad (1)$$

where $\underline{v}$ is the particle velocity.

If a Cartesian co-ordinate system is defined only the x and z co-ordinates together with those quantities dependent on x and z, need be considered, because of the nature of the plane wave.

Defining;

Displacement in the direction of the x-axis as u,

Displacement in the direction of the z-axis as w,

Displacement in the direction of the y-axis as v.

If an incident longitudinal wave is assumed then from (1)

$$\left.\begin{aligned} u &= \frac{\partial \phi}{\partial x} - \frac{\partial \psi}{\partial z} \\ v &= 0 \\ w &= \frac{\partial \phi}{\partial z} + \frac{\partial \psi}{\partial x} \end{aligned}\right\} \qquad (2)$$

As there is no incident transverse wave, the vector potential, $\underline{\Psi}$, is zero (Ref. 3.2) giving

$$\left.\begin{aligned} u &= \frac{\partial \phi}{\partial x} \\ v &= \frac{\partial \phi}{\partial z} \end{aligned}\right\} \qquad (3)$$

The Cartesian co-ordinate system is defined such that the reflecting interface between the two media to be examined is placed in the z = 0 plane, and the x-axis lies along the intersection of the interface plane with the plane of incidence, as shown in Fig. 3.1.

The physical properties of the two media are given in the table below, and the two media are defined as linear isotropic homogeneous perfectly elastic media.

	MEDIUM 1	MEDIUM 2
longitudinal velocity	a_1	a_2
transverse velocity	b_1	b_2
density	ρ_1	ρ_2

It is assumed that the wave normal of the incident wave makes an angle, i, with the normal to the interface (Fig. 3.1). The potential of the incident longitudinal wave can thus be written as

$$\phi_o = \exp\left[jk\,(x \sin i + z \cos i) - jwt\right] \qquad (4)$$

where w is the angular frequency and k is the wave number (Ref. 3.3). Assuming that there is continuity across the interface and, hence, requiring equal normal and tangential stresses on both sides of the interface, the potential of the reflected longitudinal wave may be expressed as

$$\phi^o = A_o(e_o) \exp\left[jk\,(x \sin i - z \cos i) - jwt\right] \qquad (5)$$

where $e_o = \sin i$.

$A_o(e_o)$ is defined as the Reflection Coefficient for plane waves. The value of $A_o(e_o)$ may be calculated from the above mentioned boundary conditions which are listed below;

Continuity Conditions

(i) normal displacement

(ii) tangential displacement

(iii) normal stress

(iv) tangential stress

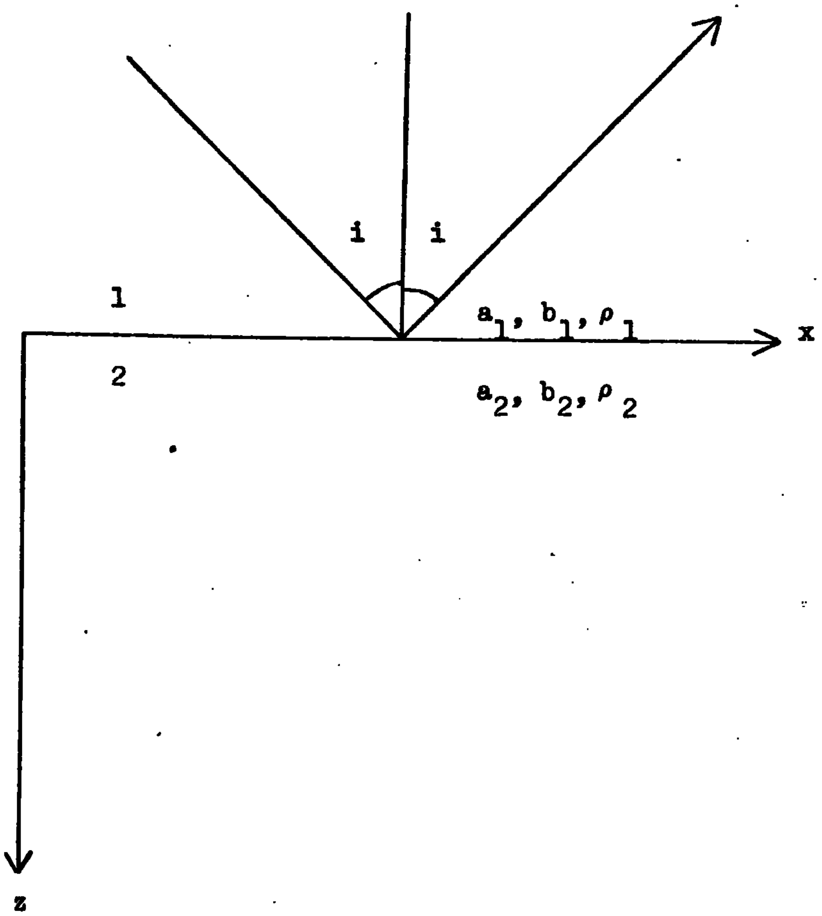

Fig. 3.1 Cartesian Co-ordinate System

which may be rewritten as (Ref. 3.4)

$$\left.\begin{aligned} &\text{(i)} & \sum u_1 &= \sum u_2 \\ &\text{(ii)} & \sum w_1 &= \sum w_2 \\ &\text{(iii)} & \sum(\sigma_{xx})_1 &= \sum(\sigma_{xx})_2 \\ &\text{(iv)} & \sum(\sigma_{zz})_1 &= \sum(\sigma_{zz})_2 \end{aligned}\right\} \qquad (6)$$

$$\left.\begin{aligned} \text{where } (\sigma_{xx}) &= \lambda\Delta + 2\mu\frac{\partial u}{\partial x} \\ \Delta &= \left(\frac{\partial u}{\partial x} + \frac{\partial w}{\partial z}\right) \\ (\sigma_{zz}) &= \mu\left(\frac{\partial w}{\partial x} + \frac{\partial u}{\partial z}\right) \end{aligned}\right\} \qquad (7)$$

λ, μ are the Lamé constants of the media (Ref. 3.5), 1, 2 subscripts denote the corresponding media.

Substituting into equations (6), gives four equations linking the amplitudes of the four waves, reflected P, reflected S, refracted P, refracted S, generated by the incidence of the longitudinal wave, to the initial amplitude (Fig. 3.2).

Rearrangement of these equations (Ref. 3.6) and substitution for the different angles of reflection and refraction using Snell's Law (Ref. 3.7) gives an expression for the plane P wave reflection coefficient.

$$A_o(e_o) = \frac{K_2(e_o) + L_2(e_o)\sqrt{n^2 - e_o^2}}{K_1(e_o) + L_1(e_o)\sqrt{n^2 - e_o^2}} \qquad (8)$$

where

$$\begin{aligned} K_{1,2}(e_o) &= \pm e_o^2\left[n_1^2(\rho - 1) - 2e_o^2(\mu - 1)\right]^2 \\ &+ \sqrt{1 - e_o^2}\sqrt{n_1^2 - e_o^2}\left[\rho n_1^2 - 2e_o^2(\mu - 1)\right]^2 \\ &+ \sqrt{1 - e_o^2}\sqrt{n_2^2 - e_o^2}\,\rho n_1^4 \end{aligned} \qquad (9)$$

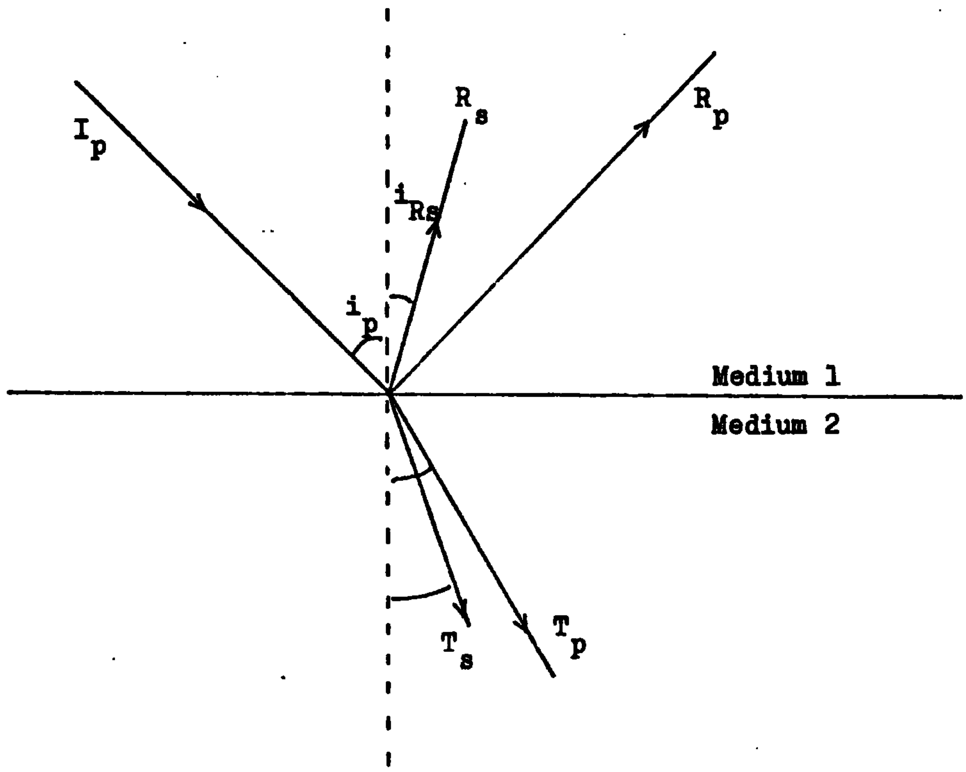

I_p - Incident P wave

R_p - Reflected P wave

T_p - Refracted P wave

T_s - Refracted S wave

R_s - Reflected S wave

Fig. 3.2 Arrangement of Reflected and Refracted P and S Waves

$$L_{1,2}(e_o) = 4\sqrt{1-e_o^2}\sqrt{n_1^2-e_o^2}\sqrt{n_2^2-e_o^2}\quad e_o^2(\mu-1)^2$$
$$\pm\sqrt{n_1^2-e_o^2}\quad \rho n_1^4 \tag{10}$$
$$\pm\sqrt{n_2^2-e_o^2}\left[n_1^2+2e_o^2(\mu-1)\right]^2$$

where $n = a_1/a_2$, the refractive index (Ref. 3.7)

$$\left.\begin{aligned} n_1 &= a_1/b_1 \\ n_2 &= a_1/b_2 \\ \rho &= \rho_1/\rho_2 \\ \mu &= \rho_2 b_2^2/\rho_1 b_1^2 \end{aligned}\right\} \tag{11}$$

$a_{1,2}$, $b_{1,2}$ being defined earlier as the P and S velocities in their respective media.

The region to be examined in detail is that near the critical angle, for which $e_o = n$

For $e_o < n$, $A_o(e_o)$ is real

$e_o > n$, $A_o(e_o)$ is complex

Only the modulus $|A_o(e_o)|$, is dealt with here; the phase changes that occur as the critical angle is passed through are discussed subsequently. The behaviour of $|A_o(e_o)|$ depends on whether $n_2 > 1$ or $n_2 < 1$.

(i) $n_2 \geq 1$

For $a_1/b_1 = a_2/b_2 = \sqrt{3}$; $\rho_2/\rho_1 = 1$ (Ref. 3.8). The numerical solution for $|A_o(e_o)|$, is shown in Fig. 3.3. This plot was obtained using the PLAMP programme, given in Appendix 1. Clearly, $|A_o(e_o)|$ changes most rapidly in the region of the critical angle.

(ii) $n_2 < 1$

In this instance, a second critical point is obtained, whose critical angle is given by $e_o = n_2$, and the $|A_o(e_o)|$ curve displays two peaks. (Fig. 3.4).

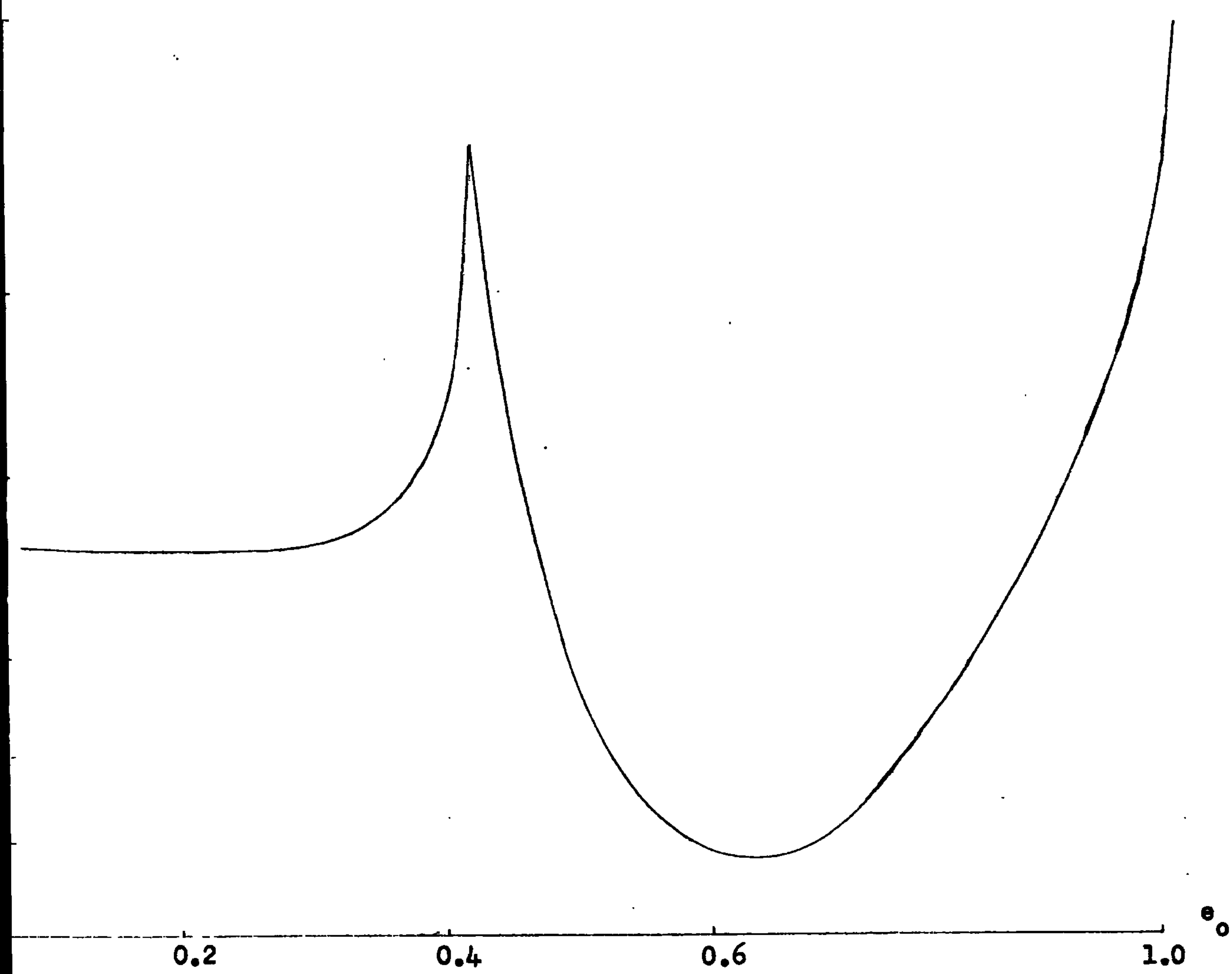

$n = 0.42,\ a_1/b_1 = a_2/b_2 = \sqrt{3},\ \rho = 1$

Fig. 3.3 Numerical Solution for Plane Wave Reflection

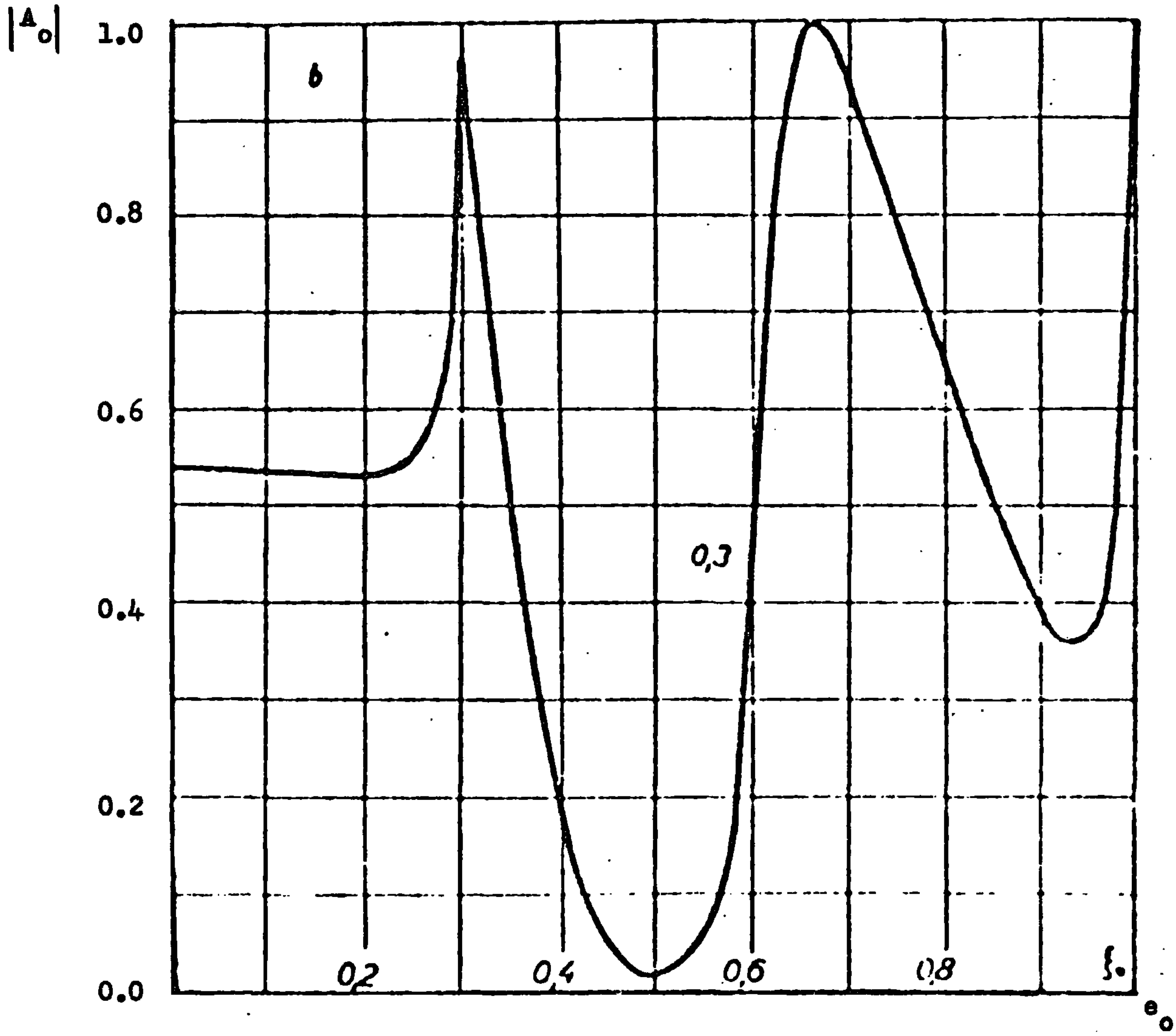

$n = 0.3,\ a_1/b_1 = a_2/b_2 = 2,\ \rho = 1.$

Fig. 3.4 Numerical Solution for Plane Wave.

$n_2 < 1$

The rapid variation in $|A_o|$ is caused by the changes in $\sqrt{n^2 - e_o^2}$ as $e_o \rightarrow n$.

Writing

$$A_o(e_o) = A_1(e_o) - A_2(e_o)\sqrt{1 - e_o^2}\sqrt{n^2 - e_o^2} \tag{12}$$

then from (8)

$$A_1(e_o) = \frac{K_1K_2 - L_1L_2\ (n^2 - e_o^2)}{K_1^2 - L_1^2(n^2-e_o^2)} \tag{13}$$

$$A_2(e_o) = \left\{\frac{K_2L_1 - K_1L_2}{K_1^2 - L_1^2(n^2 - e_o^2)}\right\} x \quad \frac{1}{\sqrt{1 - e_o^2}} \tag{14}$$

Defining $A_3(e_o)$ as

$$\left.\begin{array}{l} n < e_o\ ;\ A_3(e_o) = A_2(e_o)\sqrt{1 - e_o^2}\sqrt{e_o^2 - n^2} \\ n > e_o\ ;\ A_3(e_o) = A_2(e_o)\sqrt{1 - e_o^2}\sqrt{n^2 - e_o^2} \end{array}\right\} \text{———} \tag{15}$$

Clearly $A_1(e_o)$ and $A_2(e_o)$ change continuously in the neighbourhood of the critical point as shown in Fig. 3.5, obtained using HAL, listed in Appendix 1.

Expanding $A_1(e_o)$ and $A_2(e_o)$ in a power series in $(e_o - n)$ around the critical point and considering only the first term in the expansion

$$A_1(n) = \frac{K_2(n)}{K_1(n)} = \frac{1 - 2n^2\left[n_1^2\ (\rho - 1) - 2n^2\ (\mu - 1)\right]}{D} \tag{16}$$

$$\left.\begin{array}{l} A_2(n) = \rho n_1^4\left[\sqrt{n_1^2 - n^2}\ \left\{\rho n_1^2 - 2n^2\ (\mu - 1)\right\} + \right. \\ \left. \qquad \sqrt{n_2^2 - n^2}\ \left\{n_1^2 + 2n^2\ (\mu - 1)\right\}\right] / D \end{array}\right\} \text{———} \tag{17}$$

$$\begin{array}{rl} D = & n^2\left[n_1^2(\rho - 1) - 2n^2(\mu - 1)\right]^2 \quad + \\ & \rho n_1^4\sqrt{1 - n^2}\sqrt{n_2^2 - n^2} \quad + \\ & \sqrt{1 - n^2}\sqrt{n_1 - n^2}\left[n_1^2 - 2n^2(\mu - 1)\right]^2 \end{array} \tag{18}$$

$A_2(n)$ is the head wave coefficient.

From (15), for $e_o < n$;

$$|A_o(e_o)| = A_1(e_o) - A_2(e_o)\sqrt{1 - e_o^2}\ \sqrt{n^2 - e_o^2} \tag{19}$$

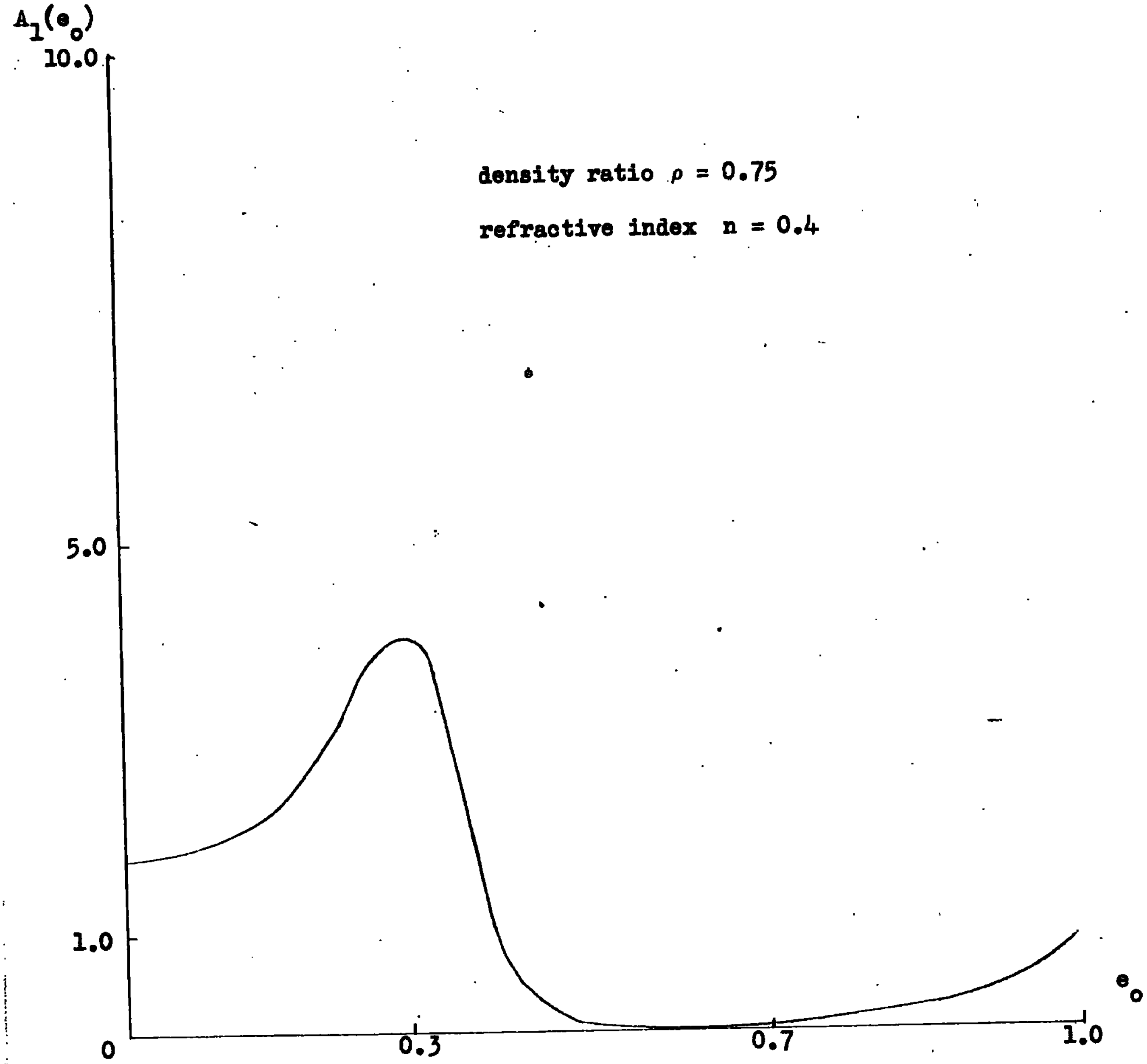

Fig. 3.5(a) **$A_1(e_o)$ against sine of angle of incidence**

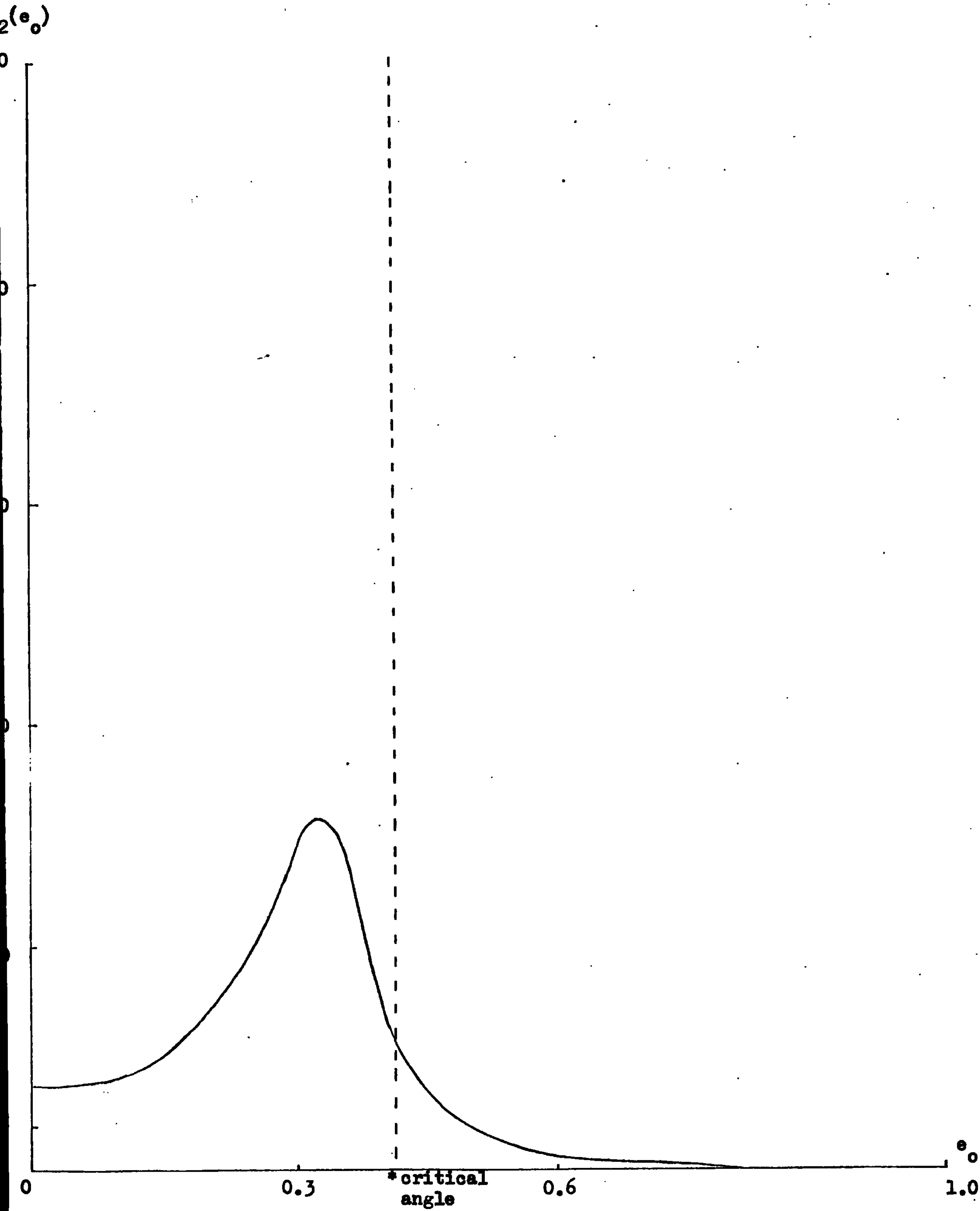

$\rho = 0.75$, $n = 0.42$

Fig. 3.5(b) $A_2(e_o)$ **against sine of angle of incidence**

$e_o > n$;

$$\left| A_o(e_o) \right| = \left[A_1^2(e_o) + A_2^2(e_o)(1 - e_o^2)(e_o^2 - n^2) \right]^{\frac{1}{2}} \qquad (20)$$

$$\left| A_o(e_o) \right| = \left[F_o(n) + F_1(n)(e_o^2 - n^2) + \ldots\ldots\ldots \right]^{\frac{1}{2}} \qquad (21)$$

where the $F_k(n)$ are functions only of the physical properties of the medium and are independent of e_o

For a change in the modulus of the reflection coefficient in the neighbourhood of the critical point,

$e_o < n$;

$$\frac{\partial A_o(e_o)}{\partial e_o} \longrightarrow \frac{n\sqrt{1-n^2}\; A_2(n)}{\sqrt{n^2 - e_o^2}} \qquad (22)$$

since in the limit as $e_o \longrightarrow n_-$ $\dfrac{\partial A_1(e_o)}{\partial e_o} \longrightarrow 0$

$e_o > n$;

$$\frac{\partial \left| A_o(e_o) \right|}{\partial e_o} \longrightarrow \frac{n\, F_1(n)}{\sqrt{F_o(n)}} \quad \text{in lim as } e_o \rightarrow n \qquad (23)$$

In the limit as $e_o \rightarrow n-$ $\dfrac{\partial A_o(e_o)}{\partial e_o} \longrightarrow \infty$

while $\lim\limits_{e_o \rightarrow n+} \dfrac{\partial \left| A_o(e_o) \right|}{\partial e_o}$ is constant.

Thus the derivative of the amplitude against angle of incidence curve is discontinuous at the critical angle, indicating that the curve itself has a sharp point at this angle as can be seen in Fig. 3.3.

Identification of this cusp by examination of the amplitude curve should, therefore, give information about the refractive index, and hence the velocities of the two media.

It can be seen from Fig. 3.6 that the reflected amplitude is sensitive to the density ratio between the two media. The plane wave approximation, however, has serious drawbacks. From Fig. 3.3 it is obvious that as $e_o \rightarrow 1$, $\left| A_o(e_o) \right| \longrightarrow 1$, i.e. as grazing

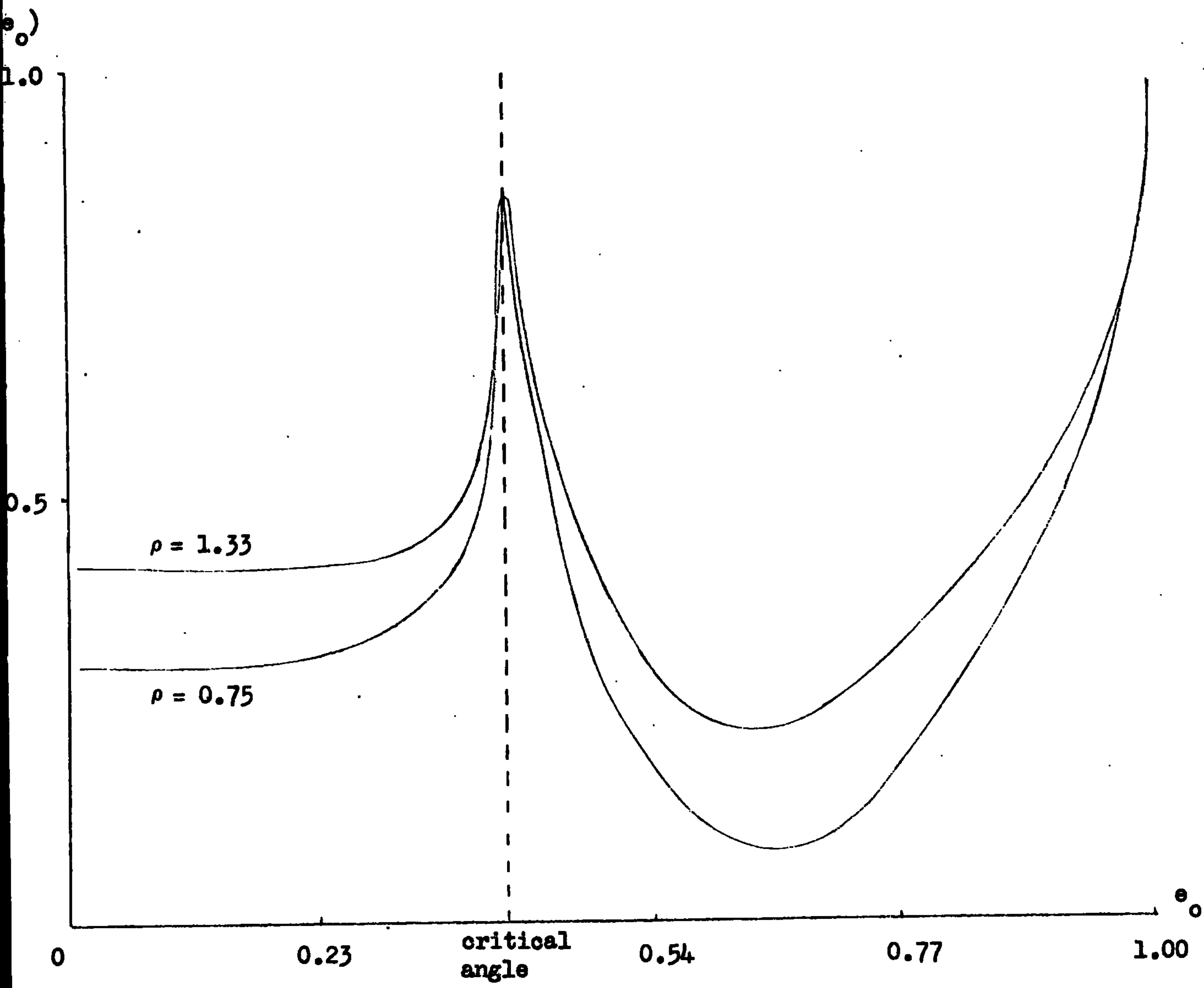

$\rho = \rho_2/\rho_1$, density ratio

Fig. 3.6 Numerical Solution - Density Dependence

incidence is approached the reflected amplitude increases to that of the incident wave. Examination of the phase of the reflected wave (Ref. 3.9), shows that it is π radians out of phase with the incident wave. Hence at grazing incidence the reflected wave completely cancels out the incident wave and no energy is propagated along the boundary, which is clearly incorrect.

Analysis using geometric ray theory (Ref. 3.10) gives zero amplitude for the head wave because the analysis itself necessitates a zero order approximation, while the head wave is a second order effect (Ref. 3.11). To obtain more meaningful results a more realistic wave must be chosen.

Although the behaviour of reflected plane waves discussed above beyond the critical angle is physically unreal the mathematical expressions derived above relating reflection coefficient to angle of incidence,density ratio, etc., are still valid in the super-critical region, in that they now refer complex angles and are themselves complex quantities. As the following analysis employs plane waves to investigate the exact nature of super-critical reflection the validity of these expressions is obviously important.

Spherical Waves

The purpose of this analysis is to approach the problem discussed above, beginning in this case with a spherical instead of a plane wave front. Mathematically, however, the technique used is to expand the spherical wave into plane waves following Weil (Ref. 3.12). The difficulty of the reflection of a spherical wave at a plane interface arises from the difference between the symmetry of the wave and the form of the boundary.

Introducing a cylindrical co-ordinate system, r, z, ϕ, with an acoustic source placed at $r = o$, $z = z_o$, the interface lies in the $z = o$ plane (Fig. 3.7).

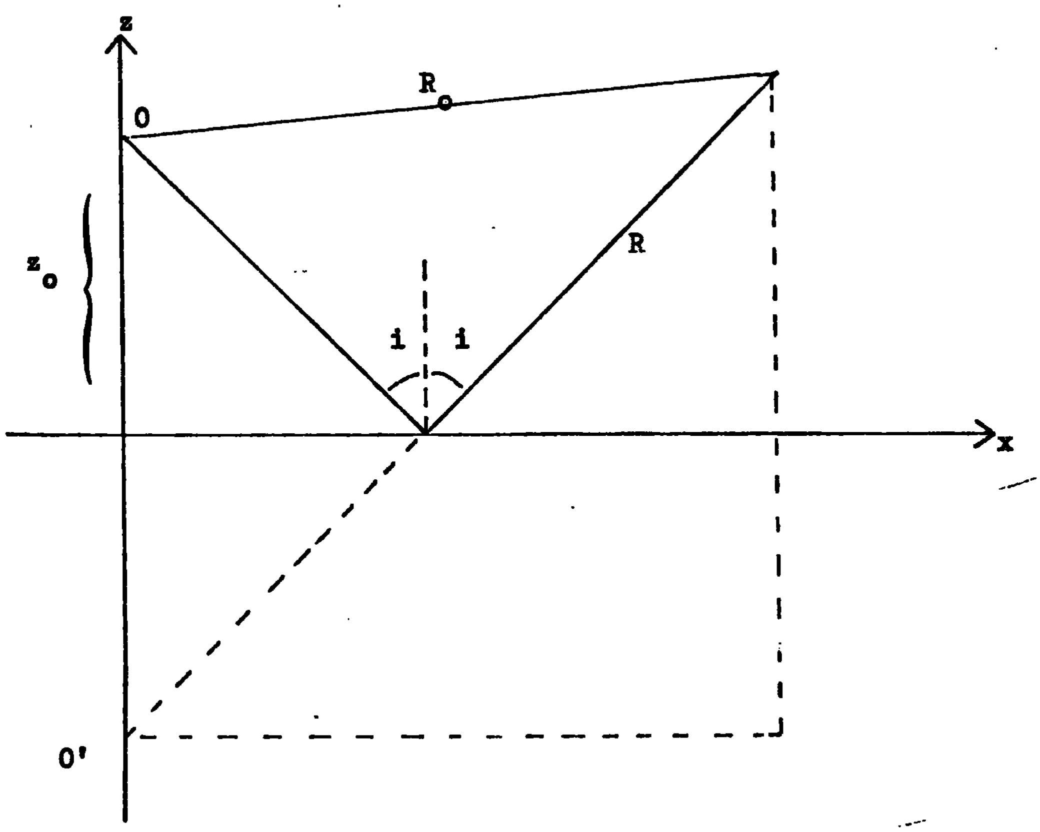

Fig. 3.7 Cylindrical Co-ordinate System

In this instance the solution is independent of ϕ.

Denoting

i) displacement in the r-direction as u

ii) displacement in the z-direction as w

and defining a longitudinal wave potential $-\Phi$ and transverse potential Ψ, so that the vector potential $\underline{\Psi}$ in (1) takes the form curl $(0,0,\Psi)$, it follows that

$$\left.\begin{aligned} u &= \frac{\partial \Phi}{\partial r} + \frac{\partial^2 \Psi}{\partial r\,\partial z} \\ w &= \frac{\partial \Phi}{\partial z} + \frac{\partial^2 \Psi}{\partial z^2} - \nabla^2 \Psi \end{aligned}\right\} \qquad (24)$$

Assuming the incident longitudinal wave has potential

$$\phi^{o} = R_o^{-1} \exp\left[jkR_o - jwt\right] \qquad (25)$$

where R_o is the distance from the source

$$R_o = \sqrt{r^2 + (z - z_o)^2}$$

and that there is no incident transverse wave we obtain, omitting the time term and assuming unit initial amplitude, the spherical wave potential, given as exp $(jkR)/R$, which can be expanded in terms of plane waves, by use of a double Fourier integral in terms of x and y, where

$$r = \sqrt{x^2 + y^2} \qquad \text{(Ref. 3.13)}$$

If, for simplicity, the source is placed at the origin, then in the plane z = o, the acoustic potential may be written as

$$\frac{\exp(jkr)}{r} = \iint_{-\infty}^{\infty} A(k_x,k_y) \exp\left[j(k_x x + k_y y)\right] dk_x dk_y \qquad (26)$$

Using the Fourier transform property, (Ref. 3.14), $A(k_x,k_y)$ is given by,

$$(2\pi)^2 A(k_x,k_y) = \iint_{-\infty}^{\infty} \frac{\exp(jkr)}{r} \exp\left[-j(k_x x + k_y y)\right] dk_x dk_y \quad (27)$$

Transforming into polar co-ordinates

$$\left.\begin{array}{ll} k_x = q\cos\psi & k_y = q\sin\psi \\ x = r\cos\phi & y = r\sin\phi \\ dxdy = rdrd\phi & \end{array}\right\} \qquad (28)$$

then (27) becomes

$$(2\pi)^2 A(k_x,k_y) = \int_0^{2\pi} d\phi \int_0^{\infty} \exp\left[jr\left\{k - q\cos(\psi-\phi)\right\}\right] dr \qquad (29)$$

The integral over r is straightforward and by assuming a slightly absorbing medium, so that the imaginary part of the wave number is positive, (Ref. 3.15), the substitution of the upper limit (∞), yields zero, giving

$$(2\pi)^2 A(k_x,k_y) = j\int_0^{2\pi} \frac{d\phi}{\left[k - q\cos(\psi-\phi)\right]}$$

$$= j/k \int_0^{2\pi} \frac{d\phi}{\left[1 - q/k\cos(\psi-\phi)\right]} \qquad (30)$$

From the Table of Integrals (Ref. 3.16)

$$A(k_x,k_y) = \frac{j}{2\pi} \frac{1}{\sqrt{k^2 - q^2}} \qquad (31)$$

From (28), $q = \sqrt{k_x^2 + k_y^2}$

$$\Longrightarrow A(k_x,k_y) = j/2\pi\sqrt{k^2 - k_x^2 - k_y^2} \qquad (32)$$

Thus (26) becomes

$$\frac{\exp(jkr)}{r} = \frac{j}{2\pi} \iint_{-\infty}^{\infty} \frac{\exp\left[j(k_x x + k_y y)\right]}{\sqrt{k^2 - k_x^2 - k_y^2}} dk_x dk_y \qquad (33a)$$

This equation describes the potential field in the x-y plane (z = o) and can be continued into space (i.e. for the source not in the plane of the interface) by using Fourier integrals (Ref. 3.17)

Each Fourier component then corresponds to a plane wave in space. In exact terms, this continuation is achieved by adding to the exponent in the integround $\pm jk_z . z$, where

$$k_z = \sqrt{k^2 - k_x^2 - k_y^2} \qquad (33b)$$

The positive quantity represents continuation in the halfspace, $z > o$.

The negative continuation denotes the halfspace $z < o$.

Thus for $z > o$;

$$\frac{\exp(jkR)}{R} = j/2\pi \iint_{-\infty}^{\infty} \exp\left[j(k_x x + k_y y + k_z z)\right] \frac{dk_x\, dk_y}{k_z}$$

for $z < o$;

$$\frac{\exp(jkR)}{R} = j/2\pi \iint_{-\infty}^{\infty} \exp\left[j(k_x x + k_y y - k_z z)\right] \frac{dk_x\, dk_y}{k_z} \qquad (34)$$

These equations (34) represent the formulae for expansion of a spherical wave into plane waves each exponent representing a plane wave propagating in a direction given by the components of the wave number.

The integration over k_x and k_y may be replaced by integration over θ and ϕ, where

$$\left.\begin{aligned} k_x &= k \sin\theta \cos\phi \\ k_y &= k \sin\theta \sin\phi \\ k_z &= k \cos\theta \end{aligned}\right\} \qquad (35)$$

as illustrated in Fig. 3.8.

The integral with respect to ϕ is between 0 and 2π, whilst that over θ is not limited to only the real values of θ. From (33b) when $k_x = k_y = o$, $k = k_z$

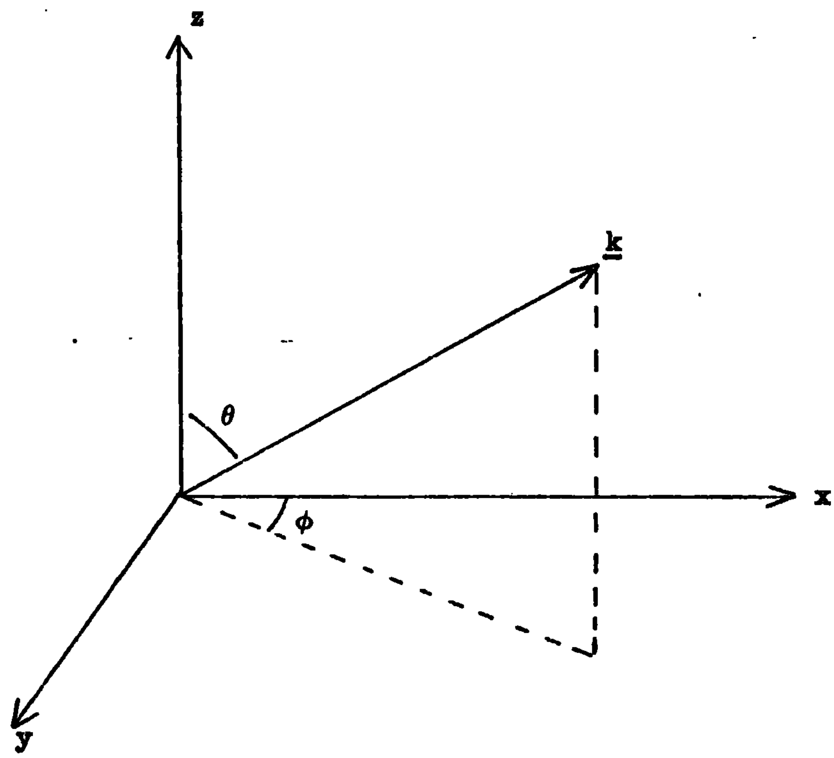

Fig. 3.8 **Spherical Co-ordinate System**

and from (35)

$\Rightarrow \theta = 0.$

When $k_x, k_y \longrightarrow \pm \infty$, $k_z \longrightarrow j\infty$

$\Rightarrow \theta \longrightarrow (\pi/2 - j\infty).$

Noting that the Jacobian of the co-ordinate transformation is given by

$$|J| = \begin{vmatrix} \frac{\partial x}{\partial u} & \frac{\partial x}{\partial v} \\ \frac{\partial y}{\partial u} & \frac{\partial y}{\partial v} \end{vmatrix} \qquad \begin{aligned} x &= \phi(u,v) \\ y &= \psi(u,v) \end{aligned}$$

where

$$\int_S f(x,y)\, d(x,y) = \int_{S^*} f\left[\phi(u,v), \psi(u,v)\right] d(u,v)\, |J| \qquad (36)$$

From (35) we obtain

$$dk_x\, dk_y = k^2 \sin\theta \cos\theta\, d\theta\, d\phi$$

$$\Rightarrow \frac{dk_x\, dk_y}{k_z} = k \sin\theta\, d\theta\, d\phi$$

Equation (33) may thus be rewritten

for $z \geq 0$;

$$\frac{\exp(jkR)}{R} = \frac{jk}{2} \int_0^{\pi/2 - j\infty} \int_0^{2\pi} \exp\left[j(k_x x + k_y y + k_z z)\right] \sin\theta\, d\theta\, d\phi$$

for $z \leq 0$;

$$\frac{\exp(jkR)}{R} = \frac{jk}{2\pi} \int_0^{\pi/2 - j\infty} \int_0^{2\pi} \exp\left[j(k_x x + k_y y - k_z z)\right] \sin\theta\, d\theta\, d\phi \qquad (37)$$

So, in addition to the waves in all possible directions, limited by $0 \leq \vartheta \leq 2\pi$, and $0 \leq \phi \leq \pi/2$, there are waves corresponding to complex values of θ, so called inhomogenous waves (Ref. 3.18)

At $\theta = \pi/2 - ja$, where a is real and positive corresponding to the integration path Γo, (Fig. 3.9), these inhomogeneous waves propagate with a shortened wavelength along a direction in the x-y plane (given by ϕ), and with an exponentially decreasing amplitude in the z-direction. Such waves are necessary since a superposition of plane waves alone would not produce a potential field having the required singularity as $R \to 0$, and still remain bounded at other points (Ref. 3.19).

<u>Evaluation of the Reflected Potential</u>

The total field is given by

$$\phi_T = \frac{\exp(jkR)}{R} + \phi_{refl}. \tag{38}$$

ϕ_{refl} may be represented as the superposition of plane waves, resulting from the reflection of the plane waves into which the original spherical wave was expanded. Upon reflection each plane wave will have an amplitude equal to the product of its original amplitude and the plane wave reflection coefficient.

i.e.

$$A_o(e_o) \exp\left[j(k_x x + k_y y + k_z (z + z_o)\right] \tag{39}$$

is the amplitude of each reflected plane wave given unit incident amplitude.

Hence,

$$\phi_{refl} = \frac{jk}{2} \int_0^{\pi/2-j\infty} \int_0^{2\pi} A_o(e_o) \exp\left[jk(x \sin\theta\cos\phi + y \sin\theta \sin\phi + (z + z_o)\cos\theta)\right] \sin\theta \, d\theta \, d\phi \tag{40}$$

The integration over ϕ reduces to a Bessel function of zero order (Ref. 3.20), and writing

$$x = r\cos\phi_1,$$

$$y = r\sin\phi_1,$$

then from (40), we have

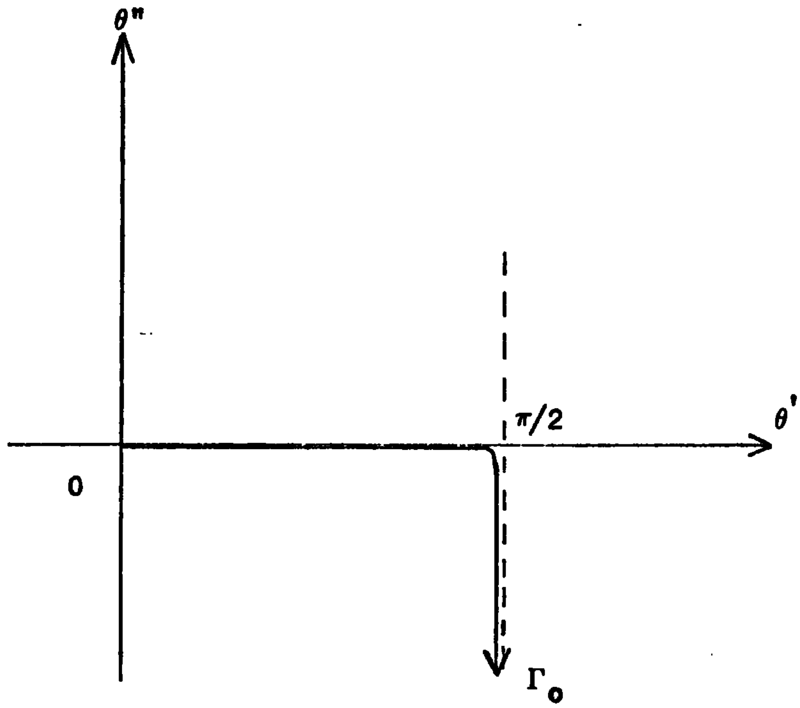

<u>**Fig. 3.9**</u> <u>**Complex Plane Diagram**</u>

$$\int_0^{2\pi} \exp\left[jk(x \cos\phi + y \sin\phi) \sin\theta\right] d\phi$$

$$= \int_0^{2\pi} \exp\left[jkr \sin\theta \cos(\phi - \phi_1)\right] d\phi \qquad \text{(41)}$$

$$= 2\pi J_o(u) \quad , \quad u = kr \sin\theta$$

Hence

$$\phi_{refl} = jk \int_0^{\pi/2 - j\infty} J_o(u) \exp\left[jk(z + z_o) \cos\theta\right] A_o(e_o) \sin\theta \, d\theta \qquad (42)$$

Rewriting $J_o(u)$ in terms of Hankel functions (Ref. 3.20)

$$J_o(u) = \tfrac{1}{2}\left[H_o^{(1)}(u) + H_o^{(2)}(u)\right] \qquad (43)$$

where $H_o^{(1)}(u)$ is a Hankel function of the first kind.

Now $H_o^{(2)}(e^{-j\pi} u) = -H_o^{(1)}(u)$ (Ref. 3.20) (44)

and $A_o(e_o) = A_o(-e_o)$, from (8).

The integral in (42) becomes the sum of two integrals. In that containing $H_o^{(2)}(u)$ if θ is replaced by $-\theta$, identical integrands are obtained, the limits of integration being respectively 0 to $\pi/2 - j\infty$ and $-\pi/2 + j\infty$ to 0.

Combining the two integrals

$$\phi_{refl} = \frac{jk}{2} \int_{-\pi/2 + j\infty}^{\pi/2 - j\infty} H_o^{(1)}(u) \exp\left[jk(z + z_o) \cos\theta\right] A_o(e_o) \sin\theta \, d\theta \qquad (45)$$

substituting for θ from (35)

$$\phi_{refl} = \frac{jk}{2} \int_{-\infty}^{\infty} A_o(e_o) \exp\left[jk(z + z_o)\sqrt{1 - e_o^2}\right] H_o^{(1)}(kre_o) \times \frac{1}{\sqrt{1 - e_o^2}} e_o \, de_o \qquad (46)$$

This expression may be evaluated by using the method of steepest descents, or saddle point integration. The method is described in detail by Morse and Feshbach (Ref. 3.21), but an outline is given below.

Method of Steepest Descents

This technique is used to evaluate integrals of the form

$$I = \int_S \exp\left[af(n)\right] \; F(n) \; dn \qquad (47)$$

where a has a large value.

The functions f(n), F(n) are arbitrary analytic functions of the complex variable, n, and S is the path of integration in the n-plane.

Within certain limits the path of integration in the complex plane may be deformed without changing the value of the integration. Knowing this, a path of integration may be chosen such that almost the entire value of the integral is given by a relatively short section of the path of integration (Ref. 3.22). Then the integrand can be replaced by another more simple function which approximates sufficiently closely to the original integrand over this region of the path.

The Hankel function in equation (46) may be extended asymtotically at the so-called saddle point (Ref. 3.23), but as the integration path cannot be deformed continuously into one passing through the saddle point without encountering pole and branch points, the initial single integral becomes several, the other contributions arising from the integrals around the pole and branch points. $\bar{\underline{\Phi}}^{o}$ represents the saddle point path contribution and physically corresponds to the acoustic potential of the truly reflected wave.

$\underline{\Phi}^{*}$ represents the contributions from the integration paths around the branch points (e_o=n) and corresponds to a P_{121} type head wave.

$\bar{\underline{\Phi}}^{z}$ represents the contribution of all the paths around other branch points and around the poles and corresponds to the remaining surface and other head waves.

Ignoring the last of these potentials,

$$\Phi = \Phi^{o} + \Phi^{*} \tag{48}$$

is the total reflected potential,

where from saddle point integration

$$\Phi^{o} = R^{-1} A_o(e_o) \exp(jkR) \tag{49}$$

$$\Phi^{*} = \frac{jnA_2(n)}{k\sqrt{r}\,L^{3/2}} \exp\left[jk(rn + (z + z_o)\sqrt{1-n^2})\right] \tag{50}$$

$A_2(n)$ is the head wave coefficient.

L is the distance travelled by the head wave in the lower medium.

i.e.
$$L = r - \frac{(z + z_o)\, n}{\sqrt{1 - n^2}} \tag{51}$$

The reflected amplitude is thus

$$R^{-1} \left|A_o(e_o)\right| \quad cm^{-1}$$

and the refracted amplitude is

$$\frac{nA_2(n)}{k\sqrt{r}\,L^{3/2}} \quad cm^{-1}$$

Assuming constant $(z + z_o)$ and defining A^o, A^*, ψ^o, ψ^* such that

$$\Phi^{o} = A^{o} \frac{\exp(j\,\psi^{o})}{(z + z_o)} \tag{52}$$

$$\Phi^{*} = A^{*} \frac{\exp(j\,\psi^{*})}{(z + z_o)} \tag{53}$$

i.e.

$$A^{o} = \left|A_o(e_o)\right| \sqrt{1 - e_o^{\,2}} \tag{54}$$

since
$$\frac{r}{(z + z_o)} = \frac{e_o}{\sqrt{1 - e_o^{\,2}}} \quad \text{(Fig. 3.7)} \tag{55}$$

and

$$A^* = \frac{nA_2(n)\ (1 - e_o^{\,2})}{k(z + z_o)e_o^{\,2}\left[1 - \frac{n\sqrt{1 - e_o^{\,2}}}{e_o\sqrt{1 - n^2}}\right]^{3/2}} \tag{56}$$

The amplitude of the truly reflected wave is given by the reflection coefficient multiplied by $\sqrt{1 - e_o^{\,2}}$.

The amplitude of the spherical waves in this solution increases very rapidly just prior to the critical point, and since $A_o(e_o)$ has a discontinuous derivative, equation (23), A^o similarly has a discontinuous derivative. The refracted wave amplitude is infinite at the critical point but decreases very rapidly as distance increases, tending to fall off as $1/r^2$ for large r.

Figures 3.10 and 3.11 show the shape of both the reflected and refracted amplitude curves. These plots were produced using programmes ASSRFLN and ASSRFRN listed in Appendix 1.

Interference will occur between the reflected and refracted waves giving a resultant potential which has different characteristics to either of its constituent members.

Write

$$\overline{\Phi} = \frac{A \exp (j\psi)}{(z + z_o)} \tag{57}$$

$$\text{where } A = \left[(A^o)^2 + (A^*)^2 + 2A^oA^* \cos(\psi^o - \psi^*)\right]^{\frac{1}{2}} \tag{58}$$

$$\text{and } \psi^o - \psi^* = k\left[R - rn - (z + z_o)\sqrt{1 - n^2}\right] + \text{am } \langle A_o(e_o)\rangle - \pi/2 \tag{59}$$

The amplitude curve for the remittant potential oscillates between an upper bound C_1 and a lower bound C_2, where

$$\left.\begin{aligned} C_1 &= A^o + A^* \\ C_2 &= A^o - A^* \end{aligned}\right\} \tag{60}$$

The frequency of oscillation depends on the frequency of the incident wave and the refractive index, as seen in Fig. 3.12. The mean curve is given by $\sqrt{(A_o)^2 + (A^*)^2}$ and analysis of the phase

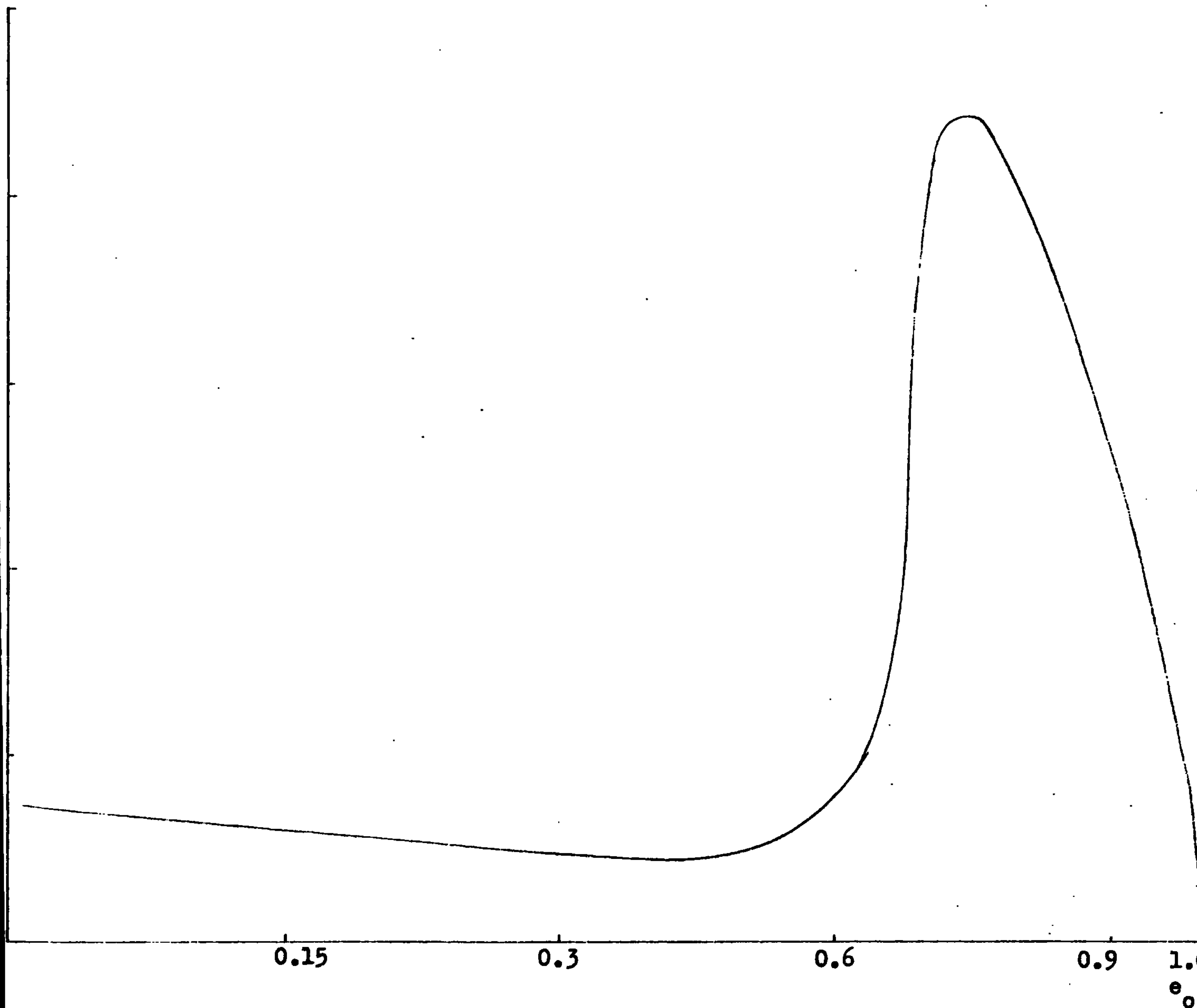

$n = 0.75$, $\rho = 1$, $b_1 = 0$

Fig. 3.10 **Reflected Amplitude Curve - Asymptotic Approximation**

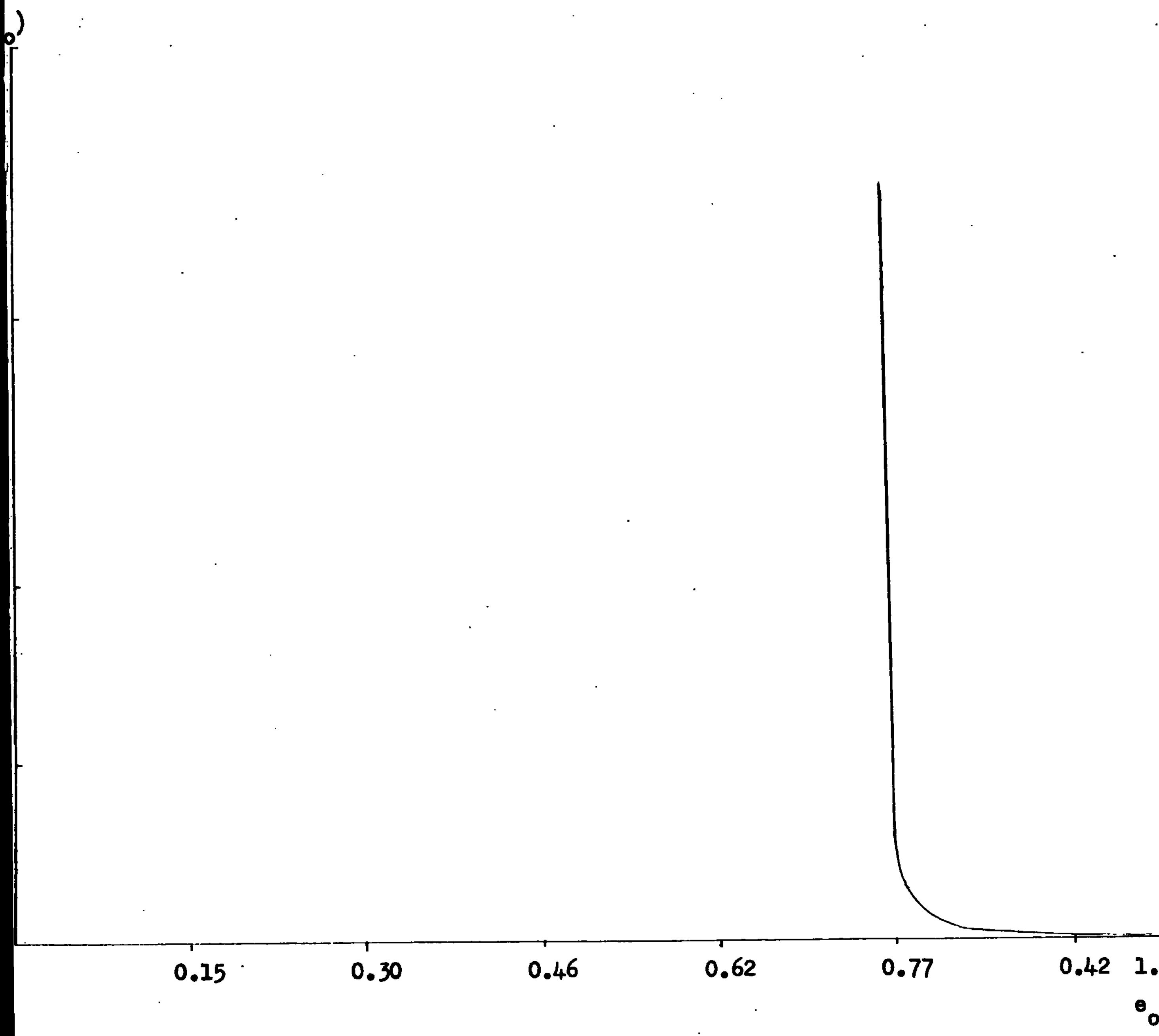

$n = 0.75$, $\rho = 1$, $b_1 = 0$.

Fig. 3.11 **Refracted Amplitude Curve - Asymptotic Approximation**

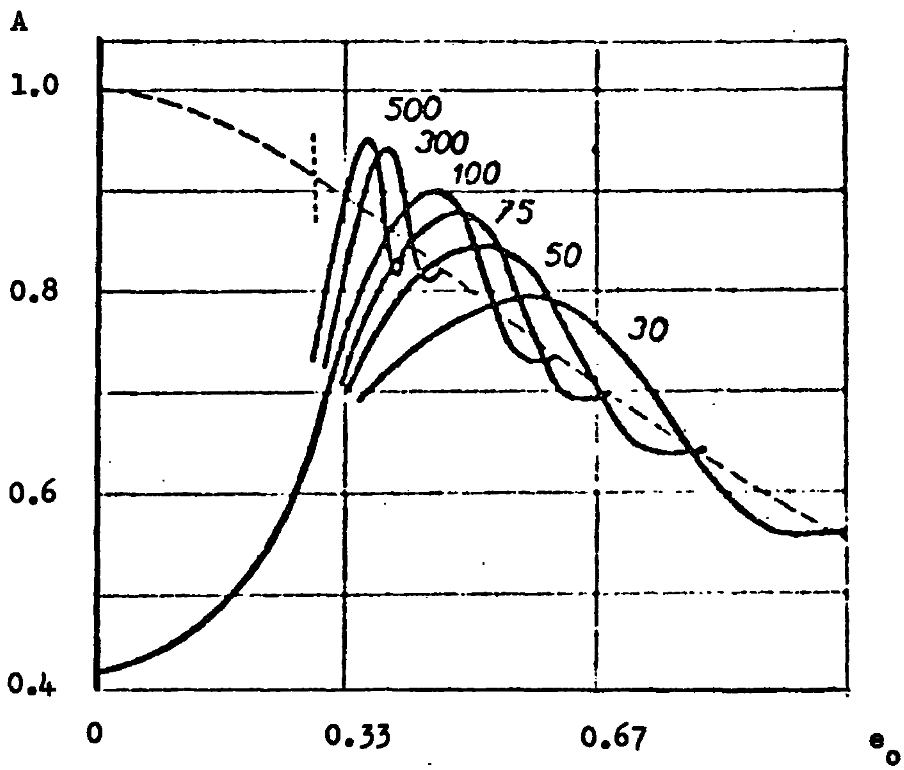

$$\frac{2\pi\nu(z + z_o)}{C} = 30,\ 50,\ 75,\ 100,\ 300,\ 500.$$

Fig. 3.12 **Frequency Dependence of Oscillations**

difference between the two waves shows that the amplitude of the oscillation decreases with increasing distance.

In the area close to the critical point equation (46) becomes invalid, since the method of steepest descents itself is invalidated when A is a rapidly varying function, as it is near the critical angle. (Ref. 3.24).

Applying a different path of integration and arranging A so that it does not vary so rapidly (equation (12)),

$$\underline{\bar{\Phi}} = R^{-1} \exp (jkR) \left\{ A_o(e_o) - e_o^3 \frac{A_2(e_o)}{kr} F(\alpha, \beta) \right\} \qquad (61)$$

where

$$F(\alpha,\beta) = j - \frac{2j}{\sqrt{\pi}} \int_{-\infty}^{\infty} \exp(-\phi^2) \left[\phi + \frac{(\alpha - \beta)}{2} \exp(j\pi/4) \times \sqrt{\phi + \alpha \exp(j\pi/4)} \times \sqrt{\phi - \beta \exp(j\pi/4)} \; d\phi \right. \qquad (62)$$

$F(\alpha,\beta)$ is obtained by employing the substitution technique used by Cerveny in Ref. 1.41.

and

$$\left.\begin{aligned} \alpha &= \sqrt{\frac{kr}{2e_o^3}} \sqrt{1-n^2} + \sqrt{1-e_o^2} \\ \beta &= \sqrt{\frac{kr}{2e_o^3}} \sqrt{1-n^2} - \sqrt{1-e_o^2} \end{aligned}\right\} \qquad (63)$$

where the branch of the Riemann surface on which the integral lies is given by

$$\left.\begin{aligned} &\text{am} \left\langle \sqrt{\phi + \alpha \exp(j\pi/4)} \right\rangle = \pi/8 \\ &\text{am} \left\langle \sqrt{\phi - \beta \exp(j\pi/4)} \right\rangle = \begin{cases} \pi/8 & e_o < n \\ 5\pi/8 & e_o > n \end{cases} \end{aligned}\right\} \qquad (64)$$

For n, e_o away from unity $\alpha \gg 1$

$$\Longrightarrow \quad F(\alpha,\beta) = \frac{kr}{R_o^{\,3}} \frac{\sqrt{1 - e_o^2}\,\sqrt{n^2 - e_o^2}}{\sqrt{\pi}} \int_{-\infty}^{\infty} \exp(-\phi^2) \times \frac{\sqrt{\phi - \beta \exp(j\pi/4)}}{\sqrt{-\beta \exp(j\pi/4)}}\, d\phi \tag{65}$$

$$\Longrightarrow \quad F(\alpha,\beta) = \frac{kr}{e_o^{\,3}} \sqrt{1 - e_o^2}\,\sqrt{n^2 - e_o^2}\,\mu_1(\beta) \tag{66}$$

where

$$\mu_1(\beta) = \frac{1}{\pi} \int_{-\infty}^{\infty} \exp(-\phi^2) \frac{\sqrt{\phi - \beta \exp(j\pi/4)}}{\sqrt{-\beta \exp(j\pi/4)}}\, d\phi \tag{67}$$

$$\mu_1(\beta) = \mu_1^R(\beta) + \mu_1^I(\beta)$$

as $\beta \longrightarrow \infty$ $\begin{cases} \mu_1^R(\beta) \longrightarrow 1 \\ \mu_1^I(\beta) \longrightarrow 0 \end{cases}$ (Ref. 3.25)

Thus

$$\underline{\Phi}^o = R^{-1} \exp(jkR) \left\{ A_1(e_o) - A_2(e_o) \sqrt{1 - e_o^2}\,\sqrt{n^2 - e_o^2}\, \mu_1(\beta) \right\} \tag{68}$$

for $e_o < n$;

$$\underline{\Phi}^o = R^{-1} \exp(jkR) \left\{ A_o(e_o) - A_3(e_o) \left[\mu_1^R(\beta) - 1 \right] - j\, A_3(e_o)\, \mu_1^I(\beta) \right\} \tag{69}$$

$e_o > n$;

$$\underline{\Phi}^o = R^{-1} \exp(jkR) \left\{ A_1(e_o) + A_3(e_o)\, \mu_1^I(\beta) - j\, A_3(e_o)\, \mu_1^R(\beta) \right\} \tag{70}$$

Hence

$e_o < n$;

$$A^o = \sqrt{1 - e_o^2}\left\{\left[A_o(e_o) - A_3(e_o)(\mu_1^R(\beta) - 1)\right]^2 + \left[A_3(e_o)\,\mu_1^I(\beta)\right]^2\right\}^{\frac{1}{2}} \qquad (71)$$

$$\psi^o = kR - \tan^{-1}\left(\frac{A_3(e_o)\,\mu_1^I(\beta)}{A_o(e_o) - A_3(e_o)\left[\mu_1^R(\beta) - 1\right]}\right) \qquad (72)$$

$e_o > n$;

$$A^o = \sqrt{1 - e_o^2}\left\{\left[A_1(e_o) + A_3(e_o)\,\mu_1^I(\beta)\right]^2 + \left[A_3(e_o)\,\mu_1^R(\beta)\right]^2\right\}^{\frac{1}{2}} \qquad (73)$$

$$\psi^o = kR - \tan^{-1}\left\{\frac{A_3(e_o)\,\mu_1^R(\beta)}{A_1(e_o) + A_3(e_o)\,\mu_1^I(\beta)}\right\} \qquad (74)$$

As $\beta \to \infty$, equations (71 - 74) give the asymptotic formulae already obtained (equation 54).

Critical Point

At the critical point itself, an indeterminacy arises in equation (50), and another expression for the totally reflected amplitude must be calculated.

From equations (66) and (67) for $\beta = 0$ and large α, $F(\alpha,\beta)$ differs depending on whether π is approached from $e_o < n$ or $e_o > n$.

$e_o \longrightarrow n-$

$$F(\alpha,\beta) \simeq 0.822\, \alpha^{3/2} \exp(j\pi/8) \tag{75}$$

$e_o \longrightarrow n+$

$$F(\alpha,\beta) \simeq 0.822\, \alpha^{3/2} \exp(j\, 5\pi/8) \qquad \text{(Ref. 3.25).} \tag{76}$$

So that

$e_o \longrightarrow n-$

$$\underline{\Phi}^o = R^{-1} \exp(jkR) \left\{ A_1(n) - \frac{0.822 A_2(n)\sqrt{n}\,(1 - n^2) \exp(j\pi/8)}{k(z + z_o)\sqrt{1 - n^2}} \right\} \tag{77}$$

$e_o \longrightarrow n+$

$$\underline{\Phi}^o = R^{-1} \exp(jkR) \left\{ A_1(n) - \frac{0.822 A_2(n)\sqrt{n}\,(1 - n^2) \exp(j5\pi/8)}{k(z + z_o)\sqrt{1 - n^2}} \right\} \tag{78}$$

which leads to

$e_o \longrightarrow n-$

$$A^o = \sqrt{1 - n^2} \left\{ \left[A_1(n) - \frac{0.759 A_2(n)\sqrt{n}\,(1 - n^2)}{\left\{ k(z + z_o)\sqrt{1 - n^2} \right\}^{\frac{1}{4}}} \right]^2 + \left[\frac{0.314 A_2(n)\sqrt{n}\,(1 - n^2)}{\left\{ k(z + z_o)\sqrt{1 - n^2} \right\}^{\frac{1}{4}}} \right]^2 \right\}^{\frac{1}{2}} \tag{79}$$

$e_o \longrightarrow n+$

$$A^o = \sqrt{1-n^2}\left\{\left[A_1(n) + \frac{0.314A_2(n)\sqrt{n}\,(1-n^2)}{\left\{k\,(z+z_o)\sqrt{1-n^2}\right\}^{\frac{1}{4}}}\right]^2 + \left[\frac{0.759A_2(n)\sqrt{n}\,(1-n^2)}{\left\{k\,(z+z_o)\sqrt{1-n^2}\right\}^{\frac{1}{4}}}\right]^2\right\}^{\frac{1}{2}} \tag{80}$$

The amplitude is thus discontinuous at the critical point, but as no head wave has been considered, this is only to be expected.

<u>Head Wave</u>

From (Ref. 3.26), the head wave potential is given by

$$\underline{\Phi}^* = \frac{-n^4A_2(n)}{kr^2}\,G\,(\delta,\eta)\,\exp\left[jk\,\left(rn + (z+z_o)\sqrt{1-n^2}\right)\right] \tag{81}$$

$$\text{where } G\,(\delta,\eta) = \frac{-4j}{\sqrt{\pi}}\int_0^\infty \exp\left[-\phi^2 - \sqrt{2}\,(1+j)\,\eta\,\phi\right] \times \sqrt{\phi}\;\times\sqrt{\phi + \delta\,\exp\,(j\,\pi/4)}\;\times\,\phi\,\times\,\frac{\delta}{2}\exp\,(j\,\pi/4)\;d\phi \tag{82}$$

$$\delta = \sqrt{\frac{2kr\,(1-n^2)}{n^3}} \qquad \eta = \sqrt{\frac{k(1-n^2)\,n}{2r}}\;L$$

For a refractive index not close to unity

$\delta >> 1$

$$G\,(\delta,\eta) \rightarrow \frac{-jr^{3/2}}{n^3L^{3/2}}\,\frac{\left[2\,\eta\,\exp\,(j\,\pi/4)\right]^{3/2}}{\Gamma\,(3/2)} \times \int_0^\infty \exp\left[-\phi^2 - \sqrt{2}\,\eta\,(1+j)\,\phi\right]\sqrt{\phi}\,d\phi \tag{83}$$

Write

$$\mu_2(\eta) = \frac{\left[2\eta\exp(j\,\pi/4)\right]^{3/2}}{\Gamma\,(3/2)} \int_0^\infty \exp\left[-\phi^2 - \sqrt{2}\,(1+j)\phi\right]\sqrt{\phi}\;d\phi \qquad (84)$$

$$G\,(\delta\,\eta) = \frac{-jr^{3/2}}{n^3 L^{3/2}}\,\mu_2(\eta)\,. \qquad (85)$$

At the critical point itself $\mu_2(\eta) = 0$

and for large r, $\mu_2(\eta) \to 1$.

Hence equation (81) may be rewritten

$$\Phi^* = \frac{jnA_2(n)\,\mu_2(\eta)}{k\sqrt{r}\,L^{3/2}} \exp\left[jk(rn + (z+z_o)\sqrt{1-n^2}\,)\right] \qquad (86)$$

At the critical point equation (86) is indeterminate since both $\mu_2(\eta)$ and L are equal to zero but $G(\delta,\eta)$ may be evaluated at $\eta = 0$ for large δ .

$$G(\delta,0) \simeq \frac{kr^2}{n}\,\frac{1.162\sqrt{n}\,(1-n^2)^{3/2}\exp\left[j\,7\pi/8\right]}{\left\{k(z+z_o)\sqrt{1-n^2}\right\}^{\frac{1}{4}}} \qquad (87)$$

giving, in general

$$\Phi^* = \frac{1.162A_2(n)\;\;n\,(1-n^2)^{3/2}}{\left\{k(z+z_o)\sqrt{1-n^2}\right\}^{\frac{1}{4}}} \exp\left[jk\,(rn + (z+z_o)\sqrt{1-n^2}) + j7\pi/8\right] \qquad (88)$$

and

$$A^* = \frac{nA_2(n)\,\mu_2(\eta)}{k\sqrt{r}\,L^{3/2}} \qquad (89)$$

$$\psi^* = k(rn + (z+z_o)\sqrt{1-n^2}) + \pi/2 + \mathrm{am} < \mu_2(\eta) > \qquad (90)$$

and at the critical point

$$A^* = \frac{1.162A_2(n)\sqrt{n}\,(1-n^2)^{3/2}}{\left[k(z+z_o)\sqrt{1-n^2}\right]^{\frac{1}{4}}} \qquad (91)$$

$$\psi^* = k(rn + (z+z_o)\sqrt{1-n^2}) + 7\pi/8 \qquad (92)$$

The amplitude of head waves decreases as r^{-p} where $p \geq 2$. p is greatest in the critical region but $\rightarrow 2$ as r increases. Figures 3.13 and 3.14 show the head wave amplitude for various acoustic parameters and were obtained using the HDGEN1 computer programme given in Appendix 1.

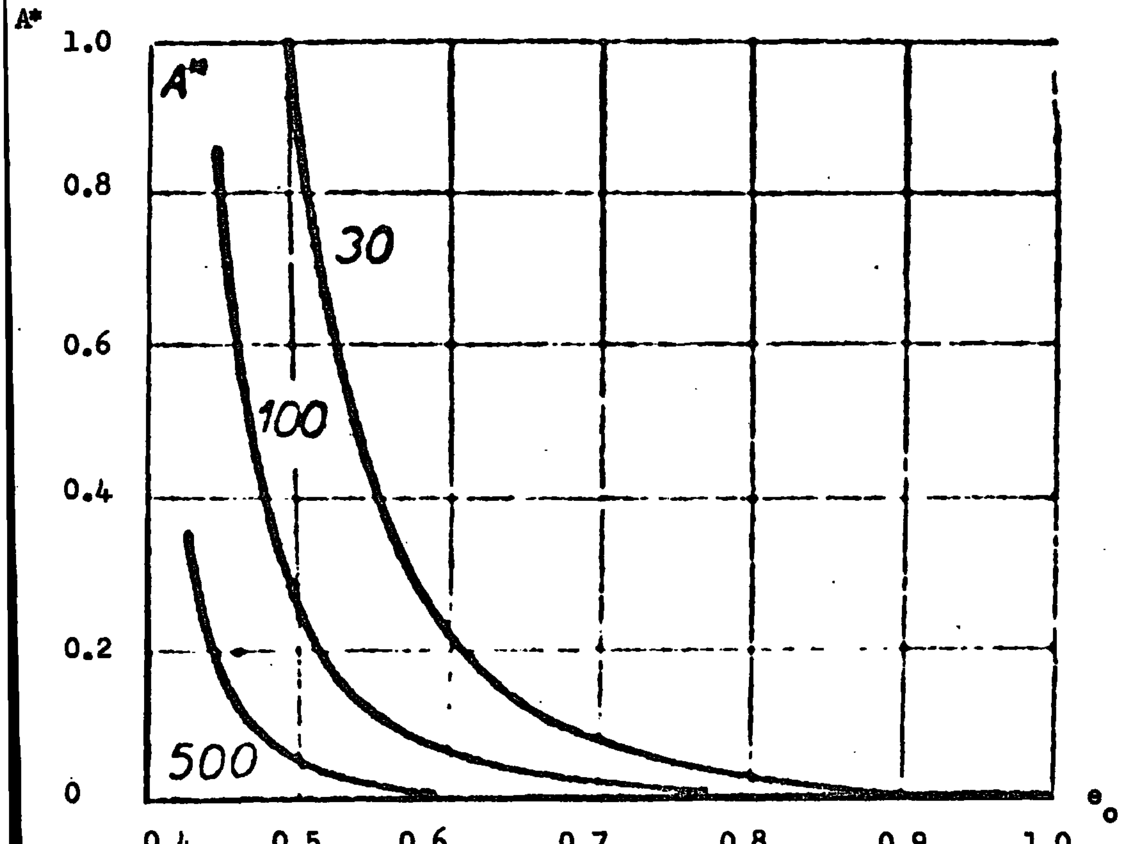

$k\ (z + z_o) = 30,\ 100,\ 500.$

Fig. 3.13 Head Wave Amplitude - Asymptotic Approximation

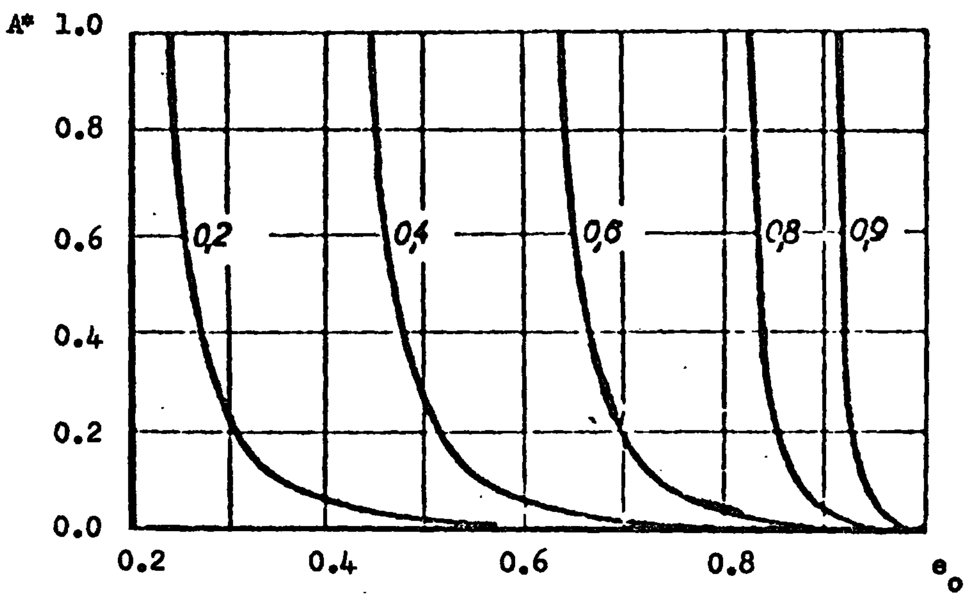

n = o.2, 0.4, 0.6, 0.8, 0.9.

Fig. 3.14 Head Wave Amplitude - Asymptotic Approximation

Total Reflection

For the totally reflected wave

$$\Phi = R^{-1} \exp(jkR) \left\{ A_1(e_o) - jA_3(e_o)\, \mu_1(\beta) \right\} + \frac{jnA_2(n)\, \mu_2(\eta)}{k\sqrt{r}\, L^{3/2}} \exp\left[jk(rn + (z + z_o)\sqrt{1 - n^2} \right] \tag{93}$$

$$\vec{\Phi} = \frac{\exp(jkR)}{(z + z_o)} \left\{ \sqrt{1 - e_o^2} \left[A_1(e_o) - j\, A_3(e_o)\, \mu_1(\beta) \right] + \frac{nA_2(n)\, (z + z_o)\, \mu_2(\eta)}{k\sqrt{r}\, L^{3/2}} \exp\left[jk(rn + (z + z_o)\sqrt{1 - n^2} - jkR + j\pi/2 \right] \right\} \tag{94}$$

Thus the total amplitude A, is given by

$$A = \sqrt{1 - e_o^2} \left\{ \left[A_1(e_o) + A_3(e_o)\, \mu_1^{I}(\beta) + \frac{nA_2(n)\sqrt{1 - e_o^2}}{k(z + z_o)\, e_o^2 \left(1 - \frac{n\sqrt{1 - e_o^2}}{e_o\sqrt{1 - n^2}} \right)^{3/2}} \times \left(\mu_2^{R}(\eta) \cos\nu - \mu_2^{I}(\eta) \sin\nu \right) \right]^2 + \left[-A_3(e_o)\, \mu_1^{R}(\beta) + \frac{nA_2(n)\sqrt{1 - e_o^2}}{k(z + z_o)\, e_o^2 \left(1 - \frac{n\sqrt{1 - e_o^2}}{e_o\sqrt{1 - n^2}} \right)^{3/2}} \left(\mu_2^{I}(\eta) \cos\nu + \mu_2^{R}(\eta) \sin\nu \right) \right]^2 \right\}^{\frac{1}{2}} \tag{95}$$

where

$$\nu = k(rn + (z + z_o)\sqrt{1 - n^2}) - kR + \pi/2 \tag{96}$$

Define

$$\Phi^{o}_{R} = \left[A_1(e_o) + A_3(e_o)\, \mu_1^{I}(\beta) \right] \sqrt{1 - e_o^2} \tag{97}$$

$$\Phi^{o}_{I} = -A_3(e_o)\, \mu_1^{R}(\beta) \sqrt{1 - e_o^2} \tag{98}$$

$$\underline{\Phi}^*_R = \frac{nA_2(n)\ (1 - e_o^2)}{k\ (z + z_o)\ e_o^2 \left(1 - \frac{n\sqrt{1 - e_o^2}}{e_o\sqrt{1 - n^2}}\right)^{3/2}} \left\{\mu_2^R(\eta)\ \cos\nu - \mu_2^I(\eta)\ \sin\nu\right\} \tag{99}$$

$$\underline{\Phi}^*_I = \frac{nA_2(n)\ (1 - e_o^2)}{k\ (z + z_o)\ e_o^2 \left(1 - \frac{n\sqrt{1 - e_o^2}}{e_o\sqrt{1 - n^2}}\right)^{3/2}} \left\{\mu_2^I(\eta)\ \sin\nu + \mu_2^R(\eta)\ \cos\nu\right\} \tag{100}$$

The amplitude of the reflected wave is

$$A^o = \left[(\underline{\Phi}^o_R)^2 + (\underline{\Phi}^o_I)^2\right]^{\frac{1}{2}} \tag{101}$$

The amplitude of the head wave is

$$A^* = \left[(\underline{\Phi}^*_R)^2 + (\underline{\Phi}^*_I)^2\right]^{\frac{1}{2}} \tag{102}$$

while the total amplitude, A, is given by

$$A = \left\{(\underline{\Phi}^o_R + \underline{\Phi}^*_R)^2 + (\underline{\Phi}^o_I + \underline{\Phi}^*_I)^2\right\}^{\frac{1}{2}} \tag{103}$$

These expressions are valid for all regions beyond the critical point, at which

$$\begin{aligned}\underline{\Phi} = R^{-1} \exp(jkR) \Bigg\{ A_1(n) &- \frac{0.822A_2(n)\sqrt{n}\,(1 - n^2)\ \exp(j5\pi/8)}{\left\{k(z + z_o)\sqrt{1 - n^2}\right\}^{\frac{1}{4}}} \\ &+ \frac{1.162A_2(n)\sqrt{n}\,(1 - n^2)^{3/2}}{\left[k\ (z + z_o)\sqrt{1 - n^2}\right]^{\frac{1}{4}}} \exp\left[jk\ (rn + (z + z_o)\sqrt{1 - n^2} + j7\pi/8\right]\end{aligned} \tag{104}$$

and since

$$R = rn + (z + z_o)\sqrt{1 - n^2} \quad \text{at the critical point}$$

$$\underline{\Phi} = R^{-1} \exp(jkR) \Bigg\{ A_1(n)\ \frac{-0.822A_2(n)\sqrt{n}\,(1 - n^2)}{\left\{k\ (z + z_o)\sqrt{1 - n^2}\right\}^{\frac{1}{4}}} \quad x \tag{105}$$

$$(1 - \sqrt{2}\,(1 + j/\sqrt{2})\ \exp\,(j5\pi/8)\Big| \qquad (105)$$

$$= R^{-1}\exp\,(jkR)\left\{A_1(n) - \frac{0.822A_2(n)\sqrt{\pi}\,(1 - n^2)\ \exp(j\,\pi/8)}{\left\{k\,(z + z_o)\sqrt{1 - n^2}\right\}^{\frac{1}{4}}}\right\} \qquad (106)$$

which is the same expression as equation (77) and thus the amplitude curve is continuous at the critical point.

$$A_{crit} = \sqrt{1 - n^2}\,\left\{A_1(n) - \frac{0.822A_2(n)\sqrt{\pi}\,(1 - n^2)\ \exp\,(j\,\pi/8)}{\left[k\,(z + z_o)\sqrt{1 - n^2}\,\right]^{\frac{1}{4}}}\right. \qquad (107)$$

Figure 3.15 shows the theoretical amplitude curve generated by the computer programme FINAL, listed in Appendix 1.

It can be seen from equations (71 - 79) and (95) that the amplitude of the reflected waves is dependent on three parameters.

i) the refractive index, $n_,\ = a_1/a_2$,

ii) the density ratio, $\rho = \rho_2/\rho_1$,

iii) the quantity, $k(z + z_o) = 2\pi\dfrac{(z + z_o)}{\lambda}$

Refractive Index

A variation in refractive index causes the position of the critical point to vary as can be seen in Figure 3.16, as is expected from plane wave theory.

Density Ratio

The only terms which involve the density ratio, ρ, are $A_1(e_o)$ and $A_2(e_o)$. The integral expressions derived for $\mu_1(\beta)$, $\mu_2(\eta)$ in equations (67) and (84) are density independent. As can be seen from Figure 3.17 a variation in density ratio hardly alters the position of the peak amplitude at all but does influence the shape of the amplitude curve to a discernible extent - the curve for a smaller density contrast being more sharply peaked than that of a higher density contrast.

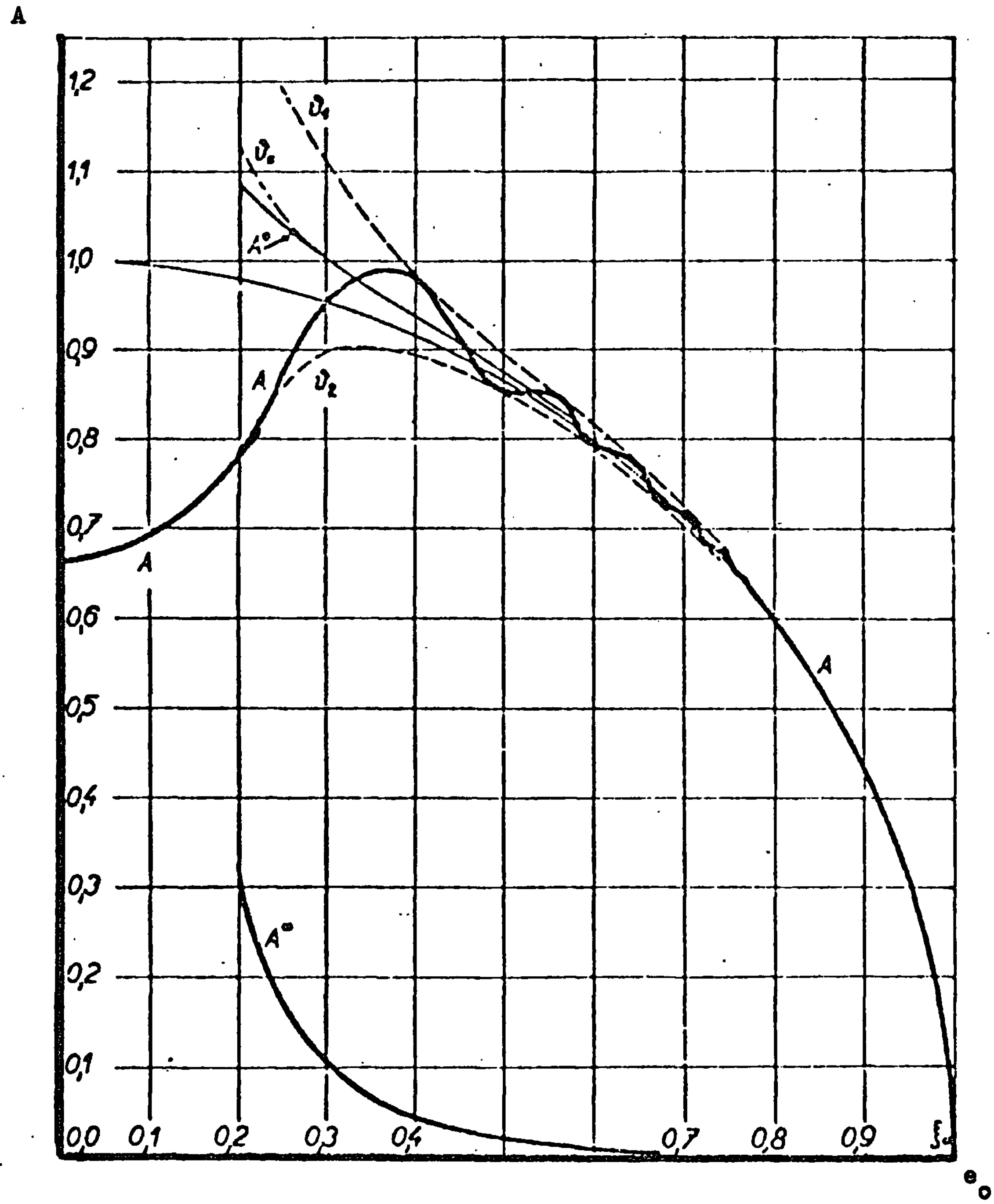

Fig. 3.15 Theoretical Amplitude Curve.

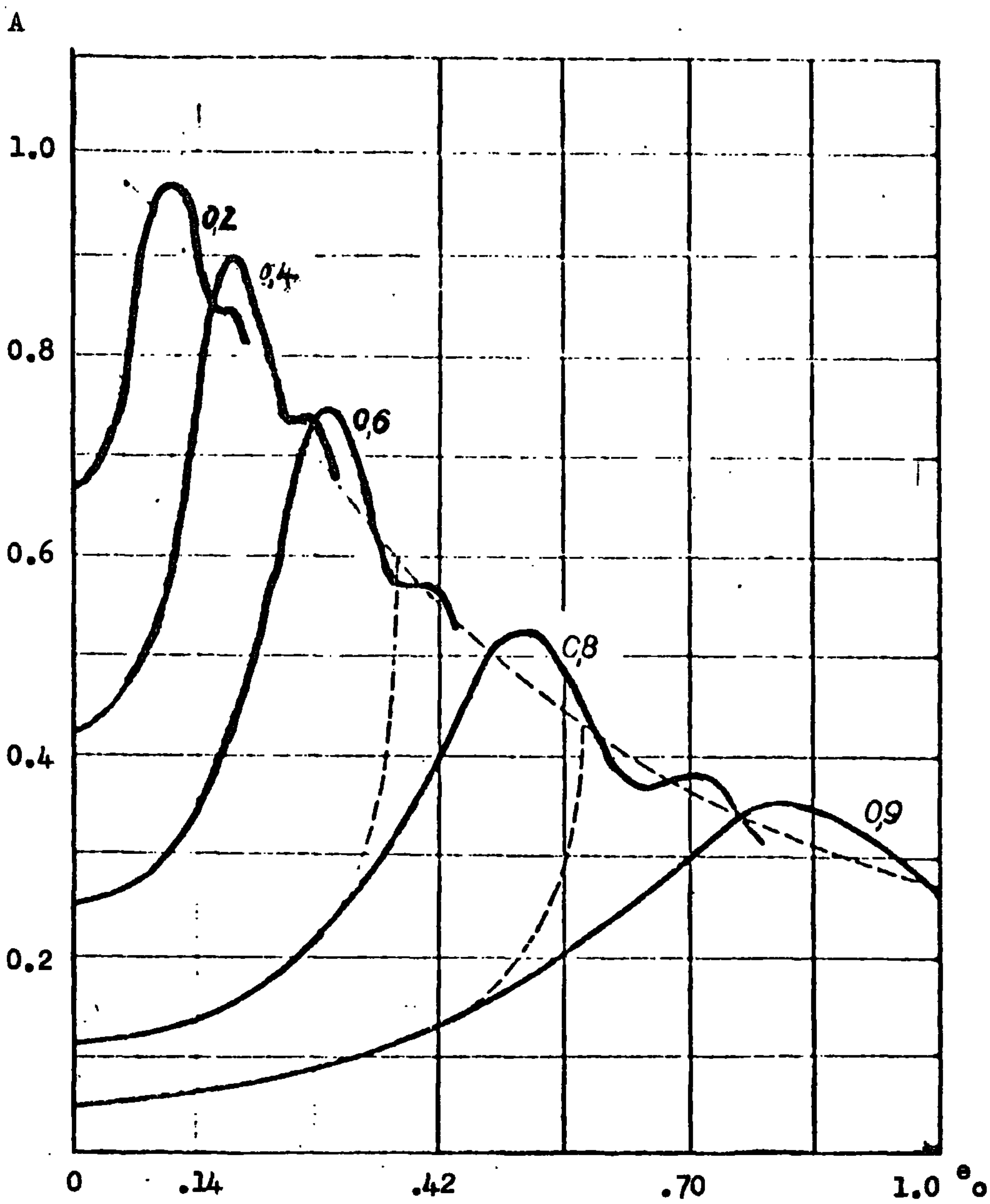

n = 0.2, 0.4, 0.6, 0.8, 0.9.

Fig. 3.16 Variation in Amplitude with Refractive Index, n.

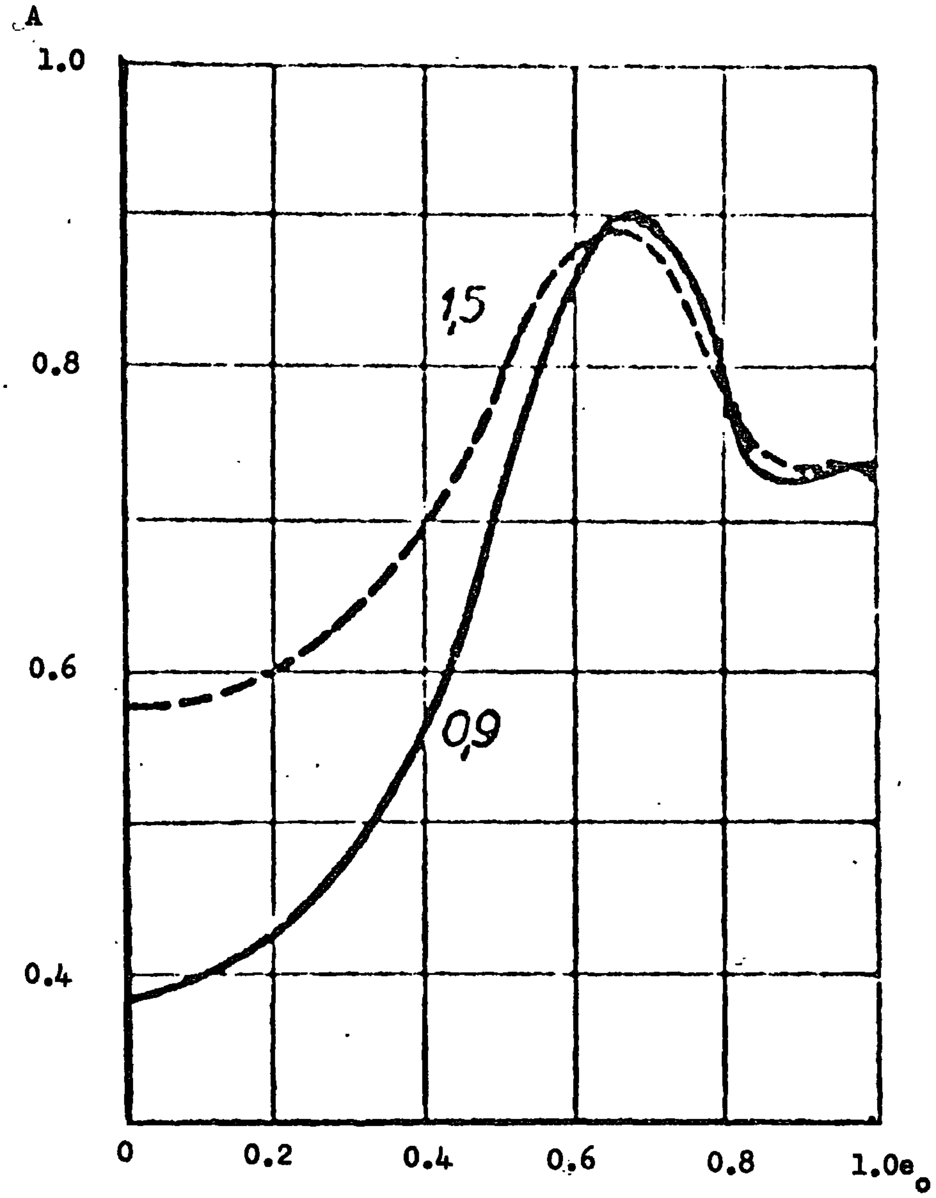

ρ = 0.9, 1.5

Fig. 3.17 Variation in Amplitude with Density Ratio.

$k(z + z_o)$

Neither $A_1(e_o)$ nor $A_2(e_o)$ depend on this quantity, but the shape of the amplitude curve and especially the position of the maximum amplitude changes considerably with a change in $k(z + z_o)$. In particular, for large k, or high frequency, the peak is sharpened and is moved nearer to the plane wave critical point position. (Fig. 3.18).

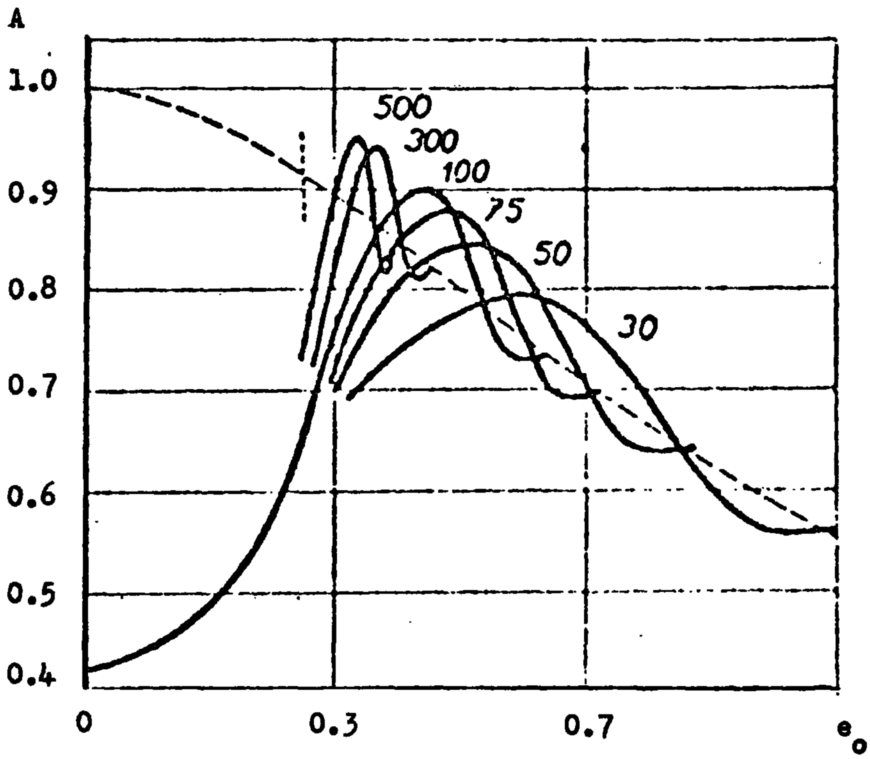

$k(z + z_o) = 30, 50, 75, 100, 300, 500.$

Fig. 3.18 Variation in Amplitude with $k(z + z_o)$.

Layered Media

In the case of reflection from an arbitrary number of layers, Brekhovskikh (Ref. 3.27) has shown that

$$Z_{1N}^{(n)} = \frac{Z_{1N}^{(n-1)} - j\, Z_N \tan\phi_n}{Z_N - j\, Z_{1N}^{(n-1)} \tan\phi_n} \quad Zn \qquad (108)$$

where

$Z_{1N}^{(n)}$ is the input impedance of the n^{th} layer,

$_n$ is the phase change in the n^{th} layer,

$_n$ is the acoustic impedance of the n^{th} layer

$$= \frac{\rho_n C_n}{\cos\theta_n}$$

where

ρ_n is the density of the n^{th} layer,

C_n is the velocity of the n^{th} layer,

θ_n is the angle of incidence at the n^{th} layer.

$$\phi_n = \alpha_n d_n$$

d_n is the thickness of the n^{th} layer,

$$\alpha_n = k_n \cos\theta_n$$

k_n is the wave number in the n^{th} layer.

The calculation of the input impedance is achieved by successive application of equation (108) and it can be shown that the reflection coefficient for a number of layers may be written as

$$R = 1 - \prod_{i=1}^{i=n} \left\{ \frac{Z_{i+1} + Z_N^{(i)}}{Z_i + Z_{1N}^{(i)}} \exp(-j\,\phi) \right\} \qquad (109)$$

The modified reflection coefficient for an arbitrary number of layers can thus be found by multiplying the expression for $A(e_o)$ in equation (95), by R, above, and dividing by the appropriate single layer plane wave reflection coefficient.

Inhomogeneous Layered Media

For an inhomogeneous layered medium, i.e. one in which the characteristics vary continually along one axis (the z-axis), provided that the variation with z is slow, the problem of wave reflection reduces to the solution of the wave equation

$$\nabla^2 \psi + k^2(z)\psi = 0 \tag{110}$$

$\psi = p/\sqrt{\rho}$ (Ref. 3.28)

Particularly this may be expressed in terms of the hypergeometric equation (Ref. 3.29) and may be solved explicitly for a transitional layer where the refractive index increases smoothly from one value to a larger one.

In this case

$$R = \frac{\Gamma(j\delta\cos\theta_o)\,\Gamma\left\{-j(\delta/2)\left[\cos\theta_o + \sqrt{\cos^2\theta_o - N}\right]\right\}}{\Gamma(-j\delta\cos\theta_o)\,\Gamma\left\{+j(\delta/2)\left[\cos\theta_o - \sqrt{\cos^2\theta_o - N}\right]\right\}} \times$$

$$\frac{\Gamma\left\{1 - j(\delta/2)\left[\cos\theta_o + \sqrt{\cos^2\theta_o - N}\right]\right\}}{\Gamma\left\{1 + j(\delta/2)\left[\cos\theta_o - \sqrt{\cos^2\theta_o - N}\right]\right\}} \tag{111}$$

where $N \equiv k(z + z_o)$

$\theta_o \equiv i$

CHAPTER FOUR

Processing

The data processing of the sonobuoy records obtained on Durham University Geological Science Department Geophysical Surveys in 1973 and 1974 may be divided into three parts.

i) Analogue playout of the Frequency Modulated (FM) tapes to a Variable Area Display (VAD) to obtain travel time information for reflection and refraction analysis programmes.

ii) Digitisation of these analogue records and subsequent amplitude investigation.

iii) Curve fitting and synthetic curve generating procedures.

The above processing was carried out on both the Durham University Departmental CTL Modular One computer and the Newcastle Universities Multiple Access Computer (NUMAC) IBM 360/67 and 370 machines.

Analogue Playout

The FM tapes recorded at sea on an EMIDATA instrumentation tape recorder by means of a V.H.F. link from sonobuoy to ship, were replayed on a "Geospace Instruments" Variable Area Display (VAD) unit. The original V.A.D. record made whilst at sea does not, usually, contain that portion of the signal corresponding to the direct or water wave arrival, if the sonobuoy was used in deep water (Fig. 4.1).

The V.A.D. record comprises only an arrival time range of 4.5 seconds, representing a water depth of 3.4 km, at normal incidence. In order to display arrivals beyond this time, a sweep delay facility is incorporated into the unit which delays the beginning of this 4.5 second sweep for up to 9 seconds in 1 second steps (Ref. 4.1).

Those sonobuoy records which were made in deep water where this facility had been used to permit examination of the bottom reflection were replayed without any sweep delay to obtain the direct arrival (Fig. 4.2). This was necessary to provide the water wave arrival time data needed for the Wide Angle Reflection programme (Appendix 1), (Ref. 4.2).

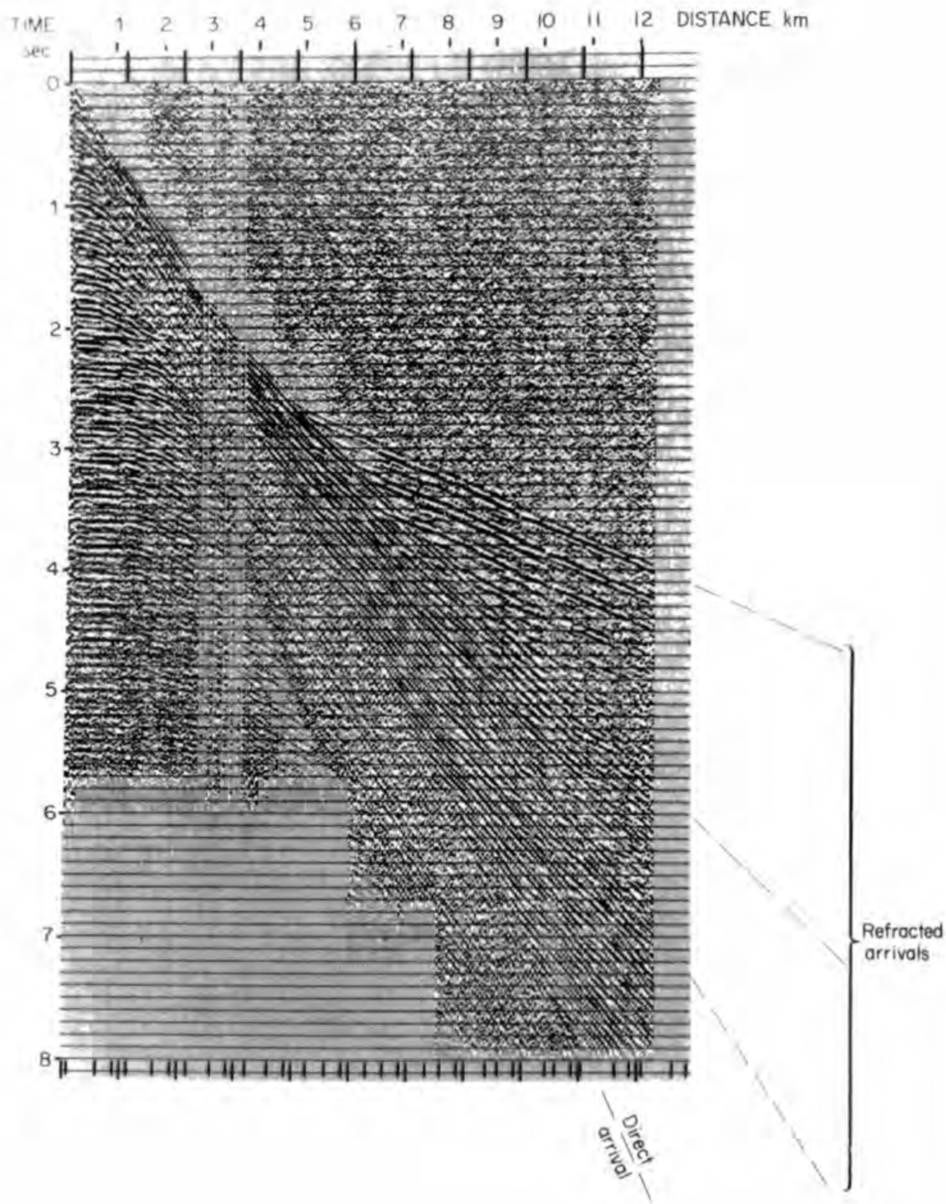

Fig. 4.1 Variable Area Display (V.A.D.) Record

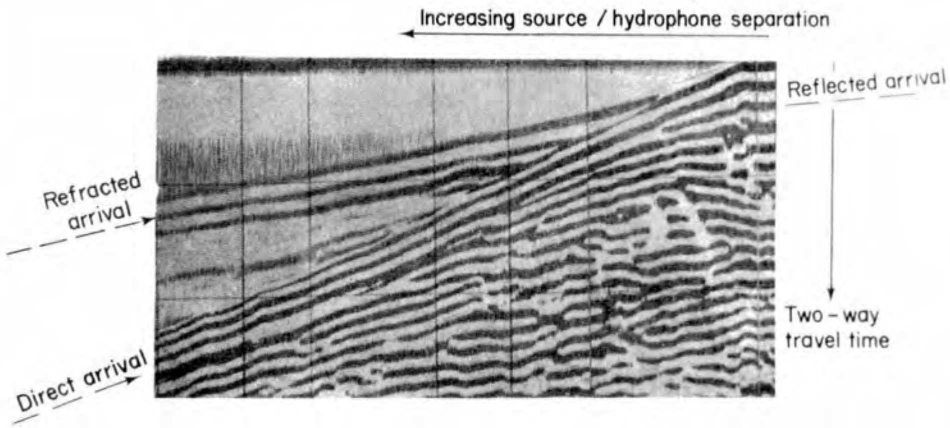

Fig. 4.2 **Outline of V.A.D. Arrivals**

On board ship, an electromagnetic log of both the ship's fore-and-aft and port-and-starboard velocities had been taken continuously and it was hoped that this knowledge of the ship's velocity through the water would be sufficiently accurate that the direct arrival times of the water wave could be calculated from this data for each sonobuoy run. An initial comparison showed that the ship's velocity relative to the sonobuoy was substantially different from that given by the E-M log, and thus all the records lacking the direct arrival were replayed to obtain corrected ship's velocities, using the surface water velocities appropriate to the area, as given in the standard tables (Ref. 4.3).

A comparison of the ship's E-M log velocity and that obtained from the water wave is given in Table 4.1.

Table 4.1

Sonobuoy No.	E-M Log Velocity Knots	Calculated Velocity Knots
1	6.2	7.09
2	5.5	5.88
4	5.0	5.21
5	4.7	4.93
6	5.3	5.78
9	4.1	4.26
11	5.7	6.09
17	4.9	5.13

Once the direct wave arrival had been obtained, each V.A.D. record was examined closely to determine the various reflecting horizons apparent on the ultra-violet sensitive paper (Ref. 4.4). A close reference was made to the continuous reflection profile immediately before the start of the sonobuoy run and also after its termination. In those instances where the acoustic basement appeared particularly rough, the continuous reflection profile which had been recorded but not displayed whilst the sonobuoy run was being made, was replayed to provide information on the dip of the bottom and sub-bottom reflecting horizons.

Those horizons discernible to the eye were transferred to tracing paper, in an effort to preserve the u-v sensitive records which aged fairly rapidly on exposure to light, and the displacements in terms of distance and time from the origin of the display measured (Fig. 4.3).

The origin of the display represents the instant of buoy drop and hence zero displacement. Horizontal displacements, proportional to separation of ship and sonobuoy, were measured at 0.05 second intervals, both for the direct and reflected arrivals. An example of the output of one such analysis is given in Table 2, (overleaf).

Reflection Processing on the 360

The information thus obtained was fed into the IBM 360/67 at Newcastle using the Durham batch processing facility. The Wide Angle Reflection programme (WAR - Appendix 1), developed from that written by Ewing, Le Pichon and Houtz (Ref. 4.5), requires the input of both direct and reflected arrival times, as mentioned above.

The programme utilised solves for interval velocities and thicknesses of N homogeneous layers with plane sloping interfaces, given a trial solution for the dip angles, which is obtained from the continuous reflection profiles made during the sonobuoy run.

The direct arrival times were calculated from the ship's velocity, which had itself been determined from the direct wave. The operation of the program may be explained by examining the single layer case. Defining:

T_o - vertical reflection time

T - reflection time at distance X, from the source

V - interval velocity in the layer

e - slope of the lower interface with respect to the upper.

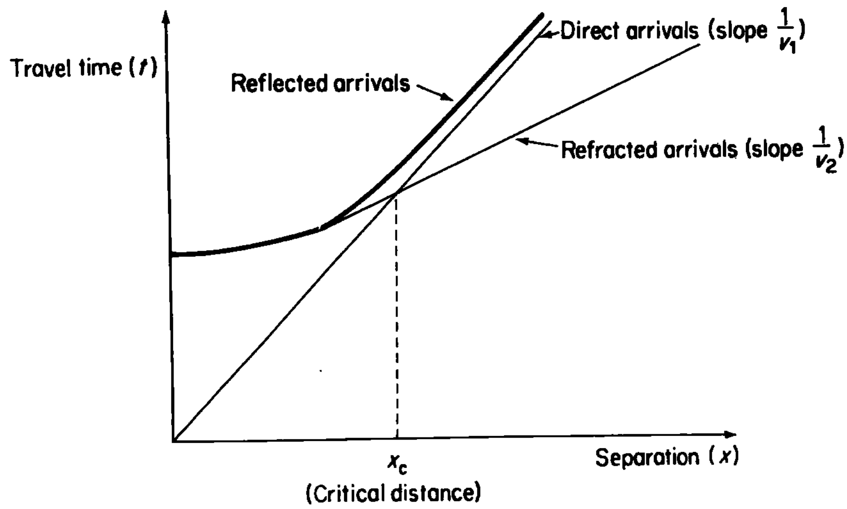

Fig. 4.3 Refraction Outline

Table 4.2 S13 Initial Analysis

Arrival Time (second)	Reflection Layer 1	Arrival Layer 2	Displacement Layer 3 (inches)
0.05	0.89	1.02	1.18
0.10	0.89	1.03	1.19
0.15	0.90	1.04	1.19
0.20	0.91	1.05	1.20
0.25	0.92	1.06	1.20
0.30	0.93	1.08	1.22
0.35	0.95	1.09	1.23
0.40	0.97	1.10	1.25
0.45	1.00	1.12	1.26
0.50	1.02	1.15	1.27
0.55	1.05	1.18	1.29
0.60	1.08	1.21	1.32
0.65	1.10	1.24	1.33
0.70	1.13	1.26	1.35
0.75	1.16	1.29	1.37
0.80	1.20	1.32	1.40
0.85	1.24	1.35	1.42
0.90	1.27	1.38	1.45
0.95	1.31	1.42	1.48
1.00	1.34	1.45	1.50
1.05	1.38	1.48	1.53

Then

$$T^2 = T_o^2 + X^2/V^2 - \frac{2T_oX}{V} \sin e \qquad (1)$$

from simple geometric ray theory (Ref. 4.6).

Given a direct wave travel time, D, and a horizontal water velocity, VH,

$$T^2 = T_o^2 + \frac{D^2 \times VH^2}{V^2} - \frac{2T_o.D.VH}{V} \sin e \qquad (2)$$

For the water layer, the interval velocity is known to be a slowly varying function (Ref. 4.7), and the solution to the water layer case can give X(V), the separation of ship and sonobuoy by entering the correct water interval velocity found from Matthew's Tables.

Assuming plane layering (e = o) equation (2) becomes

$$T^2 = T_o^2 + D^2\left(\frac{VH}{V}\right)^2 \qquad (3)$$

which is the equation of a straight line in D^2 and T^2, the velocity being obtained from the square root of the slope of the line. Hence, in its simplest form, the interval velocity for a given reflection may be found by a least squares analysis of the D^2 against T^2 plot (Ref. 4.8).

In fact, this method leads to large errors since the least squares fit is that of a tangent to an extremity of a curve, beyond which there is no data.

A solution is obtained for each layer proceeding downwards, and each layer is reduced to a single flat layer case, using the solutions obtained for the upper layers to remove their effects.

For each layer below the water layer the procedure outlined below is applied:

1) The angle of emergence, b, of the sound ray at the sea water interface, is obtained at each data point, by differentiation of a fourth order polynomial fitted to the original T/X data by least squares, according to $\sin b/V_1 = dT/dX$ (4)

2) This emergence angle is used to find the theoretical time corresponding to the travel in the layers above the one of interest, using as a first approximation the trial velocity and corresponding slope of the previous layer.

3) This computed time is subtracted from the observed time to give a reduced travel time corresponding to the travel in the layer for which a solution is required. The equivalent reduced X distance along the upper interface of the layer is found in the same way.

4) The travel time in this layer is finally reduced to the flat layer case using equation (2) and by removing, at each data point, the value.

$$T_o^2 - \frac{2T_o X \sin e}{V}$$

to obtain the reduced times

$$T^2 = X^2/V^2 \qquad (5)$$

5) The velocity is obtained from a least squares fit of this equation.

6) The solution from (5) replaces the original trial solution, with the dip modified according to, $\tan e_{(2)} = \tan e_{a(2)} \cdot \frac{V_{(2)}}{V_{a(2)}}$, (2)
and the computation goes back to (2) for a second iteration.

7) Finally, the reduced times, $T^{1\,2}$, in the layer with the corresponding deviations from the least squares fit are calculated, as are the velocity and it standard deviation derived from the standard deviation of the slope of the T^2/X^2 line.

A detailed description of the operation of this programme is given in Appendix 2.

Refraction Analysis

Any refracting horizons prevent on the VAD record were analysed using a refraction analysis programme, TWAT (Fig. 4.3)(Appendix 1). This programme simply performs a linear regression to obtain the velocity statistics - slope, intercept and standard error - for one layer with corrections for overlying layers. In practice to obtain the best fit more than just the simple regression of time onto distance is used. Regressions of both distance onto time and reciprocal time onto distance are carried out (Appendix 1). A complete list of the output from TWAT for all the sonobuoy runs is given, together with the wide angle reflection velocities obtained from WAR is given in the next chapter.

Amplitude Analysis

For the amplitude analysis it was decided to use the Departmental Modular One computer normally employed for seismic array processing. The analogue records were digitised onto magnetic tape using a digitisation programme, STORE, listed in Appendix 1. In order to prevent saturation occurring on digitisation the analogue signals were fed through an anti-aliasing and gain control unit, whose gain could be adjusted manually to prevent saturation.

A level detection programme, LEVEL, (Appendix 1), was run on the computer at a saturation voltage level of ± 5V. This figure represents the maximum signal that can be exactly digitised by the Modular One; any signal greater than this value is stored as ± 5V, or in the 60dB dynamic range of the computer input as ± 1024. (Fig. 4.4).

The EMIDATA analogue deck was started up just prior to the instant of buoy drop and the teletype output of the Modular One printed any input channel (only channels 1-5 were used to transfer from analogue to digital tape), (Fig. 4.5), greater than ± 5V at any digitisation instant. The gain of the anti-aliasing and gain control filter was adjusted manually to give the maximum signal level at which

1
2
3
4
6

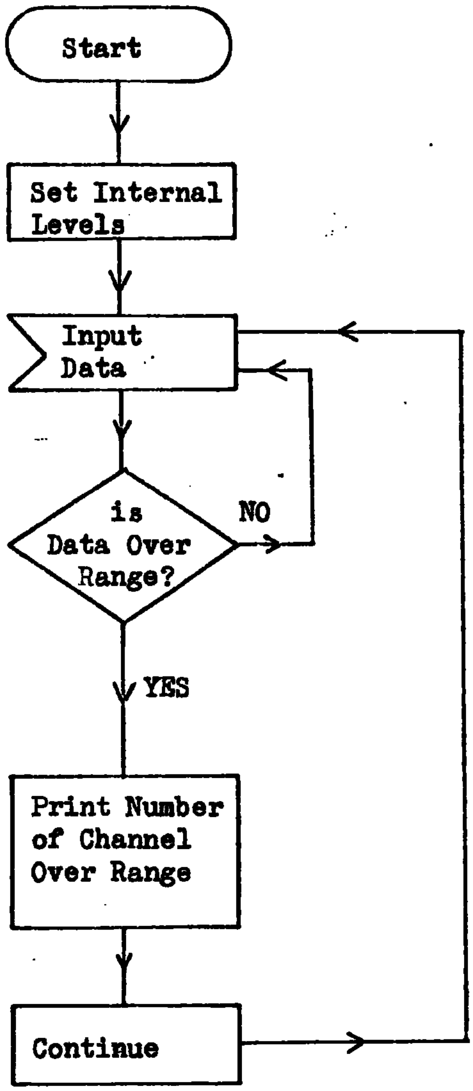

Fig. 4.4 Level Setting Programme - Flow Diagram

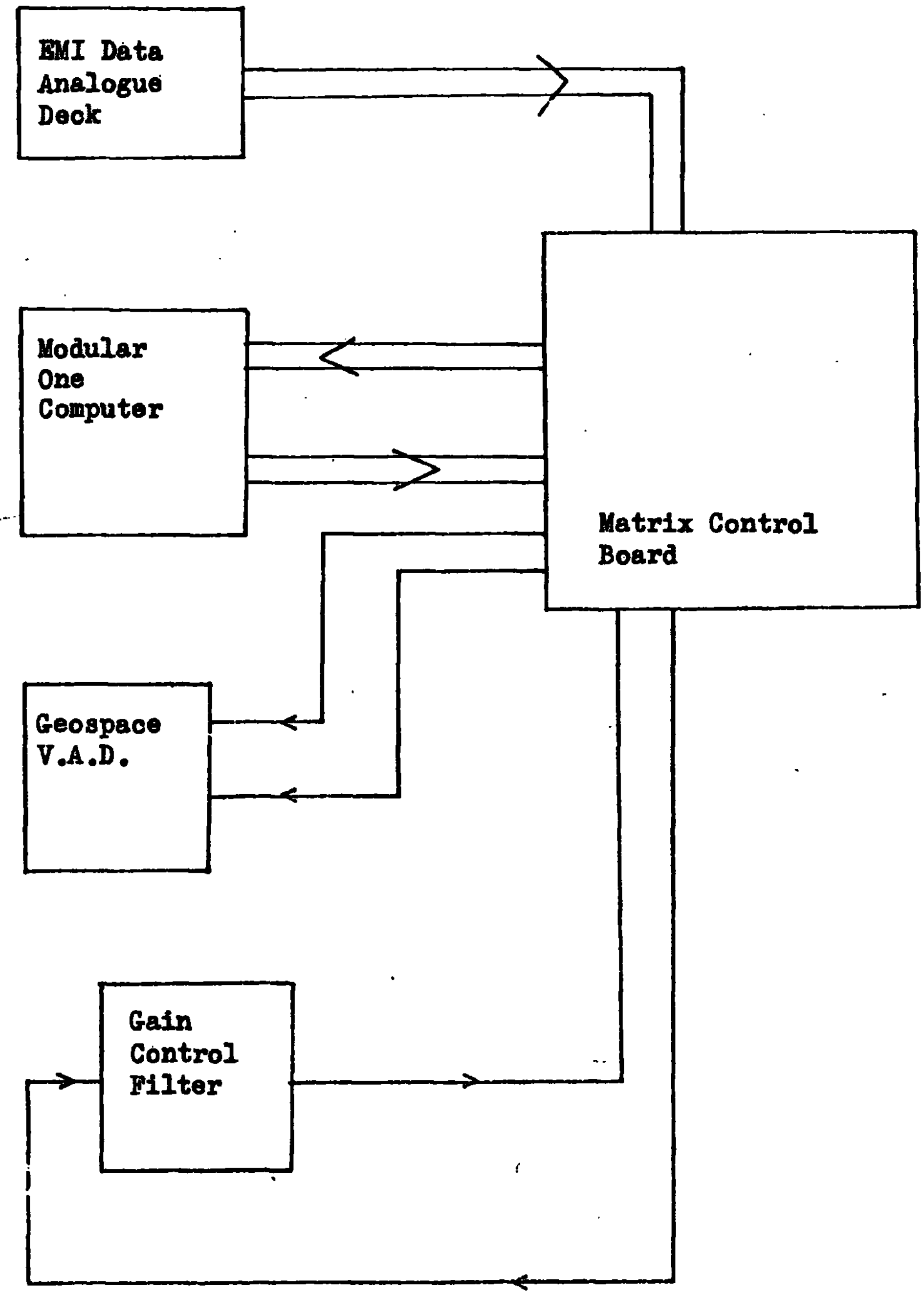

Fig. 4.5 Modular One/Analogue Link Up

saturation did not occur.

The analogue tape was then rewound to its initial pre-buoy drop position and the STORE programme loaded into the computer. The digital tape recorder, attached to the Modular One, was loaded with a tape, and a first file number written onto it to enable the STORE sequence operation to proceed.

The programme operates in the following fashion (Fig. 4.6):

On one analogue input channel is the shot instant command, which is recorded on board ship and governs the firing rate of the Bolt airgun system. It consists, essentially, of a 1 second duration 2.2 volt pulse, with a positive excursion from zero volts. On the other analogue input channel to the Modular One is the telemetered output from the sonobuoy system. The programme waits for receipt of the shot instant signal, and then transfers information from the input buffer to the digital magnetic tape at a rate governed by the digitisation rate chosen for the recording. A count is taken of the number of samples stored and this number is continuously compared with the required number of samples, specified at the beginning of each run, for each shot. Once this number has been reached the programme writes an end-of-file (EOF) mark onto the tape and resets the various interval counters to zero, to await the next shot instant signal. The process continues until the requisite number of shots (files) has been recorded.

Once the tape has been filled, it is ready for analysis, accomplished by using the REPLAY programmes. Several REPLAY programmes were written, each one increasing the flexibility of the original, whose flow diagram is shown in Fig. 4.7 (Appendix 1).

The programme operates in the following fashion;

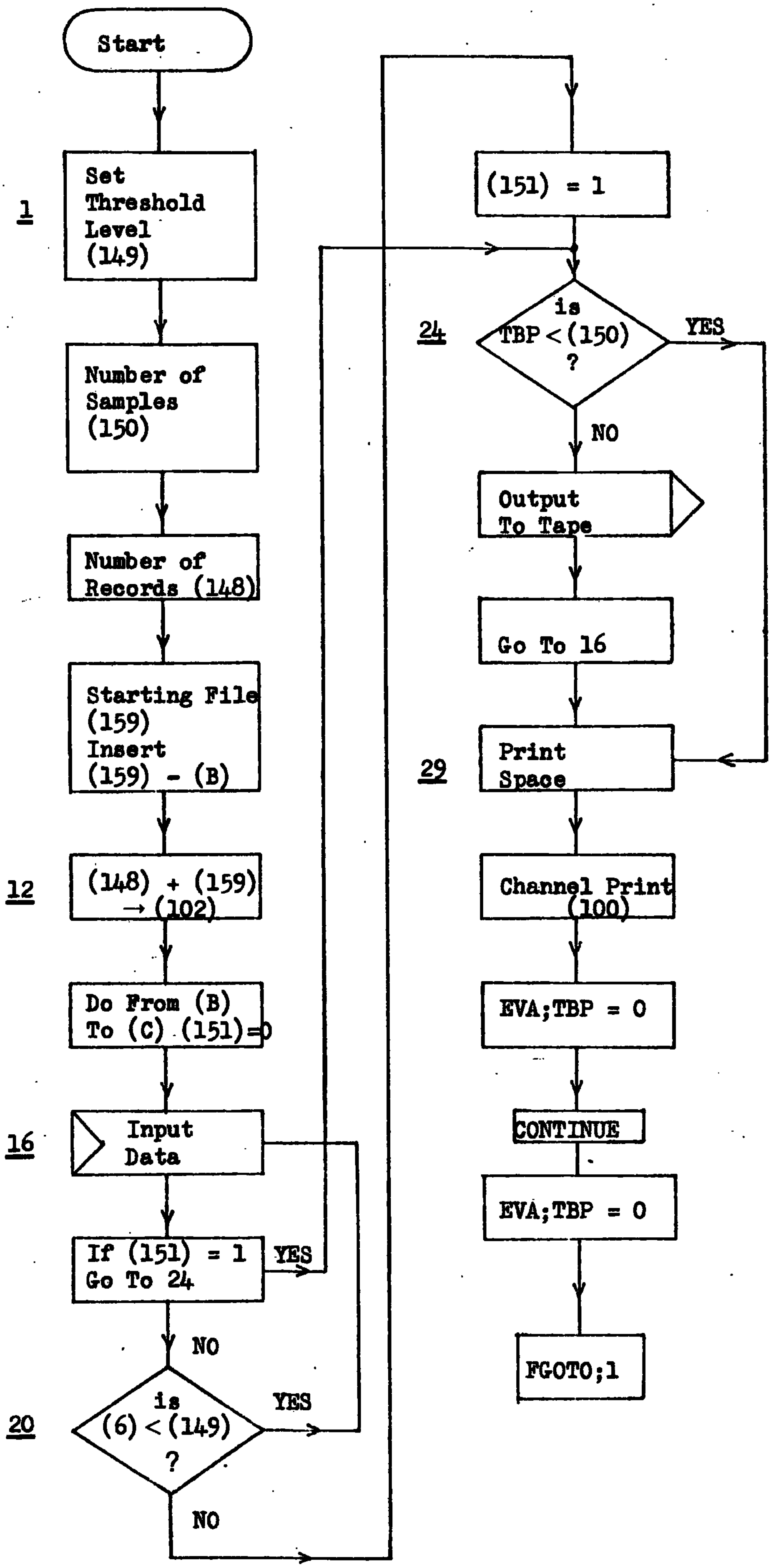

Fig. 4.6 **Store Flow Diagram**

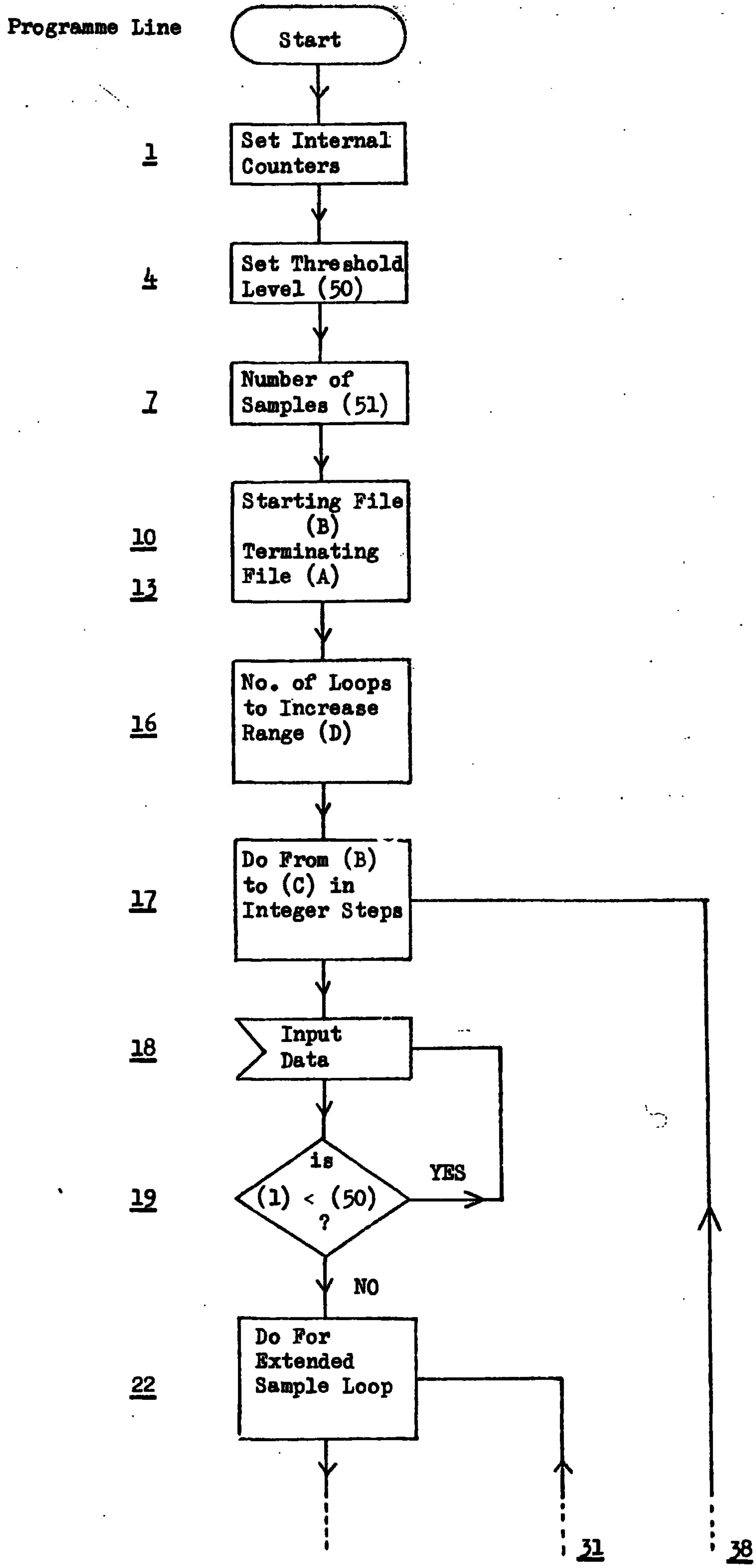

Fig. 4.7(a) More Advanced Store Programme - Flow Diagram

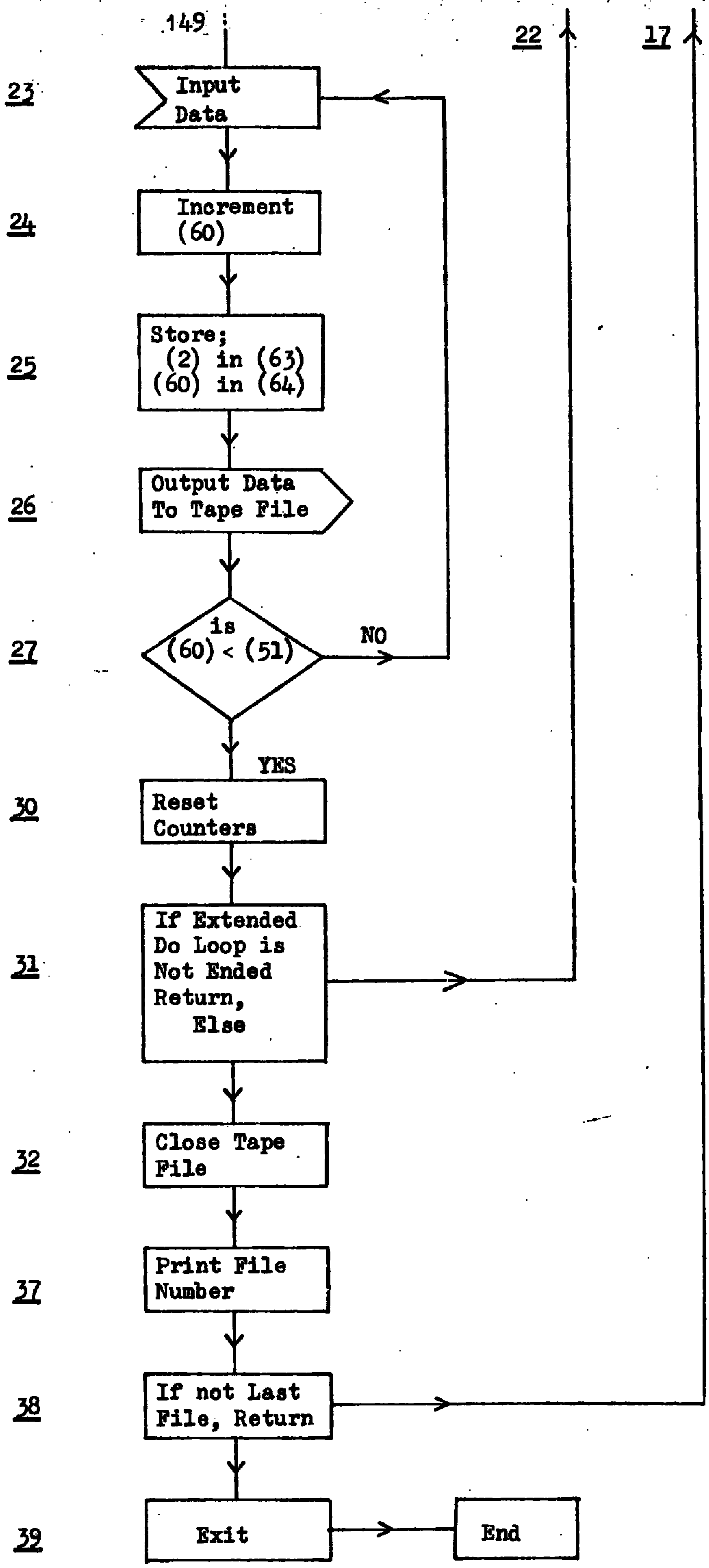

Fig. 4.7(b) More Advanced Store Programme - Flow Diagram

Step 1

'IGNORE N SAMPLES'

A count is taken for the specified number of samples before beginning amplitude comparison. Once this delay has been achieved.

Step 2

The modulus of the signal value present in Channel (1), is taken and compared with the value of ch(53), which is initially set to zero. If $|ch(1)|$ is greater than $|ch(53)|$ the former is stored in ch(53), the real value of ch(1) in ch(71) and the sample number at which this storage occurred placed in ch(57).

Step 3

A check is made to determine whether the number of samples required for analysis has been achieved, and if this is not so the next data sample is taken before returning to Step 2.

Step 4

If the window length count has been achieved the information contained in ch(53), ch(58) and ch(100), being respectively the absolute value of the maximum signal, the sample number at which this maximum occurred, and the shot (tape file) number under examination, is sent to disc for storage.

Step 5

A count is taken to see if the desired number of windows has been examined, if more than one window is to be inspected the programme goes back to Step 2, as often as there are required windows (Fig. 4.8).

Step 6

If only one window is needed or the indicated number of windows has been analysed, the computer checks if any more files are to be examined, having already reset the delay counter, ch(50), to zero. If more files are required, the programme goes back to Step 1, and works through the entire scheme again.

A sample of the output of the programme, as stored on disc, is

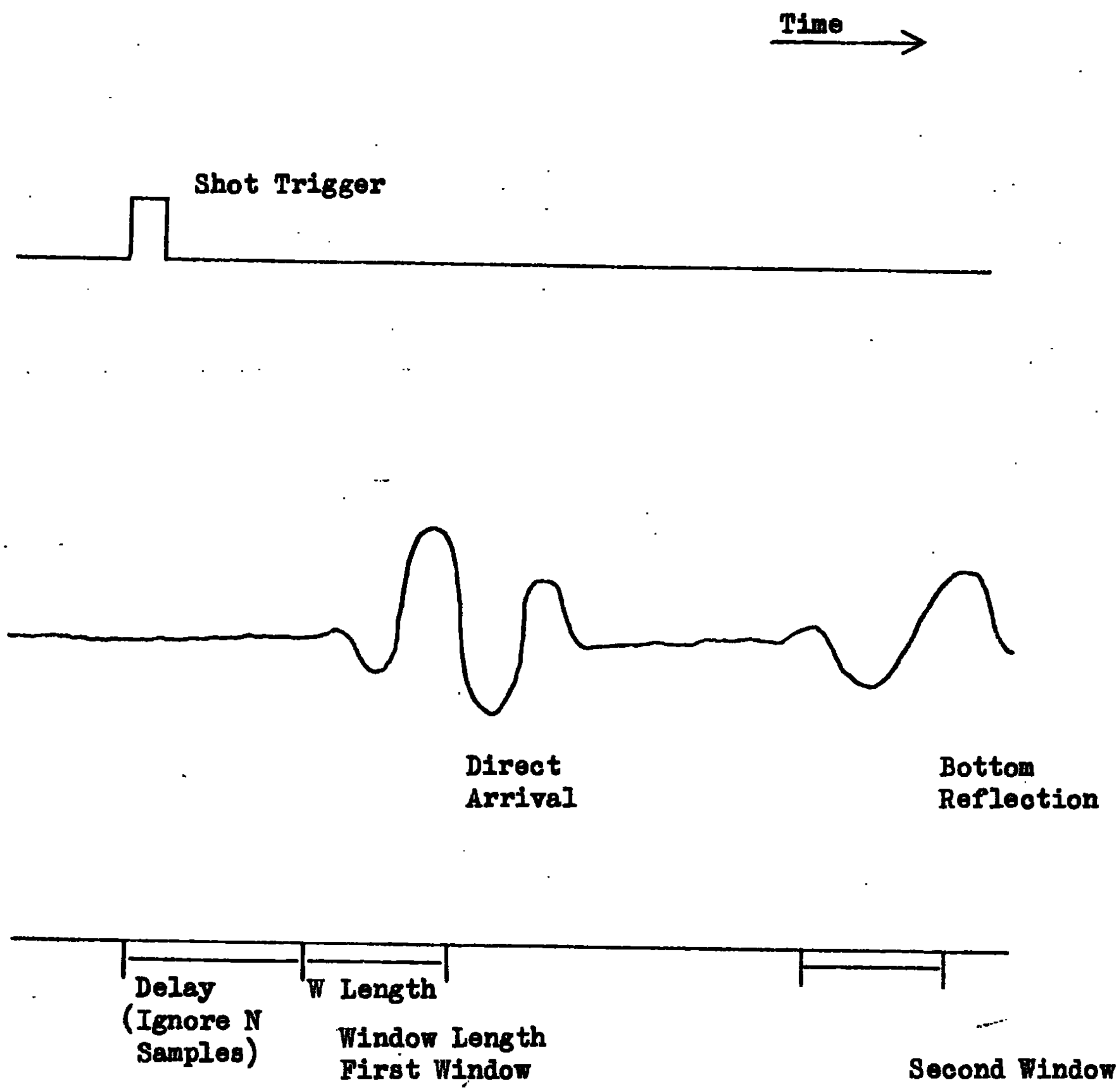

Fig. 4.8 Time Diagram For Store Programmes

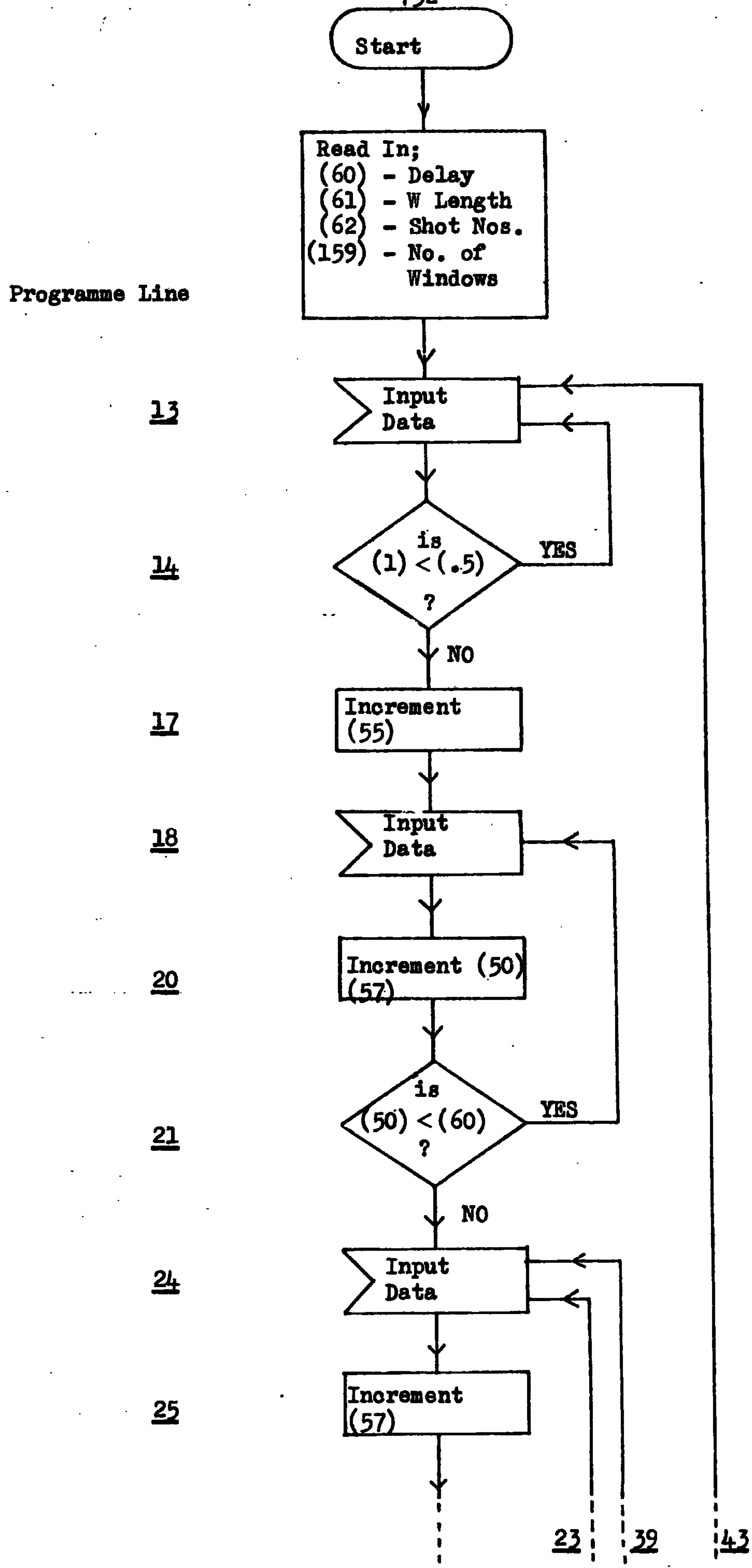

Fig. 4.9(a) **Replay Programme - Flow Diagram** (continued over)

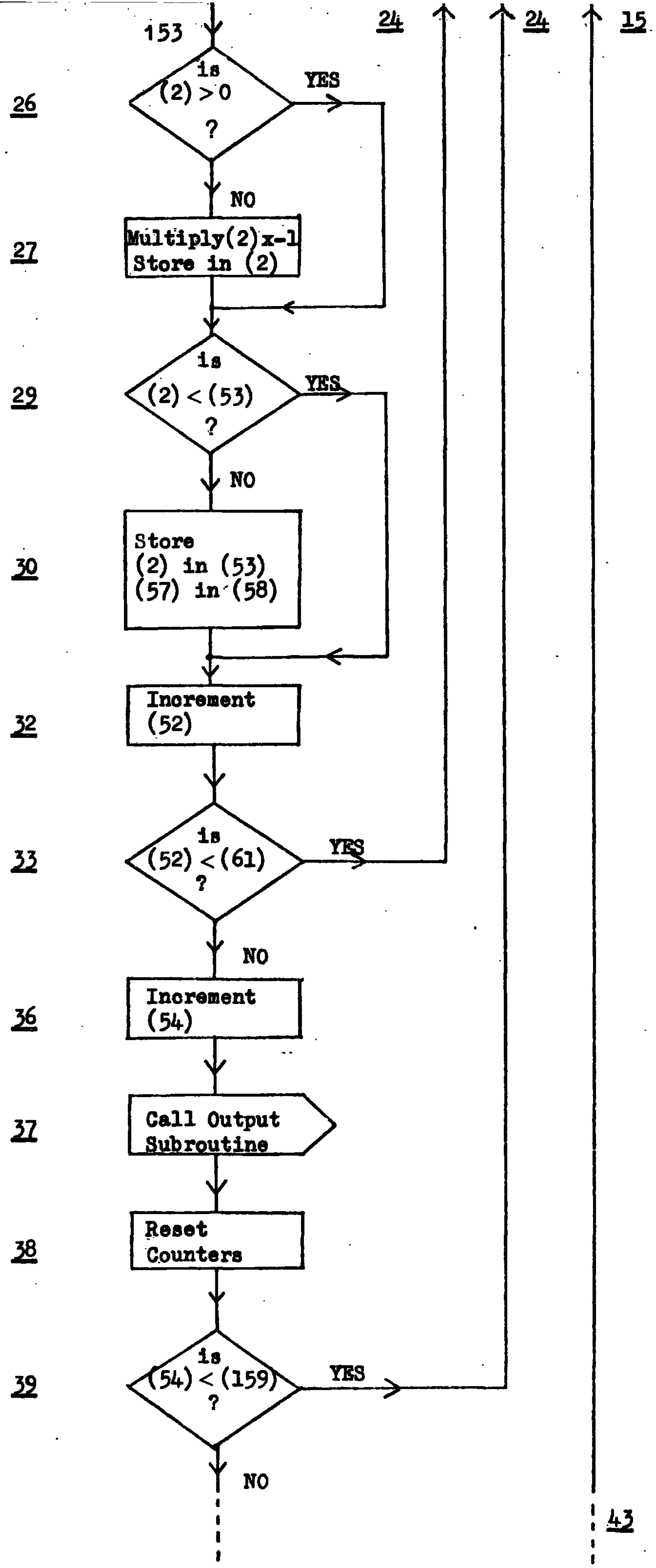

Fig. 4.9(b) **Replay Programme Flow Diagram**

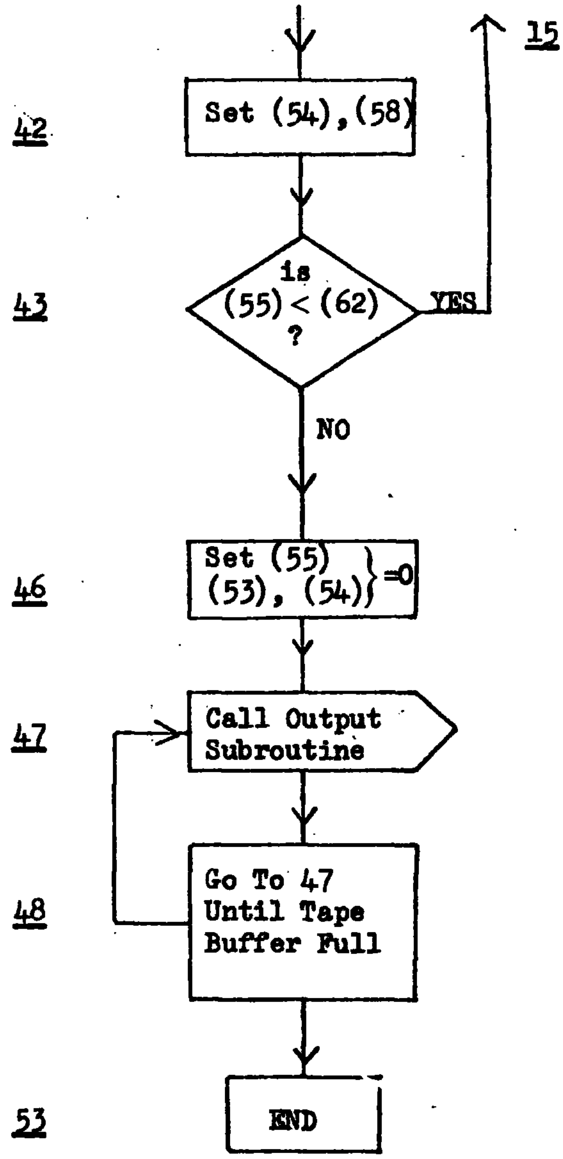

Fig. 4.9(c) Replay Programme - Flow Diagram

given below, in Fig. 4.10. This was read from disc file using the PRINT programme (Appendix 1).

Transfer of Data from Modular One to IBM 360/67

This transfer of data from the Modular One machine to the IBM 360/67 proved necessary because the Modular One did not have sufficient storage capability to enable it to handle numbers smaller than 0.01 or greater than 30.0. Several attempts were made to write a programme to convert the sample number and shot number for a particular peak amplitude into separation distance of ship and buoy and normalised amplitude, but this proved fruitless owing to the great dynamic range of the input data.

Hence the output from the REPLAY programme (Fig. 4.9) was transferred somewhat laboriously using paper tape to the 360/67. The conversion of this data for quantitative analysis is straight forward. Assuming a linear propagation path in the water layer the shot number may be converted to distance knowing the ship's velocity and the rate of discharge of the Bolt airgun system.

The arrival sample number is simply reduced to time by utilising the digitisation rate and this arrival time converted to distance as above, the additional distance being added to the shot distance to give the exact distance.

Given ; shot number, s_n

ship velocity, k knots

$\equiv k^* \text{ km hr}^{-1} \; (= k^*/3.6 \times 10^{-3} \text{kms}^{-1})$

firing interval = F seconds

The distance between successive shots, is given by

$$dL_{i,j} = F \times (k^*/3.6) \times 10^{-3} \text{ km} \qquad (6)$$

Thus the separation of ship and buoy at the nth shot is given by

$$L_n = S_n \times F \times (k^*/3.6) \times 10^{-3} \text{ km} \qquad (7)$$

```
CPN?:FILTER ?:STATMT ?:
N TIME SERIES CHS?        20    1275        0       2
FILE        0 -     4     0      0
IGNORE N SAMPLESS=?:
WLENGTH=?7.6;
NO.OF WINDOWS=?.01;
STARTING FILE=?.01;
TERMINATING FILE=?7.2;
CPN?:FILTER ?1:STATMT ?;
N TIME SERIES CHS?        20    1275        0       2
F
CPN?:FILTER ?1:STATMT ?;
N TIME SERIES CHS?        20    1275        0       2
FILE        0 -     4     0      0
      42      85      1
      40     244      2
     526     290      3
     693     756      4
     493     336      5
     619     378      6
     411       9      7
     438     338      8
     537     329      9
     539      18     10
     631     337     11
     525      27     12
     630     329     13
     407      31     14
     563      24     15
     601      34     16
     518      28     17
     473     491     18
     685      31     19
     542      33     20
```

Fig. 4.10 **Example of Output from Modular One**

For an arrival sample number, N, at a digitisation rate, r samples sec^{-1}, the additional separation of ship and buoy is given by

$$D = (N/r) \times (k^*/3.6) \times 10^{-3} \text{ km} \quad (8)$$

Thus the total separation is

$$R_n = (S_n F + N/r)\ (k^*/3.6 \times 10^{-3}) \text{ km} \quad (9)$$

The distance the reflected ray traverses is calculated from the mean water depth and the separation distance, calculated above, using Pythagoras' Theorem, and the normalised amplitude found simply by multiplying the Modular One output amplitude value, in approximately 5mV units, by this distance in kilometres.

In the case of sub-bottom reflections, the conversion is accomplished by introducing an 'effective water layer thickness' at each shot point. This e.w.l. thickness is found from the W.A.R. and refraction analysis data. Then give estimates of the thickness(es) of the sediment(s) above the sub-bottom reflection of interest. By using these estimates, a two-way travel time for the passage of the sound wave through the sediment layers is calculated and converted to an equivalent water depth using the water velocities obtained from Matthew's tables. This equivalent water depth is added to the exact water depth to provide the 'effective water layer thickness', from which the separation of ship and sonobuoy may be found. (Appendix 1).

In an effort to determine the accuracy of the digitisation procedure, a series of digitisation tests were run on the Modular One and the analysis of these is given in Appendix 3.

Curve Fitting and Synthetic Curve Generating Procedures

In an effort to smooth out the expected experimental error effects in the amplitude data thus produced, various curve fitting routines available in the *NAG (Nottingham Algorithim Group) subroutine package were employed to fit polynomial expressions by means of a least-squares or cubic spline approximation to the amplitude/ angle of incidence (ship-sonobuoy separation) plot. These curve fitting routines are given in Appendix 1, RAT (+ *NAG E02 ABF).

The output from these routines is then fed to a double precision curve plotting routine, GEN(Appendix 1), which simply produces a smoothed output plot of the input amplitude data.

CHAPTER FIVE

RESULTS

Analysis of Sonobuoy Records

The variable area display records obtained using the Ultra Electronics disposable sonobuoys were analysed to provide information on the velocity-depth structure of the sea floor sediments in the areas shown in Fig. 5.1. The reflection parabolae were digitised by hand and the resultant information processed using the Wide Angle Reflection (W.A.R.) analysis programme, as outlined in the preceeding chapter.

Those portions of the records which contained refracted arrivals were examined using a travel-time reduction programme, TWAT, (Appendix 1), with a view to producing further information concerning the sedimentary velocity structure, for correlation and cross-reference with that derived from the reflection studies.

The results of these analyses and the precise geographical location of each sonobuoy run are given below.

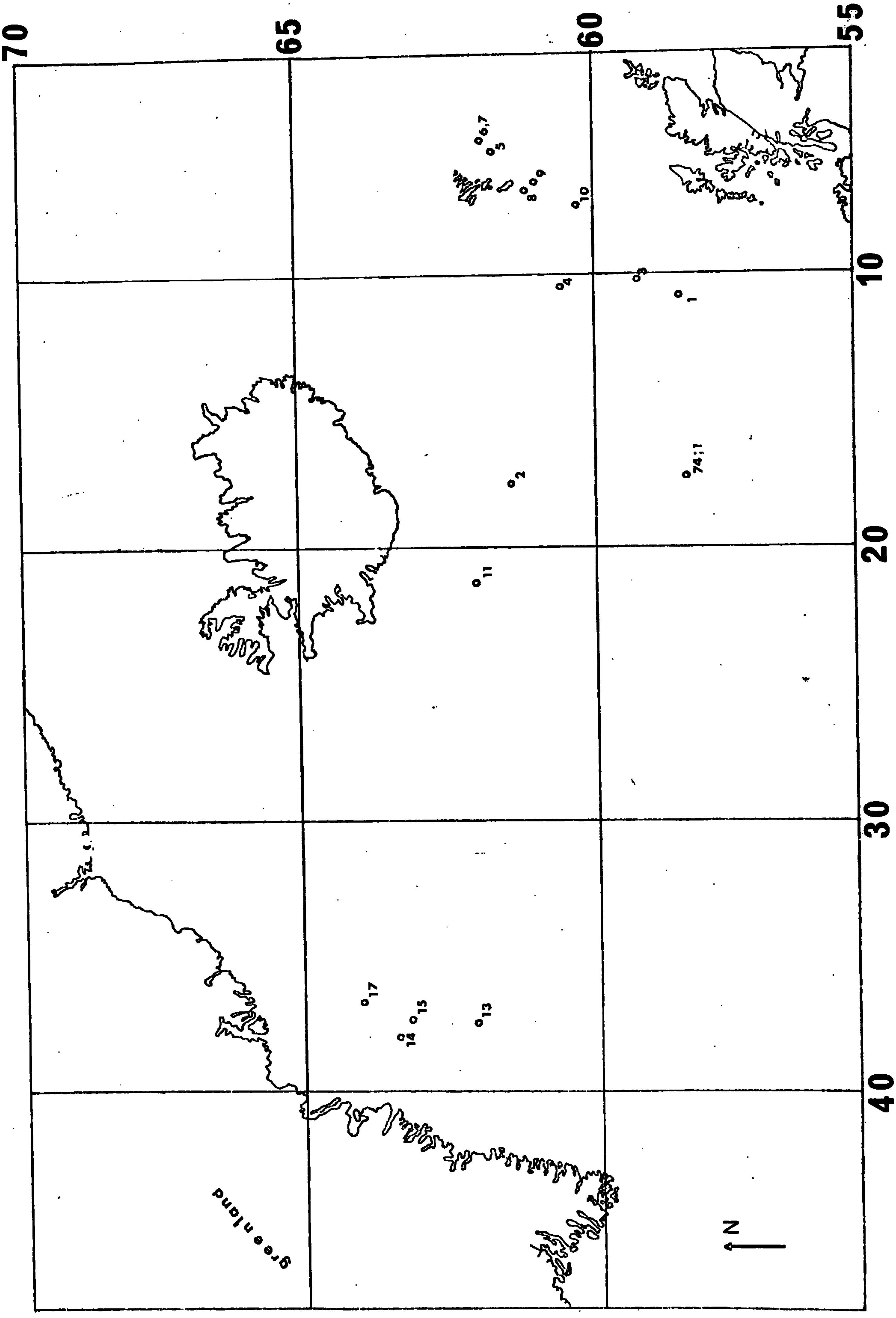

Fig 5.1 Sonobuoy Locations

TABLE 1

SONOBUOY NUMBER	TIME	JULIAN DAY/YEAR	LATITUDE	LONGITUDE	DEPTH (fathoms)
S_1	19:01:45	167/73	58° 34.8' N	10° 46.8' W	1005
S_2	16:29:18	169/73	61° 23.3' N	17° 24.2' W	1287
S_3	17:52:12	171/73	59° 13.0' N	10° 13.6' W	293
S_4	10:26:20	174/73	60° 28.0' N	10° 22.5' W	104
S_5	01:06:18	190/73	61° 42.8' N	5° 33.3' W	94
S_6	05:06:47	190/73	61° 56.3' N	5° 21.8' W	96
S_7	06:03:00	190/73	RE-RUN PAST S_6		91
S_8	22:38:18	192/73	61° 02.5' N	7° 25.8' W	292
S_9	01:49:16	193/73	60° 58.5' N	7° 18.0' W	396
S_{10}	16:04:23	193/73	60° 18.2' N	7° 40.7' W	55
S_{11}	17.06:54	195/73	62° 06.7' N	21° 18.3' W	815
S_{12}	23:22:17	199/73	FAILURE	-	-
S_{13}	00:26:42	200/73	62° 08.7' N	36° 46.7' W	1413
S_{14}	02:41:46	202/73	63° 14.0' N	37° 16.3' W	1028
S_{15}	04:57:13	202/73	63° 08.1' N	36° 57.4' W	1292
S_{16}	23:49:28	203/73	AUDIO FAILURE		-
S_{17}	00:32:27	204/73	64° 01.3' N	36° 40.9' W	194
S_{18}	17:29:04	208/73			618
S_{19}	00:28:57	210/73	AQUIFLEX FAILURE		-
$S_{74/1}$	13:04:47	248/74	58° 17.21' N	16° 37.8' W	600
$S_{74/2}$	04:38:36	257/74	53° 58.4' N	17° 59.4' W	800
$S_{74/3}$	18:31:50	251/74	53° 47.8' N	17° 33.6' W	850

Table 5.1(a) Sonobuoy Locations

Sonobuoy Number	Calculated Ship Velocity (knots)	Matthew's Area	Water Velocity $km\ s^{-1}$		Depth (km)
			Vertical	Horizontal	
S_1	7.09	8	1.488	1.495	1.84
S_2	5.88	7	1.481	1.485	2.35
S_3	6.01	8	1.493	1.495	0.54
S_4	5.21	7	1.485	1.488	0.19
S_5	4.93	2	1.461	1.461	0.17
S_6	5.78	2	1.461	1.461	0.18
S_7	4.68	2	1.461	1.461	0.17
S_8	4.14	2	1.458	1.461	0.53
S_9	4.26	2	1.458	1.461	0.72
S_{10}	4.31	3	1.474	1.474	0.10
S_{11}	6.09	7	1.481	1.488	1.49
S_{13}	6.11	6	1.478	1.476	2.58
S_{14}	4.51	7	1.482	1.476	1.84
S_{15}	6.40	6	1.478	1.476	2.36
S_{17}	5.13	6	1.475	1.476	0.36
S_{18}	5.74	6	1.482	1.476	1.13
$S_{74/1}$	5.99	10	1.495	1.496	1.20
$S_{74/2}$	6.73	10	1.495	1.497	1.62

Table 5.1(b) Sonobuoy Parameters

RESULTS

S_1

	Reflection		Refraction	
Layer	Velocity (km s^{-1})	Reflection Time (sec)	Velocity (km s^{-1})	Intercept (sec)
1	1.49 $\pm$ .01	2.51		
2	2.17 $\pm$ .1	2.68	2.17 $\pm$ .05	2.11
3			2.62 $\pm$ .05	4.35

Layer	Velocity (km s^{-1})	Thickness km	Dip ($^{\circ}$)
1	1.49 $\pm$ .01	1.99 $\pm$ .01	-
2	2.17 $\pm$ .05	3.81 $\pm$ .05	$0^{\circ} \pm 4^{\circ}$
3	2.62 $\pm$ .05		$0^{\circ} \pm 4^{\circ}$

Water depth is 1.84 km from P.E.S. records implying a thin layer of unconsolidated sediments overlying the 2.17 km s^{-1} layer.

Table 5.2(a) S_1 Results

S_2

	Reflection		Refraction	
Layer	Velocity (km s^{-1})	Reflection Time (sec)	Velocity (km s^{-1})	Intercept (sec)
1	1.485 ± .01	3.29		
2	1.99 ± .09	3.52		
3	2.31 ± .1	3.81		
4			5.52 ± .2	4.40

Layer	Velocity (km s^{-1})	Thickness km	Dip degree
1	1.485 ± .01	2.44 ± .02	-
2	1.99 ± .09	.23 ± .01	$0^\circ \pm 2^\circ$
3	2.31 ± .1	.34 ± .015	$0^\circ \pm 3^\circ$
4	4.33 ± .1	3.25 ± .08	$0^\circ \pm 3^\circ$ *
5	5.52 ± .2		$0^\circ \pm 3^\circ$

* On the continuous profile records there is a reflector at 5.3 seconds down. The two way travel time for the fourth layer is thus 1.5 seconds and from the delay time equation

$$I = \sum_{j=o}^{n} \frac{2z_j \cos i_{j,j+1}}{v_j}$$

with I = 4.40, z_o = 2.44 etc, the resulting quartic equation in v_3 may be solved (ANAL 1) to give a velocity of 4.33 km s^{-1}, which implies a thickness of 3.25 km.

Table 5.2(b) S_2 Results

S_3

Layer	Reflection Velocity (km s^{-1})	Reflection Time (sec)	Refraction Velocity (km s^{-1})	Intercept (sec)
1	1.495 ± .01	0.749		
2	2.35 ± .2	0.945	2.12 ± .1	.53
3			5.77 ±	1.13

Layer	Velocity (km s^{-1})	Thickness km	Dip (degree)
1	1.49 ± .01	.56 ± .00(3)	-
2	2.235 ± .2	.46 ± .04	$0^o \pm 3^o$
3	5.77 ± .15		$0^o \pm 8^o$

Table 5.2(c) S_3 Results

S_4

Layer	Reflection Velocity (km s^{-1})	Reflection Time (sec)	Refraction Velocity (km s^{-1})	Intercept (sec)
1	1.49 $\pm$ .08	0.13		
2	2.30 $\pm$ .1	0.87		
3			8.40 $\pm$ .2	0.92

Layer	Velocity (km s^{-1})	Thickness km	Dip (°)
1	1.49 $\pm$ .08	.19 $\pm$ .01	-
2	2.30 $\pm$ .1	1.70 $\pm$ .08	$0^\circ \pm 5^\circ$
3	4.97 $\pm$ .15		11° 42' $\pm 1^\circ$

From the continuous reflection profile this run is up dip. The dip angle is calculated as 11°42'.

Table 5.2(d) S_4 Results

S_5

	Reflection		Refraction	
Layer	Velocity ($km\ s^{-1}$)	Reflection Time (sec)	Velocity ($km\ s^{-1}$)	Intercept (sec)
1	1.495 $\pm$ .01	0.19		
2	2.07 $\pm$ .05	1.11	2.03 $\pm$ .05	0.14
3			5.19 $\pm$ .1	1.17

Layer	Velocity ($km\ s^{-1}$)	Thickness km	Dip ($^{\circ}$)
1	1.495 $\pm$ .01	0.14 $\pm$ .01	-
2	2.05 $\pm$ 0.5	0.95 $\pm$ .03	$0^{\circ} \pm 2^{\circ}$
3	5.19 $\pm$ .1	-	0°(?) $\pm 5^{\circ}$

Table 5.2(e) S_5 Results

S_6

	Reflection		Refraction	
Layer	Velocity ($km\ s^{-1}$)	Reflection Time (sec)	Velocity ($km\ s^{-1}$)	Intercept (sec)
1	$1.46 \pm .01$	.12		
2	$1.73 \pm .05$	.134	$1.68 \pm .1$	0.14
3	$2.25 \pm .05$	.760	$2.39 \pm .1$	0.88
4			$5.81 \pm .1$	1.08

Layer	Velocity ($km\ s^{-1}$)	Thickness km	Dip ($^{\circ}$)
1	$1.46 \pm .01$	$0.18 \pm .01$	-
2	$1.70 \pm .1$	$0.88 \pm .04$	$0^{\circ} \pm 2^{\circ}$
3	$2.25 \pm .05$	$0.29 \pm .03$	$5^{\circ} \pm 2^{\circ}$
4	$4.78 \pm .1$		$5^{\circ}3' \pm 20'$

From the continuous reflection profile this run is up dip, and the angle of dip is $5^{\circ}3'$.

Table 5.2(f) S_6 Results

S_7

Layer	Reflection Velocity ($km\ s^{-1}$)	Reflection Time (sec)	Refraction Velocity ($km\ s^{-1}$)	Intercept (sec)
A. 1	1.46 ± .01	0.12		
2	1.72 ± .05	0.59	1.65 ± .05	0.112
3	2.08 ± .05	0.74	1.95 ± .06	0.710
4			4.66 ± .1	1.120
B. 1	1.46 ± .01	0.12		
2	1.73 ± .04	0.62	1.70 ± .1	0.115
3	2.04 ± .86	0.75	2.03 ± .05	0.720
4			4.92 ± .05	1.140

Layer	Velocity ($km\ s^{-1}$)	Thickness km	Dip (°)
1	1.46 ± .01	.18 ± .01	-
2	1.65 ± .05	.80 ± .05	0° ± 2°
3	1.99 ± .05	.30 ± .04	1°39' ± 20'
4	4.78 ± .1		0°42' ± 20'

S_7 is a re-run past S_6 as the ship moved past the sonobuoy again.

Table 5.2(g) S_7 Results

S_8 and S_9 (Reverse of S_8)

	Reflection		Refraction	
Layer	Velocity (km s^{-1})	Reflection Time (sec)	Velocity (km s^{-1})	Intercept (sec)
1	1.458 ± .01	0.49		
2	1.96 ± .05	1.16	1.95 ± .05	0.83
3	2.40 ± .1	1.41	2.65 ± .08	2.00
4			6.38 ± .1	2.68
1	1.458 ± .01	0.49		
2	1.97 ± .08	1.20	1.93 ± .05	0.84
3	2.41 ± .1	1.44	2.32 ± .1	-
4			5.00 ± .15	

Layer	Velocity (km s^{-1})	Thickness km	Dip (°)
1	1.458 ± .01	.74 ± .03	-
2	1.95 ± .05	1.32 ± .05	4° ± 20'
3	2.45 ± .09	.59 ± .03	4°27' ± 20'
4	5.61 ± .15		7°49' ± 10'

S_9 is the reversed line of S_8 and from the up and down dip refraction velocities the time velocities and dips were found.

Table 5.2(h) S_8 and S_9 Results

S_{10}

Layer	Reflection Velocity (km s^{-1})	Reflection Time (sec)	Refraction Velocity (km s^{-1})	Intercept (sec)
1	1.474 ± .01	0.14		
2*	1.65 ± .20	0.33		
3			4.55 ± .1	0.22

* shallow depth leading to pronounced reverberation made this apparent reflector very difficult to follow and hence this result is very inaccurate.

Layer	Velocity (km s^{-1})	Thickness km	Dip (°)
1	1.474 ± .01	.10 ± .01	-
2	1.65 ± .2	.07 ± .02	0° ± 10°
3	4.55 ± .1	-	0° ± 2°

Table 5.2(i) S_{10} Results

S_{11}

	Reflection		Refraction	
Layer	Velocity (km s^{-1})	Reflection Time (sec)	Velocity (km s^{-1})	Intercept (sec)
1	1.482 ± .01	2.134		
2	1.685 ± .09	2.550		
3	2.210 ± .1	2.920	2.15 ± .05	0.34

Layer	Velocity (km s^{-1})	Thickness km	Dip (°)
1	1.482 ± .01	1.44 ± .02	-
2	1.685 ± .09	.025 ± .04	0° ± 3°
3	2.18 ± .1	-	0° ± 2°

Undulating Reflectors but no overall dip. Deep water record.

Table 5.2(j) S_{11} Results

S_{13}

	Reflection		Refraction	
Layer	Velocity (km s^{-1})	Reflection Time (sec)	Velocity (km s^{-1})	Intercept (sec)
1	1.478 ± .01	3.488		
2	1.54 ± .06	3.64		
3	4.84 ± .1	4.687		

Layer	Velocity (km s^{-1})	Thickness km	Dip (°)
1	1.478 ± .01	2.578 ± .03	-
2	2.16 ± .06	.165 ± .02	0° ± 3°
3	4.84 ± .1	1.13 ± .05	0° ± 5°

No refractors noted. Deep water.

Table 5.2(k) S_{13} Results

S_{14}

Layer	Reflection Velocity (km s^{-1})	Reflection Time (sec)	Refraction Velocity (km s^{-1})	Intercept (sec)
1	1.476 ± .01	2.47		
2	2.326 ± .1	2.90		
3	2.52 ± .05	3.24		
4	2.55 ± .05	3.64		
5			6.49 ± .1	3.57

Layer	Velocity (km s^{-1})	Thickness km	Dip (°)
1	1.476 ± .01	1.84 ± .01	-
2	2.33 ± .1	0.50 ± .03	0° ± 2°
3	2.52 ± .05	0.42 ± .03	0° ± 2°
4	2.56 ± .05	0.54 ± .03	0° ± 2°
5	6.49 ± .1		0° ± 2°

Table 5.2 (1) S_{14} Results

S_{15}

Layer	Reflection Velocity (km s^{-1})	Reflection Time (sec)	Refraction Velocity (km s^{-1})	Intercept (sec)
1	1.487 $\pm$ .01	0.792		
2	2.02 $\pm$ .05	0.983		
3	2.57 $\pm$ .08	1.091		

Layer	Velocity (km s^{-1})	Thickness km	Dip ($^\circ$)
1	1.487 $\pm$ .01	2.36 $\pm$ .03	-
2	2.02 $\pm$ .05	0.19 $\pm$ .03	$0^\circ \pm 5^\circ$
3	2.57 $\pm$ .08	0.14 $\pm$ .04	$0^\circ \pm 6^\circ$

No refractors present.

Table 5.2(m) S_{15} Results

S_{17}

Layer	Reflection Velocity (km s^{-1})	Reflection Time (sec)	Refraction Velocity (km s^{-1})	Intercept (sec)
1	1.475 ± .01	0.25		
2	1.616 ± .07	0.43		
3	1.950 ± .09	0.85	1.96 ± .05	.46
4			2.44 ± .05	.84

Layer	Velocity (km s^{-1})	Thickness km	Dip (°)
1	1.475 ± .01	0.187 ± .01	-
2	1.616 ± .07	0.41 ± .03	0° ± 2°
3	1.96 ± .05	0.42 ± .03	0° ± 3°
4	2.44 ± .05		0° ± 2°

Table 5.2(n) S_{17} Results

S_{18}

	Reflection		Refraction	
Layer	Velocity ($km\ s^{-1}$)	Reflection Time (sec)	Velocity ($km\ s^{-1}$)	Intercept (sec)
1	1.482 ± .01	0.76		
2	1.980 ± .05	1.06		
3	2.31 ± .08	1.67		

Layer	Velocity ($km\ s^{-1}$)	Thickness km	Dip (^{o})
1	1.482 ± .01	1.13 ± .01	-
2	1.98 ± .05	0.30 ± .03	$0^{o} \pm 3^{o}$
3	2.31 ± .05	0.70 ± .04	$0^{o} \pm 4^{o}$

No refractors present.

Table 5.2(p) S_{18} Results

$S_{74/1}$

Layer	Reflection Velocity (km s^{-1})	Reflection Time (sec)	Refraction Velocity (km s^{-1})	Intercept (sec)
1	1.495 $\pm$ .01	1.576		
2	2.22 $\pm$ .07	2.292		
3			3.09 $\pm$ .1	2.38

Layer	Velocity (km s^{-1})	Thickness km	Dip (°)
1	1.495 $\pm$ .01	1.18 $\pm$ .01	-
2	2.22 $\pm$ .07	1.60 $\pm$ .05	$0^{\circ} \pm 3^{\circ}$
3	3.09 $\pm$ .1		$0^{\circ} \pm 1.5^{\circ}$

Table 5.2(q) $S_{74/1}$ Results

$S_{74/2}$

Layer	Reflection Velocity (km s^{-1})	Reflection Time (sec)	Refraction Velocity (km s^{-1})	Intercept (sec)
1	$1.497 \pm .01$	1.672		
2	$2.10 \pm .05$	2.24		
3			$3.31 \pm .05$	2.93

Layer	Velocity (km s^{-1})	Thickness km	Dip (°)
1	$1.497 \pm .01$	$1.25 \pm .01$	-
2	$2.10 \pm .05$	$0.6 \pm .03$	$0^{\circ} \pm 3^{\circ}$
3	$3.31 \pm .05$	-	$0^{\circ} \pm 2^{\circ}$

Deep water.

Table 5.2(r) $S_{74/2}$ Results

Experimental Results

The experimental results discussed here, were obtained using the Modular One computer and the amplitude analysis programmes described in the previous chapter.

Initial trials on several sonobuoy records revealed that the problem of determining the peak amplitude arrival time of a given reflecting horison was not quite as straight forward as might be imagined. It was thought that the primary reflection from the sea bed itself would give the highest reflection amplitude, as this boundary represents the greatest change in acoustic impedance present (Ref. 5.1), and that a detailed investigation into the behaviour of the amplitude of this arrival for increasing angles of incidence would indicate whether the theoretical predictions would be borne out by the practical results.

An examination of Table 5.3 and Fig. 5.2 shows that the matter is not quite so simple. The table lists the arrival time (in milliseconds) and amplitude of the peak signal for the entire detectable range of sonobuoy run, S2. The figure in column three is the shot number and is related to ship-buoy separation as explained previously.

As expected, at very close ranges, the direct wave is the largest arrival and for a short interval, subsequently, a bottom reflection predominates. The picture, however, becomes more random in character beyond this area, which corresponds to an approximate separation of 2 km, and is hence, well within the limit of discernible arrivals.

Another disquieting feature is the wide variation in amplitude of the arrivals (Fig. 5.3). Fig. 5.4 shows the jet pen record of a sample of return signals from sonobuoy run, S2, from shot 1 to shot 71 corresponding to a range of approximately 5.6km and if one inspects the first and second peaks of the return, it can be seen that the same

D.W ?

735	682	1
456	339	2
543	339	3
444	337	4
433	339	5
442	421	6
501	340	7
457	414	8
538	416	9
443	340	10
499	342	11
472	340	12
481	342	13
519	343	14
502	345	15
359	345	16
376	34[illegible]	17
381	[illegible]	18
387	348	19
345	349	20
376	557	21
362	352	22
401	353	23
377	354	24
400	[illegible]	25
342	357	26
35[illegible]	358	27
320	360	28
461	1525	29
41[illegible]	1[illegible]11	[illegible]
32[illegible]	[illegible]	31
42[illegible]	[illegible]	[illegible]
314	[illegible]	33
266	364	34
475	1334	35
416	538	36
479	432	37
360	374	38
351	331	39
367	732	40
407	450	41
298	[illegible]	42
[illegible]	[illegible]	[illegible]
415	443	44
434	449	45
487	451	46
525	453	47
544	403	48
564	463	49
559	459	50
564	453	51
566	469	52
[illegible]23	472	53
[illegible]	[illegible]	54
587	476	55
536	471	56
517	473	57
546	475	58
501	479	59
584	481	60

Table 5.3 **Amplitude, Arrival Time, Shot Number (S2).**

cont. over/...

395	[illegible]	61	407	[illegible]	121
446	[illegible]	62	379	651	122
501	[illegible]	63	385	[illegible]	123
447	462	64	392	651	124
495	[illegible]	65	434	[illegible]	125
575	452	66	408	[illegible]	126
505	462	67	507	670	127
427	[illegible]	68	359	[illegible]	128
467	[illegible]	69	453	[illegible]	129
463	471	70	432	[illegible]	130
358	474	71	357	678	131
353	1545	72	419	683	132
611	1722	73	357	[illegible]	133
397	470	74	413	690	134
531	[illegible]	75	349	701	135
352	[illegible]	76	322	[illegible]	136
523	[illegible]	77	392	710	137
552	[illegible]	78	300	713	138
[illegible]	[illegible]	[illegible]	[illegible]	[illegible]	[illegible]
[illegible]	[illegible]	[illegible]	298	[illegible]	140
593	[illegible]	81	643	[illegible]	141
622	510	82	273	[illegible]	142
647	513	83	305	724	143
517	[illegible]	84	341	[illegible]	144
535	[illegible]	85	284	[illegible]	145
497	523	86	292	[illegible]	146
633	524	87	301	741	147
627	[illegible]	[illegible]	245	[illegible]	148
522	[illegible]	89	271	[illegible]	149
527	[illegible]	90	245	753	150
541	[illegible]	91	235	[illegible]	151
652	[illegible]	92	208	[illegible]	152
566	[illegible]	93	197	[illegible]	153
537	[illegible]	94	262	[illegible]	154
490	[illegible]	95	206	[illegible]	155
539	[illegible]	96	189	777	156
556	[illegible]	97	224	[illegible]	157
595	562	98	401	[illegible]	158
523	567	99	138	[illegible]	159
664	851	100	213	[illegible]	160
555	[illegible]	101	175	[illegible]	161
541	577	102	164	810	162
590	[illegible]	103	190	814	163
513	[illegible]	104	185	[illegible]	164
553	591	105	130	[illegible]	165
809	1245	106	173	[illegible]	166
498	595	107	161	82	167
590	[illegible]	108	191	[illegible]	168
438	602	109	186	[illegible]	169
509	[illegible]	110	237	387	170
606	609	111	248	[illegible]	171
483	[illegible]	112	251	[illegible]	172
618	617	113	289	[illegible]	173
623	614	114	193	[illegible]	174
523	621	115	238	[illegible]	175
564	627	116	201	[illegible]	176
482	632	117	208	[illegible]	177
449	634	118	194	[illegible]	178
457	641	119	259	871	179
446	642	120	156	881	180

Table 5.3. Amplitude, Arrival Time, Shot Number (S2).

cont. over/...

202	1085	181	67	544	241
168	994	182	74	1243	242
199	894	183	45	1297	243
190	898	184	55	1305	244
214	[illegible]	185	75	[illegible]	245
182	906	186	74	1314	246
147	909	187	43	1167	247
194	1174	188	47	[illegible]	248
192	916	189	47	[illegible]	249
200	921	190	58	1322	250
146	925	191	43	1332	251
149	1117	192	103	655	252
181	933	193	45	1340	253
134	946	194	66	1343	254
103	943	195	64	[illegible]	255
175	272	196	41	1641	256
102	953	197	63	1335	257
105	471	198	72	[illegible]	258
[illegible]	[illegible]	[illegible]	[illegible]	[illegible]	[illegible]
118	[illegible]	[illegible]	55	[illegible]	260
85	961	201	107	937	261
153	951	202	57	1690	262
143	457	203	57	1371	263
138	[illegible]	204	51	[illegible]	264
113	984	205	61	1244	265
115	[illegible]	206	78	[illegible]	266
79	665	207	55	[illegible]	267
104	993	208	51	[illegible]	268
135	[illegible]	209	53	1281	269
81	[illegible]	210	58	[illegible]	270
119	1211	211	57	315	271
92	1135	212	64	725	272
103	1189	213	53	811	273
74	1131	214	726	1555	274
81	1071	215	171	1569	275
112	1733	216	657	[illegible]	276
79	1203	217	103	[illegible]	277
68	1435	218	80	642	278
714	443	219	441	1104	279
83	1144	220	1003	[illegible]	280
66	1035	221	1003	603	281
78	1052	222	1003	1611	282
87	1057	223	[illegible]	[illegible]	283
64	1058	224	1003	[illegible]	284
95	1224	225	1003	[illegible]	285
113	1734	226	225	[illegible]	286
77	1238	227	1003	1015	287
65	[illegible]	228	1003	859	288
73	1249	229	1005	[illegible]	289
67	1253	230	954	332	290
63	1259	231	1002	1607	291
134	[illegible]	232	1003	513	292
55	1265	233	115	593	293
70	1744	234	1001	1491	294
58	1271	235	1004	1005	295
75	1276	236	1003	612	296
71	1274	237	90	734	297
90	1129	238	196	1125	298
64	1289	239	1003	971	299
91	1199	240	1003	1195	300

Table 5.3 Amplitude, Arrival Time, Shot Number (S2).

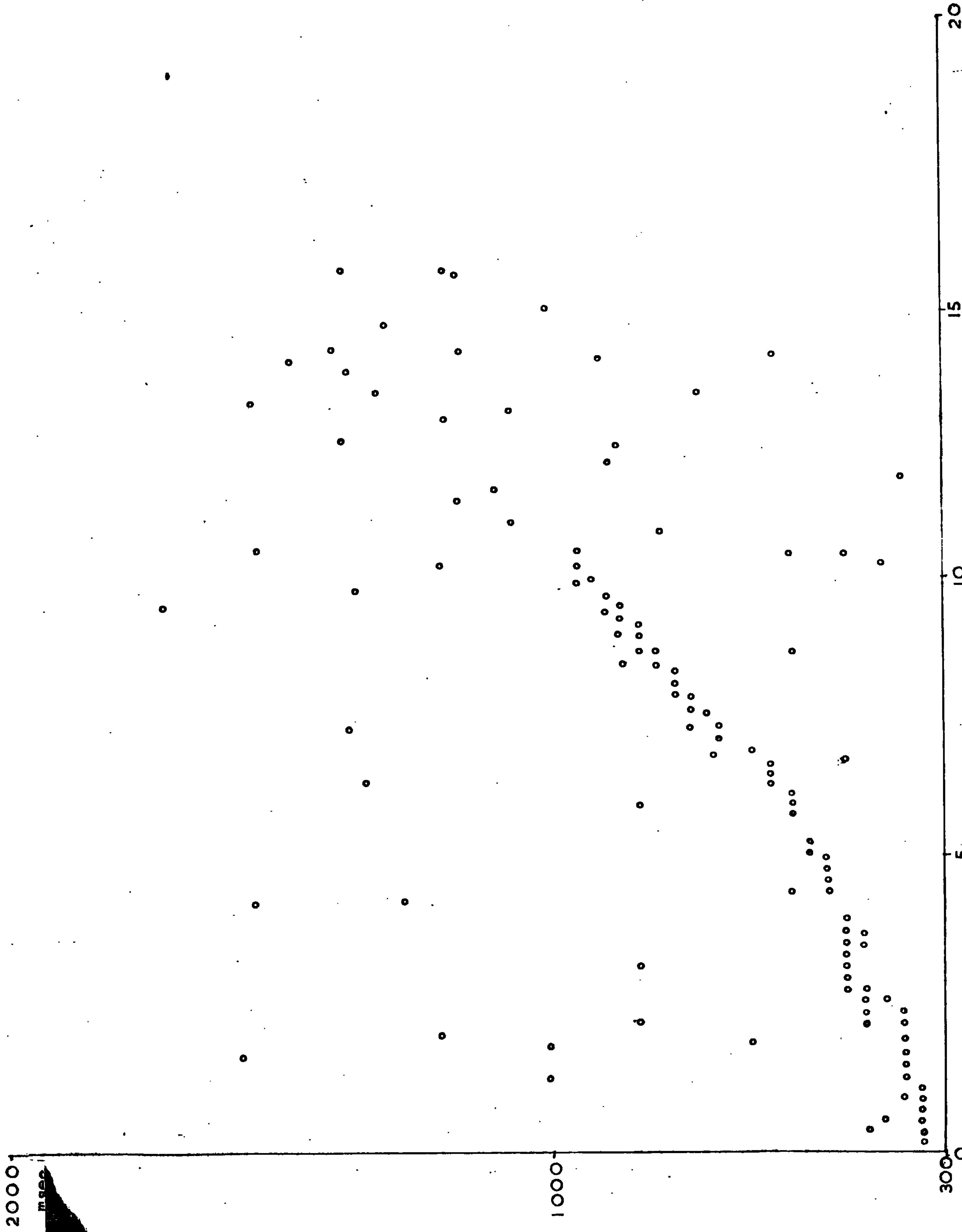

Fig. 5.2 S2 Arrival Time - All Record

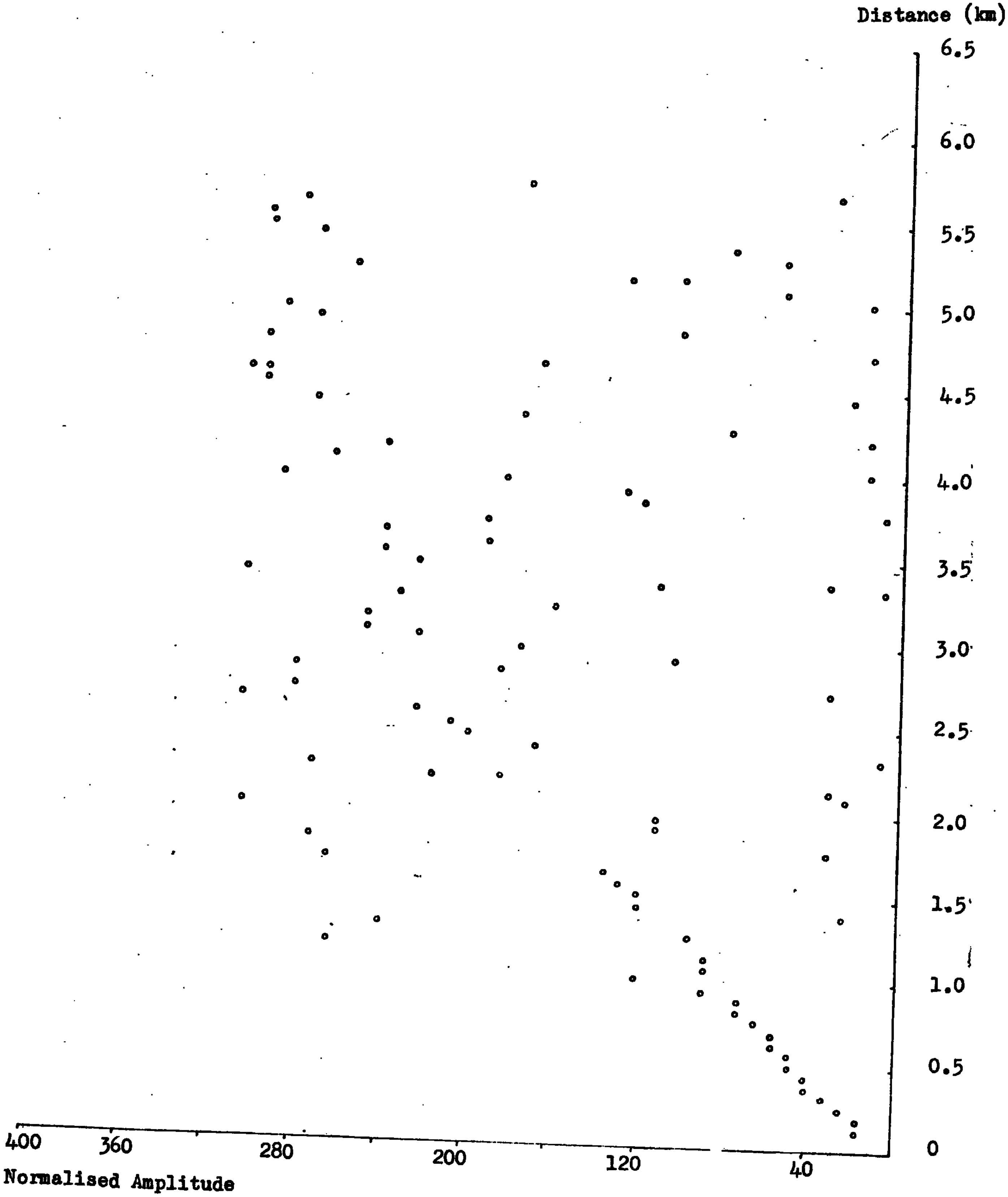

Fig. 5.3 S2 Amplitude vs. Distance

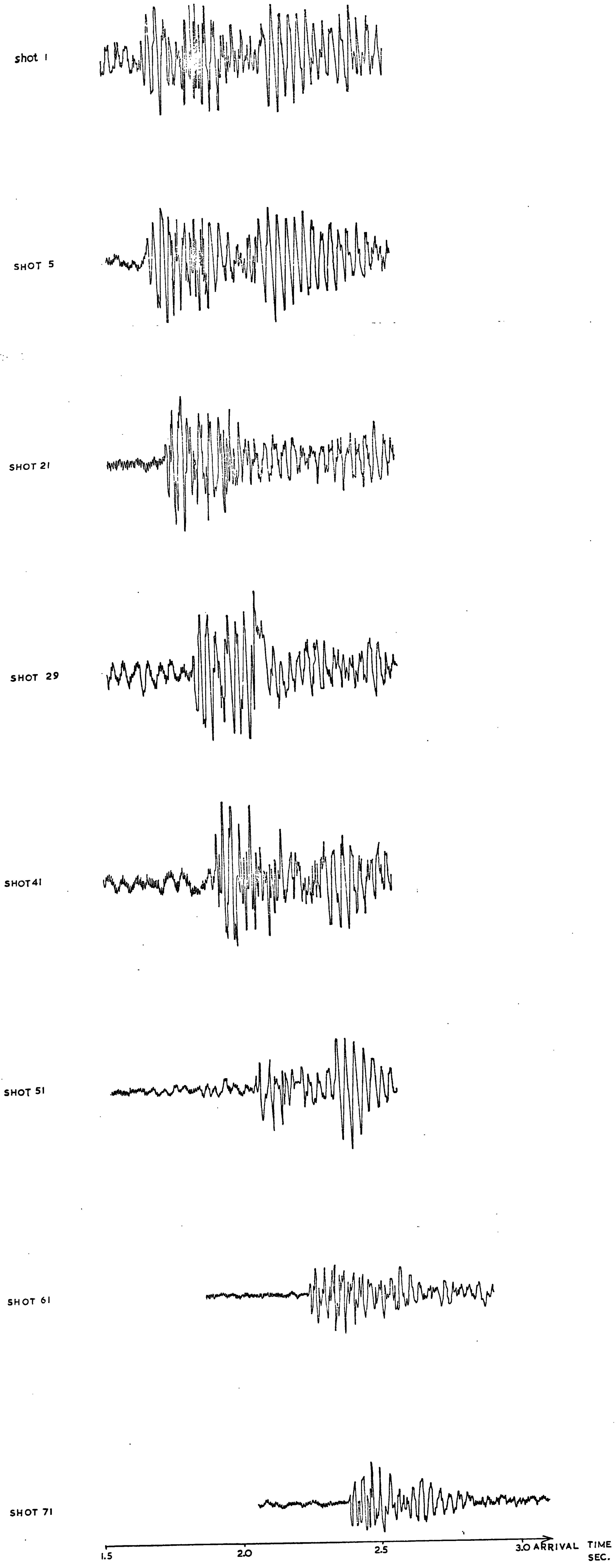

FIG.5.4 RETURN SIGNAL—SONOBUOY RUN, S2

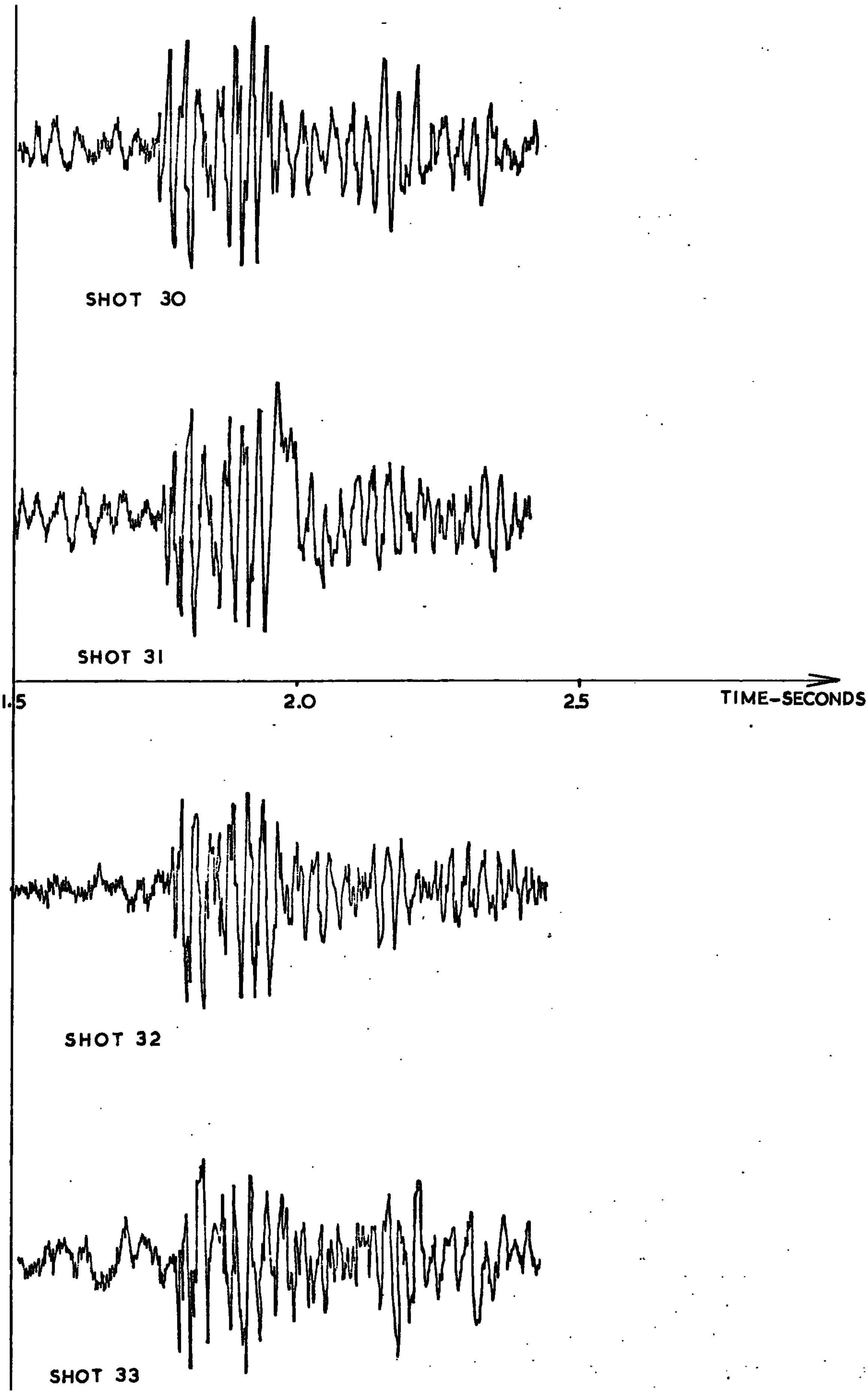

Fig. 5.5 Detailed Analysis of Sonobuoy Signal

FIG 5.6 NOISE BURST ON TYPICAL SIGNAL

reflection arrival is being examined for each shot.

Four consecutive shots are given in Fig. 5.5 and even this apparently coherent set of returns, which show good agreement as to arrival time, display a large amount of amplitude variation. The separation between each shot is of the order of 80m, which should not be sufficient to produce this degree of scatter assuming that inhomogeneities of such a small nature are not likely to be present in the sea floor surface.

The arrival time/amplitude/distance relationships for all the other sonobuoy runs were examined similarly, and it was found that this problem was not limited to this particular sonobuoy run. Examples are given in Fig. 5.7, 5.8 and 5.9.

Several complete shots were played out to the jet pen system described earlier, a laborious task since the disc file used to capture the amplitude data in the Modular One was only capable of storing 3.5 seconds of record at one time, given the high digitisation rate necessary to give the requisite resolution for this work (Appendix 3).

A close inspection of this jet pen output revealed that the records, in general, are subject to short (30-80 msec) bursts of (Fig. 5.6) noise, which saturate or nearly saturate, the Modular One analogue input are responsible for some of the scatter in the peak amplitude arrival times and levels and it is thought that they may have emanated from the steering gear of the ship used for the survey, the R.R.S. "Shackleton", and be radio frequency (R.F.) interference breaking through on the carrier frequency of the F.M. link from sonobuoy to ship. This phenomenon was apparent on all the records examined.

A more detailed analysis of the signal was undertaken, the window of record examined for each shot being calculated as that section of the record in which the bottom arrival was expected to occur, from simple geometric ray theory (Ref. 5.2). By utilising a

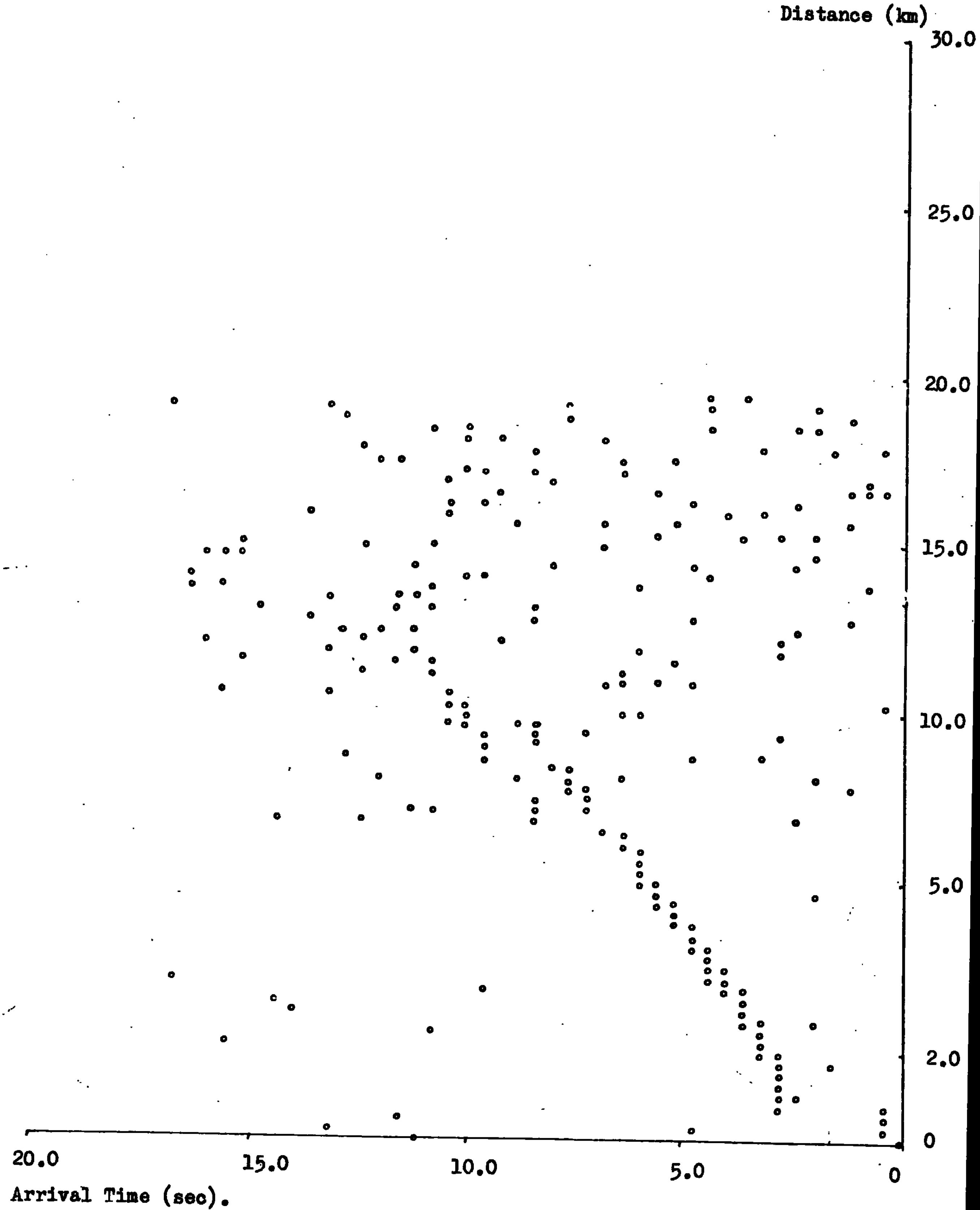

Fig. 5.7 S1 Arrival Time vs. Distance

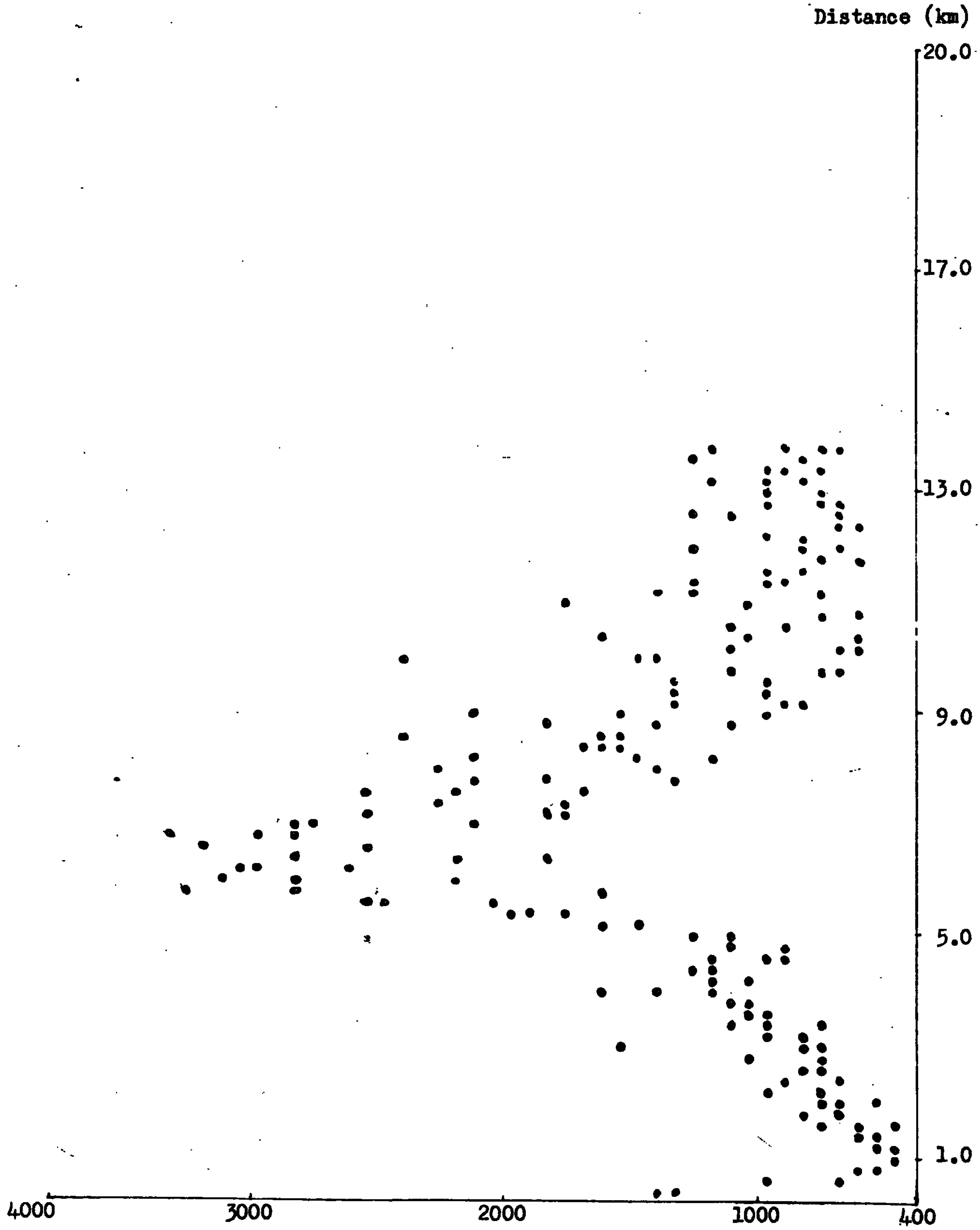

Fig. 5.8 S1 Amplitude vs. Distance (196 shots only)

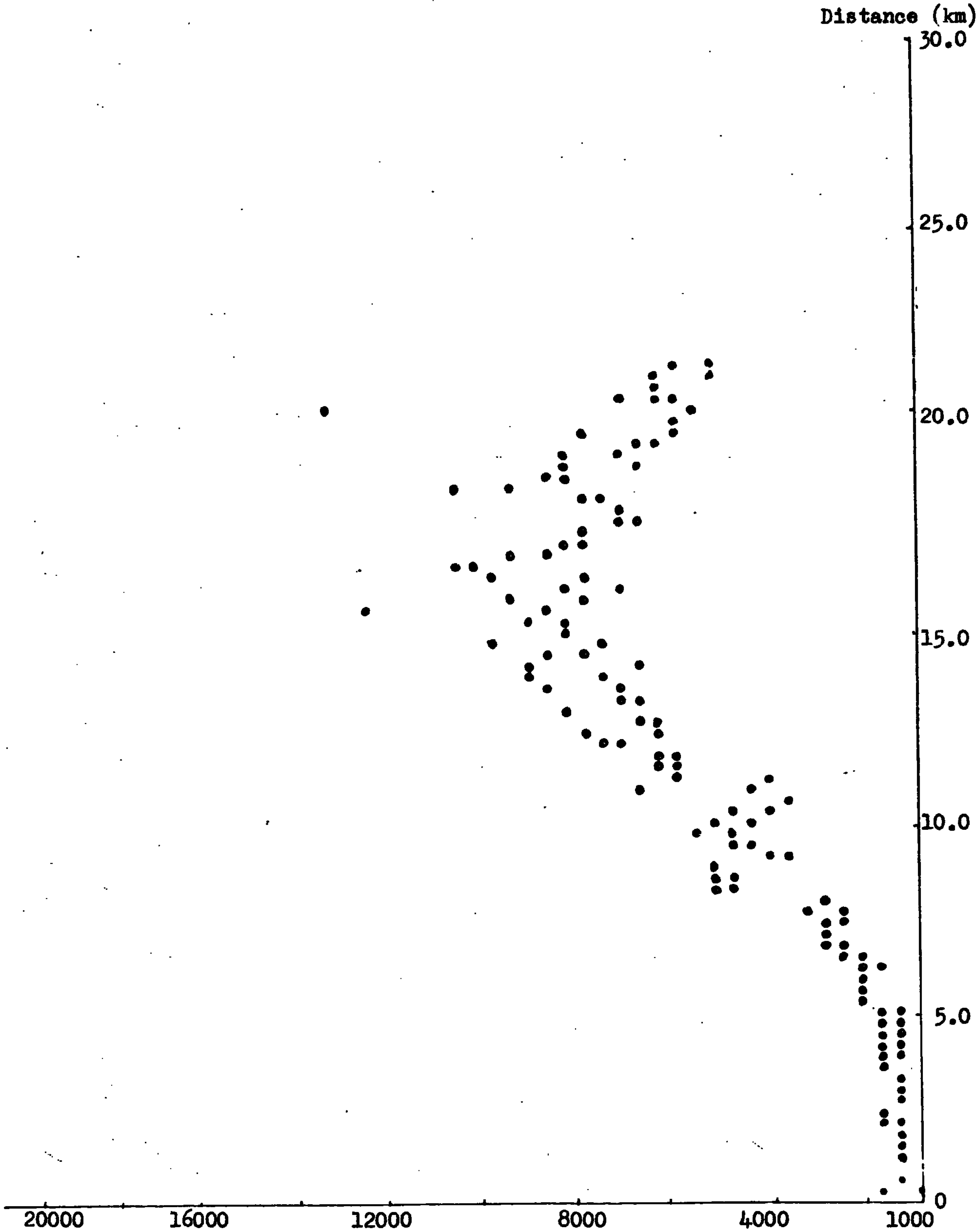

Fig. 5.9 S11 Amplitude vs. Distance

short window length and incorporating several windows per shot, a teletyped output of the relevant section of the arrival was obtained. This proved to be an extremely long and time consuming process, the actual computer operation being accomplished fairly rapidly, but the mechanical limitation of the teletype itself, at 10 characters/second, greatly slowing down the data output, an example of which is given in table 5.4. A further drawback to this process of detailed investigation was the fact that only a limited number of shots could be examined with a given window, the arrival of interest moving beyond the group of windows chosen initially, within the space of five or ten shots. It was not possible to write the window lengths and window positions into an incrementing 'do-loop' because of a software limitation on the number of data location statements and nesting levels which could occur in any one programme. This necessitated the repeated termination and re-starting of the replay programmes to enable the entire range of arrival times to be encompassed.

Fig. 5.10 shows the result of one such examination. The arrival time/distance plot is better than the equivalent 'all-record' result, but the amplitude/distance curve (Fig. 5.11) still shows a distinctly scattered nature. Repeated investigations were made of the areas of the record where there was some doubt as to the validity of the correct identification of the arrival, in an effort to remove the anomalous variations.

In order to obtain these plots, it was necessary to go over and over each particular shot examining each sample almost individually, playing out small sections of the record(s) to the jet pen system and printing out the numerical amplitudes time and time again, the nature of the arrival being so hard to follow.

This laborious technique provided dividends, and it can be seen from Fig. 5.10 that the same horizon is being investigated throughout the record and as its computed depth tallies with that given by the Precision Depth Recorder (P.D.R.) whilst the run was

|Amp|	Time	Shot No.	True Amp	Window No.
14	2056	62 -	14	411
17	2061	62 -	17	412
15	2066	62 -	15	413
39	2075	62 -	39	415
45	2076	62 -	45	415
46	2081	62 -	46	416
37	2086	62 -	37	417
20	2091	62 -	20	418
29	2099	62	29	420
44	2105	62	44	421
45	2109	62	45	422
30	2114	62	30	423
21	2119	62	21	424
20	2122	62 -	20	424
34	2126	62 -	34	425
24	2132	62 -	24	426
21	2137	62 -	21	427
29	2141	62 -	29	428
28	2146	62 -	28	429
29	2005	63	29	401
26	2010	63	26	402
27	2015	63	27	403
22	2016	63	22	403
29	2023	63 -	29	405
12	2027	63 -	12	405
38	2032	63 -	38	406
58	2038	63 -	58	408
26	2043	63 -	26	409
38	2048	63 -	38	410
47	2053	63 -	47	411
23	2058	63 -	23	412
27	2065	63	27	413
32	2066	63	32	413
38	2071	63	38	414
48	2076	63	48	415
21	2082	63	21	416
20	2089	63 -	20	418
28	2094	63 -	28	419
18	2099	63 -	18	420
20	2105	63	20	421
41	2107	63	41	421
30	2112	63	30	422
42	2116	63	42	423
42	2122	63	42	424
26	2129	63 -	26	426
38	2134	63 -	38	427
46	2139	63 -	46	428
62	2144	63 -	62	429
47	2149	63 -	47	430

Table 5.4 Extended Analysis

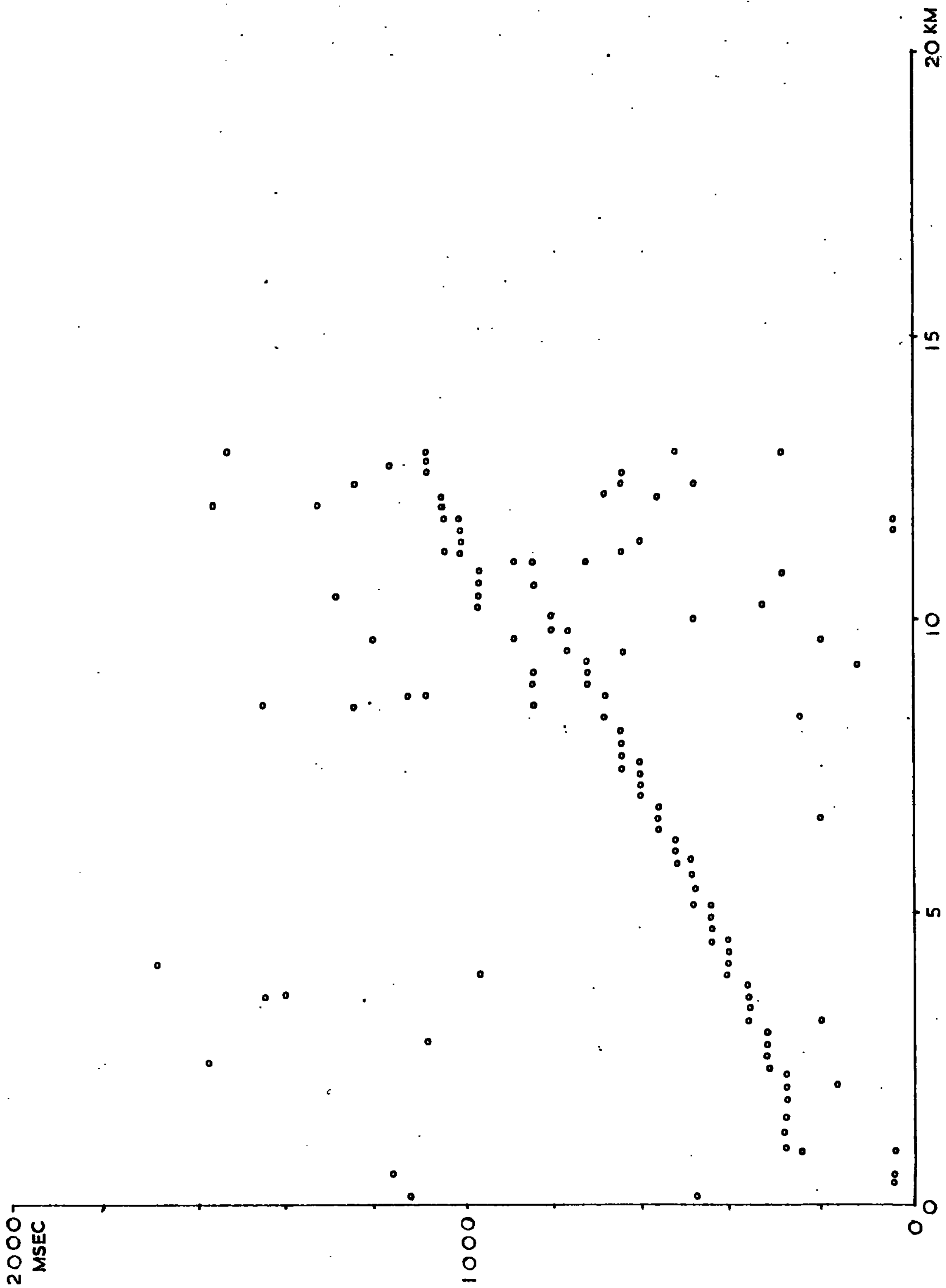

Fig. 5.10 **S1 Arrival Time/Distance**

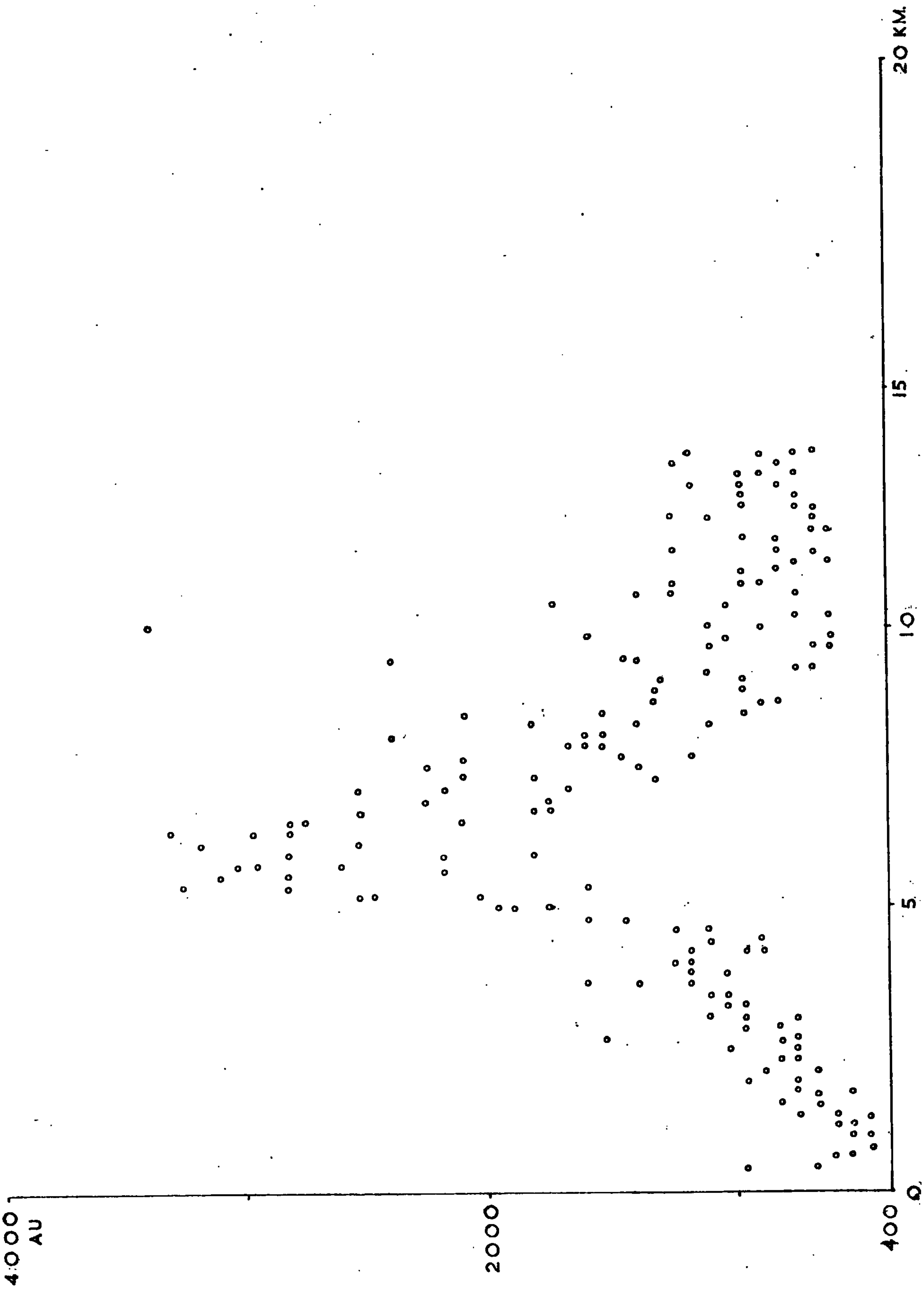

Fig. 5.11 **S1 Amplitude/Distance**

being made, it is certain that it is indeed the bottom reflection that is being considered.

The amplitude/distance plot is also an improvement but still shows considerable variation and in an effort to smooth these out the curve fitting techniques discussed in Chapter IV were applied to the data points.

These routines calculate the best fit of a polynomial of specified maximum degree to the given data points, using either a least squares or cubic spline method. A weighting factor is allocated to each data point and in the first instance all those amplitude values which were clearly incorrect were given a weighting of zero. An example of the output from one such fit, RAT + *NAG (Appendix 1), is given below.

Table 5.5

Curve-Fitting Output for Sonobuoy, S3 - All Record

Coefficient*	Error
0.246813D 03	0.223967D 06
-0.512474D 03	0.216590D 06
0.134282D 04	0.558046D 05
-0.954251D 03	0.434825D 05
0.343339D 03	0.394150D 05
-0.640666D 02	0.353928D 05
0.582796D 01	0.352825D 05
-0.204074D 00	0.350956D 05

*The numbers in the first column are the coefficients, a_i, in the expression

$$y = \sum_{i=o}^{n} a_i x^i$$

A plot of the output produced from this data by the curve generation routine, GEN (Appendix 1) is given in Fig. 5.12.

Clearly the errors involved in this fit to the amplitude curve

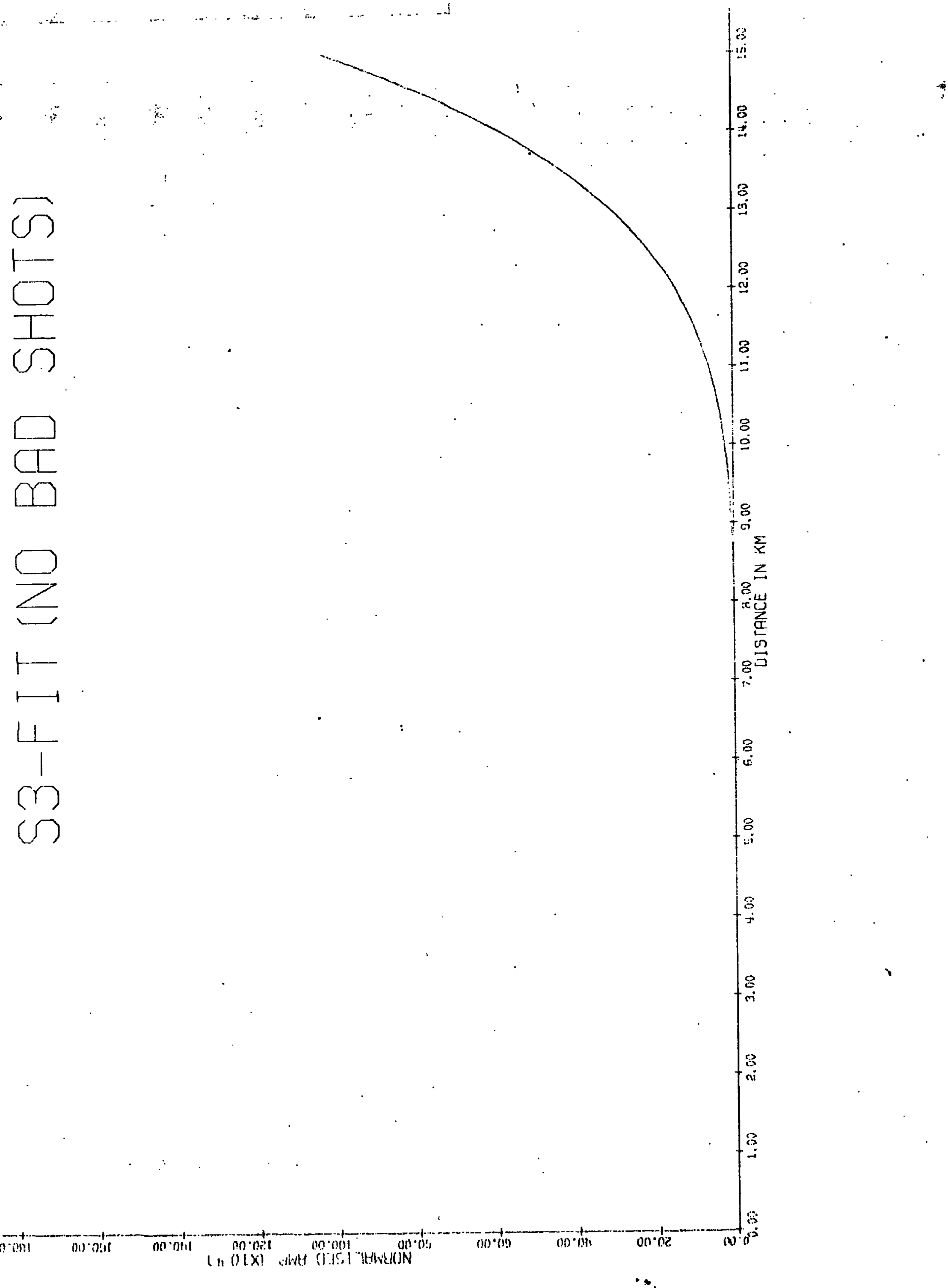

Fig. 5.12 S3 Bottom Reflection - No Bad Shots Fit

are unacceptable, and once it had been established that this was not confined to this particular sonobuoy run, it was decided to attempt a re-fit of the data by instructing the curve fitting programme to weigh other erroneous amplitude points with a zero value, and also to restrict the range of returns to within 8km of the ship to improve the signal to noise ratio.

Fig. 5.13 shows the amplitude/distance curve to be fitted and Fig. 5.14 the output from the generation programme, including 15 'bad' shots, which have been assigned zero weights in the fitting procedure. Table 5.6 gives the errors.

Table 5.6

Curve-Fitting Output - S3 15/87 Shots

Coefficient	Error
0.146842D 03	0.235336D 04
0.139719D 03	0.226152D 04
0.228739D 03	0.683976D 03
-0.144930D 03	0.548240D 03
0.476507D 02	0.524916D 03
-0.739646D 01	0.491260D 03
0.404793D 00	0.489284D 03

In this instance the generated curve follows the input curve quite well, to the eye, but the error bar shown on Fig. 5.14 indicates the amount of scatter present in the input data. For a peak reading of approximately 1500 amplitude units (mV-km^2), an error of $\pm$500 is totally unacceptable.

As a check to ensure that the curve fitting (RAT + *NAG) and generating programmes (GEN) were functioning correctly, a test was made using a known polynomial expression and the results displayed graphically in Fig. 5.15 and Fig. 5.16.

Fig. 5.17 and 5.18 show the detailed arrival time/distance

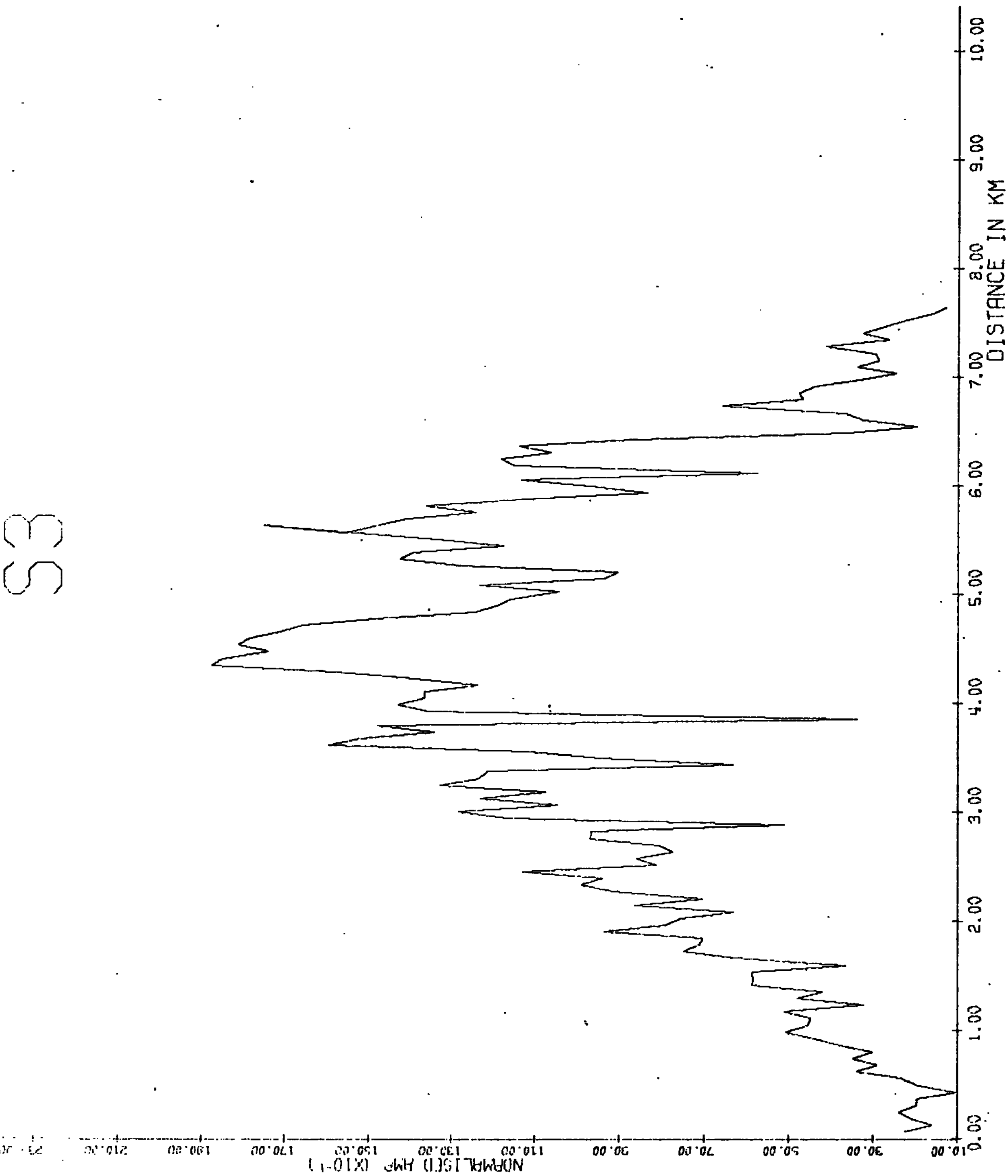

Fig. 5.13 S3 Bottom Reflection Amplitude

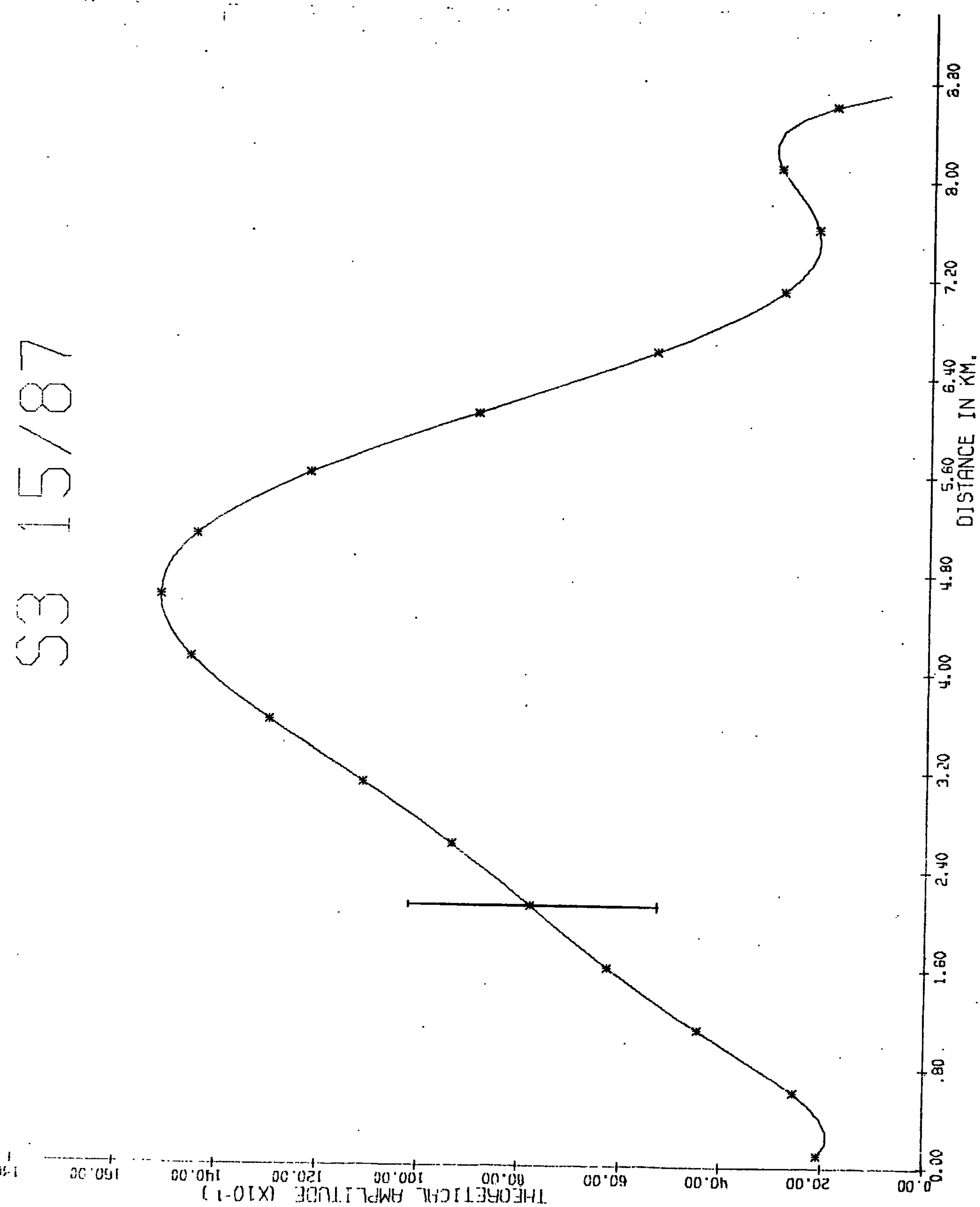

Fig. 5.14 **S3 Bottom Reflection (Fitted Curve)**

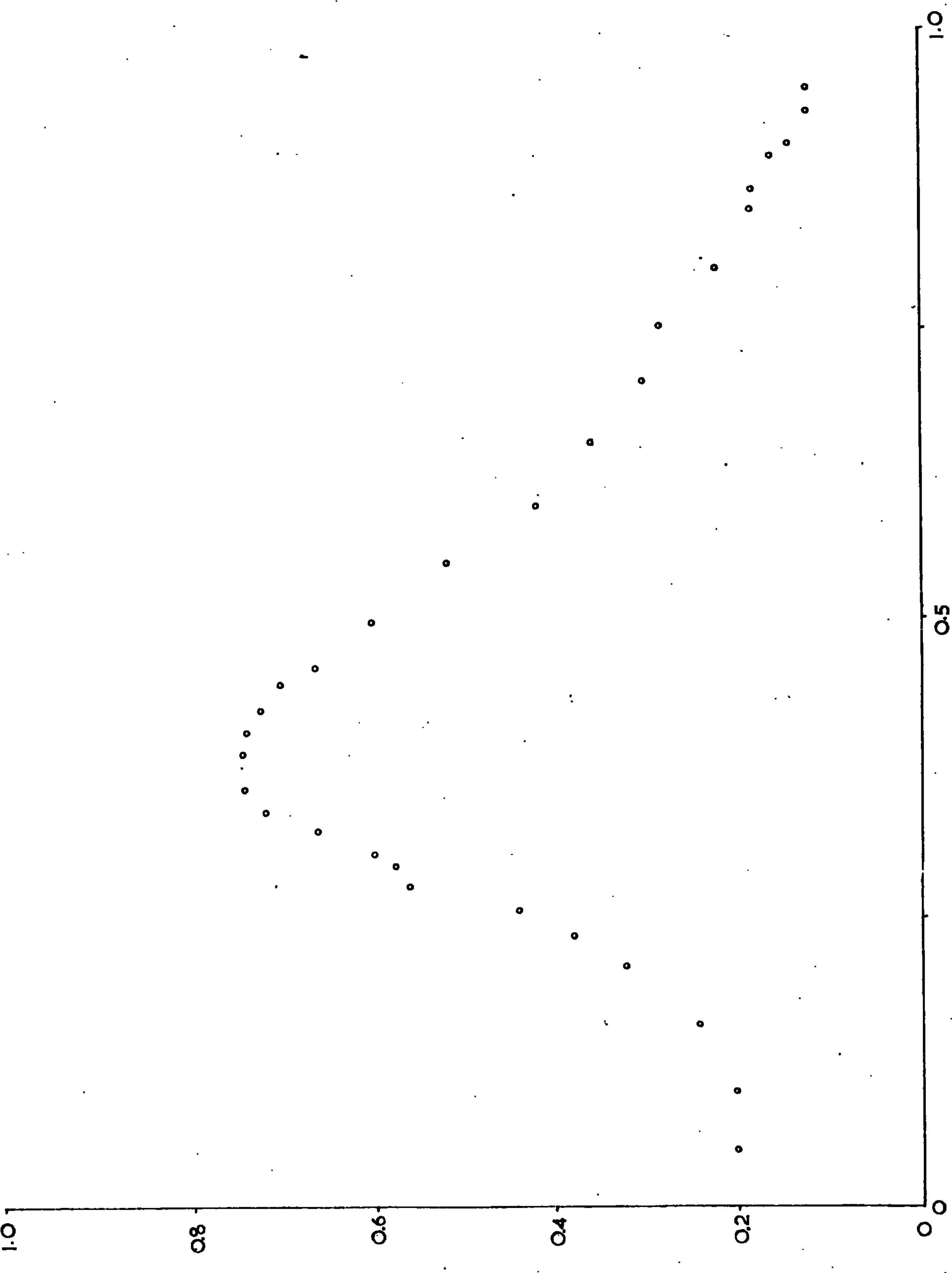

Fig. 5.15   Input Test Data For Curve Fitting

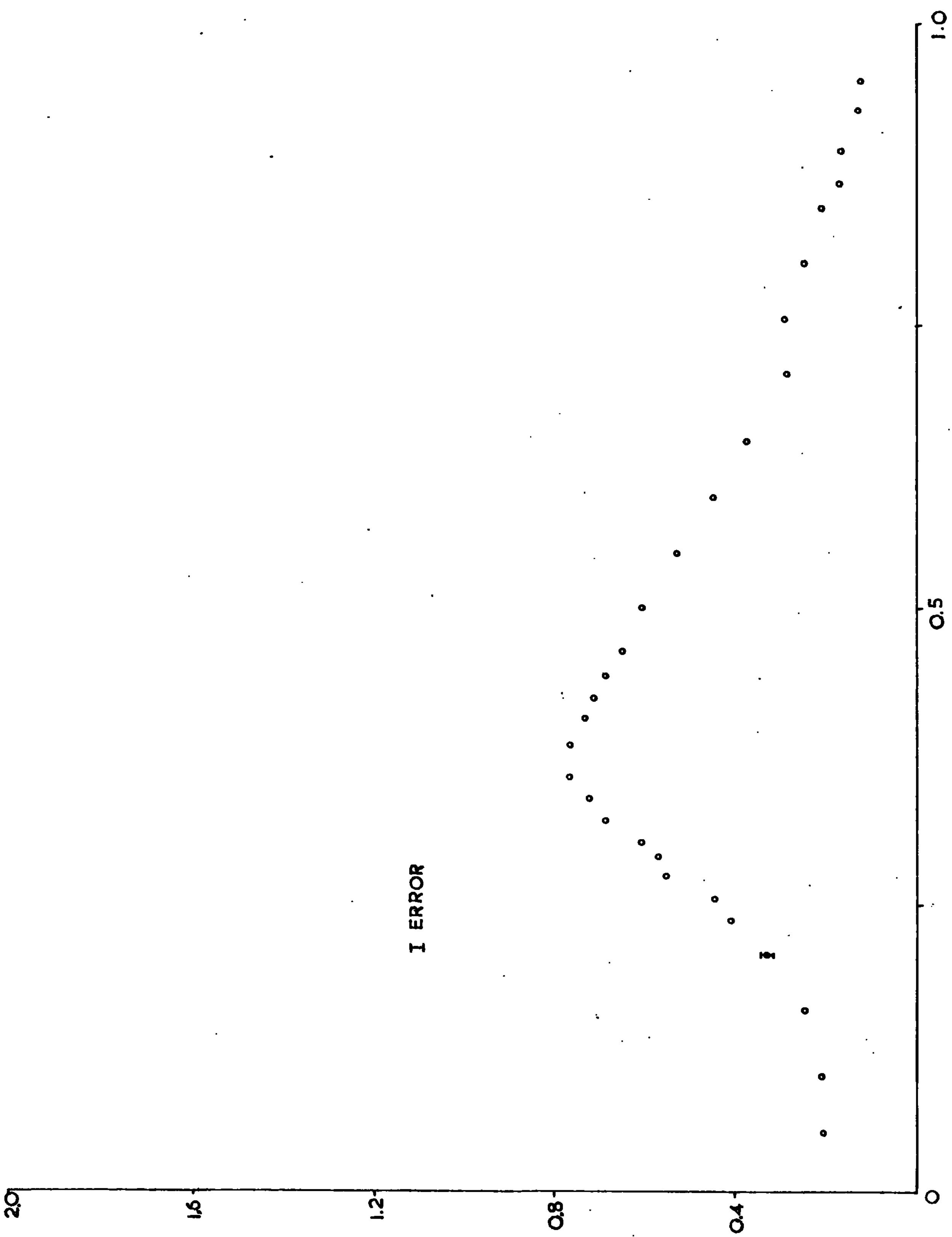

Fig. 5.16 Curve Fit to Test Data

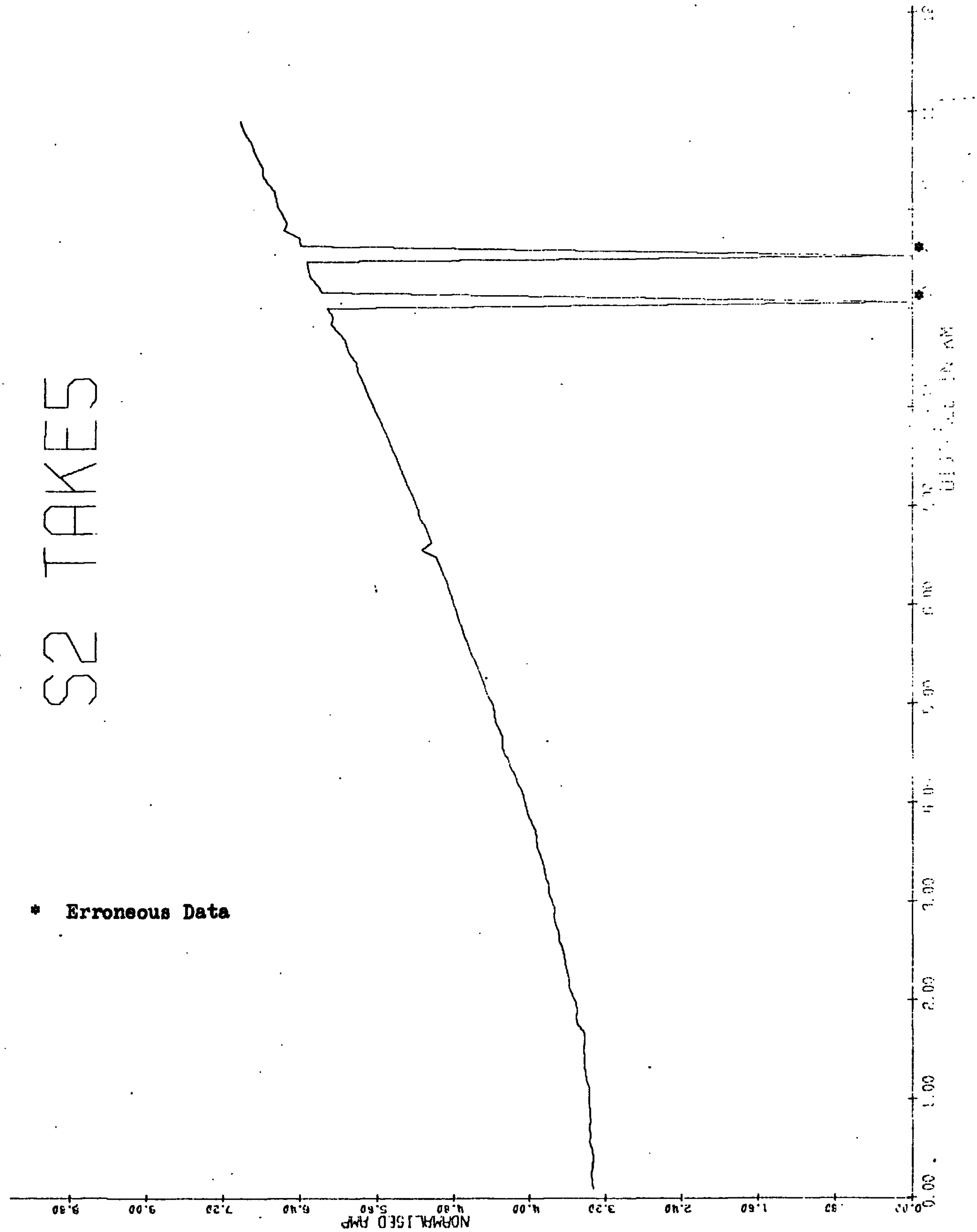

Fig. 5.17 **S2 Arrival Time**

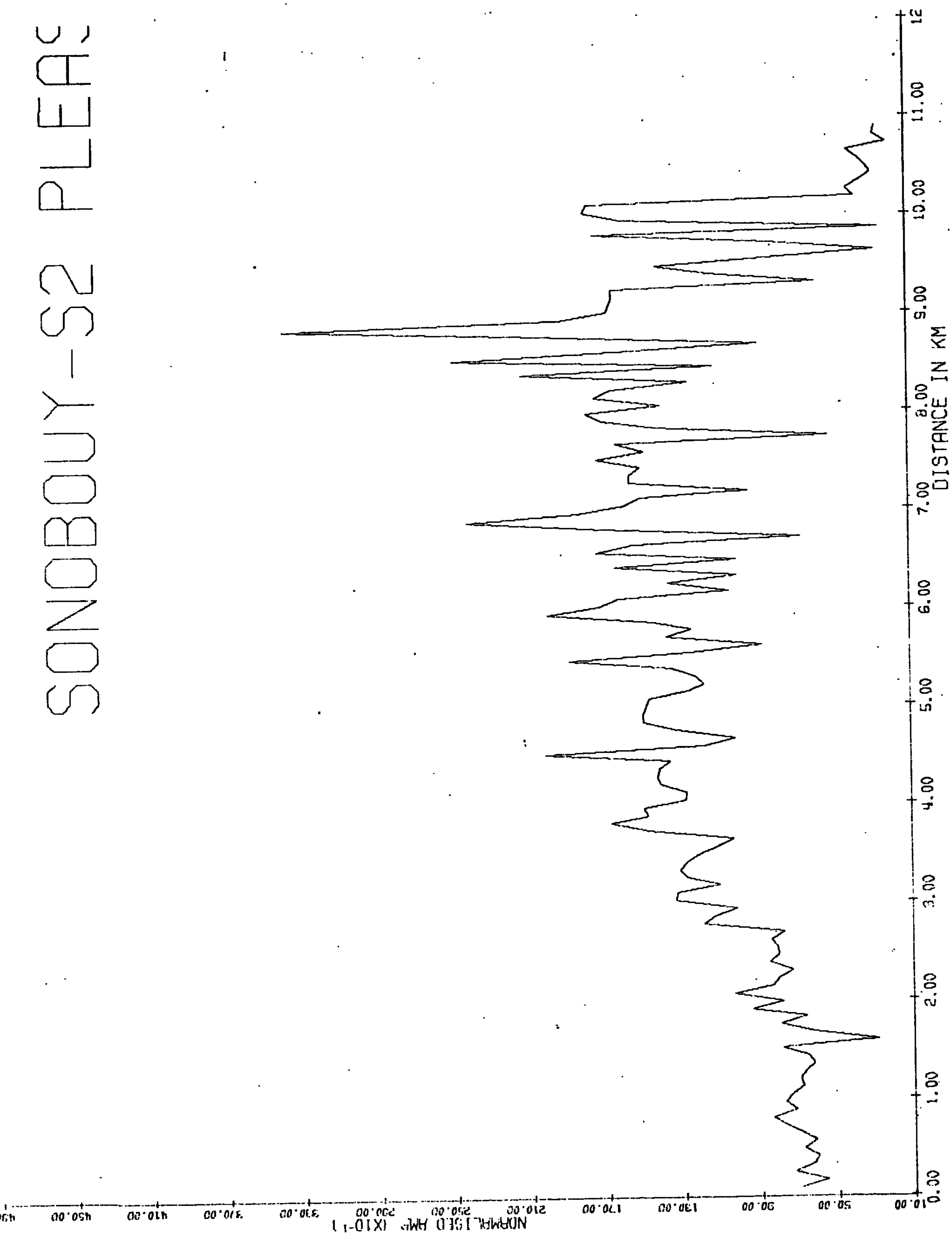

Fig. 5.18 **S2 Bottom Reflection Amplitude**

and amplitude/distance curves derived from sonobuoy run S2 by the methods described above. Fig. 5.19 depicts the output from GEN for 20 'bad' shots, while table 5.7, the errors produced by this fit.

Table 5.7

Curve-Fitting Output - S2 20/109 Shots

Coefficient	Error
0.488454D 03	0.242256D 04
0.103438D 04	0.230565D 04
-0.154229D 04	0.128955D 04
0.969357D 03	0.924444D 03
-0.281216D 03	0.867053D 03
0.410683D 02	0.855402D 03
-0.293341D 01	0.794388D 03
0.813374D 00	0.685829D 03

Again, it can be seen that the error of fit at ±680 in 1500 a.u. represents a minimum percentage error of 90% which is not very good.

Fig. 5.20 shows the expected amplitude variation with density ratio for a typical water/unconsolidated sediment reflection as calculated according to the theory developed in Chapter III. A change in lower medium density from 1.00 to 3.00 corresponds to a percentage change in peak amplitude of 56% which is considerably less than the error in the fitted curve, so that it is unlikely that any meaningful information on density variation could be obtained from this analytic method.

At this point, the sonobuoy runs examined in detail above were re-investigated attention being paid to the second and third positive peaks in the bottom reflection arrival, instead of the first positive peak used above. These secondary peaks are of slightly smaller amplitude than the initial peak and correspond to the airgun

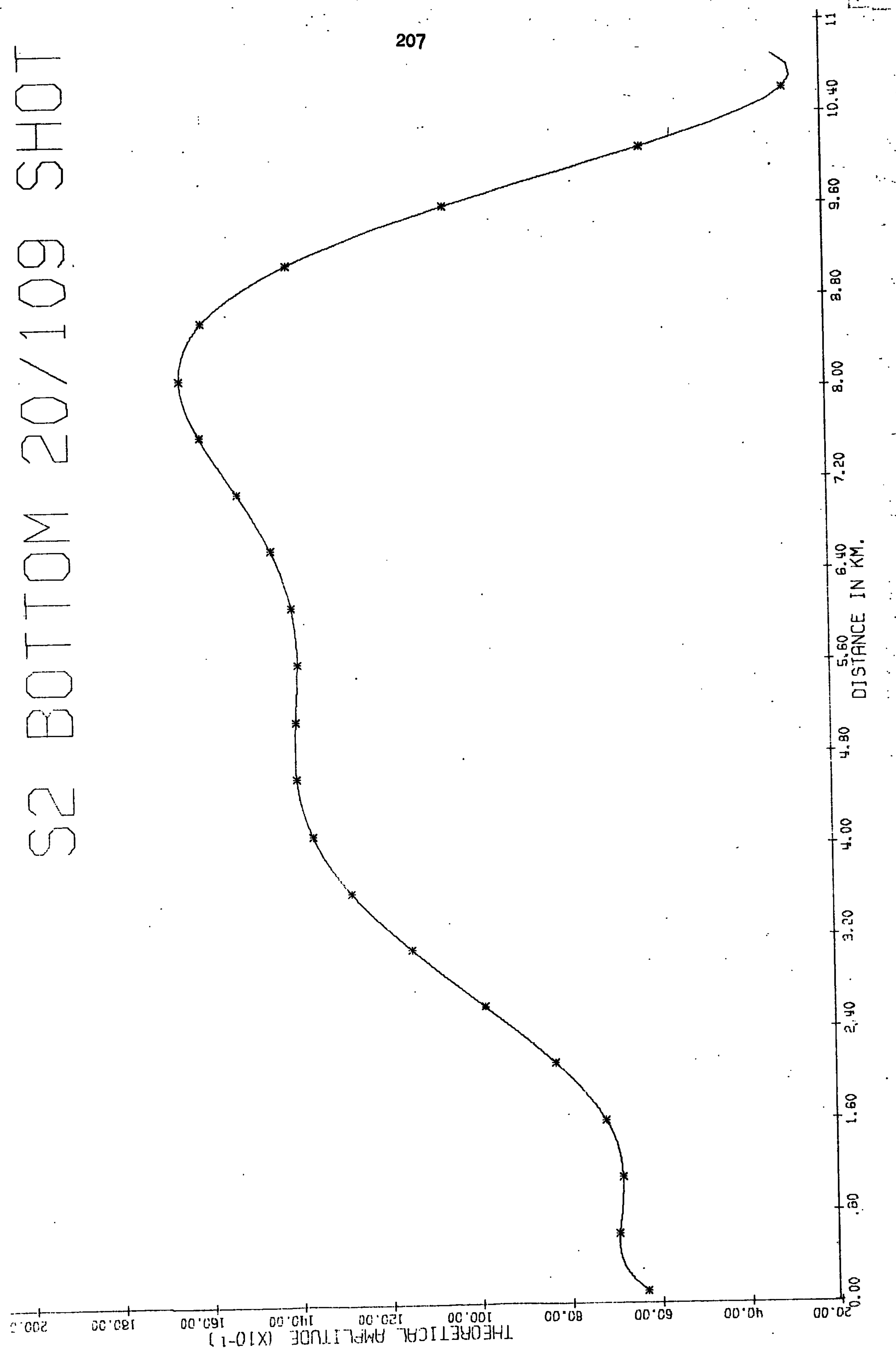

Fig. 5.19 S2 Bottom Reflection (Fitted Curve)

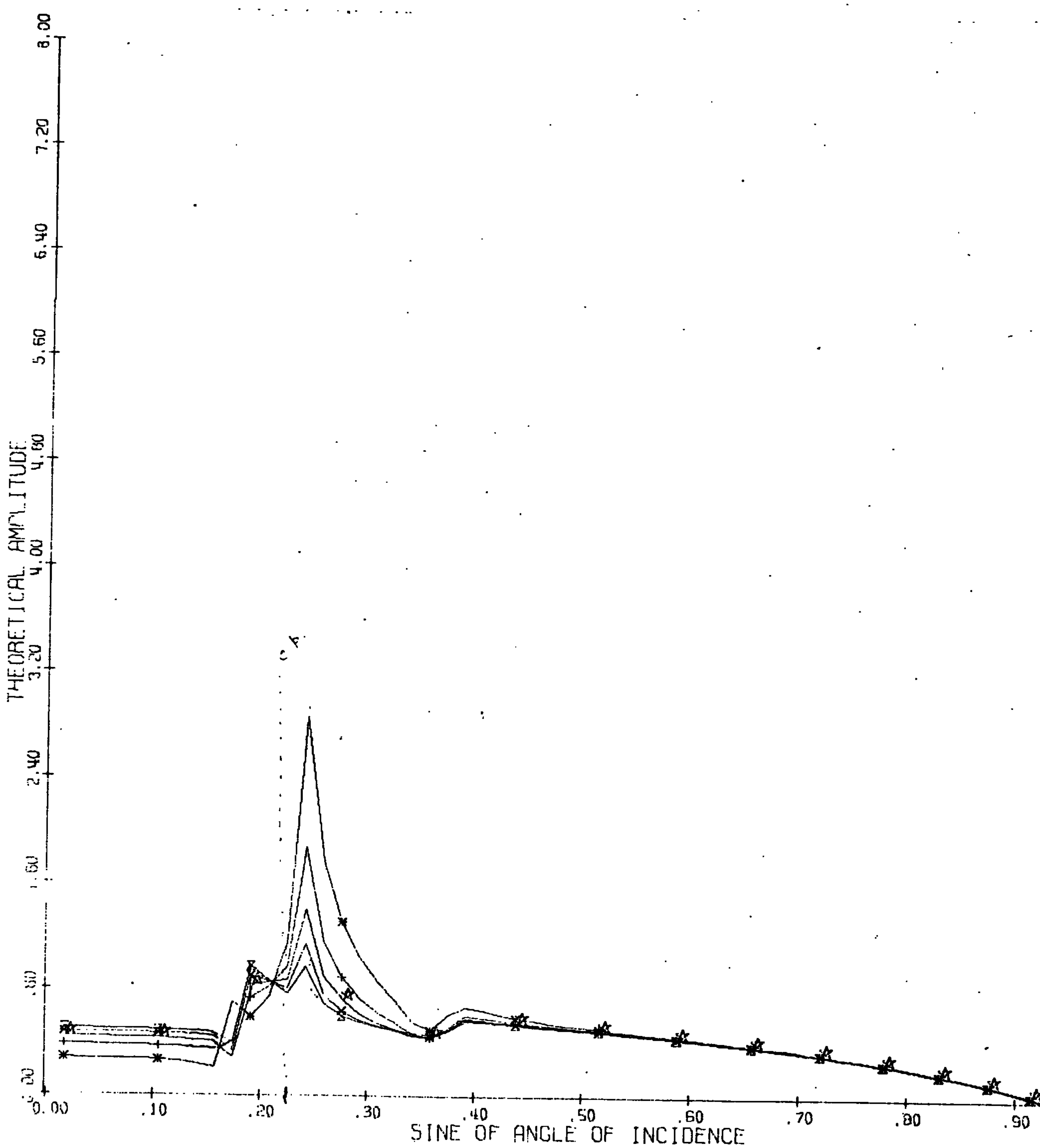

Fig. 5.20 **Theoretical Amplitude Variation with Density**

signature or bubble pulse oscillation of the acoustic source. Detailed printouts of the amplitudes of these peaks were laboriously obtained as before but a preliminary analysis indicated that they were no more consistent than the original.

Acoustic Basement Investigation

Although this initial investigation had proved unsuccessful, the entire procedure was repeated on reflections from the acoustic basement. The techniques employed for this examination are identical to those used previously, except that an effective water depth is calculated to allow for the passage of the sound wave through the upper sediment layers, as discussed in Chapter IV. Given that the signal level was somewhat lower than in the bottom reflection case, the wide angle reflections were even harder to discern.

Fig. 5.21 and 5.22 show the arrival time/ distance and amplitude/ distance curves obtained for the basement arrival for sonobuoy run, S2. Fig. 5.21 indicates that the same horizon is being examined throughout the record, whilst the amplitude plot displays considerable variation.

Fig. 5.23 shows the generated plot from the curve fitting output given in Table 5.8.

Table 5.8

Curve-Fitting Output - S2 Basement

Coefficient	Error
0.138160D 04	0.224691D 06
-0.924186D 03	0.160043D 06
0.282323D 03	0.137366D 06
-0.167946D 02	0.953289D 05

It is clear that this 'fit' is of even worse quality than those obtained for the bottom reflections.

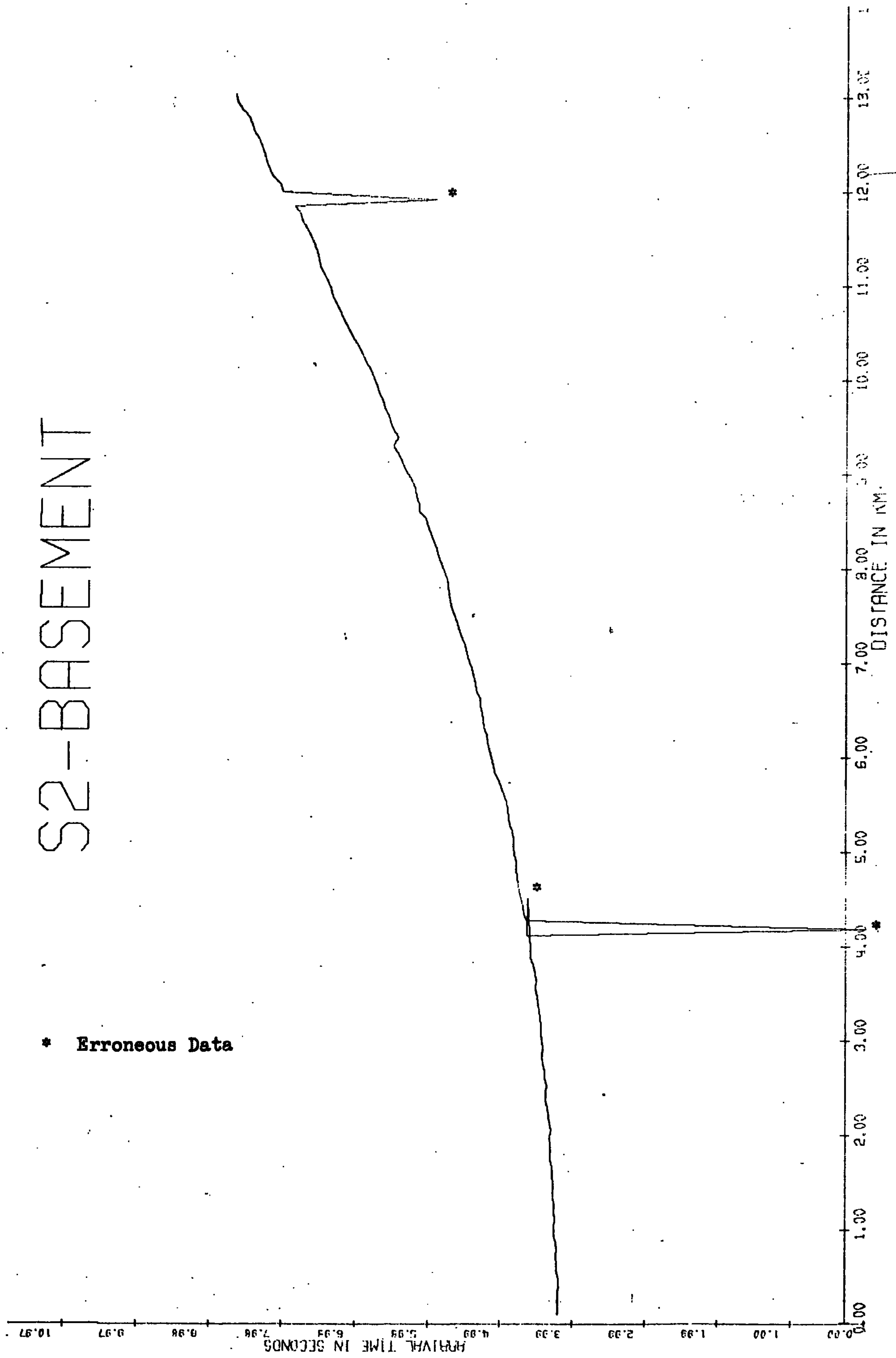

Fig. 5.21 **S2 Basement Arrival Time**

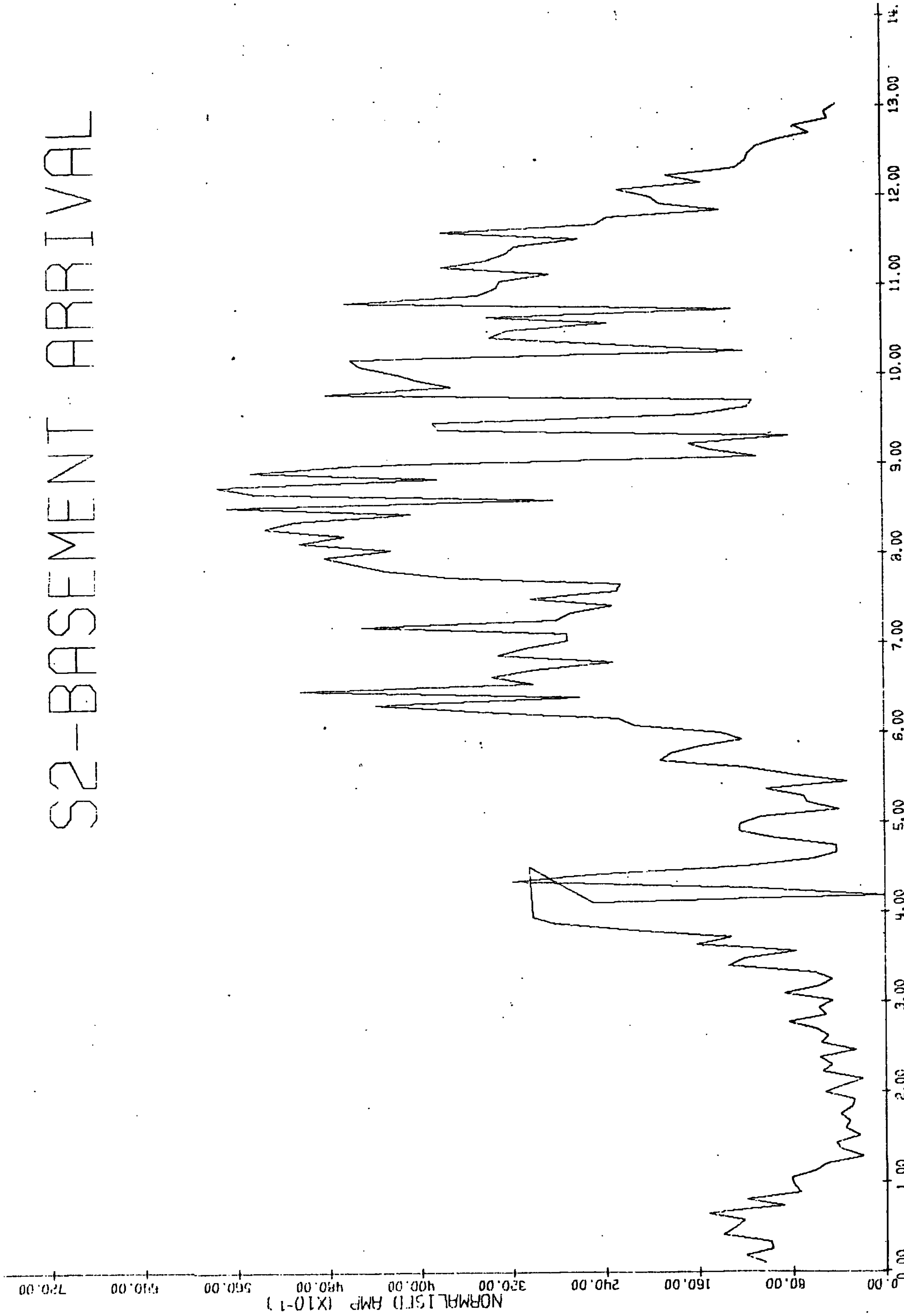

Fig. 5.22 S2 Basement Amplitude

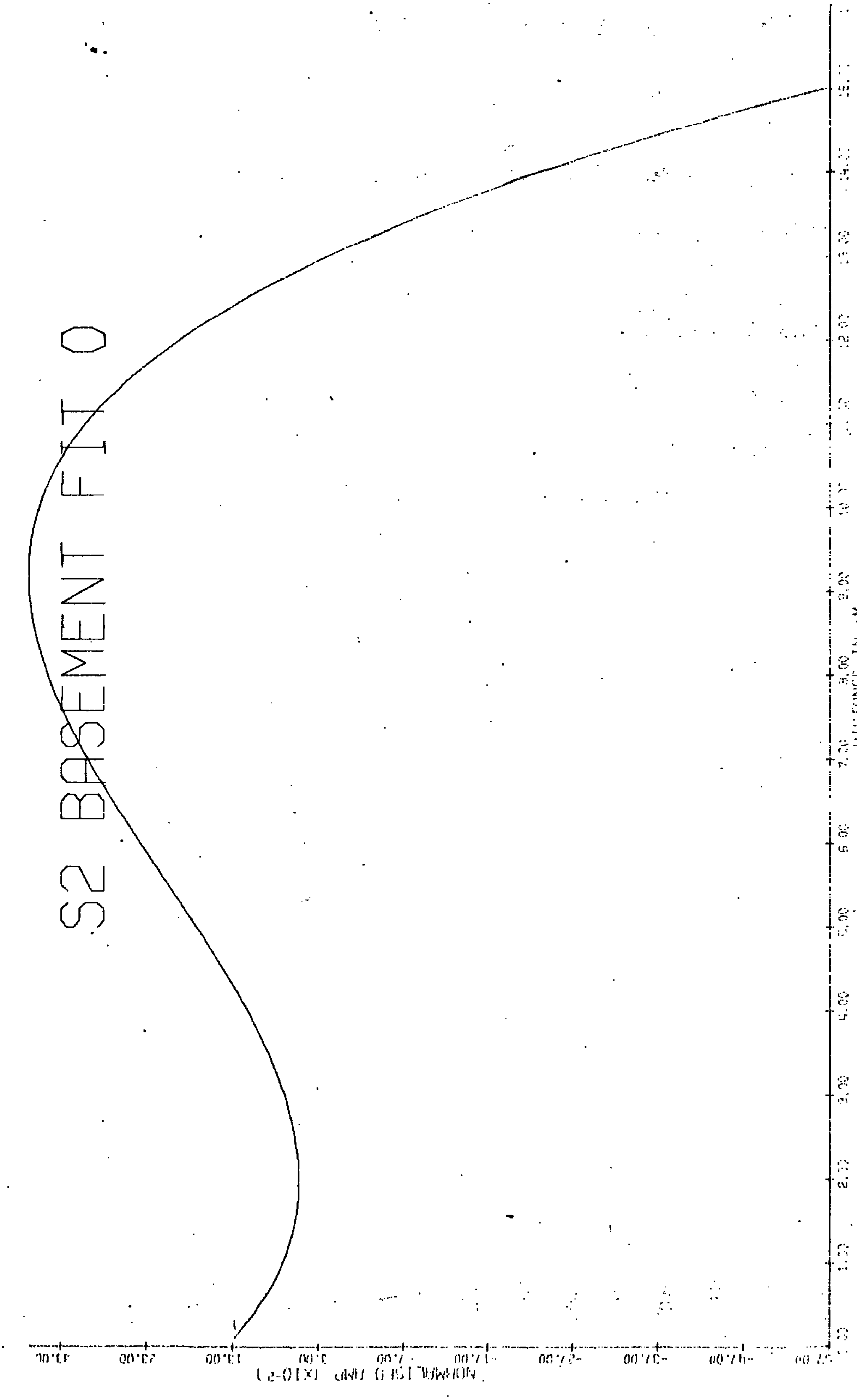

Fig. 5.23 Curve Fitting S2 Basement

Fig. 5.24 gives the fitted curve with ten 'bad' shot weighted to zero, but whilst this is an improvement over the previous case, the errors arising from this fit are still of the order of $\pm 10^3$ a.u. which renders the fit meaningless, as far as density identification is concerned.

The theoretical amplitude curves, shown in Fig. 5.20, were generated using the computer programme, FINAL, (Appendix 1) incorporating the acoustic velocities obtained from the wide angle refraction and reflection programmes discussed previously. The data input for the programme consists of the P and S velocities for the two media (Ref. 5.3) together with the appropriate densities (Ref. 5.4). Assuming an upper water layer of known density, a family of curves is obtained for a given input frequency band, for different density contrasts, and it was hoped that an estimate of the correct density value for the lower medium could be obtained by use of a multi-dimensional pattern recognition rechnique (Ref. 5.5).

In this process the Cartesian co-ordinates of the entire family of curves are input to the computer and then compared, point by point, with the co-ordinates of the experimental curve, using a least squares fit. That theoretical curve which matches the experimental at the greatest number of data points, or dimensions, is taken to be the most similar to the latter and hence is the curve with the closest approximation to the correct density.

The spread of a family of curves for the expected range of density ratios (Ref. 5.6), is unfortunately, as mentioned above, less than the error estimates for the fitted curves, and thus these could not be used in this pattern recognition procedure. Attempts to use the raw data itself were similarly unsuccessful.

It was not anticipated that the frequency dependent oscillations in the supercritical region would be observed, as one is examining a window of frequencies (5-50Hz), over which one would

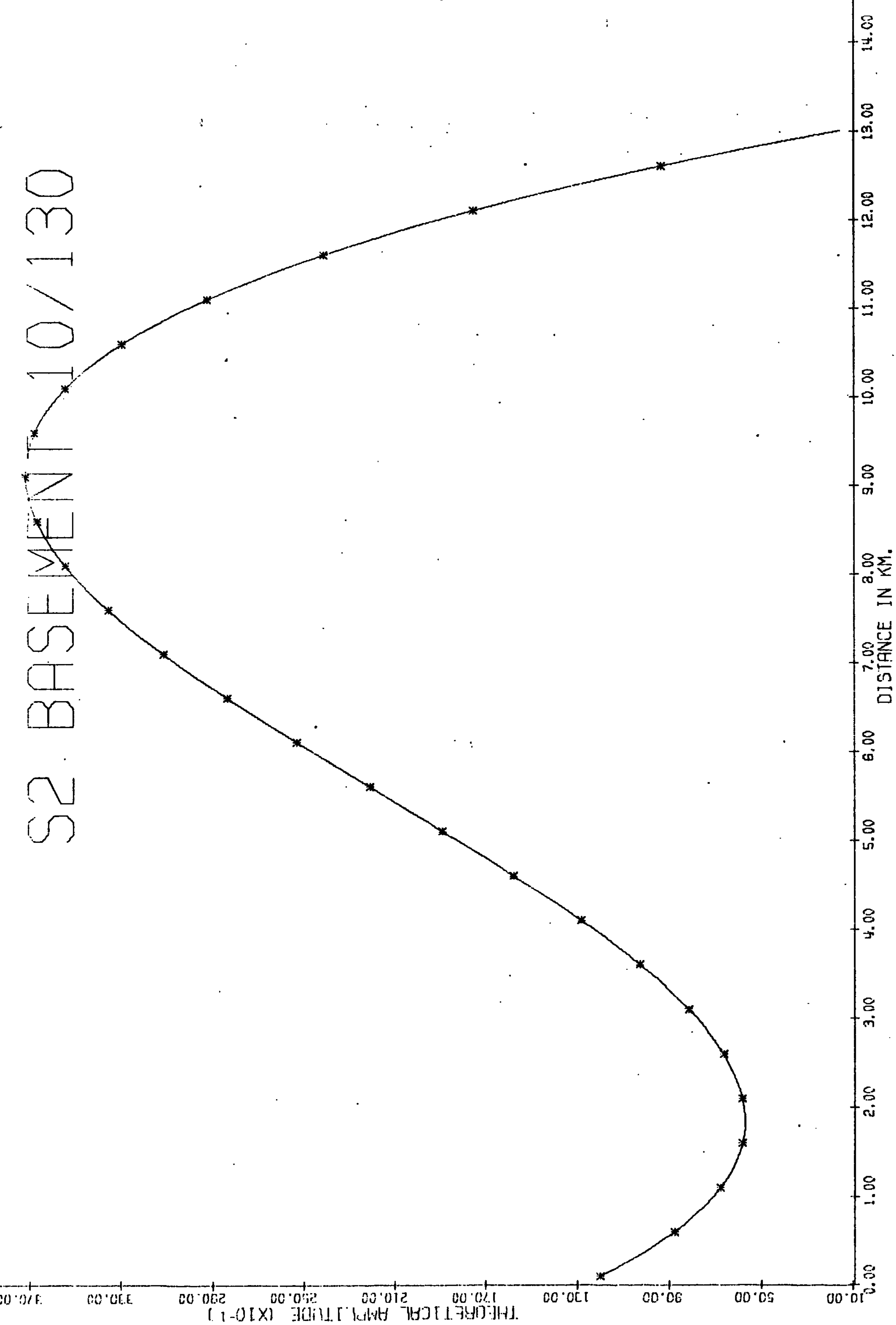

Fig. 5.24 Curve Fitting - S2 Basement

expect this feature to be averaged out, but it was hoped that the subcritical curve shape and the position of the amplitude maximum would be seen. As this was not so, it was decided not to undertake the extremely time consuming and laborious process of analysing further sonobuoy records using these techniques.

Programme Check

As a check to test that the theoretical curves themselves were valid, a model of the continental crust in the Bavarian Molasse basin (Ref. 5.7, 5.8), was used to generate a theoretical amplitude curve. The actual crustal model is simewhat complicated, involving a differentiated gradient zone at the transition between crust and mantle, (Ref. 5.9), and this was simplified to the model shown in Fig. 5.25 to enable FINAL to be used by introducing a space varying velocity function. The results are shown in Fig. 5.25, and it can be seen that whilst the curve is not exactly correct it behaves in a reasonable manner, indicating that the theory does provide a valid result. The curve presented is the mean curve for frequencies between 10 and 15Hz, following Meissner (Ref. 5.10), in which the arrivals between 9 and 17Hz are those which are least affected by multiple and ghost events.

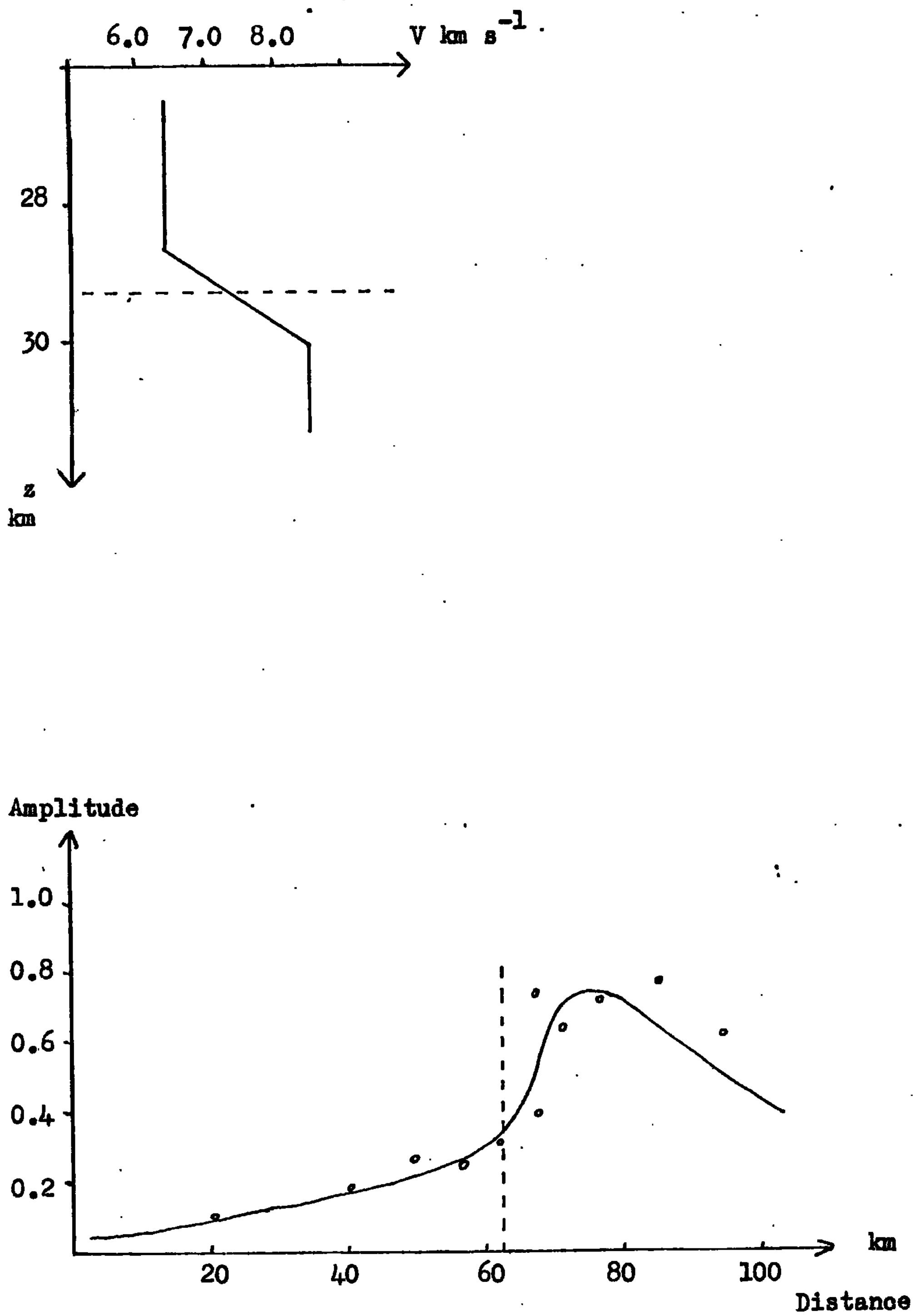

Fig. 5.25 Crustal Amplitude Model (after Meissner, 1967)

Signal Processing

In order to improve the quality of seismic records, by removing unwanted multiple reverberations and bubble pulse oscillations, it is conventional to deconvolve the records with functions representing these unwanted signals (Ref. 5.11).

Due to the nature of the wide angle reflection standard deconvolution operators are not applicable in that the path length of the shot and hence the shape of the incident waveform vary with increasing separation of ship and sonobuoy, so that a time varying deconvolution method must be sought (Ref. 5.12).

An attempt was made to use a continuously adaptive linear prediction operator in which the operator coefficients are updated using a simple adaptive algorithm. New values for the coefficients are compared for each sample of data so as to minimise the mean square errors, following Griffith's method (Ref. 5.13). This method differs from the time varying deconvolution techniques used by Wang and others (Ref. 5.14), in which autocorrelation estimates of the data are calculated, in order to solve a set of normal equations to determine the coefficients of the deconvolution operator which is, in turn, applied to the data to obtain the deconvolved output.

Griffiths' extension of Wiener filtering has proved successful in its application to conventional marine reflection data, where the removal of multiple arrivals is excellent, but when his programme was applied to the data here, it was unsatisfactory, the portion of the programme designed to remove multiples of the refraction arrivals also removing the wide angle events (Ref. 5.15).

If the problem, howerer, is treated using 'Cepstrum' analysis techniques (Ref. 5.16), this particular limitation does not occur. Consider the complex natural logarithm of the amplitude and phase spectra, log $\left[A(w)e^{i\phi(w)}\right]$ as a complex time series and take the inverse Fourier transform of this series to produce the complex cepstrum (Ref. 5.17, 5.18).

Deconvolution in the time domain becomes subtraction in the complex cepstrum and so time varying deconvolution becomes much easier to implement.

Following the work by Stoffa, Buhl et al (Ref. 5.19), a preliminary study was made to see if their homomorphic deconvolution techniques would be applicable to the problem encountered here. Only one shot was analysed and the deconvolved output from Stoffa's programme is shown in Fig. 5.26. The reflecting horizons present in the record can be seen more clearly than in the original.

By varying the period for which the complex cepstrum contributions are set to zero in performing the deconvolution, it is possible to look at the reflection of different frequency bands whthin the original waveform, and it can be seen from Fig. 5.27 that there is an apparent shift in the reflection position of the higher frequency portion of the signal. The two traces in Fig. 5.27 correspond to incident frequency bands of (5-25)Hz and (30-50)Hz.

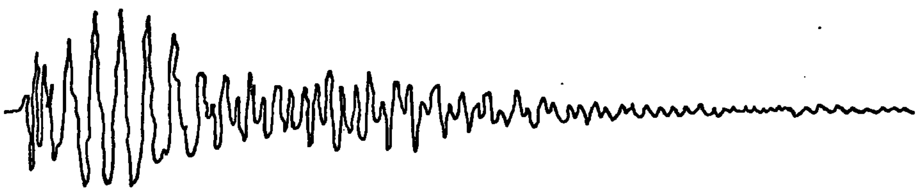

Input waveform

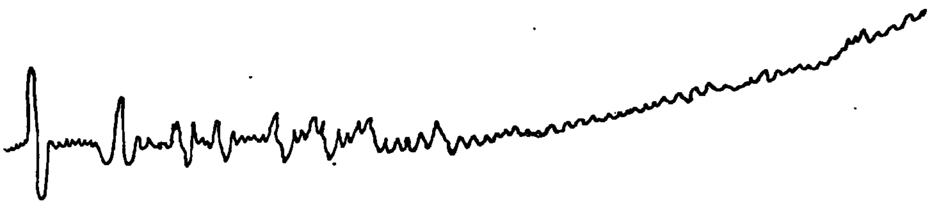

Deconvolved waveform

(corresponding to all cepstrum contributions
-T ≤ 18 ≤ T, being set to zero).

Fig. 5.26 Cepstrum Deconvolution of One Shot

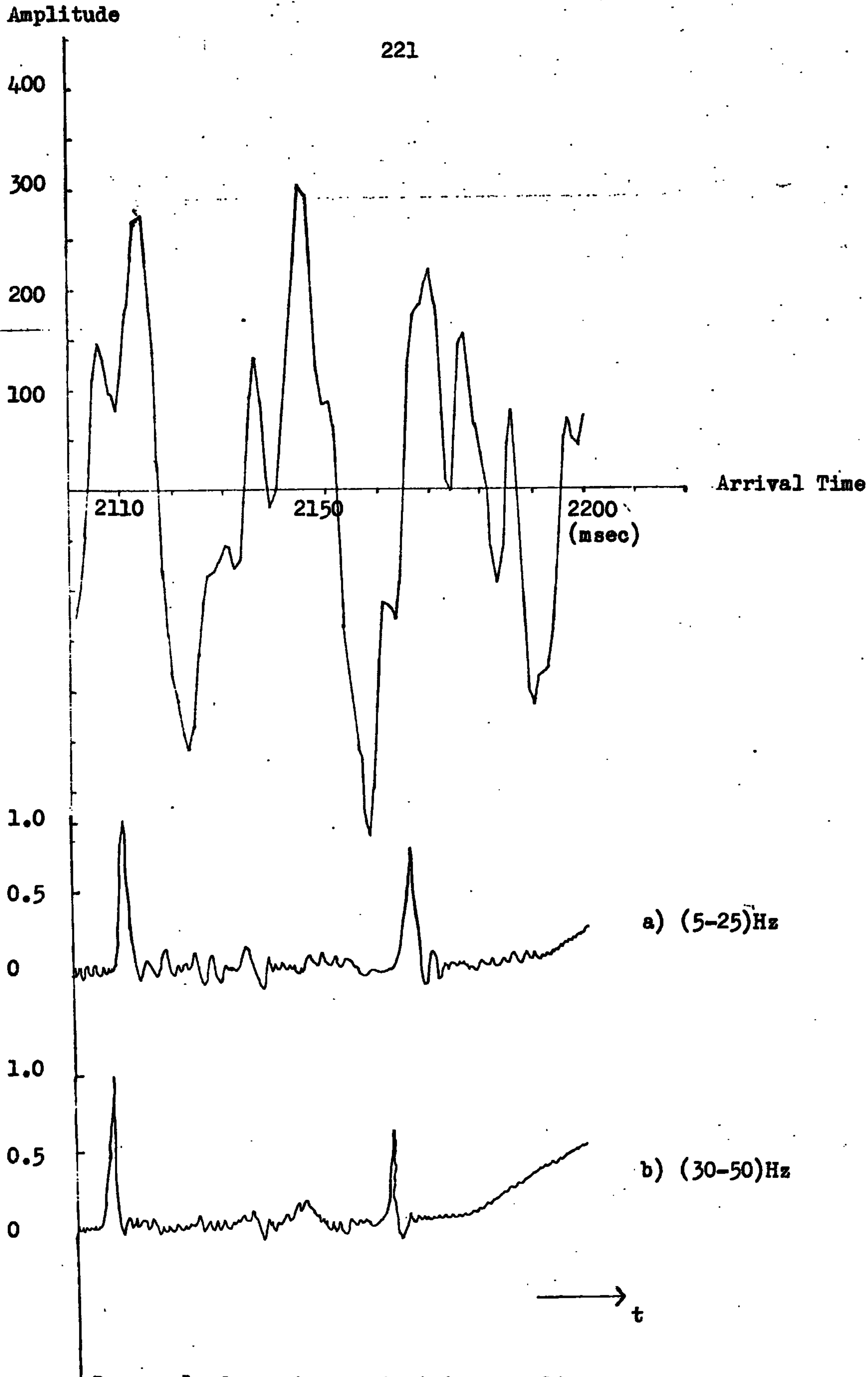

Deconvolved cepstrum output is normalised.

<u>Fig. 5.27</u> <u>Detailed Deconvolution - Shot 56, S2</u>

Discussion

The major question to be considered is the cause of the failure to obtain correlation between the predicted and practical results. The problem arises in the actual recorded amplitude, the arrival time plots given in the preceeding section indicating that the same reflecting horizon is being examined.

When one considers the physical processes involved in obtaining the record, the following possible sources of error come to mind.

i) Hydrophone

A change in the ambient noise level due to aperiodic wave motion/current noise might influence the record.

By examining, at some length, the recorded portion of the tape prior to any seismic arrivals for several sonobuoy runs, at varying separations in different depths of water, it was decided that the variation in mean noise level was not sufficient, within one run, to explain the extremes of amplitude variation present in the peak amplitude arrival.

ii) Variations in Airgun Intensity

This was considered as the airgun/compressor system on board the R.R.S. "Shackleton" was subject to periodic venting, but the time interval between successive vents was of the order of 15-20 minutes which would hardly manifest itself on the records examined. An examination of the direct wave from the airgun at close range for three sonobuoy runs indicated that the signal emanating from the airgun was of extreme regularity both in frequency content and amplitude.

iii) Frequency Demodulation/Tape

The question of the F.M. demodulator misindexing and giving rise to spurious results was considered but rejected as this would result in the loss of the record during the period of misindexing. The tape deck used was also used for recording a continuous reflection profile simultaneously with the wide angle record and a brief analysis of the normal incidence reflection amplitude did not reveal variations coincident with the wide angle measurements, thus indicating there were no tape 'drop-outs' or irregularities responsible for a loss of signal strength.

iv) Digitisation

The idea that aliasing of some description was responsible occurred, but the signals having been digitized at 500Hz, had been passed through an 80Hz low pass filter which was some 81dB down to 125Hz, before being written onto digital tape. The signals were also band pass filtered (5-50Hz) before analysis, (Appendix 3).

v) Superposition

Returning to Fig. 5.4 and 5.5, showing the bottom reflection for consecutive shots and referring to Fig. 5.27, it is apparent from these plots that the wave group as a whole is moving along the time axis of the plot, and it can be seen that different peaks within the bottom reflection wavelet are displaced by varying amounts, so that enhancement and cancellation between the various peaks is occurring.

Fig. 5.27 demonstrates that the higher frequency portion of the waveform is being reflected at a different time to the lower frequencies i.e. the lower frequency components are being reflected at a slightly lower point in the medium than the higher frequencies, and hence have a alightly different time of travel. The reason for this differential reflection, well known in echo-sounding studies (Ref. 5.20), is that the typically water saturated unconsolidated sediments that constitute the uppermost layers of the ocean floor are little more than colloidal suspensions, whose suspended particle size increases with depth, thus resulting in the higher frequencies being reflected 'above' the lower frequencies (Ref. 5.21).

Thus it is conceivable that this relatively microscopic phenomenon, which is possibly subject to lateral variations, of short wavelengths in comparison to the range covered by successive wide angle reflections, due to differing bottom current levels, turbidity, temperature and particle size could cause this superposition. During the course of one sonobuoy run over what is macroscopically homogeneous sediment according to the continuous reflection profile, these variations could effect the wide angle reflections in the manner observed. Those reflections from the acoustic basement would pass through such small scale inhomogeneities and would be similarly subject to these frequency selective phase shifts.

vi) Interference

Another possible cause of this wide variation in amplitude return level may be discerned by examining Fig. 5.5 and 5.26, from which it seems that interference is occurring between different portions of the return leading to cancellation and enhancement of the signal which is obscuring the true amplitude.

This interference could be between the reflected and refracted portions of the wave but as this would only be expected at certain water depths/velocity structures and ship to sonobuoy separations, there must be some interference occurring between different reflections at almost all angles of incidence, caused by the relatively long pulse length of the air gun in combination with the nature of the reflecting horizons themselves.

Conclusion

From this preliminary analysis of the dynamic properties of wide angle reflections it is obvious that no clear picture can emerge from the simple amplitude investigation techniques developed here, as to the physical constitution of the reflecting horizons as was anticipated from the theoretical analysis.

Amplitude information is being lost due to either superposition within the reflected waveform possibly produced by a non-linear effect in the uppermost sediment layers, or interference between different reflection and refraction arrivals in the return signal or perhaps a combination of the two. This is leading to such large variations in the measured amplitudes that no exact determination of the lower medium density was able to be made.

Recent developments in signal processing techniques may give better results by allowing smaller frequency bands to be investigated separately as illustrated briefly above, but it is unlikely that the arrangement used to collect the data in this case would be suitable, a shorter range system of higher resolution being probably required to allow either examination of the fine structure which may have been detected in this range of experiments or to enable the different pulses producing the interference effect noted above to be separated for detailed examination.

BIBLIOGRAPHY

References

1.1 Dobrin, M.B., (1960).
'Introduction to Geophysical Prospecting'.
Chapter II. McGraw Hill.

1.2 Grant, F.S., and West, G.F., (1968).
'Interpretation Theory in Applied Geophysics', 49 - 63

1.3 Sheriff, R.E., (1974).
'Seismic Detection of Hydrocarbons - The Underlying Physical Principles'.
OTC Reprints, 1, 637-660.

1.4 Schoenberger, M., and Mifsud, J.F., (1974).
'Hydrophone Streamer Noise'.
Geophys., 39, 781-794.

1.5 Ewing, J., and Ewing, H., (1961).
'A Telemetering Ocean Bottom Seismograph'.
J. Geoph. Res., 66, 3863 - 3877.

1.6 Wenz, G.M., (1962).
'Acoustic Ambient Noise in the Ocean : Spectra and Sources'.
J. Ac. Soc. Am., 34, 1936-1956.

1.7 Whitmarsh, R.B., (1967).
'Explosion Seismology on the Sea Bed'.
Unpublished Ph.D. Thesis, University of Cambridge.

1.8 Hamilton, E.L., Moore, D.G., Buffington, E.C., Sherrer, P.L., and Curray, J.R., (1974).
'Sediment Velocities from Sonobuoys - Bay of Bengal, Bering Sea, Japan Sea and N. Pacific'.
J. Geophys., Res., 79, 2653.

1.9 Dobinson, A., (1971).
'The Development of a Marine Seismic Recording System'.
Pt I, unpubl. Ph.D. Thesis, University of Durham.

1.10 Berman, A., and Saur, A.J., (1960).
'Ambient Noise as a Function of Depth'.
J. Ac. Soc. Am., 32, 19.

1.11 Anstey, N.A., (1970).
'Seismic Prospecting Instruments, Volume I, Signal Characteristics and Instrumental Specifications'.
Gebrüder Borntraeger.

1.12 Gray, F., and Owen, T.R.E., (1969).
'A Recording Sono-Radio Buoy for Seismic Reflection Work'.
presented at Oceanology Conf., Brighton, England.

1.13 Mayne, W.H., and Quay, R.G., (1970).
'Seismic Signatures of Air Guns'.
presented at 2nd Annual Off. Tech. Conf., Austin, Texas.

1.14 Cagniard, L., (1962).
'Reflection and Refraction of Progressive Seismic Waves'.
Trans. from French (Gantlier-Villars, Paris, 1939).
by E.A. Flinn and C.H. Dix.
McGraw Hill, New York.

1.15 Rayleigh, Lord, (1885).
'On Waves Propagated along the Plane Surface of an Elastic Solid'.
Proc. London Math. Soc., 17, 4-11.

1.16 Lamb, M., (1904).
'On the Propagation of Tremors over the Surface of an Elastic Solid'.
Phil. Trans. Roy. Soc. London A, 203, 1-42.

1.17 Sommerfeld, A., (1909).
'Über die Ausbreitung des Wellen in der Drahtlosen Telegraphie'.
Ann. Physik, 28, 665-736.

1.18 Smirnov, V., and Sobolev, S., (1933).
'On the Application of a New Method of Investigation of the Elastic Vibrations in a Space with Axial Symmetry'.
Trudy Inst., Seism. Akad. Nauk. USSR., 29.

1.19 Spencer, T., (1960).
'The Method of Generalized Reflection and Transmission Coefficients'.
Geophys., 25, 625-641.

1.20 Pekeris, C.L., (1955).
'The Seismic Surface Pulse'.
Proc. Natl. Acad. Sci. U.S., 41, 469-80.

1.21 Petrashen, G.I., (1957).
'Materials for the Quantitative Investigation of the Dynamics of Seismic Waves'. Vol II.
Leningrad University Press, Leningrad.

1.22 Sherwood, J.W.C., (1958).
'Elastic Wave Propagation in a Semi-Infinite Solid Medium'.
Proc. Phys. Soc. (London), 71, 207-219.

1.23 Zoeppritz, K. (1919).
'Erdbebenwellen VIII B, Über Reflexion und Durchgang Seismischer Wellen durch Unstetigkeitsflachen'.
Gottinger Nachr., 1, 66-84.

1.24 Knott, C.G., (1899).
'Reflexion and Refraction of Elastic Waves, with Seismological Applications'.
Phil. Mag. (London), 48 64-97.

1.25 Macolwane, J.B., (1936).
'Introduction to Theoretical Seismology, Part I, Geodynamics'.
St. Louis University, St. Louis.

1.26 Muskat, M., and Meres, M.W., (1940).
'Reflection and Transmission Coefficients for Plane Waves in Elastic Media'.
Geophys., 5, 115-148.

1.27 Love, A., (1944).
'A Treatise on the Mathematical Theory of Elasticity'.
Dover, New York.

1.28 Gutenberg, B., (1944).
'Energy Ratio of Reflected and Refracted Seismic Waves'.
Bull. Seism. Soc. Am., 34, 85-102.

1.29 Richter, C.F., (1958).

'Elementary Seismology'.

W.H. Freeman, San Francisco.

1.30 McCamy, K., Meyer, R.P., and Smith, T.J., (1962).

'Generally Applicable Solutions of Zoeppritz Amplitude Equations'.

Bull. Seism. Soc. Am., 52, 923-955.

1.31 Koefoed, O., (1962).

'Reflection and Transmission Coefficients for Plane Longitudinal Incident Waves'.

Geoph. Prosp., 10, 304-351.

1.32 Costain, J.K., Cook, K.L., and Algermissen, S.T., (1963).

'Amplitude, Energy and Phase Angles of Plane SV Waves and Their Application to Earth Crustal Studies'.

Bull. Seism. Soc. Am., 53,1039-1074.

1.33 Costain, J.K., Cook, K.L., and Algermissen, S.T., (1965).

'Corrigendum : Amplitude, Energy and Phase Angles of Plane SV Waves and Their Application to Earth Crustal Studies'.

Bull. Seism. Soc. Am., 55, 567-575.

1.34 Tooley, R.D., Spencer, F.W., and Sagoci, H.F., (1965).

'Reflection and Transmission of Plane Compressional Waves'.

Geophys., 30, 552-570.

1.35 Singh, S.J., Ben-Menahem, A., and Shimshoni, M., (1970).

'Comments on Papers by Costain et al. and McCamy et al. on the Solutions of Zoeppritz Amplitude Equations'.

Bull. Seism. Soc. Am., 60, 277-280.

1.36 O'Doherty, R.F., and Anstey, N.A., (1971).

'Reflections on Amplitudes'.

Geophys. Prosp., 19, 43)-458.

1.37 Cerveny, V., and Ravindra, R., (1971).

'Theory of Seismic Head Waves'.

U. of Toronto Press.,Toronto.

1.38 Hales, A.L. and Roberts, J.L. (1974).
'The Zoeppritz Amplitude Equations : More Errors'.
Bull. Seism. Soc. Am., 64, 285.

1.39 Berry, M.J., and West, G.F., (1966).
'Reflected and Head Wave Amplitudes in a Medium of Several Layers'.
The Earth Beneath the Continents, J.S. Steinhart and T.J. Smith (Eds.), 464-81.
Geophysical Monograph 10, Am. Geophys. Union, Washington.

1.40 Brekhovskikh, L.M., (1949).
'Reflection and Refraction of Spherical Waves'.
Uspekhi Fiz. Nauk., 38, 1-42.

1.41 Cerveny, V., (1959).
'On the Reflection of Spherical Waves at a Plane Interface with a Refractive Index Near to One'.
Studia Geoph. et Geod., 3, 1959, 116.

References

2.1 'P-27 Hydrophone Operation and Service Manual'.

Mark Products, Houston, Texas.

2.2 Peacock, J.H., (1973).

'A Binary Ranging Analogue to Digital Converter'.

Int. Rep., University of Durham.

— Malmstadt, H.V., and Enke, C.G., (1969).

'Digital Electronics for Scientists'

McGraw Hill, New York.

— Webar, P.J., (1963).

'The Tape Recorder as an Instrumentation Device'

Ampex Corporation.

— Texas Instruments (1971).

Semiconductor Components, Data Book Two, Digital Integrated Circuits.

— Motorola (1972).

MCMOS Data Handbook.

— RCA (1971).

COS/MOS IC's For Low Voltage Applications.

— Millman, J., and Taub, H., (1965).

'Pulse and Digital Circuits'

McGraw Hill, New York.

— Whitmarsh, R.B., (1970).

'An Ocean Bottom Pop-Up Seismic Recorder'.

Mar. Geophys. Res., 1, 91-98.

— Donnell, W.F., (1967).

'Sources of Error in a Seismic Digital Recording System'.

Geophys. Prosp., 15, 246-261.

— Nagra IV Instruction Manual (1973).

Nagra Tape Recorders, Kudelski, S.A., Switzerland.

-- Ferrograph Series Seven Tape Recorder Handbook (1974).
Ferrograph (U.K.) Ltd., Slough, England.

-- 'Small Computer Handbook' (1968).
Digital Equipment Corporation, Maynard, Mass.

-- 'Seismic Sonobuoy Type SB6E4 Handbook' (1970).
Ultra Electronics Ltd., London.

-- Walker, W.F., (1968).
'Digital Instruments'
Electronic Data Library, Vol 1.
Product Journals Ltd.

References

3.1 Frank, F. and Von Mises, R. (1937).

'The Differential and Integral Equations of Mechanics and Physics',

O.N.T.I., Chapter III.

3.2 Brekhovskikh, L.M. (1949).

'Reflection of Plane Waves from Layered Inhomogeneous Media'.

J. Tech. Physics (U.S.S.R.), 19, 1126.

3.3 Knott, C.G. (1899).

'Reflexion and Refraction of Elastic Waves with Seismological Applications'.

Phil. Mag. (5), 48.

3.4 Kolsky, H. (1963).

'Stress Waves in Solids'.

Dover, Chapter II.

3.5 Bullen, K.E. (1965).

'An Introduction to the Theory of Seismology'.

Cambridge University Press, Chapter II.

3.6 Macelwane, J.B. and Somon, F.W. (1936).

'Theoretical Seismology'

Chapter III. New York Wiley.

3.7 Bortfield, R. (1962).

'Reflection and Refraction of Spherical Compressional Waves at Arbitrary Plane Interfaces'.

Geophys. Prosp. 10 p.517-531.

3.8 Birch, F. (1960).

'Velocities of Compressional Waves in Rocks'.

J. Geoph. Res. 65, 1083-1102.

3.9 Muskat, M. and Meres, M.W., (1940).

'Reflection and Transmission Coefficients for Plane Waves in Elastic Media'.

Geophysics, 5, 115.

3.10 Heelan, P.A., (1953).

'On the Theory of Head Waves'.

Geophysics, 18, 871.

3.11 Helmberger, D.V. (1968).

'Head Waves from the Mohorovicic Discontinuity'.

Bull. Seis. Soc. Am. 58, 179-214.

3.12 Weil, H. (1919).

'Analysis of Electromagnetic Waves Above a Conducting Layer'.

Ann. Physik 60, 481.

3.13 Papoulis, A., (1962).

'The Fourier Integral and its Applications'.

McGraw Hill, Chapter IV.

3.14 Hsu, H.P. (1970).

'Fourier Analysis'.

Techoutlines, Simon and Schuster.

3.15 Gorshkov, N.F. (1957).

'The Propagation of Pulses in an Elastic Absorptive Medium'.

J. Acoust. Soc. U.S.S.R. 3, p.163-172.

3.16 Abramowitz, M., and Stegun, I.A., (1965).

'Handbook of Mathematical Functions'.

National Bureau of Standards, Applied Mathematics Series.

3.17 Bland, D.R. (1964).

'Solutions of Laplace's Equation'.

Routledge and Keegan Paul.

3.18 Brekhovskikh, L.M. (1960).

'Waves in Layered Media'.

Academic Press, Chapter I.

3.19 Brekhovskikh, L.M. (1949).

'The Reflection and Refraction of Spherical Waves'.

Uspekhi Fiz. Nank. 38, 1.

3.20 Watson, G.N., (1949).

'Theory of Bessel Functions'

3.21 Morse, P., and Feshbach, H., (1953).
'Methods of Theoretical Physics'.
McGraw Hill, Chapter V.

3.22 Courant, R, and Hilbert, D., (1933).
'Methods of Mathematical Physics', Vol. I.

3.23 Kahan, T., and Eckart, G., (1949).
'A General Account of Asymtotic Expansion in Wave Propagation'.
Rev. Sci. Paris 87, 3.

3.24 Matthews, J., and Walker, D., (1970).
'Mathematical Methods of Physics'.
Benjamin Press. Chapter IV.

3.25 Smirnova, N.S., and Ermilova, N.I., (1959).
'On the Construction of Theoretical Seismograms in the Neighbourhood of the Critical Point'.
Questions on the Dynamic Theory of the Spread of Seismic Waves. III. Leningrad University.

3.26 Cerveny, V., (1957).
'On the Amplitudes of Refracted Waves'.
Studia Geophys. and Geod. 1, 256.

3.27 Brekhovskikh, L.M. (1960).
'Waves in Layered Media'.
Academic Press, Chapter III.

3.28 Brekhovskikh, L.M. (1960).
'Waves in Layered Media'.
Academic Press, Chapter IV.

3.29 Kreyszig, E. (1967).
'Advanced Engineering Mathematics'.
Wiley.

References

4.1 'Geospace', Variable Area Display Operating Manual.
Texas Instruments.

4.2 Le Pichon, X., Ewing, J., and Houte, R.E. (1968).
'Deep Sea Sediment Velocity Determination Made While Reflection Profiling'.
J. Geoph. Res., 73, 2597-2614.

4.3 Matthews, D.J., (1939).
'Tables of the Velocity of Sound in Pure Water and Sea Water'.
Hydr. Dept. Ad. London.

4.4 Maynard, G.L., Sutton, G.H., Hussong, D.M., and Kroenke, L.W. (1973).
'The Seismic Wide Angle Reflection Method in the Study of Ocean Sediment Velocity Structure'.
Symp. on Physics of Sound in Marine Sediments, Austin, Texas.

4.5 Houts, R.E., Ewing, J., and Le Pichon, X., (1968).
'Velocity of Deep Sea Sediments from Sonobuoy Data'.
J. Geoph. Res., 73, 2615-2641.

4.6 Bullen, K.E. (1965).
'An Introduction to the Theory of Seismology'
Chapter 6.
Cambridge University Press.

4.7 Dix, C.H., (1955).
'Seismic Velocities from Surface Measurements'.
Geophys., 20, 68.

4.8 Clay, C.S., and Rona, P.A. (1965).
'Studies of Seismic Reflections from Thin Layers on the Ocean Bottom, in the Western North Atlantic'.
J. Geophys. Res., 70, 855.

References

5.1 Cole, B.F., (1965).

'Marine Sediment Attenuation and Ocean Bottom Reflected Sound'.

J. Acoust. Soc. Am., 38, 291-297.

5.2 White, J.E., (1965).

'Seismic Waves, Prediction, Transmission and Attenuation'.

McGraw Hill.

5.3 Birch, F., (1960).

'Velocities of Compressional Waves in Rocks'.

J. Geoph. Res., 65, 1083-1102.

5.4 Nafe, J.E., and Drake, C.L. (1963).

'Physical Properties of Marine Sediments', in "The Sea",

Vol III : M.N. Hill, Ed., New York, I.P., 794-815.

5.5 Corneil, D.G., and Gotlieb, C.C., (1970).

'An Efficient Algorithm for Graph Isomorphism'.

J. Ass. Comp. Mach., 17, 51-64.

5.6 Hamilton, E.L., (1970).

'Sound Velocity and Related Properties of Marine Sediments,

North Pacific : J. Geophys. Res., 75, 4423-4446.

5.7 The German Research Group for Explosion Seismology, (1966).

'Seismic Wide Angle Measurements'.

Geoph. Prosp., 14, 1-6.

5.8 Meissner, R., (1966).

'Interpretation of Wide Angle Measurements'.

Geoph. Prosp., 14, 7-16.

5.9 Meissner, R., (1967).

'Exploring Deep Interfaces by Seismic Wide Angle Measurements'.

Geoph. Prosp., 15, 598-617.

5.10. Meissner, R., (1967).

'Zur Struktur der Erdkrust...'.

Gerl. Beitr. Z. Geoph., 76 Heft 3 and 4.

5.11 Robinson, E.A., (1967).

'Statistical Communication and Detection'.

Griffin. Chapter 7.

5.12 Clarke, G.K.C., (1968).

'Time Varying Deconvolution Filters'.

Geophys., 39, 1-13.

5.13 Griffiths, L.J., (1969).

'A Simple Adaptive Algorithm for Real Time Processing in Antenna Arrays'.

Proc. IEEE, 57, 1696-1704.

5.14 Wang, R.J., and Treitel, S., (1971).

'Adaptive Signal Processing Through Stochastic Approximation'.

Geoph. Prosp., 19, 718-727.

5.15 Griffiths, L.J., Smolka, F.R., and Trembly, L.D., (1977).

'Adaptive Deconvolution : A New Technique for Processing Time Varying Seismic Data'.

Geoph., 42, 742-759.

5.16 Bogert, B., Healey, M.J., and Tukey, J.W. (1963).

'The Quefrency Analysis of Time Series for Echoes, Cepstrum, Pseudo Autocovariance, Cross-Cepstrum and Saphe Cracking'.

Proc. Symp. on Time Series Analysis, M. Rosenblatt, Ed., New York, Wiley, 209-243.

5.17 Oppenheim, A.V., (1965).

'Superposition in a Class of Non-linear Systems'.

Tech. Rep. 432., MIT, Res. Lab. of Electr.

5.18 Shafer, R.W., (1969).

'Echo Removal by Discrete Generalised Linear Filtering'.

Tech. Rep. 466, MIT, Res. Lab. of Electr.

5.19 Stoffa, P.L., Buhl, P., and Bryan, G.M., (1974).

'The Application of Homomorphic Deconvolution to Shallow Water Marine Seismology. Parts I and II. Geoph., 39, 401-427.

5.20 Breaker, L.C., and Winokur, R.S., (1967).
'The Variability of Bottom Reflected Signals Using the Deep Research Vehicle, Alvin'.
U.S.N. Oceanogr. Of. IR, 67-92.

5.21 Breslau, L.R. (1967).
'The Normally Incident Reflectivity of the Sea Floor at 12kc and its Correlation with Physical and Geological Properties of Naturally Occurring Sediments.'
Woods Hole Oceanog. Inst. Ref. 67-16.

APPENDIX 1

<u>PLAMP</u>

a) This programme calculates the plane wave amplitude as a function of the sine of angle of incidence (e_o).

b) This programme computes the value $A1(e_o)$ as a function of e_o.

c) This programme computes $A2(e_o)$ as a function of e_o.

```
      DIMENSION AO(100),XKI(100),XK1(100),XL1(100),XL2(100),EO(100),
     1E1(100),RANG(100),ANG(100),XK2(100),
     2T0(100),T1(100),T2(100),T3(100),T4(100),T5(100),T6(100),
     4XI(100),
     3T7(100),T8(100)
      READ(5,1) A1,A2,B1,B2,D1,D2
    1 FORMAT(10F7.2)
      D=D2/D1
      XN1=A1/B1
      XN2=A2/B2
      RI=A1/A2
      U=(D2*B2*B2)/(D1*B1*B1)
      WRITE(6,3)
    3 FORMAT(' ','SINE OF ANGLE',5X,'AMPLITUDE')
      DO 2 I=1,89
      ANG(I)=I
      RANG(I)=(ANG(I)*3.1416)/180.
      EO(I)=SIN(RANG(I))*SIN(RANG(I))
      T0(I)=SQRT(1-EO(I))
      T1(I)=SQRT(XN1*XN1-EO(I))
      T2(I)=SQRT(XN2*XN2-EO(I))
      T3(I)=EO(I)*(U-1)
      XK1(I)=(EO(I)*(((XN1*XN1*(D-1))-(2.*T3(I)))**2))+(T0(I)*T1(I)*(((
     1D*XN1*XN1)-(2.*T3(I)))**2))+(T0(I)*T2(I)*D*(XN1**4))
      XK2(I)=XK1(I)-(2.*(EO(I)*(((XN1*XN1*(D-1))-(2.*T3(I)))**2)))
      XL1(I)=(4.*T0(I)*T1(I)*T2(I)*(T3(I)*(U-1)))+(T1(I)*D*(XN1**4
     1))+(T2(I)*(((XN1*XN1)+(2.*T3(I)))**2))
      E1(I)=SIN(RANG(I))
      XL2(I)=(4.*T0(I)*T1(I)*T2(I)*(T3(I)*(U-1)))-(T1(I)*D*(XN1**4
     1))-(T2(I)*(((XN1*XN1)+(2.*T3(I)))**2))
      RI2=RI*RI
      IF(EO(I).GT.RI2) GO TO 47
      T5(I)=SQRT(RI2-EO(I))
      T6(I)=(XK2(I)+(XL2(I)*T5(I)))
      XI(I)=I
      T7(I)=(XK1(I)+(XL1(I)*T5(I)))
      AO(I)=T6(I)/T7(I)
      GO TO 2
   47 T5(I)=(EO(I)-RI2)
      T6(I)=SQRT(ABS(XK2(I)**2+(XL2(I)**2)*T5(I)))
      T7(I)=SQRT(ABS(XK1(I)**2+(XL1(I)**2)*T5(I)))
      AO(I)=T6(I)/T7(I)
    2 CONTINUE
      WRITE(6,44) (E1(I),AO(I),I=1,89)
   44 FORMAT(2F14.3)
      WRITE(6,45) RI
   45 FORMAT(' ','REFRACTIVE INDEX='F7.3)
```

```
C       PROG CALCULATES A1(E0) AS A FUNCTION OF E0
C       AND PLOTS IT .
        DIMENSION A1(100),A2(100),XK1(100),XK2(100),XL1(100),XL2(100)
       1,T1(90),T2(90),T3(90),T4(90),T5(90),T6(90),T7(90),T8(90),T9(90),
       2ANG(90),RANG(90),E(90),E1(90),S1(90),S2(90),S3(90),S4(90),S5(90),
       5X(2048),Y(2048),
       3R1(90),R2(90),R3(90),R11(90)
        READ(5,1) V1,V2,B1,B2,D1,D2
      1 FORMAT(6F7.2)
        RI=V1/V2
        XN1=V1/B1
        XN2=V2/B2
        D=D2/D1
        U=D*((B2/B1)**2)
        D1=D-1.
        U1=U-1.
        DO 2 I=1,89
        ANG(I)=I
        RANG(I)=(ANG(I)*3.14159)/180.
        E1(I)=SIN(RANG(I))
        E(I)=E1(I)**2
        T1(I)=SQRT(1-E(I))
        T2(I)=SQRT((XN1**2)-E(I))
        T3(I)=SQRT((XN2**2)-E(I))
        T4(I)=2.*E(I)*U1
        T5(I)=((XN1**2)*D1-T4(I))**2
        T6(I)=(D*(XN1**2)-T4(I))**2
        T7(I)=E(I)*T5(I)
        T8(I)=T1(I)*T2(I)*T6(I)
        T9(I)=T1(I)*T3(I)*D*(XN1**4)
        XK1(I)=T7(I)+T8(I)+T9(I)
        XK2(I)=(T8(I)+T9(I))-T7(I)
        S1(I)=E(I)*(U1**2)
        S2(I)=((XN1**2)+T4(I))**2
        S3(I)=4.*T1(I)*T2(I)*T3(I)*S1(I)
        S4(I)=T2(I)*D*(XN1**4)
        S5(I)=T3(I)*S2(I)
        XL1(I)=S3(I)+S4(I)+S5(I)
        RI2=RI**2
        XL2(I)=S3(I)-(S4(I)+S5(I))
        R1(I)=(XK1(I)*XK2(I))
        R2(I)=RI2-E(I)
        R3(I)=(XL1(I)*XL2(I)*R2(I))
        R11(I)=(XL1(I)**2)*R2(I)
        A1(I)=(R1(I)-R3(I))/((XK1(I)**2)-R11(I))
      2 CONTINUE
        WRITE(6,45) RI,XN1,XN2,D
        X(I)=E1(I)
        Y(I)=A1(I)
        WRITE(6,44) (E1(I),A1(I),I=1,89)
     44 FORMAT(1H ,'SINE OF ANGLE',5X,'A1(E0)',/2F14.3)
     45 FORMAT(1H ,'REFRACTIVE INDEX='F7.3/'N1(=A1/B1)='F7.3
       1/'N2(=A2/B2)='F7.2/'DENSITY RATIO='F7.3)
```

```
C      PROG CALCULATES A2(E0) AS A FUNCTION OF E0
C      AND PLOTS IT .
      DIMENSION A1(100),A2(100),XK1(100),XK2(100),XL1(100),XL2(100)
     1,T1(90),T2(90),T3(90),T4(90),T5(90),T6(90),T7(90),T8(90),T9(90),
     2ANG(90),RANG(90),E(90),E1(90),S1(90),S2(90),S3(90),S4(90),S5(90),
     5X(2048),Y(2048),

     3R1(90),R2(90),R3(90),R11(90)
      READ(5,1) V1,V2,B1,B2,D1,D2
    1 FORMAT(6F7.2)
      RI=V1/V2
      XN1=V1/B1
      XN2=V2/B2
      D=D2/D1
      U=D*((B2/B1)**2)
      D1=D-1.
      U1=U-1.
      DO 2 I=1,89
      ANG(I)=I
      RANG(I)=(ANG(I)*3.14159)/180.
      E1(I)=SIN(RANG(I))
      E(I)=E1(I)**2
      T1(I)=SQRT(1-E(I))
      T2(I)=SQRT((XN1**2)-E(I))
      T3(I)=SQRT((XN2**2)-E(I))
      T4(I)=2.*E(I)*U1
      T5(I)=((XN1**2)*D1-T4(I))**2
      T6(I)=(D*(XN1**2)-T4(I))**2
      T7(I)=E(I)*T5(I)
      T8(I)=T1(I)*T2(I)*T6(I)
      T9(I)=T1(I)*T3(I)*D*(XN1**4)
      XK1(I)=T7(I)+T8(I)+T9(I)
      XK2(I)=(T8(I)+T9(I))-T7(I)
      S1(I)=E(I)*(U1**2)
      S2(I)=((XN1**2)+T4(I))**2
      S3(I)=4.*T1(I)*T2(I)*T3(I)*S1(I)
      S4(I)=T2(I)*D*(XN1**4)
      S5(I)=T3(I)*S2(I)
      XL1(I)=S3(I)+S4(I)+S5(I)
      RI2=RI**2
      XL2(I)=S3(I)-(S4(I)+S5(I))
      R1(I)=(XK2(I)*XL1(I))-(XK1(I)*XL2(I))
      R2(I)=RI2-E(I)
      R3(I)=(XL1(I)**2)*R2(I)
      R11(I)=((XK1(I)**2)-R3(I))*T1(I)
      A2(I)=R1(I)/R11(I)
    2 CONTINUE
      WRITE(6,45) RI,XN1,XN2,D
      WRITE(6,44)
   44 FORMAT('SINE OF ANGLE',5X,'AMPLITUDE')
      WRITE(6,46) (E1(I),A2(I),I=1,89)
   46 FORMAT(2F14.3)
   45 FORMAT(1H ,'REFRACTIVE INDEX='F7.3/'N1(=A1/B1)='F7.3
     1/'N2(=A2/B2)='F7.2/'DENSITY RATIO='F7.3)
```

ASSRFLN

This programme computes the reflected amplitude of an incident spherical wave according to the asymtotic approximation.

```
      DIMENSION ANG(90),RANG(90),XK1(90),XK2(90),XL1(90),XL2(90),T1(90),
     1T2(90),T3(90),T4(90),T5(90),T6(90),T7(90),T8(90),T9(90),E(90),E1(9
     20),S1(90),S2(90),S3(90),S4(90),S5(90),S6(90),R1(90),R2(90),R3(90),
     3R4(90),R5(90),R6(90),A(90),A1(90),A2(90),A3(90),X(2048),Y(2048),BE
     4TA(90),IBETA(90),ETA(90),IETA(90),RMU(90),XMU(90),SMU(90),XSMU(90)
     5,RMU1(20),XMU1(20),XMU2(9),RMU2(9),XSMU1(38),W1(90),W2(90),Z1(
     690),Z2(90),Z3(90),Z4(90),Z7(90),Z8(90),Z9(90),W3(90),W4(90),XX1(90
     7),XX2(90),XX3(90),YY1(90),YY2(90),XNU(90),CNU(90),SNU(90),ZZ1(90),
     8ZZ2(90),ZZ3(90),ZZ4(90),ZZ5(90),ZZ6(90),ZZ7(90),ZZ8(90),ZZ9(90),BB
     91(90),BB2(90),BB3(90),BB4(90),BB5(90),BB6(90),BB7(90),BB8(90),BB9(
     190),CC1(90),CC2(90),TITLE(20),A0(90),RR1(90),SMU1(38)
      DATA RMU1/ 1.63,1.30,1.17,1.11,1.07,1.05,1.04,1.03,1.02,1.01,
     11.01,1.01,1.01,1.00,1.00,1.00,1.00,1.00,1.00,1.00/
      DATA XMU1/ 0.51,0.31,0.22,0.16,0.13,0.10,0.09,0.07,0.06,0.05,
     10.04,0.03,0.03,0.03,0.02,0.02,0.02,0.02,0.01,0.01/
      DATA RMU2/ 16.3,8.15,5.26,4.07,3.26,2.72,2.61,2.04,1.81/
      DATA XMU2/ 5.10,2.55,1.70,1.28,1.02,0.85,0.73,0.64,0.57/
      DATA SMU1/ 0.03,0.08,0.15,0.22,0.30,0.38,0.46,0.53,0.59,
     10.64,0.70,0.74,0.78,0.81,0.84,0.86,0.88,0.90,0.91,0.92,0.93,
     20.94,0.95,0.96,0.96,0.96,0.97,0.97,0.97,0.98,0.98,0.98,
     30.98,0.99,0.99,0.99,0.99,1.00/
      DATA XSMU1/ 0.05,0.12,0.18,0.24,0.28,0.31,0.33,0.33,
     10.68,0.32,0.32,0.31,0.29,0.28,0.26,0.24,0.23,0.21,0.20
     2,0.19,0.17,0.16,0.15,01.4,0.13,0.12,0.11,0.10,0.09,0.08,
     30.07,0.06,0.05,0.04,0.03,0.02,0.01,0.00/
      READ(4,10) N
      READ(5,1) V1,V2,B1,B2,D1,D2
      READ(15,9) NMAX,IND,INK,(TITLE(I),I=1,INK)
   10 FORMAT(I5)
    1 FORMAT(6F7.2)
    9 FORMAT(3I7,10A4)
      RI=V1/V2
      RI2=RI**2
      XN1=V1/B1
      XN2=V1/B2
      D=D2/D1
      U=D*((B2/B1)**2)
      DD=D-1.
      U1=U-1.
      FLAG=0
      WRITE(8,21) N,V1,V2,B1,B2,D1,D2,
     1U,DD,U1,RI,RI2,XN1,XN2
   21 FORMAT(I5,13F5.2)
C     CRITICAL POINT CALCULATION
      T1C=SQRT(1.-RI2)
      T2C=SQRT((XN1**2)-RI2)
      T3C=SQRT((XN2**2)-RI2)
      T4C=2*RI2*U1
      T5C=((XN1**2)*DD-T4C)**2
      T6C=(D*(XN1**2)-T4C)**2
      T7C=RI2*T5C
      T8C=T1C*T2C*T6C
      T9C=T1C*T3C*D*(XN1**4)
      XK1C=T7C+T8C+T9C
      XK2C=(T8C+T9C)-T7C
      S1C= RI2*(U1**2)
      S2C= (RI2+T4C)**2
      S3C= 4.*T1C*T2C*T3C*S1C
      S4C= T2C*D*(XN1**4)
      S5C= T3C*S2C
```

```
      XL1C= S3C+S4C+S5C
      XL2C= S3C-(S4C+S5C)
      R1C= (XK2C*XL1C)-(XK1C*XL2C)
      R2C=(XK1C**2)*T1C
      A2C=R1C/R2C
      Z4C=  0.822*A2C*SQRT(RI)*(1-RI2)
      Z5C= SQRT(N*T1C)
      Z6C=SQRT(Z5C)
      Z7C=Z4C/Z6C
      Z8C=(COS(3.14159/8.))*Z7C
      Z9C=(SIN(3.14159/8.))*Z7C
      A1C= XK2C/XK1C
      W3C= (A1C-Z8C)**2
      W4C= SQRT(W3C+(Z9C**2))
      AC=T1C*W4C
      WRITE(6,115) AC
  115 FORMAT(' ','CRITICAL AMPLITUDE='F10.4)
      U1=U-1.
      DO 2  I=1,89
      ANG(I)=I
      RANG(I)=(ANG(I)*3.1416)/180.
      E1(I)=SIN(RANG(I))
      E(I)= E1(I)**2
      T1(I)=SQRT(1-E(I))
      T2(I)=SQRT((XN1**2)-E(I))
      IF(XN2.LT.E1(I))GO TO 130
      T3(I)=SQRT((XN2**2)-E(I))
      T4(I)=2.*E(I)*U1
      T5(I)=((XN1**2)*DD-T4(I))**2
      T6(I)=(D*(XN1**2)-T4(I))**2
      T7(I)=E(I)*T5(I)
      T8(I)=T1(I)*T2(I)*T6(I)
      T9(I)=T1(I)*T3(I)*D*(XN1**4)
      XK1(I)=T7(I)+T8(I)+T9(I)
      XK2(I)=(T8(I)+T9(I))-T7(I)
      S1(I)=E(I)*(U1**2)
      S2(I)=((XN1**2)+T4(I))**2
      S3(I)=4.*T1(I)*T2(I)*T3(I)*S1(I)
      S4(I)=T2(I)*D*(XN1**4)
      S5(I)=T3(I)*S2(I)
      XL1(I)=S3(I)+S4(I)+S5(I)
      XL2(I)=S3(I)-(S4(I)+S5(I))
      GO TO 131
CC    FOR N2 LESS THAN E1(I)
C     I.E. T3(I),T9(I),XK1(I),XK2(I)
C     S3(I),S5(I),XL1(I),XL2(I) COMPLEX
  130 T3(I)=SQRT(E(I)-(XN2**2))
      IF(FLAG.NE.0) GO TO 133
      FLAG=ANG(I)
  133 CONTINUE
      T4(I)=2.*E(I)*U1
      T5(I)=((XN1**2)*DD-T4(I))**2
      T6(I)=(D*(XN1**2)-T4(I))**2
      T7(I)=E(I)*T5(I)
      T8(I)=T1(I)*T2(I)*T6(I)
      T9(I)=T1(I)*T3(I)*D*(XN1**4)
      XK1(I)=SQRT((T7(I)+T8(I))**2+(T9(I)**2))
      XK2(I)=SQRT((T8(I)-T7(I))**2+(T9(I)**2))
      S1(I)=E(I)*(U1**2)
      S2(I)=((XN1**2)+T4(I))**2
```

```
      S3(I)=4.*T1(I)*T2(I)*T3(I)*S1(I)
      S4(I)=T2(I)*D*(XN1**4)
      S5(I)=T3(I)*S2(I)
      XL1(I)=SQRT((S4(I)**2)+(S3(I)+S5(I))**2)
      XL2(I)=SQRT((S4(I)**2)+(S3(I)-S5(I))**2)
C  REST OF CALC. DOES NOT INVOLVE COMPLEX VALUES.
  131 R1(I)=(XK1(I)*XK2(I))
      R1(I)=(XK1(I)*XK2(I))
      R2(I)=RI2-E(I)
      R3(I)=(XL1(I)*XL2(I)*R2(I))
      R4(I)=(XL1(I)**2)*R2(I)
      A1(I)=(R1(I)-R3(I))/((XK1(I)**2)-R4(I))
      R5(I)=(XK2(I)*XL1(I))-(XK1(I)*XL2(I))
      R6(I)=((XK1(I)**2)-(XL1(I)**2)*R2(I))*T1(I)
      A2(I)= R5(I)/R6(I)
      IF(RI2.LT.E(I)) GO TO 99
      A0(I)= A1(I)-(A2(I)*T1(I)*SQRT(RI2-E(I)))
      GO TO 100
   99 RR1(I)= E(I)-RI2
      A0(I)= SQRT(A1(I)**2+(A2(I)**2)*RR1(I))
  100 SI2=SQRT(1.-RI2)
      W1(I)=SI2-T1(I)
C   N IS THE FACTOR K(Z+ZO)
      WRITE(8,24) (R1(I),R2(I),R3(I),R4(I),A1(I),R5(I)
     1,R6(I),A2(I),A0(I),SI2)
   24 FORMAT(10F8.3)
      W2(I)=SQRT(N/(2.*E(I)*T1(I)))
      BETA(I)=W2(I)*W1(I)
      BETA(I)=ABS(BETA(I))
      IF(BETA(I).GE.2.0) GO TO 47
      IF(BETA(I).LT.0.1) GO TO 48
      IBETA(I)=(BETA(I)*10.0+0.53)
      J=IBETA(I)
      RMU(I)=RMU1(J)
      XMU(I)=XMU1(J)
      GO TO 49
   48 IBETA(I)=(BETA(I)*100.+0.53)
      J=IBETA(I)
      RMU(I)=RMU2(J)
      XMU(I)=XMU2(J)
      GO TO 49
   47 RMU(I)=1.0
      XMU(I)=0.0
   49 IF(RI2-E(I)) 111,2,113
  113 A3(I)= A2(I)*T1(I)*SQRT(RI2-E(I))
      Z1(I)=(A3(I)*XMU(I))**2
      Z2(I)= A3(I)*(RMU(I)-1.)
      Z3(I)= A0(I)-Z2(I)
C  A(I) CALC. ABOVE IS AMPLITUDE BEFORE C.P.
      A(I)=T1(I)*(SQRT((Z3(I)**2)+Z1(I)))
      GO TO 2
C BEYOND CRITICAL POINT
  111 XX1(I)=E1(I)/T1(I)-RI/SQRT(1.-RI2)
      XX2(I)=(N*(1.-RI2)*RI*T1(I))/(E1(I)*2.)
      XX3(I)=SQRT(XX2(I))
      ETA(I)=XX3(I)*XX1(I)
      IF(ETA(I).GE.2.60) GO TO 147
      IETA(I)=(ETA(I)*10.0+0.53)
      J=IETA(I)
      SMU(I)=SMU1(J)
```

```
      XSMU(I)=XSMU1(J)
      GO TO 148
  147 SMU(I)=1.0
      XSMU(I)=0.0
  148 YY1(I)=(RI*E1(I))/T1(I)
      YY2(I)=(SQRT(1.-RI2))-(1./T1(I))
      XNU(I)=N*(YY1(I)+YY2(I))+3.1416/2.
      CNU(I)=COS(XNU(I))
      SNU(I)=SIN(XNU(I))
      ZZ1(I)=A3(I)*XMU(I)
      ZZ2(I)=SMU(I)*CNU(I)
      ZZ3(I)=XSMU(I)*SNU(I)
      ZZ4(I)=ZZ2(I)-ZZ3(I)
      ZZ5(I)=RI*A2C*T1(I)
      ZZ6(I)=(RI*T1(I))/(E1(I)*SQRT(1.-RI2))
      ZZ7(I)= 1.-ZZ6(I)
      ZZ8(I)=SQRT(ZZ7(I)**3)
      ZZ9(I)=N*E(I)*ZZ8(I)
      BB1(I)=ZZ5(I)/ZZ9(I)
      BB2(I)=BB1(I)*ZZ4(I)
      BB3(I)=XSMU(I)*CNU(I)
      BB4(I)=SMU(I)*SNU(I)
      BB5(I)=BB3(I)+BB4(I)
      BB6(I)= BB5(I)*BB1(I)
      BB7(I)= A1(I)+ZZ1(I)+BB2(I)
      BB8(I)= A3(I)*RMU(I)
      BB9(I)=(BB6(I)-BB8(I))
      CC1(I)=((BB7(I))**2)+(BB9(I)**2)
      CC2(I)=SQRT(CC1(I))
      A(I)=T1(I)*CC2(I)
    2 CONTINUE
      DO 499 I=1,89
      X(I)=E1(I)
      Y(I)=A(I)
  499 CONTINUE
      WRITE(6,14) FLAG
   14 FORMAT(1H ,'SINE(ANG.OF INCID. BECAME GREATER
     1THAN N2(=V1/B2) WHEN THE ANGLE WAS='I3)
      WRITE(6,11) (X(I),Y(I),I=1,89)
   11 FORMAT(1H,2F14.3)
      STOP
      END
C OF FILE
```

<u>ASSRFRN</u>

This programme computes the head wave amplitude as given by the asymtotic approximation.

```
      DIMENSION ANG(90),RANG(90),XK1(90),XK2(90),XL1(90),XL2(90),T1(90),
     1T2(90),T3(90),T4(90),T5(90),T6(90),T7(90),T8(90),T9(90),E(90),E1(9
     20),S1(90),S2(90),S3(90),S4(90),S5(90),S6(90),R1(90),R2(90),R3(90),
     3R4(90),R5(90),R6(90),A(90),A1(90),A2(90),A3(90),X(2048),Y(2048),BE
     4TA(90),IBETA(90),ETA(90),IETA(90),RMU(90),XMU(90),SMU(90),XSMU(90)
     5,RMU1(20),XMU1(20),XMU2(9),RMU2(9),XSMU1(38),W1(90),W2(90),Z1(
     690),Z2(90),Z3(90),Z4(90),Z7(90),Z8(90),Z9(90),W3(90),W4(90),XX1(90
     7),XX2(90),XX3(90),YY1(90),YY2(90),XNU(90),CNU(90),SNU(90),ZZ1(90),
     8ZZ2(90),ZZ3(90),ZZ4(90),ZZ5(90),ZZ6(90),ZZ7(90),ZZ8(90),ZZ9(90),BB
     91(90),BB2(90),BB3(90),BB4(90),BB5(90),BB6(90),BB7(90),BB8(90),BB9(
     190),CC1(90),CC2(90),TITLE(20),AC(90),BP1(90),SMU1(38)
      DATA RMU1/ 1.63,1.30,1.17,1.11,1.07,1.05,1.04,1.03,1.02,1.01,
     11.01,1.01,1.01,1.00,1.00,1.00,1.00,1.00,1.00,1.00/
      DATA XMU1/ 0.51,0.31,0.22,0.16,0.13,0.10,0.08,0.07,0.06,0.05,
     10.04,0.03,0.03,0.03,0.02,0.02,0.02,0.02,0.01,0.01/
      DATA RMU2/ 16.3,8.15,5.26,4.07,3.26,2.72,2.61,2.04,1.81/
      DATA XMU2/ 5.10,2.55,1.70,1.28,1.02,0.85,0.73,0.64,0.57/
      DATA SMU1/ 0.03,0.08,0.15,0.22,0.30,0.38,0.46,0.53,0.59,
     10.64,0.70,0.74,0.78,0.81,0.84,0.86,0.88,0.90,0.91,0.92,0.93,
     20.94,0.95,0.96,0.96,0.96,0.97,0.97,0.97,0.98,0.98,0.98,
     30.98,0.99,0.99,0.99,0.99,1.00/
      DATA XSMU1/ 0.05,0.12,0.18,0.24,0.28,0.31,0.33,0.33,
     10.68,0.32,0.32,0.31,0.29,0.28,0.26,0.24,0.23,0.21,0.20
     2,0.19,0.17,0.16,0.15,01.4,0.13,0.12,0.11,0.10,0.09,0.08,
     30.07,0.06,0.05,0.04,0.03,0.02,0.01,0.00/
      READ(4,10) N
      READ(5,1) V1,V2,B1,B2,C1,D2
   10 FORMAT(I5)
    1 FORMAT(6F7.2)
      RI=V1/V2
      RI2=RI**2
      XN1=V1/B1
      XN2=V1/B2
      D=D2/D1
      U=D*((B2/B1)**2)
      D1=D-1.
      U1=U-1.
      FLAG=0
C     CRITICAL POINT CALCULATION
      T1C=SQRT(1.-RI2)
      T2C=SQRT((XN1**2)-RI2)
      T3C=SQRT((XN2**2)-RI2)
      T4C=2*RI2*U1
      T5C=((XN1**2)*D1-T4C)**2
      T6C=(D*(XN1**2)-T4C)**2
      T7C=RI2*T5C
      T8C=T1C*T2C*T6C
      T9C=T1C*T3C*D*(XN1**4)
      XK1C=T7C+T8C+T9C
      XK2C=(T8C+T9C)-T7C
      S1C= RI2*(U1**2)
      S2C= ((XN1**2)+T4C)**2
      S3C= 4.*T1C*T2C*T3C*S1C
      S4C= T2C*D*(XN1**4)
      S5C= T3C*S2C
      XL1C= S3C+S4C+S5C
```

```
      XL2C= S3C-(S4C+S5C)
      R1C= (XK2C*XL1C)-(XK1C*XL2C)
      R2C=(XK1C**2)*T1C
      A2C=R1C/R2C
      Z4C=  0.822*A2C*SQRT(RI)*(1-RI2)
      Z5C= SQRT(N*T1C)
      Z6C=SQRT(Z5C)
      Z7C=Z4C/Z6C
      Z8C=(COS(3.14159/8.))*Z7C
      Z9C=(SIN(3.14159/8.))*Z7C
      A1C= XK2C/XK1C
      W3C= (A1C-Z8C)**2
      W4C= SQRT(W3C+(Z9C**2))
      AC=T1C*W4C
      WRITE(6,115) AC
  115 FORMAT(' ','CRITICAL AMPLITUDE='F10.4)
      DO 2  I=1,89
      ANG(I)=I
      RANG(I)=(ANG(I)*3.1416)/180.
      E1(I)=SIN(RANG(I))
      E(I)= E1(I)**2
      T1(I)=SQRT(1-E(I))
      T2(I)=SQRT((XN1**2)-E(I))
      IF(XN2.LT.E1(I))GO TO 130
      T3(I)=SQRT((XN2**2)-E(I))
      T4(I)=2.*E(I)*U1
      T5(I)=((XN1**2)*D1-T4(I))**2
      T6(I)=(D*(XN1**2)-T4(I))**2
      T7(I)=E(I)*T5(I)
      T8(I)=T1(I)*T2(I)*T6(I)
      T9(I)=T1(I)*T3(I)*D*(XN1**4)
      XK1(I)=T7(I)+T8(I)+T9(I)
      XK2(I)=(T8(I)+T9(I))-T7(I)
      S1(I)=E(I)*(U1**2)
      S2(I)=((XN1**2)+T4(I))**2
      S3(I)=4.*T1(I)*T2(I)*T3(I)*S1(I)
      S4(I)=T2(I)*D*(XN1**4)
      S5(I)=T3(I)*S2(I)
      XL1(I)=S3(I)+S4(I)+S5(I)
      XL2(I)=S3(I)-(S4(I)+S5(I))
      GO TO 131
CC    FOR N2 LESS THAN E1(I)
C     I.E. T3(I),T9(I),XK1(I),XK2(I)
C     S3(I),S5(I),XL1(I),XL2(I) COMPLEX
  130 T3(I)=SQRT(E(I)-(XN2**2))
      IF(FLAG.NE.0) GO TO 133
      FLAG=ANG(I)
  133 CONTINUE
      T4(I)=2.*E(I)*U1
      T5(I)=((XN1**2)*D1-T4(I))**2
      T6(I)=(D*(XN1**2)-T4(I))**2
      T7(I)=E(I)*T5(I)
      T8(I)=T1(I)*T2(I)*T6(I)
      T9(I)=T1(I)*T3(I)*D*(XN1**4)
      XK1(I)=SQRT((T7(I)+T8(I))**2+(T9(I)**2))
      XK2(I)=SQRT((T8(I)-T7(I))**2+(T9(I)**2))
      S1(I)=E(I)*(U1**2)
      S2(I)=((XN1**2)+T4(I))**2
      S3(I)=4.*T1(I)*T2(I)*T3(I)*S1(I)
      S4(I)=T2(I)*D*(XN1**4)
```

```
      S5(I)=T3(I)*S2(I)
      XL1(I)=SQRT((S4(I)**2)+(S3(I)+S5(I))**2)
      XL2(I)=SQRT((S4(I)**2)+(S3(I)-S5(I))**2)
C  REST OF CALC. DOES NCT INVCLVE COMPLEX VALUES.
  131 R1(I)=(XK1(I)*XK2(I))
      R2(I)=RI2-E(I)
      R3(I)=(XL1(I)*XL2(I)*R2(I))
      R4(I)=(XL1(I)**2)*R2(I)
      A1(I)=(R1(I)-R3(I))/((XK1(I)**2)-R4(I))
      R5(I)=(XK2(I)*XL1(I))-(XK1(I)*XL2(I))
      R6(I)=((XK1(I)**2)-(XL1(I)**2)*R2(I))*T1(I)
      A2(I)= R5(I)/R6(I)
      IF(RI2.LT.E(I)) GO TO 99
      A0(I)= A1(I)-(A2(I)*T1(I)*SQRT(RI2-E(I)))
      GO TO 100
   99 RR1(I)= E(I)-RI2
      A0(I)= SQRT(A1(I)**2+(A2(I)**2)*RR1(I))
  100 SI2=SQRT(1.-RI2)
      W1(I)=SI2-T1(I)
C   N IS THE FACTOR K(Z+Z0)
      W2(I)=SQRT(N/(2.*E(I)*T1(I)))
      BETA(I)=W2(I)*W1(I)
      BETA(I)=ABS(BETA(I))
      IF(BETA(I).GE.2.0) GO TO 47
      IF(BETA(I).LT.0.1) GO TO 48
      IBETA(I)=(BETA(I)*10.0+0.53)
      J=IBETA(I)
      RMU(I)=RMU1(J)
      XMU(I)=XMU1(J)
      GO TO 49
   48 IBETA(I)=(BETA(I)*100.+0.53)
      J=IBETA(I)
      RMU(I)=RMU2(J)
      XMU(I)=XMU2(J)
      GO TO 49
   47 RMU(I)=1.0
      XMU(I)=0.0
   49 IF(RI2-E(I)) 111,2,113
  111 A3(I)=A2(I)*T1(I)*SQRT(E(I)-RI2)
      Z1(I)=(A3(I)*XMU(I))**2
      YY1(I)=(A1(I)+Z1(I))**2
      YY2(I)=(A3(I)*RMU(I))**2
      A(I)=T1(I)*SQRT((YY1(I)+YY2(I)))
  113 CONTINUE
    2 CONTINUE
      DO 499 I=1,89
      X(I)=E1(I)
      Y(I)=A(I)
  499 CONTINUE
      WRITE(6,500) (X(I),Y(I),I=1,89)
  500 FORMAT(2F14.3)
      STOP
      END
```

ND OF FILE .

HDGEN 1

This programme calculates the refracted amplitude of an incident spherical wave.

```
      DIMENSION ANG(90),RANG(90),XK1(90),XK2(90),XL1(90),XL2(90),T1(90),
     1T2(90),T3(90),T4(90),T5(90),T6(90),T7(90),T8(90),T9(90),E(90),E1(9
     20),S1(90),S2(90),S3(90),S4(90),S5(90),S6(90),R1(90),R2(90),R3(90),
     3R4(90),R5(90),R6(90),A(90),A1(90),A2(90),A3(90),X(2048),Y(2048),BE
     4TA(90),IBETA(90),ETA(90),IETA(90),RMU(90),XMU(90),SMU(90),XSMU(90)
     5,RMU1(20),XMU1(20),XMU2(9),RMU2(9),XSMU1(38),W1(90),W2(90),Z1(
     690),Z2(90),Z3(90),Z4(90),Z7(90),Z8(90),Z9(90),W3(90),W4(90),YX1(90
     7),XX2(90),XX3(90),YY1(90),YY2(90),XNU(90),CNU(90),SNU(90),ZZ1(90),
     8ZZ2(90),ZZ3(90),ZZ4(90),ZZ5(90),ZZ6(90),ZZ7(90),ZZ8(90),ZZ9(90),BB
     91(90),BB2(90),BB3(90),BB4(90),BB5(90),BB6(90),BB7(90),BB8(90),BB9(
     190),CC1(90),CC2(90),TITLE(20),AC(90),RR1(90),SMU1(38)
      DATA RMU1/ 1.63,1.30,1.17,1.11,1.07,1.05,1.04,1.03,1.02,1.01,
     11.01,1.01,1.01,1.00,1.00,1.00,1.00,1.00,1.00,1.00/
      DATA XMU1/ 0.51,0.31,0.22,0.16,0.13,0.10,0.08,0.07,0.06,0.05,
     10.04,0.03,0.03,0.03,0.02,0.02,0.02,0.02,0.01,0.01/
      DATA RMU2/ 16.3,8.15,5.26,4.07,3.26,2.72,2.61,2.04,1.81/
      DATA XMU2/ 5.10,2.55,1.70,1.28,1.02,0.85,0.73,0.64,0.57/
      DATA SMU1/ 0.03,0.08,0.15,0.22,0.30,0.38,0.46,0.53,0.59,
     10.64,0.70,0.74,0.78,0.81,0.84,0.86,0.88,0.90,0.91,0.92,0.93,
     20.94,0.95,0.96,0.96,0.96,0.97,0.97,0.97,0.98,0.98,0.98,
     30.98,0.99,0.99,0.99,0.99,1.00/
      DATA XSMU1/ 0.05,0.12,0.18,0.24,0.28,0.31,0.33,0.33,
     10.68,0.32,0.32,0.31,0.29,0.28,0.26,0.24,0.23,0.21,0.20
     2,0.19,0.17,0.16,0.15,01.4,0.13,0.12,0.11,0.10,0.09,0.08,
     30.07,0.06,0.05,0.04,0.03,0.02,0.01,0.00/
      READ(4,10) N
      READ(5,1) V1,V2,B1,B2,D1,D2
   10 FORMAT(I5)
    1 FORMAT(6F7.2)
      RI=V1/V2
      RI2=RI**2
      XN1=V1/B1
      XN2=V1/B2
      D=D2/D1
      U=D*((B2/B1)**2)
      D1=D-1.
      U1=U-1.
      FLAG=0
C     CRITICAL POINT CALCULATION
      T1C=SQRT(1.-RI2)
      T2C=SQRT((XN1**2)-RI2)
      T3C=SQRT((XN2**2)-RI2)
      T4C=2*RI2*U1
      T5C=((XN1**2)*D1-T4C)**2
      T6C=(D*(XN1**2)-T4C)**2
      T7C=RI2*T5C
      T8C=T1C*T2C*T6C
      T9C=T1C*T3C*D*(XN1**4)
      XK1C=T7C+T8C+T9C
      XK2C=(T8C+T9C)-T7C
      S1C= RI2*(U1**2)
      S2C= ((XN1**2)+T4C)**2
      S3C= 4.*T1C*T2C*T3C*S1C
      S4C= T2C*D*(XN1**4)
      S5C= T3C*S2C
      XL1C= S3C+S4C+S5C
      XL2C= S3C-(S4C+S5C)
      R1C= (XK2C*XL1C)-(XK1C*XL2C)
      R2C=(XK1C**2)*T1C
```

```
      R1C= (XK2C*XL1C)-(XK1C*XL2C)
      R2C=(XK1C**2)*T1C
      A2C=R1C/R2C
      DO 2  I=1,89
      ANG(I)=I
      RANG(I)=(ANG(I)*3.1416)/180.
      E1(I)=SIN(RANG(I))
      E(I)= E1(I)**2
      T1(I)=SQRT(1-E(I))
      IF(E1(I).LE.RI) GC TO 2
      ZZ5(I)=RI*A2C*(T1(I)**2)
      ZZ6(I)=(RI*T1(I))/(E1(I)*SQRT(1.-RI2))
      ZZ7(I)= 1.-ZZ6(I)
      ZZ8(I)=SQRT(ZZ7(I)**3)
      ZZ9(I)=N*E(I)*ZZ8(I)
      BB1(I)=ZZ5(I)/ZZ9(I)
    2 CONTINUE
      DO 499 I=1,89
      X(I)=E1(I)
      Y(I)=PB1(I)
  499 CONTINUE
      WRITE(6,500) (X(I),Y(I),I=1,89)
  500 FOPMAT(2F14.3)
      STOP
      END
```

FINAL

This programme computes the totally reflected amplitude of an incident spherical wave according to the exact derivation.

```
      DIMENSION ANG(90),RANG(90),XK1(90),XK2(90),XL1(90),XL2(90),T1(90),
     1T2(90),T3(90),T4(90),T5(90),T6(90),T7(90),T8(90),T9(90),F(90),E1(9
     20),S1(90),S2(90),S3(90),S4(90),S5(90),S6(90),R1(90),R2(90),R3(90),
     3R4(90),R5(90),R6(90),A(90),A1(90),A2(90),A3(90),X(2048),Y(2048),BE
     4TA(90),IBETA(90),ETA(90),IETA(90),RMU(90),XMU(90),SMU(90),XSMU(90)
     5,RMU1(20),XMU1(20),XMU2(9),RMU2(9),XSMU1(38),W1(90),W2(90),Z1(
     690),Z2(90),Z3(90),Z4(90),Z7(90),Z8(90),Z9(90),W3(90),W4(90),XX1(90
     7),XX2(90),XX3(90),YY1(90),YY2(90),XNU(90),CNU(90),SNU(90),ZZ1(90),
     8ZZ2(90),ZZ3(90),ZZ4(90),ZZ5(90),ZZ6(90),ZZ7(90),ZZ8(90),ZZ9(90),BB
     91(90),BB2(90),BB3(90),BB4(90),BB5(90),BB6(90),BB7(90),BB8(90),BB9(
     190),CC1(90),CC2(90),TITLE(20),A3(90),BP1(90),SMU1(38)
      DATA RMU1/ 1.63,1.30,1.17,1.11,1.07,1.05,1.04,1.03,1.02,1.01,
     11.01,1.01,1.01,1.00,1.00,1.00,1.00,1.00,1.00,1.00/
      DATA XMU1/ 0.51,0.31,0.22,0.16,0.13,0.10,0.08,0.07,0.06,0.05,
     10.04,0.03,0.03,0.03,0.02,0.02,0.02,0.02,0.01,0.01/
      DATA RMU2/ 16.3,6.15,5.26,4.17,3.26,2.72,2.61,2.14,1.81/
      DATA XMU2/ 5.10,2.55,1.70,1.28,1.02,0.85,0.73,0.64,0.57/
      DATA SMU1/ 0.03,0.08,0.15,0.22,0.30,0.38,0.46,0.53,0.59,
     10.64,0.71,0.74,0.78,0.81,0.84,0.86,0.88,0.90,0.91,0.92,0.93,
     20.94,0.95,0.96,0.96,0.96,0.97,0.97,0.97,0.98,0.98,0.98,
     30.98,0.99,0.99,0.99,0.99,1.00/
      DATA XSMU1/ 0.05,0.12,0.18,0.24,0.28,0.31,0.33,0.33,
     10.68,0.32,0.32,0.31,0.29,0.28,0.26,0.24,0.23,0.21,0.20
     2,0.19,0.17,0.16,0.15,0.14,0.13,0.12,0.11,0.10,0.09,0.08,
     30.07,0.06,0.05,0.04,0.03,0.02,0.01,0.00/
      READ(4,10) N
      READ(5,1) V1,V2,B1,B2,D1,D2
   10 FORMAT(I5)
    1 FORMAT(6F7.2)
      RI=V1/V2
      RI2=RI**2
      XN1=V1/B1
      XN2=V1/B2
      D=D2/D1
      U=D*((B2/B1)**2)
      D1=D-1.
      U1=U-1.
      FLAG=0
C     CRITICAL POINT CALCULATION
      T1C=SQRT(1.-RI2)
      T2C=SQRT((XN1**2)-RI2)
      T3C=SQRT((XN2**2)-RI2)
      T4C=2*RI2*U1
      T5C=((XN1**2)*D1-T4C)**2
      T6C=(D*(XN1**2)-T4C)**2
      T7C=RI2*T5C
      T8C=T1C*T2C*T6C
      T9C=T1C*T3C*D*(XN1**4)
      XK1C=T7C+T8C+T9C
      XK2C=(T8C+T9C)-T7C
      S1C= RI2*(U1**2)
      S2C= ((XN1**2)+T4C)**2
      S3C= 4.*T1C*T2C*T3C*S1C
      S4C= T2C*D*(XN1**4)
      S5C= T3C*S2C
      XL1C= S3C+S4C+S5C
      XL2C= S3C-(S4C+S5C)
      R1C= (XK2C*XL1C)-(XK1C*XL2C)
      R2C=(XK1C**2)*T1C
      A2C=R1C/R2C
```

```
      Z4C=  C.822*A2C*SQRT(RI)*(1-RI2)
      Z5C= SQRT(N*T1C)
      Z6C=SQRT(Z5C)
      Z7C=Z4C/Z6C
      Z8C=(COS(3.14159/8.))*Z7C
      Z9C=(SIN(3.14159/8.))*Z7C
      A1C= XK2C/XK1C
      W3C= (A1C-Z8C)**2
      W4C= SQRT(W3C+(Z9C**2))
      AC=T1C*W4C
      WRITE(6,115) AC
  115 FORMAT(' ','CRITICAL AMPLITUDE='F10.4)
      DO 2  I=1,89
      ANG(I)=I
      RANG(I)=(ANG(I)*3.1416)/180.
      E1(I)=SIN(RANG(I))
      E(I)= E1(I)**2
      T1(I)=SQRT(1-E(I))
      T2(I)=SQRT((XN1**2)-E(I))
      IF(XN2.LT.E1(I))GO TO 130
      T3(I)=SQRT((XN2**2)-E(I))
      T4(I)=2.*E(I)*U1
      T5(I)=((XN1**2)*D1-T4(I))**2
      T6(I)=(D*(XN1**2)-T4(I))**2
      T7(I)=E(I)*T5(I)
      T8(I)=T1(I)*T2(I)*T6(I)
      T9(I)=T1(I)*T3(I)*D*(XN1**4)
      XK1(I)=T7(I)+T8(I)+T9(I)
      XK2(I)=(T8(I)+T9(I))-T7(I)
      S1(I)=E(I)*(L1**2)
      S2(I)=((XN1**2)+T4(I))**2
      S3(I)=4.*T1(I)*T2(I)*T3(I)*S1(I)
      S4(I)=T2(I)*D*(XN1**4)
      S5(I)=T3(I)*S2(I)
      XL1(I)=S3(I)+S4(I)+S5(I)
      XL2(I)=S3(I)-(S4(I)+S5(I))
      GO TO 131
CC    FOR N2 LESS THAN E1(I)
C     I.E. T3(I),T9(I),XK1(I),XK2(I)
C      S3(I),S5(I),XL1(I),XL2(I) COMPLEX
  130 T3(I)=SQRT(E(I)-(XN2**2))
      IF(FLAG.NE.0) GO TO 133
      FLAG=ANG(I)
  133 CONTINUE
      T4(I)=2.*E(I)*U1
      T5(I)=((XN1**2)*D1-T4(I))**2
      T6(I)=(D*(XN1**2)-T4(I))**2
      T7(I)=E(I)*T5(I)
      T8(I)=T1(I)*T2(I)*T6(I)
      T9(I)=T1(I)*T3(I)*D*(XN1**4)
      XK1(I)=SQRT((T7(I)+T8(I))**2+(T9(I)**2))
      XK2(I)=SQRT((T8(I)-T7(I))**2+(T9(I)**2))
      S1(I)=E(I)*(L1**2)
      S2(I)=((XN1**2)+T4(I))**2
      S3(I)=4.*T1(I)*T2(I)*T3(I)*S1(I)
      S4(I)=T2(I)*D*(XN1**4)
      S5(I)=T3(I)*S2(I)
      XL1(I)=SQRT((S4(I)**2)+(S3(I)+S5(I))**2)
      XL2(I)=SQRT((S4(I)**2)+(S3(I)-S5(I))**2)
C   REST OF CALC. DOES NOT INVOLVE COMPLEX VALUES.
```

```
131 R1(I)=(XK1(I)*XK2(I))
    R2(I)=RI2-E(I)
    R3(I)=(XL1(I)*XL2(I)*R2(I))
    R4(I)=(XL1(I)**2)*R2(I)
    A1(I)=(R1(I)-R3(I))/((XK1(I)**2)-R4(I))
    R5(I)=(XK2(I)*XL1(I))-(XK1(I)*XL2(I))
    R6(I)=((XK1(I)**2)-(XL1(I)**2)*R2(I))*T1(I)
    A2(I)= R5(I)/R6(I)
    IF(RI2.LT.E(I)) GO TO 99
    A0(I)= A1(I)-(A2(I)*T1(I)*SQRT(RI2-E(I)))
    GO TO 100
 99 RR1(I)= E(I)-RI2
    A0(I)= SQRT(A1(I)**2+(A2(I)**2)*RR1(I))
100 SI2=SQRT(1.-RI2)
    W1(I)=SI2-T1(I)
C   N IS THE FACTOR K(Z+Z0)
    W2(I)=SQRT(N/(2.*E(I)*T1(I)))
    BETA(I)=W2(I)*W1(I)
    BETA(I)=ABS(BETA(I))
    IF(BETA(I).GE.2.0) GO TO 47
    IF(BETA(I).LT.0.1) GO TO 48
    IBETA(I)=(BETA(I)*10.0+0.53)
    J=IBETA(I)
    RMU(I)=RMU1(J)
    XMU(I)=XMU1(J)
    GO TO 49
 48 IBETA(I)=(BETA(I)*100.+0.53)
    J=IBETA(I)
    RMU(I)=RMU2(J)
    XMU(I)=XMU2(J)
    GO TO 49
 47 RMU(I)=1.0
    XMU(I)=0.0
 49 IF(RI2-E(I)) 111,2,113
111 A3(I)=A2(I)*T1(I)*SQRT(E(I)-RI2)
    Z1(I)=(A3(I)*XMU(I))
    BB2(I)=(A1(I)+Z1(I))**2
    BB3(I)=(A3(I)*RMU(I))**2
    A(I)=T1(I)*SQRT((BB2(I)+BB3(I)))
    C5=RI*A2C
    ZZ6(I)=(RI*T1(I))/(E1(I)*SQRT(1.-RI2))
    ZZ7(I)= 1.-ZZ6(I)
    ZZ8(I)=SQRT(ZZ7(I)**3)
    ZZ9(I)=N*E(I)*ZZ8(I)
    BB1(I)=C5/ZZ9(I)
    XX1(I)=E1(I)/T1(I)-RI/SQRT(1.-RI2)
    XX2(I)=(N*(1.-RI2)*RI*T1(I))/(E1(I)*2.)
    XX3(I)=SQRT(XX2(I))
    ETA(I)=XX3(I)*XX1(I)
    IF(ETA(I).GE.3.30) GO TO 147
    IETA(I)=(ETA(I)*10.0+0.53)
    J=IETA(I)
    SMU(I)=SMU1(J)
    XSMU(I)=XSMU1(J)
    GO TO 148
147 SMU(I)=1.0
    XSMU(I)=0.0
148 YY1(I)=(RI*E1(I))/T1(I)
    YY2(I)=(SQRT(1.-RI2))-(1./T1(I))
    XNU(I)=N*(YY1(I)+YY2(I))+3.1416/2.
```

```
      CC1(I)=SQRT((SMU(I)**2)+(XSMU(I)**2))
      BB6(I)=BB1(I)*CC1(I)*(T1(I)**2)
      CC2(I)=(XSMU(I)/SMU(I))
      CC2(I)=ATAN(CC2(I))
      BB4(I)=((SQRT(BB3(I)))/(SQRT(BB2(I))))
      BB4(I)=ATAN(BB4(I))
      BB5(I)=-(XNU(I)+BB4(I)+CC2(I))
      BB9(I)=(N/T1(I))+XNU(I)+CC2(I)
C       BB7(I) CALCULATED BELOW IS THE SUPERCRITICAL AMPLITUDE
      BB7(I)=SQRT((A(I)**2)+(BB6(I)**2)+2*A(I)*BB6(I)*COS(BB5(I)))
C       BB8(I) CALCULATED BELOW IS THE MEAN SUPERCRITICAL AMPLITUDE
      BB8(I)=SQRT((A(I)**2)+(BB6(I)**2))
C       ZZ1(I) IS THE UPPER BOUND AMPLITUDE-THETA1
      ZZ1(I)=A(I)+BB6(I)
C       ZZ2(I) IS THE LOWER BOUND AMPLITUDE-THETA2
      ZZ2(I)=A(I)-BB6(I)
      GO TO 2
  113 A3(I)= A2(I)*T1(I)*SQRT(R12-E(I))
      Z1(I)=(A3(I)*XMU(I))**2
      Z2(I)= A3(I)*(RMU(I)-1.)
      Z3(I)= A0(I)-Z2(I)
C   BB7(I) CALC. BELOW IS AMPLITUDE BEFORE C.P.
      BB7(I)=T1(I)*(SQRT((Z3(I)**2)+Z1(I)))
    2 CONTINUE
      DO 499 I=1,89
      X(I)=E1(I)
      Y(I)=BB7(I)
      Z4(I)=BB6(I)
      Z7(I)=BB8(I)
      Z8(I)=ZZ1(I)
      Z9(I)=ZZ2(I)
  499 CONTINUE
      WRITE(6,500) (X(I),Y(I),I=1,89)
C       OUTPUT ON '6' IS THE TOTAL AMPLITUDE
      WRITE(1,500) (X(I),Z4(I),I=1,89)
C       OUTPUT ON '1' IS THE HEAD WAVE AMPLITUDE
      WRITE(2,500) (X(I),Z7(I),I=1,89)
C       OUTPUT ON '2' IS THE MEAN SUPERCRITICAL AMPLITUDE
      WRITE(7,500) (X(I),Z8(I),I=1,89)
C       OUTPUT ON '7' IS THE UPER BOUND -THETA1
      WRITE(8,500) (X(I),Z9(I),I=1,89)
C       OUTPUT ON '8' IS THE LOWER BOUND -THETA2
  500 FORMAT(2F14.6)
      STOP
      END
```

WAR

This programme calculates the interval velocities in sediments from wide angle reflection data.

```
C***************    WIDE ANGLE REFLECTION PROGRAM    ***************
C                   ******************************
C
C                       CARD INPUT FOR THE PROGRAM
C
C     CARD 1 - IDENTIFICATION OF THE STATION ; NO. OF LAYERS
C     CARD2 - GUESS AT THE VELOCITY OF EACH LAYER
C     CARD3 - SLOPE OF EACH LAYER
C     CARD4 - VERTICAL & HORIZONTAL WATER VELOCITIES
C     CARD5 - LAYER REFERENCE NO. ; NO. OF READINGS FOR THAT LAYER
C     CARD 6 - DIRECT ARRIVAL TIMES
C     CARD 7 - REFLECTED ARRIVAL TIMES
C
C     A LOOP IS SET UP SUCH THAT THE PROGRAM GOES BACK TO READ NEW
C     DATA FOR ANOTHER LAYER STARTING AT CARD 5.
      DIMENSION TO(10),HH(10),V(10),W(10),SW(10),CW(10),TW(10),D(100),
     1R(100),ZH(100),P(5,6),X(5),TI(100),U(100),S(100)
      COMMON TO,HH,V,W,TR,DR,SW,CW,TW,D,R,ZH,P,C,M,IND,KO,SVN,VH,X,TIT
C     ADEN1 & ADEN2 ARE IDENTIFICATION MARKERS OF EACH LAYER
C     NREF=NO. OF LAYERS
      READ(5,100)NREF
  100 FORMAT(I5)
C     V(I)=ESTIMATES OF VELOCITIES OF EACH LAYER (GUESS ON SMALL SIDE)
C     W(I)=SLOPE OF LAYER IN DEGREES & 1/10 THS. OF A DEGREE
      READ(5,107)(V(I),I=1,NREF)
      READ(5,107)(W(I),I=1,NREF)
  107 FORMAT(10F6.0)
      KW=2
      WT=0.0
      DO 6000 I=1,NREF
 6000 WT=WT+ABS(W(I))
      IF(WT-1.E-10)6001,6001,6002
 6001 KW=1
 6002 WRITE(6,103)NREF
  103 FORMAT('NO. OF LAYERS READ IN=',I5,//)
      WRITE(6,600)
      WRITE(6,607)(V(I),W(I),I=1,NREF)
  600 FORMAT(//,'TRIAL VELOCITIES & SLOPES IN DEGREES',//)
  607 FORMAT(F11.5,2X,F11.5)
C     CONVERT ANGLE TO DEGREES
      DO 1300 I=1,NREF
 1300 W(I)=W(I)*0.0174533
C     VV=VERTICAL WATER VELOCITY ; VH=HORIZONTAL WATER VELOCITY
      READ(5,107)VV,VH
      V(1)=VV
      WRITE(6,608)VV,VH
```

```
  608 FORMAT(//,'VV=',F11.5,2X,'VH=',F11.5,//)
C     THE FOLLOWING LOOP 12 IS THE MAIN ONE
C     IREF=LAYER NO. IDENTIFICATION ; KO=NO. OF POINTS TAKEN ON EACH
      DO 12 L=1,NREF
      READ(5,734)IREF,KO
  734 FORMAT(2I5)
      WRITE(6,735)IREF,KO
  735 FORMAT(///,'LAYER NO. REFERENCE',I5,2X,'NO. OF READINGS',I5,//)
C     U(K)=DIRECT ARRIVAL TIME IN SECONDS
C     S(K)=REFLECTED ARRIVAL TIME IN SECONDS
      READ(5,107)(U(K),K=1,KO)
      READ(5,107)(S(K),K=1,KO)
      WRITE(6,83)
      WRITE(6,84)(U(K),S(K),K=1,KO)
   83 FORMAT(//,4X,'U(K)',5X,'S(K)',//)
   84 FORMAT(2F8.5)
      IF(L-1)1210,1210,1211
C     IF NOT THE FIRST LAYER CONVERT U(K) TO DISTANCE
 1211 DO 796 KL=1,KO
  796 U(KL)=U(KL)*VH
 1210 CONTINUE
      WRITE(6,7491)VH
 7491 FORMAT(//,'VH=',F11.5,//)
C     FIT CURVE TO DATA TO OBTAIN TO AND LATER DIFFERENTIATE FOR ANGLE E
C     MERGENCE
C     IND IS AND INDEXUSED IN MOINS
      IF(U(1))923,3,923
  923 IND=-1
      DO 90 K=1,KO
      R(K)=S(K)**2
   90 D(K)=U(K)**2
      WRITE(6,80)
   80 FORMAT(//,'PASSED ST. NO. 90',//)
      CALL MAIND(1,L)
      TO(L)=SQRT(Y(1))
      IND=1
      IF(L-1)2,2,3
C     IF FIRST LAYER COMPUTE THICHNESS AND VH BY T2/X2
    2 CON=2.*TO(1)*SIN (W(1))
      HE(1)=V(1)*TO(1)/2.
      DO 200 I=1,KO
C     BRING BACK TO FLAT LAYER CASE
      R(I)=S(I)**2+CON*U(I)
  200 D(I)=U(I)**2
      WRITE(6,81)
   81 FORMAT(//,'PASSED ST. NO. 200',//)
      IND=1
      CALL MAIND(1,1)
      VH=SQRT(X(2))*V(1)
      GO TO 32
C     COMPUTE COEFFICIENTS DERIVATIVE FOR EMERGENCE ANGLE
    3 DO 92 K=1,KO
      R(K)=S(K)
   92 D(K)=U(K)
      WRITE(6,7492)
      WRITE(6,1985)(U(K),K=1,KO)
 7492 FORMAT(//,'U(K) ARRAY AFTER ST. NO. 92',//)
      WRITE(6,82)
   82 FORMAT(//,'PASSED ST. NO. 92',//)
      CALL MAIND(4,L)
```

```
      X(2)=X(2)*V(1)
      X(3)=X(3)*2.*V(1)
      X(4)=X(4)*3.*V(1)
      X(5)=X(5)*4.*V(1)
      WRITE(6,8456)V(1),X(2),X(3),X(4),X(5)
 8456 FORMAT(//,'V(1)=',F8.5,2X,'X(2)=',F8.5,2X,'X(3)=',F8.5,2X,'X(4)=',
     1F8.5,2X,'X(5)=',F8.5,//)
      IF(D(1))920,921,920
  921 TO(L)=X(1)
  920 IF(L-1)2,2,922
C     FIND ANGLE EMERGENCE ZM FOR EACH POINT EXCEPT LAST
  922 KO=KO-1
      IND=1
      DO 30 I=2,KO
      ZM(I)=X(2)+X(3)*U(I)+X(4)*U(I)**2+X(5)*U(I)**3
   30 ZM(I)=ATAN (ZM(I)/SQRT (1.-ZM(I)**2))
      D(1)=-1.E20
      TI(1)=0.
   31 IND=-IND
      CON=2.*SIN(W(L))/V(L)
      IK=0
      WRITE(6,1986)DR
 1986 FORMAT(//,'DR=',F11.5,//)
      DO 300 I=2,KO
      CALL KAUS(L,ZM(I),IK)
      WRITE(6,1986)DR
      IK=1
C     NOTE THAT D IS IN KM
      D(I)=U(I)-DR
      R(I)=S(I)-TR
      TI(I)=TIT
      D(I)=D(I)/C
      WRITE(6,2947)C
 2947 FORMAT('C=',F11.5)
C     ELIMINATE POINTS WITH NEGATIVE REDUCED D
      IF(D(I))300,3601,3601
C     REDUCE TO FLAT LAYER CASE
 3601 R(I)=R(I)**2+CON*D(I)*TI(I)-TI(I)**2
      D(I)=D(I)**2
  300 CONTINUE
      WRITE(6,1984)
      WRITE(6,1985)(D(I),I=1,KO)
 1984 FORMAT(//,'ARRAY D(I) WHICH GOES INTO MAIND AT ST. NO. 6',//)
 1985 FORMAT(10F11.5)
C     SOLVE FOR VELOCITY
      GO TO (5,6),KW
    5 IND=1
    6  CALL MAIND(1,L)
      VV=V(L)
C     CHECK FOR IMAGINARY VELOCITY
      IF(X(2))3100,3101,3101
 3101 WRITE(6,8455)X(2),V(L)
      WRITE(6,8455)X(2),V(L)
 8455 FORMAT(//,'X(2)=',F8.5,2X,'V(L)=',F8.5,2X,//)
      V(L)=SQRT (1./X(2))
C     RESET ANGLE ACCORDING TO NEW VELOCITY
      TW(L)=TW(L)*V(L)/VV
      W(L)=ATAN (TW(L))
      CALL KAUS(L,ZM(2),0)
C     IF IND NEGATIVR RESTART PROCESS
```

```
      IF(IND)31,31,32
   32 WW=W(L)/0.0174533
      WRITE(6,104)L,V(L),TO(L),SVN,WW
  104 FORMAT(//,'LAYER',I3,5X,'VELOCITY=',F11.5,2X,'REFLECTION TIME=',F1
     11.5,2X,'SV=',E13.7,2X,'SLOPE=',F11.5,//)
   12 CONTINUE
      WRITE(6,111)VH
  111 FORMAT(//,'VH=',F11.5,//)
 3100 WRITE(6,3200)L
 3200 FORMAT('*******  VELOCITY NEGATIVE REMOVE LAYER  *******',I5,//)
      STOP
      END
      SUBROUTINEMAIND(LL,L)
C     THIRD VERSION SUBROUTINE FOR SLOPING WIDANG JULY 1966
      DIMENSIONTO(10),HH(10),V(10),W(10),                    SW(10),
     1CW(10),TW(10),D(100),R(100),ZM(100),P(5,6),X(5)
      COMMONTO,HH,V,W,TR,DR,  SW,CW,TW,D,R,ZM,P,C,      M,IND,KO,SVN,VH
      COMMONX,TIT
      WRITE(6,734)
  734 FORMAT(//,'THE FOLLOWING ARE FROM SUBROUTINE MAIND',//)
      IN=LL
      INO=IN+1
      NO=INO+1
      KN=INO-1
      DO 1000 M=1,INO
      DO 1001 N=1,M
      P(M,N)=0.
      DO 1001 I=1,KO
      IF(D(I))1001,9001,9001
 9001 IF(M+N-2)6000,6000,6001
 6000 TX=1.
      GO TO 6002
 6001 TX=D(I)**(M+N-2)
 6002 P(M,N)=P(M,N)+TX
 1001 CONTINUE
      P(M,NO)=0.
      DO 1000 I=1,KO
      IF(D(I))1000,9002,9002
 9002 IF(M-1)6003,6003,6004
 6003 TX=R(I)
      GO TO 6005
 6004 TX=D(I)**(M-1)*R(I)
 6005 P(M,NO)=P(M,NO)+TX
 1000 CONTINUE
      DO 1010 N=1,INO
      DO 1010 M=1,N
 1010 P(M,N)=P(N,M)
      DO 1022 K=1,KN
      DO 1002 I=1,K
      II=I+1
      KK=K+1
      A1=ABS(P(I,I))
      A2=ABS (P(KK,I))
      IF(A1-A2)1020,1021,1021
 1020 DO 1200 IIN=I,NO
      AA=P(KK,IIN)
      P(KK,IIN)=P(I,IIN)
 1200 P(I,IIN)=AA
 1021 IF(A1-1.E-30)1002,1002,1210
 1210 DO 1201 MM=II,NO
```

```
1201  P(KK,NM)=P(KK,NM)-(P(I,NM)*P(KK,I)/P(I,I))
1002  CONTINUE
1022  CONTINUE
C     SOLVE MATRIX
      DO 1005 K=1,INO
      I=NO-K
      II=I+1
      X(I)=P(I,NO)
      IF(I-INO)1006,1050,1050
1006  DO 1060 KX=II,INO
1060  X(I)=X(I)-(P(I,KX)* X(KX))
1050  A1=ABS (P(I,I))
      IF(A1-1.E-30)1500,1500,1005
1005  X(I)=X(I)/P(I,I)
      A=IN+1
      IF(IN-1)1701,1701,4
1701  IF(IND)4 ,4 ,21
21    DDO=0.
      OK=KO
      DO 1061 K=1,KO
      RR=0.
      IF(D(K))9003,9004,9004
9003  OK=OK-1.
      WRITE(6,9173)OK,KO
 9173 FORMAT(//,'PASSED ST. NO. 9003 IN MAIND',2X,'OK=',F11.5,2X,'KO=',
     1I10,//)
      GO TO 1061
9004  DO 1062 I=1,INO
      IF(I-1)6006,6006,6007
6006  TX=X(I)
      GO TO 1062
6007  TX=X(I)*(D(K)**(I-1))
1062  RR=RR+TX
      DK=R(K)-RR
      DDO=DDO+DK**2
      WRITE(6,1700)D(K),R(K),RR,DK
 1700 FORMAT(3F10.5,E15.7)
1061  CONTINUE
      WRITE(6,89)DDO,OK,A
   89 FORMAT(//,'DDO=',F8.5,2X,'OK=',F8.5,2X,'A=',F8.5,//)
      DDO=SQRT (DDO/(OK-A ))
      WRITE(6,1802)DDO
 1802 FORMAT(//,'STANDARD DEVIATION FROM MAIND=',E15.7,//)
      STD=DDO
      VA=1./X(2)
      WRITE(6,1900)X(1),X(2)
1900  FORMAT(2F10.5)
      STD=STD**2
      D11=0.
      D21=0.
      DO 6 M=1,KO
      IF(D(M))6,9010,9010
9010  D2=D(M)**2
      D21=D2+D21
      D11=D(M)+D11
6     CONTINUE
      D211=OK*D21-D11**2
      SX=STD/D211
      SVN=OK*SX
      SVN=SVN*VA**4
```

```
      WRITE(6,90)SVN,OK,SX,VA,STD,D211
   90 FORMAT(//,'SVN=',F8.5,2X,'OK=',F8.5,2X,'SX=',F8.5,2X,'VA=',F8.5,2X
     1,'STD=',F8.5,2X,'D211=',F8.5,//)
      SVN=SQRT (SVN)
      GO TO 4
 1500 WRITE(6,1501)I,I
 1501 FORMAT(//,I3,',',I3,'=0   PROBLEM UNDETERMINED',//)
4     RETURN
      END
      SUBROUTINE KAUS(L,ZZ,IK)
C     SUBROUTINE TO COMPUTE REFLECTIONS FOR T2/X2 METHOD
C     L IS NUMBER LAYER,ZZ IS EMERGENCE ANGLE,IK IS INDEX TO INDICATE FI
C     RST POINT LAYER,PARAMERERS TRANSMITTED BY COMMON
C     TR,DR,AND TI ARE RETURNED
C     VERSION MAY 1967
      DIMENSION TO(10),HH(10),V(10),W(10),X(10),XX(10)          ,SW(10),
     1CW(10),TW(10),D(100),R(100),ZM(100),P(5,6),Y(5)
      COMMONTO,HH,V,W,TR,DR,   SW,CW,TW,D,R,ZM,P,C      M,IND,KO,SVN,VH
      COMMONY,TI
C     CHECK IF FIRST POINT
      IF(IK)9990,9990,9991
C     FIND THICHNESSES  ,COMPUTE SIN COS TAN
 9990 DO 1000 I=1,L
      SW(I)=SIN (W(I))
      CW(I)=COS (W(I))
 1000 TW(I)=SW(I)/CW(I)
      C=1.
      IF(L-1)1003,1003,1002
 1002 L1=L-1
      WW=0.
      DO 1001 I=1,L1
 1001 WW=WW+W(I)
      C=COS (WW)
C     FIND ANGLE CORRESPONDING VERTICAL REFLECTION
 1003 I=L
      Q=W(I)
      IF(L-1)11,11,10
   10 SIX=(V(I-1)/V(I))*SIN (Q)
      COX=SQRT (1.-SIX*SIX)
      Q=ATAN (SIX/COX)+W(I-1)
      I=I-1
      IF(I-1)11,11,10
11    Q=C-W(I)
      ZO=0
      U=0.
      TT=0.
   12 IF(I-L)13,14,14
C     COMPUTE HH(I)
   13 HC=HH(I)-U*SIN (W(I))
      SIX=SIN (Q)
      COX=COS (Q)
      U=U*CW(I)       +HC*SIX/COX
      TT=TT+HC/(V(I)*COX)
      SIXW=V(I+1)*SIX/V(I)
      XW=ATAN (SIXW/SQRT (1.-SIXW*SIXW))
      Q=XW-W(I+1)
      I=I+1
      GO TO 12
   14 HC=(TO(I)/2.-TT)*V(I)
      HH(I)=HC+U*SW(I)
```

```
C         COMPUTE REFLECTIONS
C FIN DANGLES INCIDENCE FROM EMERGENCE ANGLE
   9991 I=0
        XX(1)=ZZ+W(1)
    924 I=I+1
        IF(L-I) 9252,9252,9250
   9250 SIX=SIN(XX(I))
        IF(SIX-V(I)/V(I+1))9253,30,30
   9253 SIXW=V(I+1)*SIX/V(I)
        XW=ATAN(SIXW/SQRT(1.-SIXW*SIXW))
        XX(I+1)=XW+W(I+1)
        GO TO 924
   9252 I=L+1
        X(L)=XX(L)
    926 I=I-1
        IF(I-1)21,21,928
    928 SIX=SIN(X(I)+W(I))*V(I-1)/V(I)
        X(I-1)=ATAN(SIX/SQRT(1.-SIX*SIX))
        GO TO 926
C         MAIN COMPUTATION
     21 TT=0
        U=0
        I=0
     24 I=I+1
        HC=HH(I)-U*SW(I)
        SIX=SIN(X(I))
        COX=COS(X(I))
        HK=HC*(SIX/COX)
        U=U*CW(I)      +HK
        TK=HC/(V(I)*COX)
        TT=TT+TK
        IF(L-I)252,252,24
    252 I=L+1
        HK=HK/COS (W(L))
        TR=TK
        DR=HK
        TI    =(HC/V(L))*2.
        PP=U
     26 I=I-1
        RR=HH(I)-PP*TW(I)
        COX=COS(XX(I)-W(I))
        HK=RR*SIN(XX(I))/COX
        PP=PP/CW(I)+HK
        TK=(RR*CW(I))/(COX*V(I))
        TT=TT+TK
        IF(I-L)262,261,261
    261 DR=DR+HK
        TR=TR+TK
    262 IF(I-1)27,27,26
     27 TP=TT-TR
        DR=PP-DR*C
      3 RETURN
     30 DR=+1.E20
        TR=0.
        TI=0.
        GO TO 3
        END
```

TWAT

This programme computes the refraction velocity for one layer with corrections for overlying layers.

```
C       REFRACTION VELOCITY STATISTICS FOR ONE LAYER WITH
C       CORRECTIONS FOR OVERLYING LAYERS. LINEAR REGRESSION TO
C       ARRIVAL TIMES.  ND = NO. OF ARRIVAL TIMES.  NL = NO. O
C       F OVERLYING LAYERS.  WV(I) = VELOCITY OF ITH OVERLYING
C       LAYER.  X(I) = DISTANCE TO ITH DATA POINT.  T(I) =
C       ARRIVAL TIME AT ITH POINT.  W(I,J) = THICKNESS OF JTH
C       OVERLYING LAYER AT ITH POINT.
C      REFRACTION  VELOCITY STATISTICS FOR ONE LAYER + CORRECTIONS
       DIMENSION X(100),T(100),A(100),W(100,5),WV(5),B(100),R(100)
       READ(5,2) ND,NL
     2 FORMAT(I3,I2)
       READ(5,3) (WV(I),I=1,NL)
     3 FORMAT(5F7.2)
       IND=1+NL
       JIM=1
       SX=0.
       ST=0.
       WRITE(6,12) ND
    12 FORMAT(1H1,20X,'ANALYSIS OF REFRACTION VELOCITY FOR ONE LAYER WITH
      1 CORRECTIONS FOR OVERLYING LAYERS'/21X,83(1H-)///'NO. OF DATA POIN
      2TS =',I3/'DIST.    TIME.    LAYER THICKNESSES'/)
       DO 10 I=1,ND
       READ(5,4) X(I),T(I),(W(I,J),J=1,NL)
     4 FORMAT(8F7.2)
       WRITE(6,6) X(I),T(I),(W(I,J),J=1,NL)
     6 FORMAT(1H ,8F8.2)
       SX=SX+X(I)
       ST=ST+T(I)
       A(I)=T(I)
    10 CONTINUE
       STM=ST/ND
       SXM=SX/ND
    15 SV=0.
       STQ=0.
       SXQ=0.
       DO 20 I=1,ND
       ET=A(I)-STM
       EX=X(I)-SXM
       SV=SV+ET*EX
       STQ=STQ+ET**2
       SXQ=SXQ+EX**2
    20 CONTINUE
       VT=SV/SXQ
       VX=SV/STQ
       DT=STM-VT*SXM
       DX=SXM-VX*STM
       RVT=1/VT
       RDT=SXM-RVT*STM
       TE=0.
       XE=0.
       RTE=0.
       DO 30 I=1,ND
       U=X(I)
       V=A(I)
       RES=(V-DT-VT*U)
```

```
      TE=TE+RES**2
      R(I)=RES
      XE=XE+(U-DX-VX*V)**2
      RTE=RTE+(U-RCT-RVT*V)**2
   30 CONTINUE
      STE=SQRT(TE/(ND-2))
      SXE=SQRT(XE/(ND-2))
      SRTE=SQRT(RTE/(ND-2))
      EV=SXE/SQRT(STC)
      EI=SQRT(STE*STE/ND+STE*STE*SXM*SXM/SXC)
      GO TO(32,45,45,32),JIM
   32 WRITE(6,36) VT,DT,STE,VX,DX,SXE,RVT,RCT,SRTE,EV,EI
   36 FORMAT(1H0,'REGRESSION OF TIME ON TO DISTANCE'//'SLOPE =',F6.3/'IN
     1TERCEPT =',F6.2/'STANDARD ERROR =',F5.2//'REGRESSION OF DISTANCE O
     2N TO TIME'//'VELOCITY =',F5.2/'INTERCEPT =',F6.2/'STANDARD ERROR =
     3',F5.2//'REGRESSION OF RECIPROCAL T ON TO D FOR V'//'VELOCITY =',
     4F5.2/'INTERCEPT =',F6.2/'STANDARD ERROR =',F5.2/'S.E. ON VELOCITY
     5=',F6.3/'S.E. ON INTERCEPT =',F6.3///)
      WRITE(6,37) (R(I),I=1,ND)
   37 FORMAT(1H0,'TIME RESIDUALS'/(13F8.3))
      GO TO (90,40,40,40,40,40),IND
   40 IND=IND-1
      JIM=1
      IT=NL+1-IND
      WRITE(6,42) IT,WV(IT)
   42 FORMAT(1H0,'VELOCITIES WITH CORRECTION FOR LAYER',I2,' WITH VELOCI
     1TY',F5.2/)
      DO 44 I=1,ND
   44 B(I)=A(I)
   45 ANG=ARSIN(WV(IT)/VX)
      FAC=1/(COS(ANG)*WV(IT))-TAN(ANG)/VX
      ST=0.
      DO 50 I=1,ND
      A(I)=B(I)-W(I,IT)*FAC
   50 ST=ST+A(I)
      STM=ST/ND
      JIM=JIM+1
      GO TO 15
   90 STOP
      END
```

Store

This programme transfers data from analogue to digital tape.

```
50;;
SET;60,61,62,63,64;0,.01,-1,0,0;
SPR;
SET THRESHOLD LEVEL;
ASK;
DEL;159;;50;
SPR;
NO.OF SAMPLES;
ASK;
DEL;159;;51;
SPR;
STARTING FILE;
ASK;
INS;B;159;
SPR;
TERMINATING FILE;
ASK;
INS;C;159;
SPR;
NO.OF DO LOOPS;
ASK;
INS;D;159;
DO;A;B;.01;C;
CALL;40;
IF;C(.01,)<C(.05,);
IGO;18;
ELS;
DO;91;0;.01;D;
CALL;40;
ADD;60,61;60;
DEL;2,60;;63,64;
CALL;42;
IF;C(.60,)<C(.51,);
IGO;23;
ELS;
SET;60,63,64;0,0,0;
CONT;
DO;90;0;.01;.31;
CALL;42;
IGO;32;
CONT;
SPR;
;
CPR;100;
CONT;
EXI;
INP;;;13,14;1,2;
RETURN;
OUT;A;;1,2;63,64;
RETURN;
END;
```

LEVEL SETTING

```
10;;
SET;50,51;0,10.0;
INP;;;13,14;1,2;
IF;C(.02,)>C(.51,);
SPR;
CHANNEL 2
ELS;
IGO;2
END
```

Replay 1, 2, 3

These programmes examine the digital tape to find the peak amplitudes and sample numbers.

PEAK DETECTION-------6.(6/2/75).

```
60;;
SET;50,51,52,53,54,55,56;0,.01,0,0,0,0,-1;
SPR;
IGNORE N SAMPLES;
ASK;
DEL;159;;60;
SPR; WLENGTH;
ASK;
DEL;159;;61;
SPR; SHOTS;
ASK;
DEL;159;;62;
SPR; NO.OF WINDOWS;
ASK;
CALL;47;
IF;C(.01,)<.50;
IGO;13;
ELS;
ADD;55,51;55;
CALL;47;
ADD;50,51;50;
IF;C(.50,)<C(.60,);
IGO;18;
ELS;
CALL;47;
IF;C(.02,)<0;
MUL;2;56;2;
ELS;
IF;C(.02,)>C(.53,);
DEL;2;;53;
ELS;
ADD;51,52;52;
IF;C(.52,)<C(.61,);
IGO;23;
ELS;
ADD;51,54;54;
CALL;49;
SET;52,53;0,0;
IF;C(.54,)<C(1.59,);
IGO;23;
ELS;
SET;54;0;
IF;C(.55,)<C(.62,0);
IGO;13;
ELS;
SET;53,54,55;0,0,0;
CALL;49;
IGO;45;
INP;;;13,14;1,2;
RETURN;
OUT;-.06;;1,2,3;53,54,55;
RETURN;
END;
```

2nd Replay

PEAK DETECTOR--------8.

```
60;;
SET;50,51,52,53,54,55,56,57,58;0,.01,0,0,0,0,-1,0,0;
SPR;
IGNORE N SAMPLES;
ASK;
DEL;159;;60;
SPR; WLENGTH;
ASK;
DEL;159;;61;
SPR; SHOTS;
ASK;
DEL;159;;62;
SPR; NO.OF WINDOWS;
ASK;
CALL;49;
IF;C(.01,)<.50;
IGO;13;
ELS;
ADD;55,51;55;
CALL;49;
ADD;50,51;50;
ADD;57,51;57;
IF;C(.50,)<C(.60,);
IGO;18;
ELS;
CALL;49;
ADD;57,51;57;
IF;C(.02,)<0;
MUL;2;56;2;
ELS;
IF;C(.02,)>C(.53,);
DEL;2,57;;53,58;
ELS;
ADD;51,52;52;
IF;C(.52,)<C(.61,);
IGO;23;
ELS;
ADD;51,54;54;
CALL;51;
SET;52,53,57;0,0,0;
IF;C(.54,)<C(1.59,);
IGO;23;
ELS;
SET;54,58;0,0;
IF;C(.55,)<C(.62,0);
IGO;13;
ELS;
SET;53,54,55;0,0,0;
CALL;51;
IGO;47;
INP;;;13,14;1,2;
RETURN;
OUT;-.06;;1,2,3,4;53,54,55,58;
RETURN;
END;
```

```
70;;

SET;50,51,52,53,54,57,58,59,70,71;0,.01,0,0,0,0,0,0,-1,0;
SPR;
IGNORE N SAMPLES( 3,1;
ASK;
DEL;159;;60;
SPR;
TIME FACTOR;
ASK;
INS;65;159;
MUL;60;65;60;
SPR;
WLENGTH;
ASK;
DEL;159;;61;
SPR;
MF FOR WLENGTH;
ASK;
INS;66;159;
MUL;61;66;61;
SPR;
NO.OF WINDOWS(MAX. NO.IS 3,000-TYPED AS 30.);
ASK;
INS;62;159;
SPR;
STARTING FILE;
ASK;
INS;B;159;
SPR;
TERMINATING FILE;
ASK;
INS;C;159;
DO;A;B;.01;C;
CALL;62;
ADD;50,51;58;
ADD;57,51;57;
IF;C(.50,)<C(.60,);
IGO;26;
ELS;
CALL;62;
ADD;51,57;57;
IF;C(.01,)<0;
MUL;1;70;3;
ELS;
IF;C(.01,)>0;
DEL;1;;3;
ELS;
IF;C(.03,)>C(.53,);
DEL;3,57,2,1;;53,58,59,71;

ELS;
ADD;51,52;52;
IF;C(.52,)<C(.61,);
IGO;32;
ELS;
ADD;51,54;54;
CALL;64;
SET;52,53,58,59,71;0,0,0,0,0;
```

Cont. over/...

```
IF;C(.54,)<C(.62,);
IGO;32;
ELS;
SET;50,54,57;0,0,0;
CONT;
DO;90;0;.01;2.55;
CALL;64;
IGO;55;
CONT;
CALL;62;
IGO;59;
EXI;
INP;A;;1,2;1,2;
RETURN;
OUT;-0.04;;1,2,3,4;53,58,100,71;
RETURN;
END;
```

PRINT

This programme O/P the contents of A (Specified) file to the T/T.

1) Give File No.

2) Starting Sample No.

3) No. of Samples.

```
 20;;
SPR;
FILEN;
ASK;
INS;A;159;
SPR;
START SAMPLE;
ASK;
INS;B;159;
SPR;
NO.OF SAMPLES;
ASK;
INP;A;B;1,2;1,2;
SPR;
;
CPR;1,2;
IF;TBP<C(1.59,);
IGO;9;
ELS;
EXI;
END;
```

CONV

a) This programme converts the Modular One output into normalised amplitude and distance.

b) This programme converts the Modular One output into arrival time and distance.

```
      IMPLICIT REAL*8(A-H,O-Z)
      DIMENSION A(400),XN(400),XSN(400),XL(400),AC(400),
     1IA(400),IN(400),ISN(400)
C      NMAX IS THENO.OF SHOTS')
      READ(3,77) NMAX
   77 FORMAT(I5)
      READ(5,1) (IA(I),IN(I),ISN(I),I=1,NMAX)
    1 FORMAT(4X,I4,3X,I4,4X,I3)
CSV IS THE SHIP VELOCITY IN KNOTS.
C  D IS THE WATER DEPTH IN KM.
C  F IS THE SHOT INTERVAL IN SEC.
      READ(4,2) SV,D,F
    2 FORMAT(3F7.2)
C      ISF IS THE CON.FACTOR TO CONVERT SAM NO. INTO DIST.
      READ(3,13) ISF
   13 FORMAT(I5)
      XK=SV*1.8288
      DO 3 I=1,NMAX
      A(I)=DFLOAT(IA(I))
      XN(I)=DFLOAT(IN(I))
      SF=DFLOAT(ISF)
      XN(I)=XN(I)/(SF*100.)
      XSN(I)=DFLOAT(ISN(I))
      XL(I)=((XSN(I)*F+XN(I))*XK)/3.6
      XL(I)=XL(I)/1000.
      AC(I)=A(I)*DSQRT(XL(I)**2+D*D)
    3 CONTINUE
      WRITE(6,4) (XL(I),AC(I),I=1,NMAX)
      WRITE(7,4) (XL(I),XN(I),I=1,NMAX)
    4 FORMAT(2F14.6)
      STOP
      END
```

```
      IMPLICIT REAL*8(A-H,O-Z)
      DIMENSION A(400),XN(400),XSN(400),XL(400),AC(400),
     1IA(400),IN(400),ISN(400)
      READ(5,1) (IA(I),IN(I),ISN(I),I=1,300)
    1 FORMAT(4X,I4,3X,I4,4X,I3)
      READ(4,2) SV,D,F
    2 FORMAT(3F7.2)
      XK=SV*1.8288
      DO 3 I=1,300
      A(I)=DFLOAT(IA(I))
      XN(I)=DFLOAT(IN(I))
      XSN(I)=DFLOAT(ISN(I))
      XL(I)=((XSN(I)*F+XN(I)/100.)*XK)/3.6
      XL(I)=XL(I)/1000.
      AC(I)=A(I)*DSQRT(XL(I)**2+D*D)
    3 CONTINUE
      WRITE(6,4) (XL(I),AC(I),I=1,300)
    4 FORMAT(2D14.6)
      STOP
      END
END OF FILE
```

RAT

This programme fits a polynomial to the given data.

```
C       THIS PROG IS A CURVE FITTING PROG
C       DATA IS FED IN ON '4'  FOR ANALYSIS
        IMPLICIT REAL*8(A-H,O-Z)
        DIMENSION X(300),Y(300),W(300),NN(300),SI(15),P(15)
C       FOLLOWING IS BAD SHOT DATA
        READ(3,17)NIS
C       NIS IS THE NO. OF BAD SHOTS
     17 FORMAT(I5)
        IF(NIS.EQ.0) GO TO 19
        READ(3,18) (NN(J),J=1,NIS)
C       NN(J) IS THE JTH BAD SHOT
     18 FORMAT(4I5)
C       M IS THE NO. OF DATA POINTS TO BE READ IN
     19 READ(5,17) M
        READ(4,2) (X(I),Y(I),I=1,M)
      2 FORMAT(2F14.6)
C       THIS DO LOOP SETS ALL THE WEIGHTS TO 1.0
        DO 3 I=1,M
        W(I)=1.0D0
     3  CONTINUE
        IF(NIS.EQ.0) GO TO 20
C       THIS DO LOOP SETS THE WEIGHTS OF THE BAD SHOT DATA POINTS TO 0.0
        DO 77 J=1,NIS
        W(NN(J))=0.0D0
     77 CONTINUE
     20 K1=15
        LOGICAL L
        L=.FALSE.
C       THE CURVE FITTING ROUTINE IN *NAG IS CALLED
        CALL E02ABF(M,X,Y,W,K1,N,SI,P,L)
C       THE OUTPUT IS THE COEFFICIENTS OF THE FITTED POLYNOMIAL
C       AND THE VARIANCE OF THE DATA FIT
C       N IS THE DEGREE OF THE POLYNOMIAL
        WRITE(6,4) (P(I),SI(I),I=1,K1)
      4  FORMAT(2E14.6)
        WRITE(6,5) N
     5  FORMAT(I5)
        STOP
        END
OF FILE
```

<u>GEN</u>

This programme produces an output from the fitted curve data from RAT.

```
      IMPLICIT REAL*8(A-H,O-Z)
      DIMENSION X(350),Y(350),T(100),A(350)
      WRITE(2,1)
    1 FORMAT('NO.OF DATA POINTS')
      READ(4,2) NP
    2 FORMAT(I5)
      READ(5,3) (A(I),I=1,NP)
    3 FORMAT(D14.6)
      DO 4 I=1,150
      X(I)=FLOAT(I)
      X(I)=X(I)/10.
      TOTAL=0.0
      DO 7 J=1,NP
      K=J-1
      T(J)=A(J)*(X(I)**K)
      TOTAL=TOTAL+T(J)
    7 CONTINUE
      Y(I)=TOTAL
    4 CONTINUE
      WRITE(6,5) (X(I),Y(I),I=1,150)
    5 FORMAT(2F14.6)
      STOP
      END
D OF FILE
```

Appendix 2

Detailed explanation of the Wide Angle Reflection Analysis Programme, W.A.R.

Layer 1

Given $T_{(1)} = f(D_{(1)})$, $e_{(1)}$ and $v_{(1)}$, where the quantities have the same meaning as in equation (2), chapter IV.

Step 1

Find $T_{o(1)}$, the minimum reflection time if the T/X curves start as X = 0, $T_{o(1)}$ is found by a fourth order least squares fit

$$T_{(1)} = T_{o(1)} + X_{(1)}.D_{(1)} + X_{(2)}.D_{(1)}^2 + X_{(3)}.D_{(1)}^3 + X_{(4)}.D_{(1)}^4 \qquad (A2.1)$$

If the T/X curves do not start at X = 0 $T_{o(1)}$ is found from a linear squares fit

$$T_{(1)}^2 = T_{o(1)}^2 + X_{(1)}.D_{(1)}^2 \qquad (A2.2)$$

From $T_{o(1)}$, $HH_{(1)}$, the perpendicular distance to the first layer is found (Fig. A2.1).

Step 2

For each $T_{(1)}$, the following is computed

$$CON_{(1)} = T_{o(1)}^2 - 2T_{o(1)} \sin e_{(1)}.D_{(1)} \qquad (A2.3)$$

where $CON_{(1)}$ is a correction term to reduce the observed times, and we obtain the reduced times

$$T_{(1)}^2 = T_1^2 - CON_{(1)} \qquad (A2.4)$$

Then, VH is found by a least squares fit of

$$T_{(1)}^2 = D_{(1)}^2 \quad \frac{VH^2}{V_{(1)}^2} \qquad (A2.5)$$

together with its standard deviation.

Layer 2

Given $T_{(2)} = f(D_{(2)})$, $e_{(1)}$, $V_{(1)}$ and knowing the apparent slope $e_{a(2)}$ as a result of the trial velocity $V_{a(2)}$.

APPENDIX 2

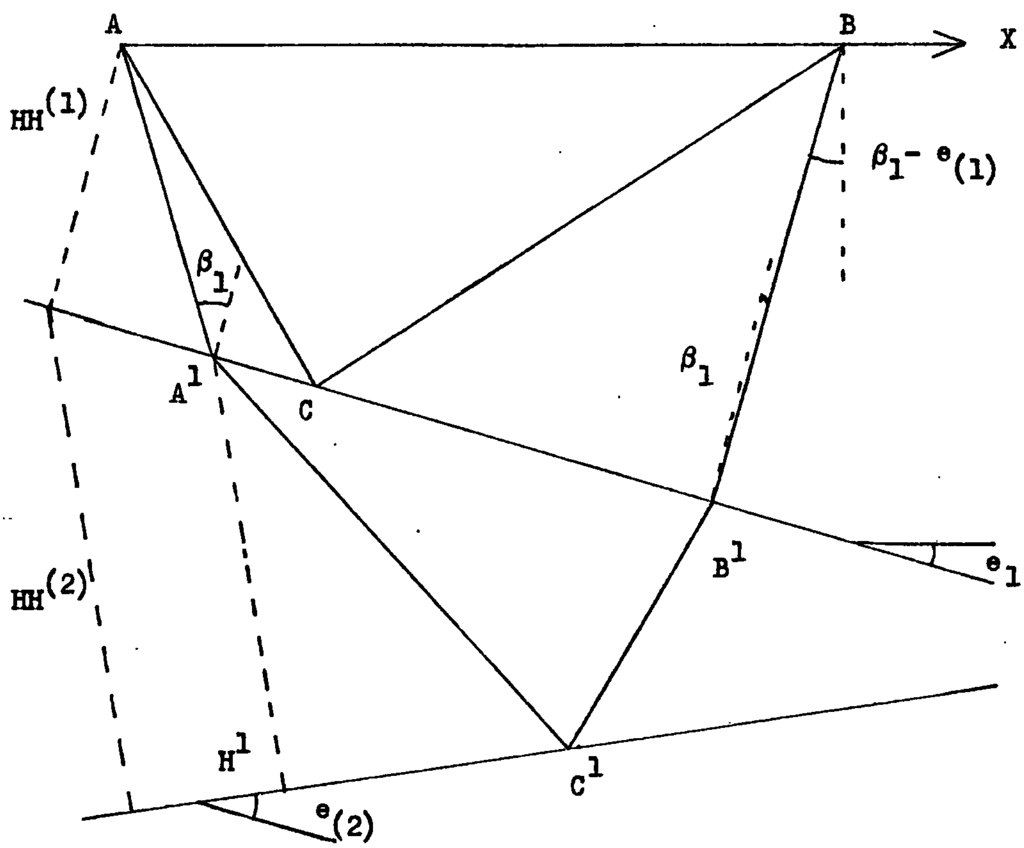

Fig. A2.1 Schematic Diagram for Velocity Computations

Step 1

$T_{o(2)}$ is found as above, where $T_{o(2)}$ is the zero excursion, $(X = 0)$, reflection time to Layer 2.

Step 2

$HH_{(2)}$ is found for the trial velocity $V_{a(2)}$.

Step 3

The fourth order polynomial

$T_{(2)} = f(X(Z))$ is differentiated to give

$$\sin(\beta_1 - e_{(1)}) = V_{(1)} \frac{dT_2}{dX} \qquad (A2.6)$$

and β' is found from β for each data point except the first and last. These are omitted because the fourth order polynomial is not constrained beyond these points and its slope often becomes erratic.

Step 4

Knowing the incident and emergent angles, $T_{BB'}$, $T_{AA'}$, $A'B'$ and $T_{A'H'}$ (Fig. A2.1) are calculated and hence the travel time in the second layer obtained

$$T_{A'C'B'} = T_{AA'C'B'} - T_{AA'} - T_{BB'} \qquad (A2.7)$$

Step 5

The reduced travel times

$$T_{(2)}{}^2 = T_{(2)}{}^2 - CON_{(2)} \qquad (A2.8)$$

are calculated, where

$$CON_{(2)} = T_{A'H'}{}^2 - 2T_{A'H'} \sin e_{a(2)} T_{A'B'} \qquad (A2.9)$$

Any negative reduced times are eliminated. These occasionally occur at near normal incidence, owing to errors in the upper layers. In such cases the corresponding data points are removed from the solution.

Step 6

The corrected layer two velocity, with its standard deviation is obtained by a least squares fit of

$$T_{(2)}{}^2 = \frac{A'B'}{V_{(2)}{}^2} \qquad (A2.10)$$

and a check made for negative velocities.

Step 7

The dip angle, $e_{(2)}$, is corrected, using

$$\tan e_{(2)} = \tan e_{a(2)} \cdot \frac{V_{(2)}}{V_{a(2)}} \qquad (A2.11)$$

and the programme returns to step 2 for a new iteration, before moving onto a third layer.

APPENDIX 3

Appendix 3

Digitisation Test

Using the STORE programme, described in Chapter IV and Appendix 1, several digitisations of the same section of record were made at different sampling rates, 100Hz, 250Hz, 500Hz and 1kHz.

The analogue signal, as mentioned previously is filtered through an anti-aliasing filter (Ref. 2.2) whose cut-off is approximately 100Hz, but a test of the digitisation accuracy, using linear interpolation for signal reconstitution, was made at different sampling rates.

For a sinusoidal waveform of frequency f, a 95% accuracy limit on the peak amplitude is given by having at least one digitisation value fall between 71.805° and 108.195°, an angle window of 36.39° (Fig. A3.1). This is equivalent to 9.893 windows per wavelength, or roughly 10 samples/wavelength. Thus for 95% accuracy (minimum), using linear interpolation, the digitisation rate must be ten times the maximum frequency of interest. For a sinusoid frequency of 20Hz sampled at a rate of 500Hz, 25 samples are taken per wavelength, giving an error window of 14.4° about the peak amplitude corresponding to an accuracy level of 96.86%.

For a frequency of 40Hz, the error window is 28.8°, giving an accuracy level of 87.63%, whilst for 100Hz, the error window is 72°, implying at 30.9% accuracy. These, of course, are the worst case figures.

The REPLAY programme (Chapter IV, Appendix 1) was run with a window length of one sample, with zero delay and taking varying sample numbers, to give exact coverage of the section of digitised record being examined. The results of this were displayed on a teletype, using the PRINT programme and the results plotted in Figs. A3.2, A3.3, A3.4. There are obvious inaccuracies prevent at the lower digitisation rates, and the results of the comparison of the amplitudes

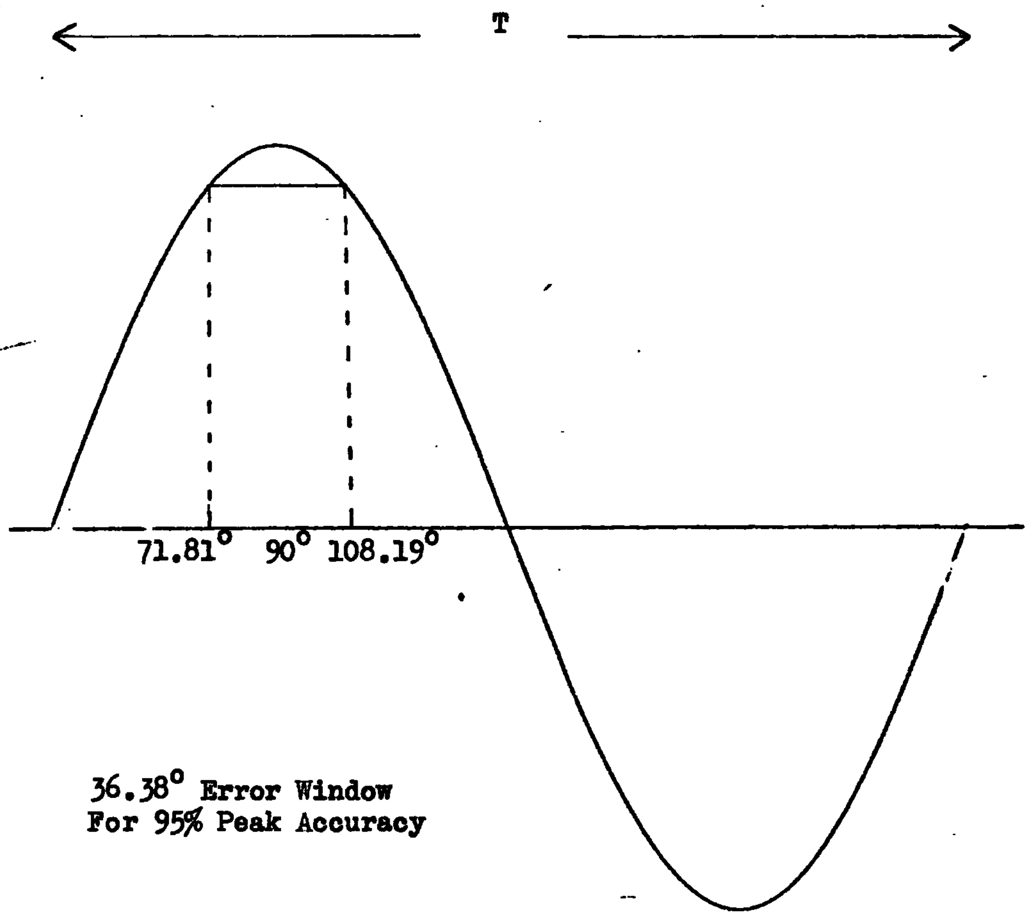

Fig. A3.1 **Digitisation of A Sinusoid**

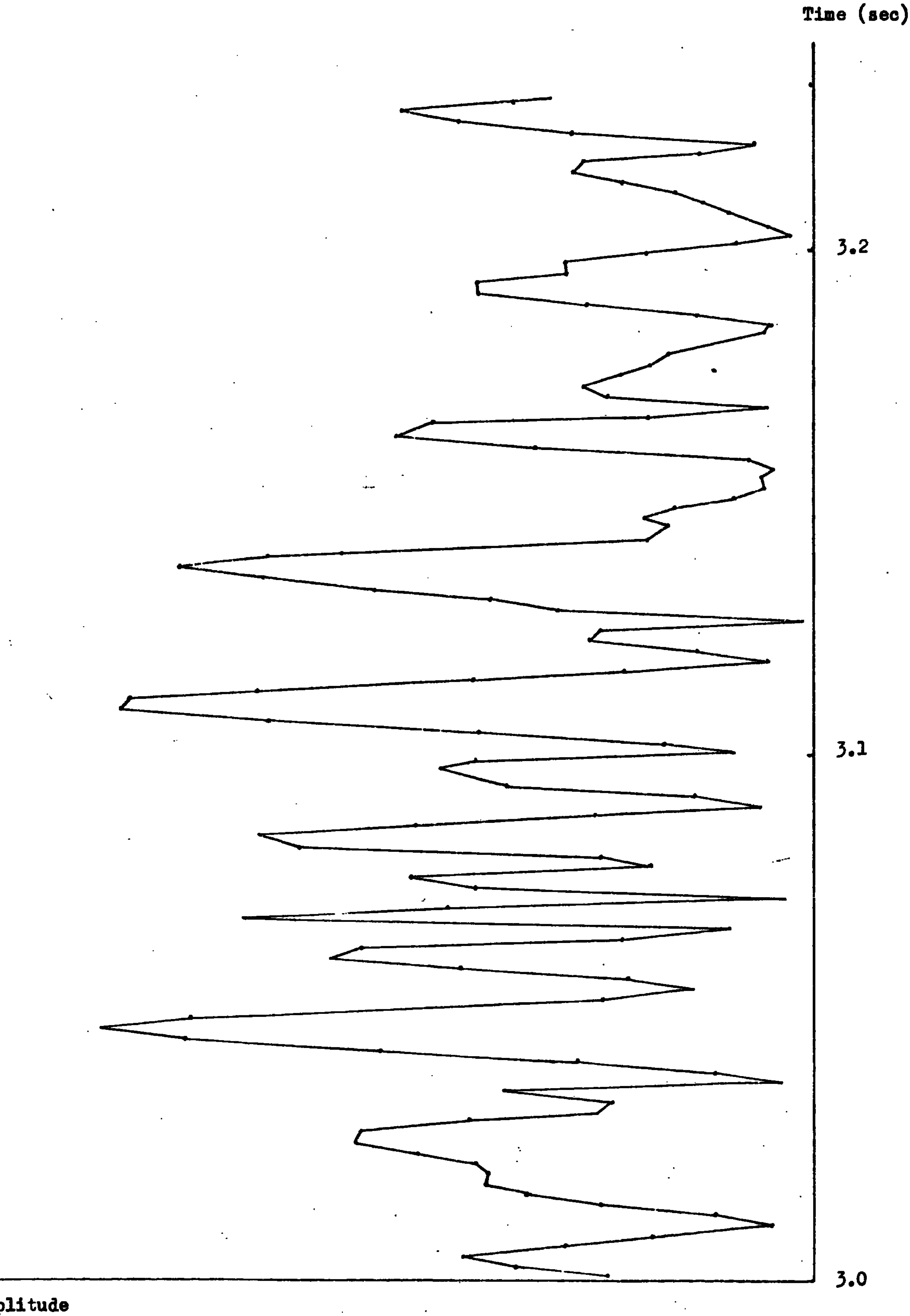

Fig. A3.2 Digitisation Test 500Hz

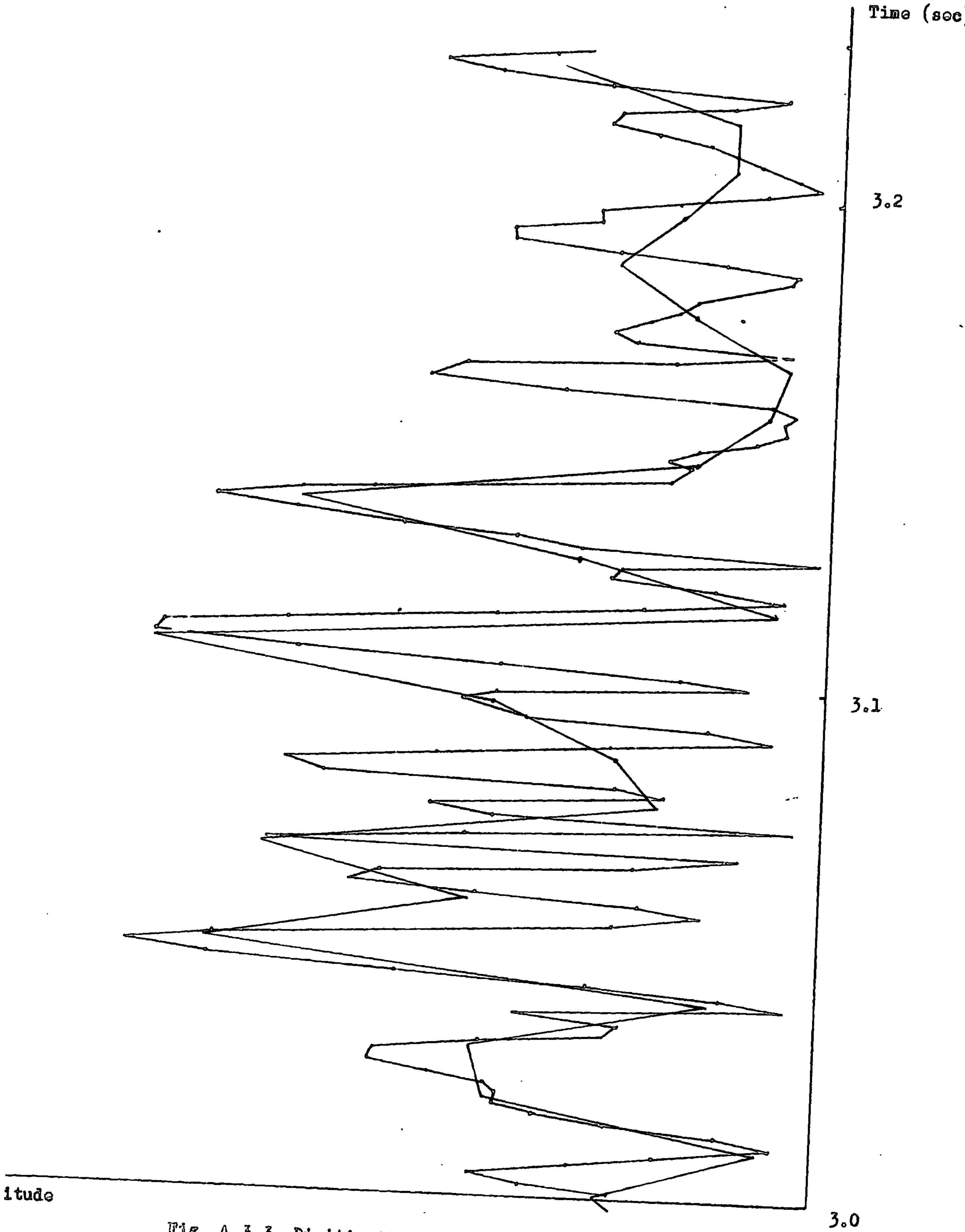

Fig. A.3.3 Digitisation Test 250Hz/500Hz

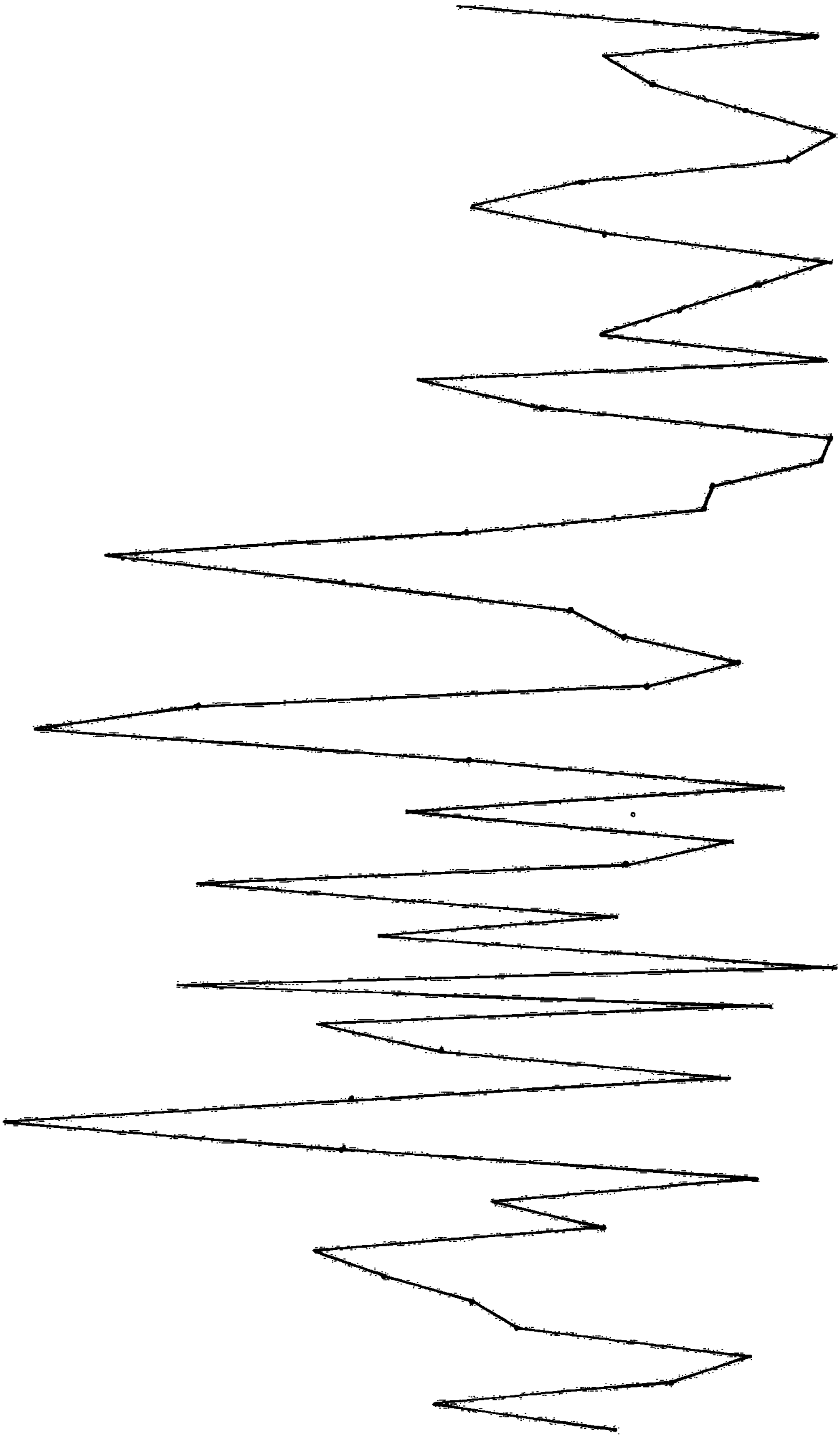

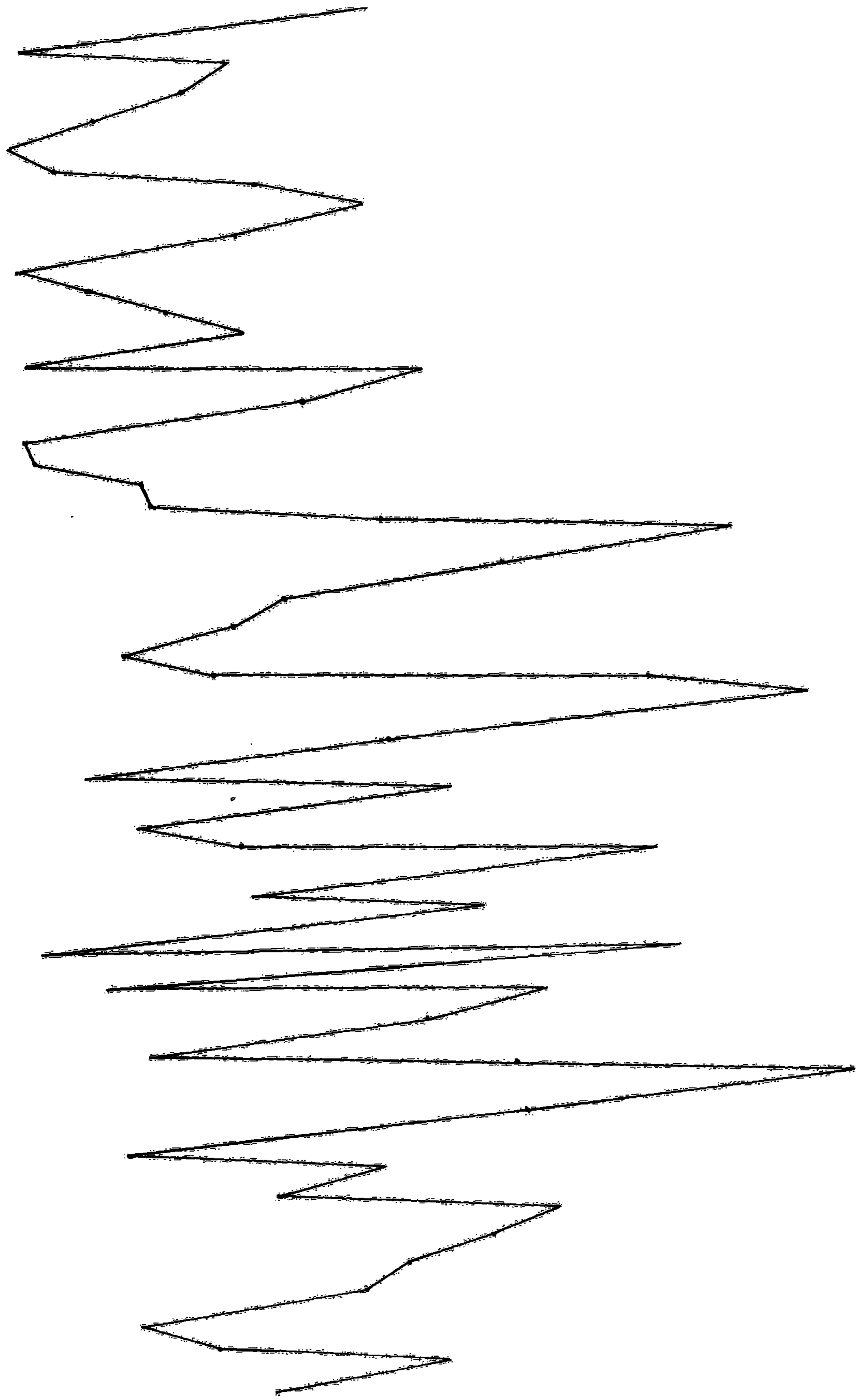

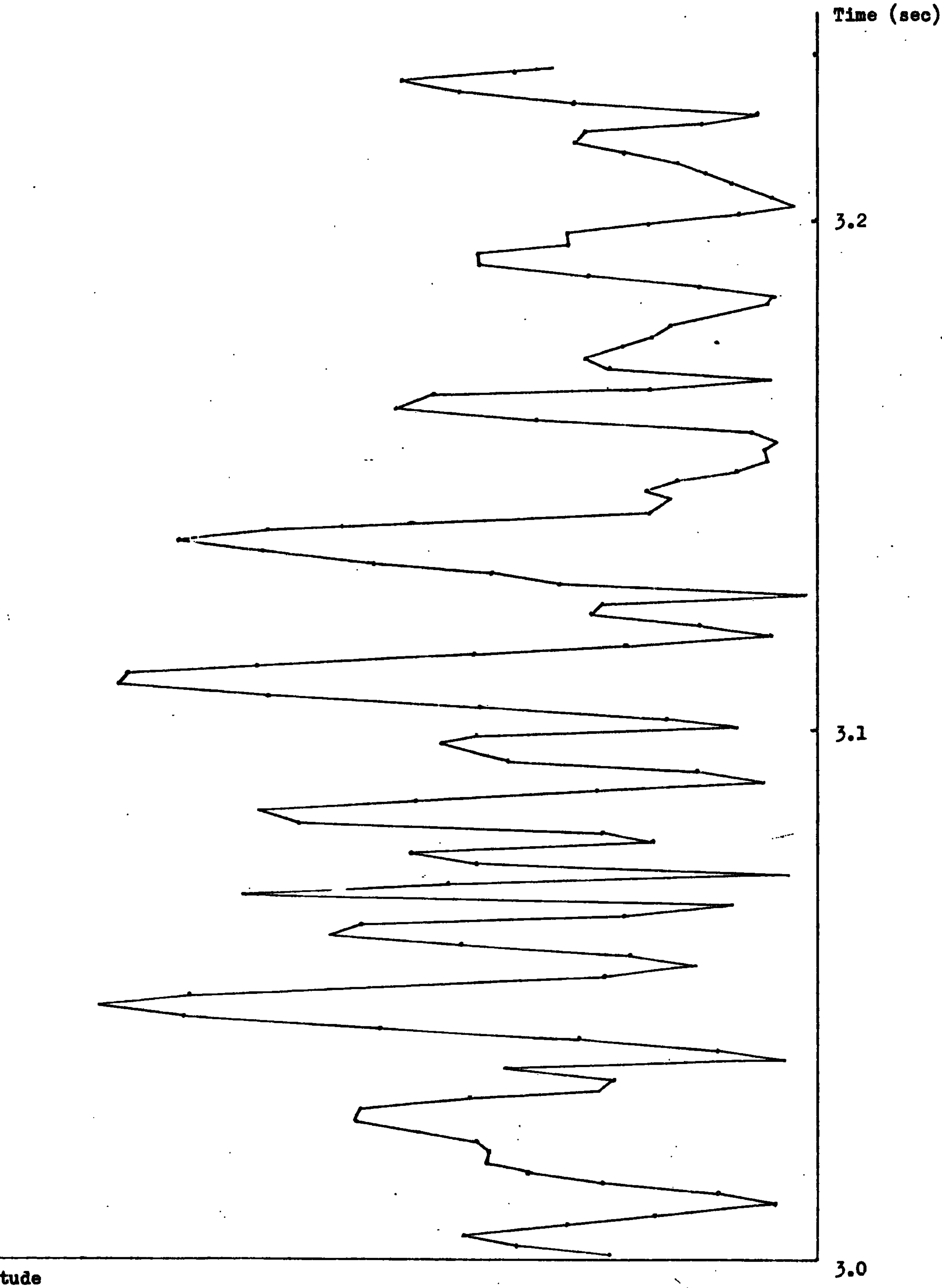

Fig. A3.4 Digitisation Test 100Hz/500Hz

for 15 different peaks listed in the table below (Table A3.1).

Table A3.1 Accuracy of Digitisation Results

Peak No.	500Hz Sample Value	250Hz Sample Value	250Hz % error	100Hz Sample Value	100Hz % error
1	223	213	4.5	217	2.7
2	122	118	3.3	94	22.9
3	148	140	5.4	114	22.8
4	158	157	0.6	156	1.3
5	279	275	1.4	192	31.2
6	260	260	0.0	172	33.9
7	307	294	4.2	294	4.2
8	329	309	6.1	260	21.0
9	277	277	0.0	243	12.3
10	239	223	7.2	222	7.1
11	223	216	3.2	79	64.6
12	276	270	2.2	269	2.5
13	247	247	0.0	213	13.8
14	167	149	10.8	24	85.3
15	136	132	2.9	88	35.3

Mean Error at 250Hz is 3.45%

Mean Error at 100Hz is 24.09%

These figures are calculated with respect to the 500Hz figure. The plots corresponding to Table A3.1 are given in Fig. A3.5.

The digitisation at 1kHz proved unsuccessful; the programme was attempting to force the data through the internal storage buffers for the magnetic tape faster than possible and this lead to corruption of the information written onto tape.

The 100Hz digitisation, as expected, gave a percentage error on the peak amplitude (averaged) of 24.09%, taking the 500Hz as the

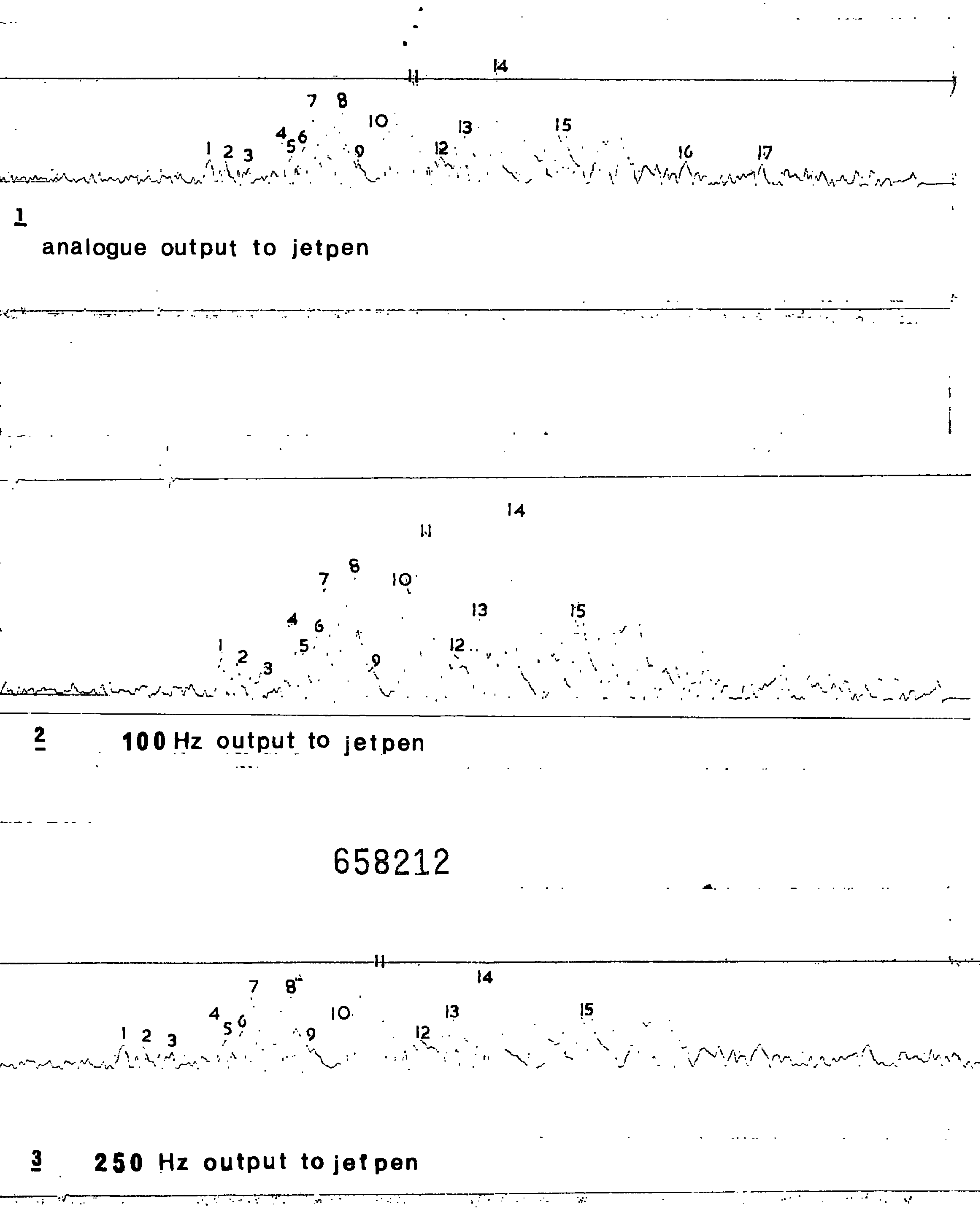

Fig. A3·5 Peak Accuracy

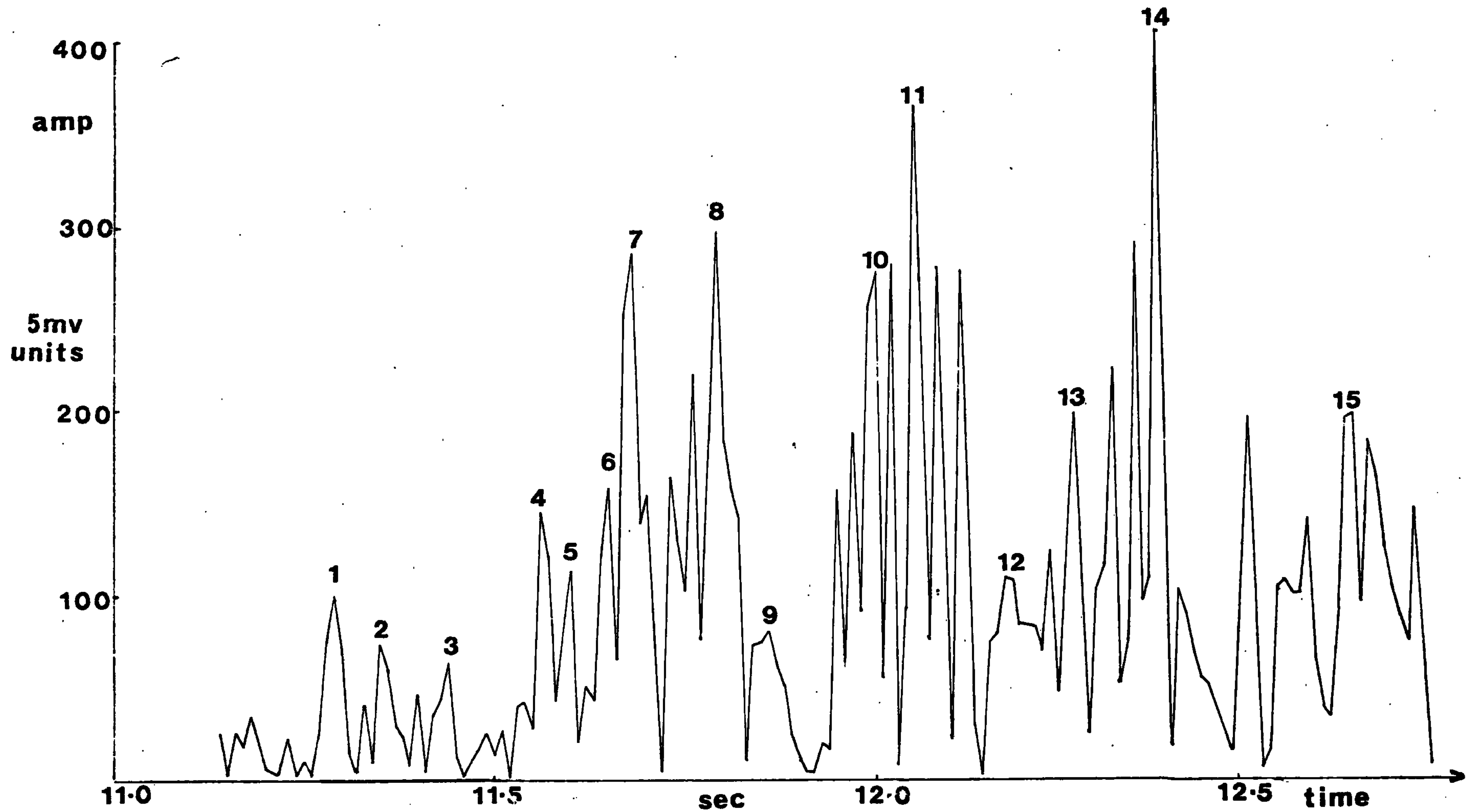

Fig. A 3·6 Disc output

true record, whilst the 250Hz sampling rate gave a predictably lower error figure of 3.45%. The 500Hz digitisation was checked against an analogue display of the analogue signal prior to digitisation, using 'jet-pen' equipment, normally used to investigate the output from an earthquake monitoring seismic array, whose characteristic frequencies are well below those encountered in this work. The low amplitude range of this display (maximum displacement 7cm) together with the impulse response of the galvanometers deflecting the pens, meant that this analogue display was not capable of producing records which could be numerically analysed to any degree of sophistication.

A listing of the relative amplitude ratios obtained, analogue source to 500Hz digital source, is, however, given in Table A3.2, from which it can be seen that the 500Hz rate seems to give a fairly accurate representation of the analogue signal.

Table A3.2 Comparison of Disc and Jet-Pen Output

Peak No.	Amplitude Ch(2) jet pen (mm)	Amplitude Ch(5) jet pen (mm)	Ch(5) / Ch(2)	Disc Output (Digital) Ch(5) 5mV/mm.
1	4.7	7.0	1.760	14.14
2	4.0	6.1	1.525	11.97
3	3.0	4.5	1.500	14.00
4	8.0	11.8	1.475	12.29
5	5.0	7.9	1.580	14.30
6	7.2	11.2	1.555	14.12
7	13.5	20.6	1.526	13.84
8	13.5	22.3	1.652	13.27
9	4.3(?)	5.7	1.325(?)	13.85
10	12.8	21.0	1.640	13.10
11	18.2	29.8	1.637	12.22
12	5.0	8.4	1.680	12.86
13	9.2	15.0	1.630	13.13
14	21.0	33.0	1.571	12.21
15	9.0	15.0	1.667	13.00
16	4.5	7.2	1.600	13.33
17	4.0	6.7	1.675	13.13

Ch(2) is analogue source/analogue output.

Ch(5) is digital source (disc file)/analogue output.

The figures in column 4 are obtained by dividing the numerical disc file output (Table A3.3), obtained on the teletype using the PRINT programme, by the corresponding analogue output from disc.

The response of the jet pen system was investigated using a computer generated square wave, and analysis of the results gave an approximate overshoot value of 25.30%.

Table A3.3 Disc File Output

Peak Number	Amplitude (1024=5mV)
1	99
2	73
3	63
4	145
5	113
6	158
7	285
8	296
9	79
10	275
11	364
12	108
13	197
14	403
15	195
16	96
17	88